RESEARCH PROGRAMME OF THE RESEARCH FUND FOR COAL AND STEEL

STEELRTD

Project carried out with a financial grant of the Research Programme of the Research Fund for Coal and Steel

DRAFT-FINAL REPORT

Technical Report N°	**07**	Issued on	**30/03/2012**
Period of Reference	**01/07/2008 – 31/12/2011**		
Technical Group	TG**8**		

DESIGN AND INTEGRITY ASSESSMENT OF HIGH STRENGTH TUBULAR STRUCTURES FOR EXTREME LOADING CONDITIONS

Project Acronym: **HITUBES**

Grant Agreement Number: **RFSR-CT-2008-00035**

Beneficiaries : **University of Trento, Italy**
Centro Sviluppo Materiali, Italy
Instituto de Soldadura e Qualidade, Portugal
Fundacion ITMA, Spain
Korrosions Och Metallforskningsinstitutet AB, Sweden
Université de Liège, Belgium
University of Thessaly, Greece

Coordinator: **Oreste S. Bursi, University of Trento**

Authors: **Oreste. S. Bursi (UTRE), Anil Kumar (UTRE)**
Giuseppe Demofonti (CSM), Giuliana Zilli (CSM),
Gian Marco Tamponi (CSM), Jan Ferino (CSM)
Helena Guvaia (ISQ), Carlos Maia (ISQ)
Sergio Rivera (ITMA), Ricardo Alvarez (ITMA),
Ricardo Lezcano (ITMA)
Eva Johansson (KIMAB), Nuria Fuertes (KIMAB),
Jean-Pierre Jaspart (ULGG), Jean-François Demonceau (ULGG), Long Van Hoang (ULGG), Ly Dong Phuong Lam (ULGG)
Spyros Karamanos (UTHESSA), Philip Perdikaris (UTHESSA), Aglaia Pournara (UTHESSA), George Varelis (UTHESSA), Charis Papatheocharis (UTHESSA)
Daniele Maio (StahlbauPichler), Manuel Sommariva (StahlbauPichler)

Commencement date: **1 July 2008**

Completion date: **31 December 2011**

Distribution list

Chairman

Expert Name: Mr Louis-Guy CAJOT
Organisation: ARCELOR PROFIL
ARCELORMITTAL BELVAL & DIFFERDANGE S.A.

Members

Expert Name: Ms Nancy BADDOO
Organisation: SCI
THE STEEL CONSTRUCTION INSTITUTE LBG

Expert Name: Prof. Darko BEG
Organisation: UNIV LJUBLJANA
UNIVERZA V LJUBLJANI

Expert Name: Prof. Antonio Augusto FERNANDES
Organisation: UNIV PORTO
UNIVERSIDADE DO PORTO

Expert Name: Mr Anthony KARAMANOS
Organisation: A.S. KARAMANOS
A.S. KARAMANOS & ASSOCIATES

Expert Name: Prof. Andrzej KLIMPEL
Organisation: SUT
SILESIAN UNIVERSITY OF TECHNOLOGY -
POLITECHNIKA SLASKA

Expert Name: Mr Jouko KOUHI
Organisation: FCSA
FINNISH CONSTRUCTIONAL STEELWORK
ASSOCIATION

Expert Name: Prof. Joaquín ORDIERES MERE
Organisation: UPM
UNIVERSIDAD POLITÉCNICA DE MADRID

Expert Name: Dr. Walter SALVATORE
Organisation: UNIV PISA
UNIVERSITA DI PISA - DIPARTAMENTO
INGEGNERIA CIVILE

Members (not reimbursed)

Expert Name: Mr Adam BANNISTER
Organisation: TATA STEEL UK
TATA STEEL UK LTD - SWINDEN TECHNOLOGY
CENTRE

Expert Name: Mr Thierry BRAINE-BONNAIRE
Organisation: ARCELOR France

ARCELOR France SA

Expert Name: Dr.-Ing. Giuseppe DEMOFONTI
Organisation: CSM
CENTRO SVILUPPO MATERIALI SPA

Expert Name: Dr. Gerhard KNAUF
Organisation: SZMF
SALZGITTER MANNESMANN FORSCHUNG GmbH

TABLE OF CONTENT

Abstract

High Strength Steel (HSS) characterized by yield strength ranging between 500MPa to 700MPa has been available for many years. However, its use in onshore engineering is quite restrictive. Reasons were threefold: i) Eurocodes covered steels with yield strength up to 460MPa; ii) higher costs than regular steel; iii) lack of conceptual design with HSS. Nonetheless very recently, there has been a growing trend for the use of HSS in tubular structures thanks to Eurocode 3 Part 1-12 (2006), that extended its scope to steel grades up to S690/S700MC. Along this line, the HITUBES project intended to develop performance-based designs and assessment procedures to make full use of HSS tubes up to S700MC for structures subject also to extreme repeated loads; in fact Eurocode 3 Part 1-12 imposes many limitations at the material, structural and design level. The ambitious targets are to increase the performance of tubular structures, reduce weights, construction and operating costs.

The project covered the period 01/07/2008-31/12/2011, and main research work focussed on several aspects listed herein: literature survey; selection of finite element-based and identification dynamic analysis codes; selection of realistic Case Studies and FE analysis for the evaluation of actions and stresses; structural identification and health monitoring of a cable-stay and arch footbridges; tests planning and execution including welding procedure specifications; simulations of welded and bolted connections under monotonic, low-cycle and high-cycle fatigue loadings; simulation of Case studies and reliability analysis for quantification of realistic performance scenarios; SWOT analysis and monitoring of project activities.

Reference:

Eurocode 3: Part 1.12 (2006), Design of steel structures: Additional rules for the extension of EN 1993 up to steel grades S700, EN, 1993-1-12

Project Overview

A brief overview of the project for the period 01 July 2008 to 31 December 2011 is presented in Table 1.

Table1: Final project overview

CATEGORY OF RESEARCH *(COAL /STEEL)*:	STEEL
TECHNICAL GROUP:	TG8
REFERENCE PERIOD:	01/07/2008-31/12/2011
GRANT AGREEMENT N°:	*RFSR-CT-2008-00035*
TITLE:	*DESIGN AND INTEGRITY ASSESSMENT OF HIGH STRENGTH TUBULAR STRUCTURES FOR EXTREME LOADING CONDITIONS*
BENEFICIARIES:	*University of Trento, Italy* *Centro Sviluppo Materiali, Italy* *Instituto de Soldadura e Qualidade, Portugal* *Fundacion ITMA, Spain* *Swerea KIMAB AB, Sweden* *Université de Liège, Belgium* *University of Thessaly, Greece*
COMMENCEMENT DATE:	01 July 2008
COMPLETION DATE:	31 December 2011
WORK UNDERTAKEN:	o Literature survey and selection of case studies o Selection of FE codes, simulations and investigations on case studies o Structural identification and monitoring of footbridges o Tests on HSS materials and welds also considering post-weld treatment o Tests on HSS tubular members and welded and bolted connections o Numerical simulations on HSS tubular members, tubular welded and bolted connections o Simulation on footbridges and fatigue checks o Development of design guidelines and reliability evaluation o Standard protocols, SWOT analysis and monitoring of project activities

MAIN RESULTS:	o Literature survey completed, case studies selected o FE and identification codes chosen, analysis and investigation on case studies completed o Identification and monitoring of the two footbridges completed o Tests completed o Numerical simulations completed o Design guidelines and reliability assessment developed o Efficient management process set o Standard protocols, SWOT analysis made o Monitoring of the project completed
FUTURE WORK TO BE UNDERTAKEN:	
ON SCHEDULE (*YES /NO)*:	YES
PROBLEMS ENCOUNTERED:	- Difficulty in the provision of HSS TS 590J2H tube material in small quantity (193.7 x 10 mm tubes – about 3.5 tons; 355.6 x 12.5 mm tubes – about 1.5 tons); - Wind turbines not studied.
CORRECTION – ACTIONS *(USE OF A TABLE IS RECOMMENDED)*:	- Tenaris Dalmine agreed and provided the small quantity of steel tubes; - Technical annex was amended
PUBLICATIONS – PATENTS :	In summary: 10 papers and 1 book; 2 papers published on international journals, 3 papers under preparation; 5 on international conferences. See Section List of Publications.

BUDGET INFORMATION PER BENEFICIARY:
Based on overall costs (independently from EU financial contribution)

BENEFICIARY (incl. coordinator)	***Total amount spent to date (€)****	***Total allowable cost (€) as foreseen in Grant Agreement***
UTRE	404300.38	372907
CSM	203223.90	186799
ISQ		169826
ITMA	176416.20	174014
KIMAB	183883.60	166809
ULGG	186276.12	186530
UTHESSA	169077.69	175612

Final summary

WP1: Review on test data and design procedures on tubular members and connections and Bayesian approaches for probabilistic risk assessment

The main objectives of WP1 were several: a) collection of literature on road foot-cycle and railway bridges made of HSS and/or tubular sections under extreme loadings; b) collection and evaluation of experimental test data and design procedures for tubular members and joints relevant to the investigated structures; c) corrosion aspects relevant to HSS employed in structures; d) evaluation of Bayesian approaches for the development of time dependent formulations in order to perform probabilistic risk assessments; e) choice of output-only identification techniques.

The bibliographic review was made at the beginning of the project in order to have knowledge of conceptual design, standards and test methods relevant to HSS tubular members, joints and connections mainly employed for selected Case Studies. The main results of this work package are summarized here. They are also widely reported in Section WP1 of Description of Activities and Discussion, in Appendix A and relevant Deliverables D1.1-D1.4 listed in the Amended Technical Annex.

From the state of the art relevant to the use of HSS for onshore construction [1], it is clear that Europe is lagging behind with respect to USA and Japan in spite of the fact that several applications in constructions are cost effective. In detail, we restricted our scope to constructions made with Circular Hollow Sections (CHS) that result to be very competitive in terms of strength relevant to compression, tension and bending and torsion. Moreover, the CHS represents the optimal shape for elements subject to wind and sea loading owing to the low drag coefficient. Nonetheless, we considered also the Nomi footbridge which is characterized by a Rectangular Hollow Sections (RHS) arch. Due to higher cost of tubular members, about 15 per cent more with respect to open sections, and HSS, up to 30 per cent more for S690 with respect to S355, sometimes it is wise just to change the material to a higher grade in a small part of the structure, in order to achieve weight savings. Nonetheless, in many cases it is necessary to change the conceptual design of a structure in order to make full use of HSS. In fact, buckling, fatigue and deflection criteria often set limits for steel grade used. Though a working group within CEN/TC250/SC3 recently issued Part 1-12 of Eurocode 3 in order to make easier for designers and steel contractors the choice of HSS, still several problems remain. Basically, elastic analysis should be used though plastic resistance would be better. For joints there are restrictions with reduction factors, for instance 0.8, for strength design methods that make use of large plastic deformations. For welded connections undermatched electrodes are allowed. Within all these uncertainties, to collect and evaluate test data on members, joints and connections under extreme loadings as well as to extract realistic specimens to be tested, the following two main case studies were selected:

1. the cable-stay footbridge “Ponte del mare” Pescara, Italy.
2. The Landegem Railway Bridge, Belgium.

The basis for selection of two different types of bridges was that on one hand, the footbridge was mainly subject to elastic or possible low-cycle fatigue behaviour owing to excessive wind and pedestrian loadings; in fact, high-cycle fatigue check were carried out for wind and pedestrians, and all checks were satisfied; on the other hand the railway bridge was mainly subject to high-cycle fatigue loading owing to loads caused by passage of railway vehicles. It was expected that the study of structures subject to two different types of loadings would provide a better comparative understanding of the behaviour of structures, tubular members and joints made of HSS, including welding, bolting, etc.

Due to higher cost of HSS, several bridges use tubular members with standard steel. In this respect, other two footbridges endowed with tubular members, i.e. the S. Michele footbridge and the Nomi footbridge, both located nearby Trento were selected and analysed. In particular: i) the twin tubular arch foot-cycle bridge at S. Michele (Trento) is characterized by S460 CHS arches; ii) the tilted bowstring arch foot-cycle bridge at Nomi (Trento) is endowed with a RHS bowstring arch. These bridges were also selected for fatigue model developments treated in Task 6.3, to reply to some open question left by the HIVOSS project [2].

The aforementioned activities and results allowed some brief conclusions to be drawn. Tubular members are very popular in bridge structures mainly for aesthetic and mechanical reasons. CHS members are preferred to RHS also for aerodynamic problems. With regard to steel grade and when strength dominates structural design, S355 and S460 are much more preferred with respect to S500 or higher grades both for costs and grade availability reasons. We understood that steel mills tend to use HSS for specific applications, e.g. tower cranes made of CHS with S690 or so, and therefore, also their adaptation to different grades is limited -taking into account material certification problems too-. With regard to structural design with HSS, though Part 1-12 of Eurocode 1993 was issued, the use of HSS both at the conceptual design level and at the checking level of members, joints, etc. remains difficult when extreme conditions in terms of actions and stresses are present. From a corrosion viewpoint, one serious drawback of HSS is its increased risk of hydrogen-related Stress Corrosion Cracking (SCC), or hydrogen embrittlement. The literature review indicates that this limit state can be reached for a suitable combination of material properties, environmental effects and stress conditions. Aggressive environmental effects, e.g. sea water, steered us to the selection of the “Ponte del mare” footbridge.

With regard to Bayesian techniques, Bridge Management Systems have become increasingly sophisticated over the past decade and provide valuable information about the structural condition of several bridges. At the same time, reliability methods have gained increasing prominence and are used to forecast life-cycle performance over many decades of structural life. In this context, reliability analyses can be updated with Bayesian techniques when inspection results are available. Nonetheless, available literature mainly focussed on reinforced concrete bridge superstructures.

Finally, modal analysis involving output-only measurements present a challenge that requires the use of special modal identification technique, which can deal with very small magnitude of ambient vibration contaminated by noise. There are two complementary modal analysis methods as rather simple Peak Picking (PP) method in frequency domain and more advanced stochastic subspace identification (SSI) method in time domain. The SSI technique can detect frequencies that may possibly be missed by the PP method and gives a more reasonable mode shapes in most cases. To be able to trace non-linear phenomena that change with time, also short-time Fourier transform techniques can be used. The choice of a time-frequency (TF) technique is made because of its robustness, i.e. its capability to clearly identify: i) signal events which manifest during a short time interval (time localization); ii) signal components which are concentrated at particular Fourier frequencies, such as sinusoids (frequency localization). We used both SSI and TF techniques in “Ponte del mare” mainly to capture the non-linear on-off behaviour of dampers used to reduce potential flutter phenomena and introduce damping.

WP2: Extreme forces and stresses on foot- cycle-bridges, railway bridges and monitoring of footbridges

The main objectives of WP2 were: a) the selection of FE codes used to perform analyses to obtain extreme forces and relevant stresses; b) to perform the aforementioned analyses; c) to further justify the choices of Case Studies also on the basis of calculations and preliminary experimental data; d) to perform both system identification and structural health monitoring of footbridges “Ponte del mare” and “S. Michele”, respectively. At this stage, we note that the wind turbine was not chosen as a possible case study owing to the variable tube cross-sections of the mast. The tube of the mast is seam and typically, the manufacturer ‘Tenaris Dalmine’ only produces seamless tubes with constant cross-sections. Hence, the study on the chosen wind turbine was abandoned. Main results of this work package are summarized here. They are also widely reported in Section WP2 of Description of Activities and Discussion, in Appendix B and relevant Deliverables D2.1 and D2.2 listed in the Amended Technical Annex.

In order to re-design the “Ponte del mare” footbridge with circular hollow sections (CHS) and to evaluate both internal actions and stresses, the SAP 2000 [3] non-linear software code was chosen. Successively, in order to perform the FE analysis on the footbridge aiming at observing the effect of wind and pedestrians, the ANSYS-11 software [4] code was selected. This software was also used for the analysis of the “S. Michele” footbridge. In order to find modal parameters, i.e. natural frequencies, mode shapes and damping, the ARTeMIS-Extractor software code [5] and some in-house software developed by Politecnico of Torino was chosen. In order to perform the numerical simulation analysis on welded connections ABAQUS-STANDARD (2000) [6] software code was selected. In order to perform numerical simulations on flange bolted joints the LAGAMINE software code, developed by University of Liege was used.

With regard to re-design of Case studies, the “Ponte del mare” footbridge was redesigned using the CHS members with grade TS590J2H provided by Tenaris. From analyses, it resulted that the possibility of exploitation of HSS was limited by deformation limit states, i.e. maximum deck deflection L/500, and maximum deck rotation ϑ=5.48 per cent corresponding to about 210 mm maximum displacement at one end. Nonetheless, the employment of CHS members provided several advantages in terms of: i) steel savings in both decks for the replacement of open sections with CHS of about 60.89 tons, i.e. 11.7 per cent; more transparency of decks and possibility to take away the hulls; ii) reductions of aerodynamic problems because of the elimination of the hulls and hence elimination of elastic-viscous-fluid dampers. As far as the “Landegem” railway bridge is concerned, the re-design mainly interested CHS arches and hangers, which were conditioned by high-cycle fatigue phenomena. We considered as reference grade S355J2, a detail category C90 and the steel price proposed by Johansson and Collin [7]. With reference to arches, if the admissible nominal stress range can exceed a value of about 120 MPa, the use of HSS will end up with an economical interest. Because high-cycle fatigue tests on TS590J2H tubes were performed, an admissible stress range of 126 N/mm^2 was obtained. Hence, 117 tons for the S355J2 arches corresponded to savings of about 14 per cent, meaning that TS590 is economically interesting if its price doesn’t exceed 116% with respect to grade S355J2. With respect to bridge hangers, there was no interest in the use of HSS for these structural elements, even if the admissible stress range could increase up to 300 MPa.

Structural identification and condition monitoring on site of the dynamic properties and stress states of “Ponte del mare” and S. Michele were performed too. These activities were much more complex for the first footbridge, indeed. In fact, the cable-stayed footbridge was characterized by two curved decks and provided with a vibration reduction system –viscous-fluid dampers- designed and installed to avoid premature aeroelastic instability and to control human-induced vibrations. The complex dynamic behaviour and the uncertainties related to numerical modelling led to a modal testing campaign of the bridge without and with dampers. Output-only ambient vibration tests, associated with low vibration levels, showed that the damping devices were basically inactive, owing to friction and connection slacks. In addition, for such low oscillation amplitudes dampers caused a stiffening effect that had not been envisaged earlier in the design process. Free decay tests, which were performed by released masses, did produce high vibration levels. In the latter tests, dampers showed a good absorption capacity and the damping doubled or even trebled on some of the vibration modes. In order to clarify these outcomes, modal quantities were calculated instantaneously, on the basis of time–frequency identification techniques. A thorough analysis of dynamic response signals revealed that the structure with dampers actually behaves like a threshold system: (i) for low vibration levels the dampers were still, so that they performed as constraints that stiffened the structure; (ii) for high vibration levels, the dampers became fully working and, as required at the design stage, they did not significantly affect main frequencies. With regard to monitoring activities, the whole monitoring system of Ponte del Mare was composed of 8 accelerometers, 4 thermo-resistances and 2 anemometers. Each of the anemometers provided two types of acquisition, that is, the wind speed and the wind direction, respectively. Three types of data were acquired during the period 17/12/2009-31/12/2010: i) temperature, wind speed and direction that were continuously monitored; ii) accelerations from all accelerometers, which were recorded at 5:58 p.m. every day for 82 seconds at 100 Hz; iii) trigger events: trigger was considered an extreme event when any of the eight accelerometers reached the limit of 0.4 m/s2 in vertical direction and 0.2 m/s2 in the horizontal direction. The maximum event happened at Christmas day (25/12/2009) with a large wind trigger that corresponded to a wind speed of 28.02 m/s. The majority of triggers occurred equally on Friday and Sunday. The accelerometer channels 4 & 7 were subject to the large number of triggers. Channel 4 was located near the end of the foot deck, while channel 7 was located in the middle of the cycle deck. The Fast Fourier Transform (FFT) of these data revealed information about the excitation frequencies. It was observed that frequencies below and near 1 Hz were well excited. This was due to the fact that wind typically excites frequencies below 1 Hz.

The corresponding structural identification and condition monitoring activities performed on the S. Michele footbridge highlighted no specific problems. In fact the footbridge was much more standard both in conceptual design and equipment. It was endowed with two twin tubular arches, far from locations of high wind and equipped with three classical tuned mass dampers for pedestrians. Nonetheless, it was very useful for fatigue model checks treated in Task 6.3.

WP3: Mechanical characterization of HSS and inelastic behaviour of HSS tubular members

The main objectives of WP3 were: a) the mechanical characterization of HSS material including high-cycle fatigue and corrosion aspects; b) execution and evaluation of tests on tubular members characterized both by buckling and inelastic behaviour. The main results of this work package are summarized here. They are also widely reported in Section WP3 of Description of Activities and Discussion, in Appendix C and relevant Deliverables D3.1-D3.3 listed in the Amend. Technical Annex.

With regard to the HSS base material, we chose TS590J2H quenched and tempered produced by Tenaris Dalmine, because they guaranteed a small production of 193.7 x 10 mm tubes – about 3.5 tons - and 355.6 x 12.5 mm tubes – about 1.5 tons – for this project. Nonetheless, we traced average yield strengths and tensile strengths of about 690 MPa and 766 MPa, respectively with elongations greater than 19 per cent. Though these properties satisfied quality control of Tenaris Dalmine, we understood that steel mills tend to use HSS for specific applications, e.g. tower cranes made of CHS with grade S690 or so, and therefore, also their adaptation to different grades can be limited. In any case, the aforementioned variability did not put at risk the under- over-matching ratios that we selected for welds. In fact, it was not that easy to conceive an intertwined experimental program comprising 63 specimens in total – see Figure 25 – and 88 tests for this WP – see Table 9 – used for: i) characterization tests on base material TS590J2H and welds with the inclusion of peening treatments; ii) testing on short and long tubular members; iii) tests on welded and bolted connections with the inclusion of corrosion; NDT tests on realized specimens. Moreover also specimens made of S355J2 were included in the test program as specimens made of reference steel.

Fatigue characterizations of base material of tubes were performed by means of relevant S-N curves. ASTM E466-07 were followed [8] for axial fatigue tests considering a load ratio R=0.1. Fatigue limits for 2×10^6 cycles corresponded to detail categories 432 MPa and 690 MPa for S355 and TS590, respectively. These values result to be more than satisfactory.

The fracture toughness characterization was performed by means of the determination of a J-R curve for each base material. The test procedure followed the requirements of ASTM E1820 [9] at ambient temperature. The corresponding energy for the onset of a stable crack growth resulted to be 620 kJ/m^2 and 440 kJ/m^2 for S355 and TS590, respectively. Moreover, inspection certificates indicate an average of 160 Joule for Charpy resilience V-notch (KCV) at -40 C much greater than J2 requirement.

Several classes of electrodes, i.e. 32, 46, 55 and 79 were selected to reproduce the following weld types: Undermatching to grade S355; Overmatching to S355; Undermatching to TS590; Overmatching to TS590; Undermatching to TS590 and Overmatching to S355. The subcontractor Stahlbau Pichler does not usually employ Electrode class 55 and 79; as a result, we prepared with them Welding Procedure Specifications (WPS). In greater detail, they specified welding variables for our specific applications to assure repeatability by trained welders and welding operators, according to EN ISO 15609-1 [10].

The specimens were categorized for three types of non-destructive tests. The specimens under monotonic and low-cycle fatigue loading were chosen for visual inspection (VI) as well as for magnetic-particle (MT) inspection. The specimens under high-cycle fatigue loading were selected for ultrasonic testing (UT). With regard to weld specimens the subcontractor followed a defect acceptance criterion according to EN 1712 and EN 1291 for ultrasonic and magnetic particle methods, respectively. In general, pre-production welding tests allow for defects up to 3 mm. Obviously, we were much below this threshold and fatigue data of welded connections prove it.

Corrosion rate measurements and Slow Strain Rate Tests (SSRT) were performed on two different materials, i.e. TS590 and S355, in order to evaluate the susceptibility of materials towards stress corrosion cracking or hydrogen embrittlement. Uniform corrosion rates of base metals were measured in two different solutions, 1 wt% and 3.5 wt% NaCl, respectively, in order to simulate offshore and sea water environments, respectively. Tests were carried out at ambient temperature. The linear polarization resistance technique, based on the change in potential and record of the polarization was used to measure the corrosion rate. The electrochemical general corrosion rate measurements showed that steel TS590 had the same corrosion resistance or a slightly better value than the reference material S355. The SSRT-measurements showed that both TS590 and S355 were sensitive to stress corrosion cracking in the presence of cathodic polarisation.

In view of tests on tubular members, both geometrical imperfections and residual stresses were detected. Imperfections satisfied the product norm for seamless tubes, i.e. EN 10210-2 [11]; whilst longitudinal residual stresses on the outer surface ranged between + 74 MPa and – 60 MPa, bending components of longitudinal residual stresses were evaluated to be less than ± 10 MPa, and circumferential residual stresses were estimated to be + 93 MPa. Under the assumption of a triangular through thickness distribution the compressive residual stress of - 93 MPa was assumed for the inner surface. Several tests were conducted on 193.7 x 10 mm tubes under M, N and M-N action combinations. Because of its large slenderness, i.e. 75, with respect to the one of other tubes, e.g. 40 for 355 x 12 mm and 44 for 323.9 x 10 mm, some tests of 193.7 x 10 mm tubes prematurely ended. So other CHS were employed. Nonetheless, the entire test programme showed that the aforementioned tubes exhibited favourable characteristics at the section level, at the member level, adequate ductility and low strength degradation.

WP4: Performance of HSS welded and bolted connections

The main objectives of WP4 were: a) the mechanical characterization of welded HSS connections including high-cycle fatigue, corrosion aspects, weld characterization; b) execution and evaluation of tests on tubular welded connections and bolted connections under monotonic, cyclic and high-cycle fatigue loadings. The main results of this work package are summarized here. They are also widely reported in Section WP4 of Description of Activities and Discussion, in Appendix D and relevant Deliverables D4.1-D4.4 listed in the Amended Technical Annex.

Also for this WP, we conceived an intertwined experimental program comprising 63 specimens in total – see see Figure 25 – and 130 tests for this WP – see Table 9 in this respect.

Fatigue characterizations were carried out on coupon specimens extracted from transverse butt weld connections of TS590J2H and S355J2 tubes, respectively. The study included the evaluation of the mismatching behaviour because welds were realized both in the overmatching and in the undermatching condition. The characterization was based on the determination of an entire S-N curve with a run-out of $2 \bullet 10^6$ cycles with a load ratio R=0.1. Test results were fitted to a $\Delta\sigma/2$ - Log N linear curve in agreement with ASTM E739 standards [12], for fatigue data evaluation. Taking into account the reference value of 96 MPa for the reference steel grade S355, the overmatching condition exhibited a better fatigue performance than the undermatching condition; in fact we got 126 MPa for the overmatching case and 105 MPa for the undermatching case; see Table 17. Note that the detail category suggested by Eurocode 1993 Part 1-9 for this detail is 71. So both cases were favourable and undermatching is in general preferred because of less electrode strength and more ductility exhibited by welds.

Crack initiation was always located in the inner part of the tube, with a crack propagation always through the thickness. Two welded connections were treated by means of an ultrasonic process, i.e. peening, that consisted of cleaning the weld toe areas of the outer surface and the creation of a weld toe groove. The weld root in the tube inner surface was not treated by means of the ultrasonic equipment, both for costs and tool access reasons. As stated above, all fatigue failures initiated from the inner surface of the tube and progressed to the outer surface of the tube, i.e. the peened surface. Therefore, the peening treatment did not affect the fatigue performance of specimens.

The fracture toughness characterization was performed by means of the determination of a J-R curve for each welded connection. The test procedure followed the requirements of ASTM E1820 [9] at ambient temperature. The corresponding energy for the onset of a stable crack growth resulted to be 440 kJ/m^2 for TS590J2H base metal, 132 kJ/m^2 for TS590 with an undermatching weld and 90 kJ/m^2 for TS590 with an overmatching weld, respectively. The better condition of undermatching weldment is evident.

In order to evaluate the susceptibility of materials to stress corrosion cracking or to hydrogen embrittlement, corrosion rate measurements and Slow Strain Rate Tests (SSRT) were performed on welds extracted from K- and X-joints and relevant Heat Affected Zones (HAZ) of two different materials, i.e. TS590J2H and S355J2, respectivley. Uniform corrosion rates of welds and materials were measured in two different solutions, i.e. 1 wt% and 3.5 wt% NaCl, respectively, in order to simulate offshore and sea water environments, respectively. Higher corrosion rates were achieved in 3.5 wt% NaCl compared to 1 wt% NaCl for all tested samples. Steel TS590 exhibited a lower corrosion rate than S355 in the most aggressive solution with 3.5 wt% NaCl, while it was slightly higher for the weld metal of TS590 in 1 wt% NaCl solution. From results, it was evident that cathodic polarisation, that it is intended to simulate cathodic protection drastically decreased the Reduction Area of all tested samples prepared, from base metal, welds and HAZ. The obtained results also indicated that the susceptibility to stress corrosion cracking increased in following order: base, HAZ and weld metal.

Additional macroscopic examinations, hardness tests, and toughness tests were performed on butt welded connections, X joints and K joints. As a result, we concluded that the WPS used for welded connections were considered qualified according to EN 15614-1:2004 [13]; moreover, toughness requirements of 27J at - 20ºC in weldments were always satisfied.

Ten tests in agreement with the Amended Technical Annex were conducted on welded connections between 193.7 x 10 mm tubes and 355 x 12 mm tubes, under in-plane axial loading, in-plane bending and out-of-plane bending loading. Both monotonic and cyclic loadings were considered; R=0.1 for cyclic loading. Test results were able to characterize both strength capacity and ductility as well as low-cycle fatigue behaviour of examined welded joints. They performed quite well and failed with ductile foreseen chord face failure and punching shear mechanisms. See Eurocode 1993 Part 1-8 [14].

A similar testing program comprising six specimens - in agreement with the Amended Technical Annex - was conducted on bolted flange connections between 355 x 12 mm tubes subject to axial loading. Different combinations of plates – 20 and 15 mm thickness – and bolts – M27 and M20 – were considered in order to favour the activation of plastic failure Mechanism 1 and Mechanism 2 foreseen in Eurocode 1993 Part 1-8 [14]. Monotonic, cyclic and high-cycle fatigue loadings were considered; fatigue loading was considered with R=0.1. Test results were able to characterize both strength capacity and ductility as well as the high-cycle fatigue behaviour of bolted connections under exam. Their behaviour was favourable both under monotonic loading in terms of ductility and under high-cycle fatigue loading when the hot spot stress approach is considered.

WP5: Numerical simulations of tubular connections; parametric study

The main objectives of WP5 were: a) to refine material parameter formula depending upon fast extreme loadings; b) response simulation both of welded and bolted connections under monotonic, cyclic and high-cycle fatigue loadings. The main results of this work package are summarized here. They are also widely reported in Section WP5 of Description of Activities and Discussion, in Appendix E and relevant Deliverables D5.1-D5.3 listed in the Amended Technical Annex.

With regard to the sensitivity of TS590J2H to strain rate, as done in previous WPs we also investigated the behaviour of reference grade S355J2 to these effects. In the case of impact or explosions this phenomenon must be necessarily considered. In the case of seismic action and at level of member, the rate of deformation can reach values of about 0.1, with increments of yield strength that can reach about 14 per cent. However in general, considering the uncertainty of seismic input and the effects of single members on the global behaviour on a structure, these effects reduce and wipe out. Conversely, the effect of strain rate on fracture toughness is much more significant, as several brittle failures occurred in members and joints close to welds during Northridge (1994) and Kobe (1995) earthquakes. In this context, we do not expect significant effects on well-designed Case studies, even if subject to typhoons or the like. Nonetheless, because of the character of this exploratory study, it was important to consider these effects on the grades to hand. As a result, low-cycle fatigue tests were carried out up to 10 Hz corresponding to a quite high strain rate of 1/s (= 10 per cent deformation * 10 Hz). Experimental tests were conducted at room temperature and to clarify the dependence of mechanical behaviour, yield strength, ultimate tensile strength and elongation (fracture strain) were observed. Distributions of yield strength, ultimate tensile strength and elongation as a function of strain rates were plotted and fitted with typical power formula. With regard to TS590J2H, it was observed that yield strength increased, with increasing of strain rate; ultimate tensile strength also increased with the growth of strain rate; however, the elongation slightly decreased with increasing strain rate. These phenomena happened because yield strength and ultimate tensile strength increase because of strain-rate hardening. Moreover, increasing rate of yield strength is generally larger than that of ultimate tensile strength due to effect of thermal softening on the deformation. In addition, coefficients of the power formula fitted, indicate that TS590J2H mechanical properties are less sensitive to strain rate than those of S355J2 steel grade.

The simulation of welded X connections of tubular members subject to monotonic loadings was performed with the general-purpose finite element program ABAQUS/STANDARD, capable of modelling the detailed weld geometry, the weld material around braces, the loading sequence as well as nonlinearities. For critical regions of failure, the analysis considered nonlinear geometry through a large-strain description of deformable tubes, as well as inelastic material behaviour, accounted for through an appropriate J2 flow (von Mises) large-strain plasticity model. We recall that the weldment profile in connections of CHS members was made according to EN 1993 Part 1-8 [14]. Nonetheless, due to the insufficient information, weld profiles for CHS X and K joints were also taken by the American Welding Society (AWS) code [15]. Numerical models of connections subject to axial loading, in-plane bending and out-of-plane bending were compared to experimental results. Therefore, chord face failure and punching shear failure which are ductile mechanisms favoured by EN 1993 Part 1-8 were checked. Apart from predicting the load-displacement behaviour of the joint, an important target of the numerical investigation was the calculation of cyclic strain variations in critical weld locations and their comparison with experimental measurements. Furthermore, test results and numerical simulations indicated effects of chord-to-brace diameter ratio, chord diameter-to-thickness ratio and chord-to-brace thickness ratio to the behaviour of examined connections.

Numerical simulations on bolted flange connections were performed by means of the FE program LAGAMINE developed at University of Liege. This program permits the analysis of mechanical, thermal and dynamic problems with large deformation taking in to account geometrical and material non-linearities. Due to symmetry of circular flange joints, only a 1/8 of a half of specimen model was sufficient for the analysis. 3D solid elements endowed with 3 DoF per node were used to model the mechanical behaviour of each specimen. Welds were also been introduced into the model to be able to study the development of hot spot stresses close to them. Moreover, several layers of elements were deployed along the flange thickness to better capture stresses at weld toes. Effective lengths of bolts were taken into account by means of the Agerskov's model. Also in this case, FE models were able to capture both monotonic and low-cycle fatigue response of specimens. In the case of monotonic loading, observed plastic failure mechanisms corresponded to the designed ones. Moreover, bolted connections exhibited a favourable behaviour in terms of strength and ductility.

High-cycle fatigue modelling both of welded and bolted connections required a deeper investigation. First of all, differently from Eurocode 1993 part 1-9 [16] that merges geometric stresses with hot spot stresses we clearly distinguished these stresses: i) the geometric stress is the maximum principal stress in the parent material that includes concentrated load effects, misalignments and macro-geometric effects in the connection, but it disregard the presence of the weld itself in a detail; ii) the hot spot stress is the maximum principal stress in the parent material that includes concentrated load effects, misalignments and macro-geometric effects in the connection, and includes the presence of the weld itself. Eurocode 1993 part 1-9 [16] tries to estimate hot spot stresses by means of the magnification factor k_1 for welded connections and the Stress Concentration Factor (SCF) k_f for bolted connections, to take account of the local stress magnification in relation to detail geometry not included in the reference S-N curves. Because values of k_1 appear quite small with respect to values provided in CIDECT reports [17], and because SCF values are hidden in the S-N curves or not provided in the Eurocode 1993 part 1-9 [16], it was decided to estimate these values either experimentally or numerically by means of strain gauges or refined finite element meshes around welds. In greater details, several extrapolation methods were considered to estimate the hot spot stress at weld toe. With regard to welded connections of X joints, the method suggested by Romeijn [18] reported in the CIDECT report [17], was considered. Conversely wit reference to bolted flange joints, the hot spot stress in plates at weld toes was estimated by : i) the Linear Surface Extrapolation method (LSE) [19]; ii) the Through Thickness at the Weld Toe method (TTWT) [20]; iii) the structural stress from the distance method based on the Dong's method [21]. The LSE method is a simplified technique that can be used both for experimental- and numerical-based approaches. Conversely, the main idea of TTWT and Dong's method are to find a structural stresses through a plate thickness that are in equilibrium with the notch stress –or hot spot stress at the weld toe-. Comparisons between experiments and simulations pointed out that the LSE method is not recommended for bolted connections; as a result, hot spot stresses provided either by TTWT or Dong's were used.

WP6: Numerical simulations of tubular members and structures; parametric study

The main objectives of WP6 were: a) to analyse and determine S-N data for welded/bolted connections with CHS; b) to simulate the behaviour of tubular members; c) to simulate some peculiar aspects of case studies. The main results of this work package are summarized here. They are also widely reported in Section WP6 of Description of Activities and Discussion, in Appendix F and relevant Deliverables D6.1-D6.3 listed in the Amended Technical Annex.

Low-cycle fatigue S-N curves of welded tubular connections were based on the hot-spot methodology described in WP5. For instance for out-of-plane bending low-cycle fatigue tests of X connections carried out in Task 4.2, the Strain Concentration Factor (SNCF) numerically estimated was equal to 7.18, higher than the experimentally evaluated value. According to CIDECT guidelines [17], the corresponding Stress Concentration Factor (SCF) for the connection under exam was equal to 9.82, whereas the numerical model entailed a SCF value equal to 6.16 using a linear extrapolation and 8.19 using a quadratic extrapolation suggested by Romeijn [18]. The above differences are attributed to the sensitivity of the strain/stress field near the weld toe owing to local conditions (notch effect). Because structural components were loaded with repeated excursions well into the inelastic range of material behaviour, we extended high-cycle fatigue curves to low-cycle regime by a method proposed by Ballio et al. [22]; an equivalent elastic stress range was introduced and a linear extension of the S-N curves in the log-log scale was made. Using this approach, the experimental number of cycles for the X-joints under consideration both for out-of-plane bending and in-plane bending endowed with overmatching and undermatching welds were beyond S-N data suggested by CIDECT manual [17]. Moreover and due to presence of monotonic tests, a cut-off criterion for very low cycle numbers is suggested.

A large set of high cycle fatigue data were produced on tensile sample coupons machined from girth welded CHS connections. These tests were performed in Task 4.1 both with Overmatching where TS590J2H elements were butt welded using a G79 consumable, and with Undermatching (U) where TS590J2H elements were butt welded using a G55 consumable. Values of stress range corresponding to 2 million of cycles were calculated with a 75% confidence level and a survival probability of 95% as recommended in Eurocode 1993 Part 1-9 [16]. Both Overmatching and Undermatching specimens satisfy the Detail Category 71 of Detail 3 of Table 8.6 – or Detail 13 of Table 8.3 - and Overmatched weldments provide a better fatigue performance. With regard to bolted connections two high-cycle fatigue tests were performed on specimens with flange thickness of 15 and 20 mm, respectively. Cracks happened always at the weld toe of tubes, and only for the ticker flange a bolt cracked too. FE simulations and the evaluation of structural stresses based on the Dong's method, allow hot spot stresses to be correctly evaluated in tubes, flanges and bolts; in this case, detail categories offered by Eurocode 1993 Part 1-9 are conservative. In other cases where stresses in the parent material or in a weld adjacent to a potential crack location are calculated in accordance with elastic theory excluding all stress concentration effects, i.e. with the nominal stress, it may lead to unsafe results; hence, components are necessarily overdesigned when using the nominal stress approach.

FE simulations of beam-column specimens tested in WP3 were performed with nonlinear finite element models by ABAQUS/STANDARD software. The tube cross-section was endowed with nominal diameter and thickness equal to 193.7 mm and 10 mm respectively. The FE models employed shell elements, which were capable of describing rigorously the behaviour of CHS members, and accounted for nonlinear deformation and plasticity of the steel, through a Linear Kinematic Hardening (LKH) model. A parametric study on beam-columns with the above cross-sectional dimensions was conducted. Moreover, both because of slenderness problems of the aforementioned section and of the need to obtain quite complete M-N diagrams, also members with cross-section ∅355.6/12.5 and ∅323.9/10 were simulated too. Ticker specimens failed after several loading cycles due to fracture near the end connection; thinner specimens sustained a few cycles until local buckling took place. As a result, detailed numerical models were developed using 8-node solid elements (C3D8H) based on a linear-hybrid formulation. Also the stiff steel stubs located between specimens and machine hinges were simulated. A key modelling issue was hardening of the cyclic plasticity model; so cyclic plasticity phenomena and the change of the cross-sectional geometry –ovalization- were captured. In this respect, two von-Mises plasticity models were used, i.e. the LKH model and the more advanced Tseng – Lee (TL) model, which adopts the "bounding surface" concept; it was implemented into ABAQUS through a UMAT user-subroutine. Relevant comparisons between experimental and numerical data are provided in Section WP6 of Description of Activities and Discussion, in Appendix F and relevant Deliverables.

Two reasons were behind simulations of some case studies: i) to analyse the performance of "Ponte del Mare" and discover possible overstressing due to various loading conditions; ii) to investigate possible high-cycle fatigue problems for the design of footbridges, as underlined in the RFS HIVOSS project [2]. With regard to the performance of "Ponte del mare", to get a robust FE model capable of simulating the actual behaviour of the footbridge, the initial FE model was updated on the basis of experimental data. The sensitivity-based model updating techniques and Powell's Dog-Leg method based on the Trust-Region optimisation approach were used. The sensitivity matrix was calculated and nine most sensitive parameters were selected. In order to check its applicability, the updated FE model was used to reproduce the acceleration response under the actual wind recorded on 25/12/2009; then several simulation were carried out for ultimate limit state conditions: the footbridge behaviour resulted to be satisfactory. With reference to high-cycle fatigue limit states, fatigue checks on three different typologies of footbridges were performed: on Ponte del Mare, S. Michele and Nomi-Calliano footbridges. Severe pedestrian loadings were taken from Technical Guide Setrà [23], where it was possible to select pedestrian load models and a methodology for vibration analysis due to human walking. For high-cycle fatigue checks, Eurocode 1993 Part 1-9 was chosen. FE analyses combined with reasonable assumptions and safety checks clearly indicated that none of the footbridge typology considered was prone to fatigue problems owing to pedestrian loading.

WP7: Development of design guidelines and recommendations for high strength tubular structures

The main objectives of WP7 were: a) to develop design guidelines and recommendations for HSS steel for onshore structures under extreme loadings, for welded connections, for bolted connections and for tubular structures; b) to develop Bayesian life-cycle models for maintenance and durability. The main results of this work package are summarized here. They are also widely reported in Section WP7 of Description of Activities and Discussion, in Appendix G and relevant Deliverables D7.1-D7.3 listed in the Amended Technical Annex.

With regard to HSS steel for onshore structures given the fact that mechanical characteristics of TS590J2H are quite good, only some aspects were deepened. With reference to transverse butt welds of sample coupons extracted by CHS subject to fatigue and considering a 75 per cent confidence level with survival probability of 95 per cent, typical reliability values used in Eurocode 1993 part 1-9 [16], details categories with nominal stresses are 71 MPa and 47 MPa for Overmatching and Undermatching weldments, respectively. Because the Detail Category suggested by Eurocode 1993 Part 1-9 is 71 MPa, overmatched welds provide better fatigue performance. Nonetheless, we have to note that only nominal stresses and not hot spot stresses were considered here. Moreover, it must be noted that Eurocode 1993 part 1-9 merges hot spot stresses with geometrical stresses and tends to underestimate Stress Concentration Factors. The corrosion resistance of TS590J2H is of essential importance in offshore applications. It was also shown that TS590J2H is sensitive to stress corrosion cracking in presence of cathodic polarisation. This susceptibility is higher for the weld metal than the base metal. The heat affected zone that arises during welding is also more susceptible to stress corrosion cracking than base metal but lower than weld metal. Nonetheless, its performance against corrosion is slightly better than S355J2 steel grade.

In welded tubular connections, failure usually occurs in the form of cracks at a discontinuity or stress raiser, associated with a microscopic defect at the weld toe. As a result, cracks under monotonic, low-cycle or high-cycle fatigue loading initiate at these locations irrespective of steel grade. Eurocode 1993 Part 1-8, Design Guides No. 1 [24] and 8 [25] present typical weld details at the main locations of welded tubular connections made of CHS. Nonetheless, additional information on weld details were needed and taken from the AWS Welding Code [26]. Weld start/stop positions for non-continuous welds should not be located at points of high stress concentration -crown and saddle points-, since these can cause themselves stress concentrations. Higher steel grades can be used to improve connections static strength, but they do not necessarily improve deformation capacity or high-cycle fatigue strength. Design provisions of EN 1993-1-8 (2002) [27] are identical to those proposed by Wardenier et al. [28] for ultimate resistance, and they are used for predicting the joint capacity under axial load or bending loading. Results of the present study have shown that static strength equations of the aforementioned specifications are adequate and that strength reduction factor equal to 0.8 for the HSS under exam with overmatching weldments suggested by EN 1993-1-12 (2009) [29] is unnecessary. With regard to high-cycle fatigue, Eurocode 1993 Part 1-9 [16] provisions for welded tubular joints adopt the “classification of details” method, which is not applicable to the majority of tubular X-joints. Therefore, hot spot stresses and stress concentration factors must be quantified. Various methods of improving the fatigue resistance of welded connections are available. Mechanical peening mainly introduces compression stresses in the weld toe to reduce tensile stresses effects. The peening treatment should be carried out in the inner part of tubes.

With regard to bolted connections subject to monotonic loadings, several methods were considered in order to estimate their plastic failure capacity. Predictions were always on the safe side and differences between predictions and experiments ranged between 4% and 40%. Predictions provided by Eurocode 1993 Part 1-8 were the most accurate ones. As far as high-cycle fatigue behaviour is concerned, it was shown that the use of Detail Category 11 of Table 8.5 in Eurocode 1993, part 1-9 overestimates fatigue strength, and therefore is unsafe. Nonetheless, the use of the hot-spot stress concept estimated through finite element analyses via the Dong’s method [21] allowed a safe prediction of the fatigue strength to be made, via a Detail Category 100. Moreover, stress concentration factors were estimated too. Initial deformation of flanges owing to heat effects during welding significantly influence the stress range both on tubes and flanges. Therefore in view of an economic design, initial deformations should be taken into account in FE models.

CHS tubes with nominal dimensions of 193.7mm in diameter and of 10mm in thickness were analysed. Considering actual mechanical properties of members -f_y = 694 MPa; D/t = 19.4- the relevant cross section was classified as Class 2 in accordance with EN 1993-1-1 [30], whilst considering its nominal strength f_y = 590 MPa a Class 1 section is obtained. Full-scale tests were performed with two different column lengths: i) short length -member slenderness 28.4- relevant to its cross sectional behaviour; ii) long length -member slenderness 74.6- relevant to member behaviour. Experimental data were compared with Eurocode 3 predictions in the N-M interaction diagram using both Method 1 -m1- and Method 2 -m2-. Experimental results are on the safe side of the interaction diagram indicating that recommended design formulae can be consistently extended to HSS members for the slenderness range investigated.

The Ponte del mare of Pescara redesigned with tubular sections offered us two possibilities for checks: on one hand both with identification and numerical data, we had the possibility to check and employ several indications provided by Eurocode 1993 Part 2 for steel decks and Eurocode 1991 Part 1-4 and Eurocode 1993 Part 3-1 for masts of Ponte del Mare with reference to along-wind and vortex-shedding wind loadings; on the other hand, we estimated the safety of footbridge decks by means of the calculation of the reliability index β -or the probability of failure P_f-, followed by a Bayesian updating technique. It can use both prior information and new inspection information to account for the relative uncertainty associated with each variable. In greater detail, assigned Weibull density probability functions for pedestrian loads and for wind loads -for corrosion rates of members Gaussian distributions were used-, we simulated the progressive reduction of painting effects and the concurrent increase of corrosion for a reference life time of 50 years. The probabilistic evaluation of the safety margin and reliability of the deck of the footbridge was conducted using non-linear simulations based on Monte Carlo Sampling (MCS). Although MCS is straightforward to apply, as it only requires repetitive executions of deterministic simulations, typically a large number of executions are needed, because solution statistics converge relatively slowly – for example the mean value typically converges as $\frac{1}{\sqrt{K}}$, where K is the number of realizations. So we have applied the Latin hypercube sampling to accelerate convergence of the brute-force MCS. Several limit states in terms of maximum strength, maximum deflection, and maximum deck rotations were considered. As a result, and with reference to the maximum deck rotation, the value of β crossed the limiting value at about 23 years and 33 years for the case without and with wind, respectively. This showed also that wind acted in the way to increase the reliability of the footbridge structure, owing to lifting effects. Moreover, the decision should be based on the critical case, i.e. the one without wind. Therefore, the repair and/or retrofit plan of footbridge decks should be activated by 23 years of lifetime in order to increase its reliability index.

WP8: Project coordination

The main objectives of WP8 were: a) to establish an efficient management process; b) to define standard protocols, c) to carry out the SWOT evaluation; d) the activity monitoring of the project. The main results of this work package are summarized here. They are also widely reported in Section WP8 of Description of Activities and Discussion, in Appendix H and relevant Deliverables D8.1 and D8.2 listed in the Amended Technical Annex. In greater detail, all coordination meetings were regularly carried out, the FTP server directory was created by UNILG and continuous exchanges favoured objectives and relevant project outcomes. Moreover, common standard testing protocols were very effective for assuring quality of test results. The evaluation of the project in terms of Strength, Weakness, Opportunity and Threat allowed a global evaluation of the research project both in terms of activity coordination and work effectiveness of each research unit. Finally, intermediate reports and set of deliverables enabled internal and external monitoring of the project advances, and of the degree of fulfillment of objectives set for various phases.

Conclusions and main results

New steel production processes have led to a remarkable improvement in steel products within the last few years, and now they allow steels to be produced according to desired mechanical and chemical properties. High Strength Steel (HSS) or High Performance Steel is the designation given to this new generation of steels that offer higher performance, especially in the case of tubular members produced for structural applications, not only in terms of strength but also toughness, weldability, cold formability and corrosion resistance, compared to the traditionally used mild steel grades. The development of HSS goes with today’s increased demand for slender lightweight structures, as for instance in footbridge and bridge design. However, on the structural engineering side there is a need for knowledge of these new steel grades combined to proper conceptual designs. Nonetheless quite often, recent design codes like Eurocode 3-1-12 do not provide sufficient information to fully exploit the advantageous properties of HSS. In this respect, the HITUBES project showed new conceptual designs and assessment procedures in order to make full use of HSS TS590 for onshore structures that employed tubes 355/12 with D/t > 29 and 193.7/10 with D/t > 19. In particular, we analysed in depth two specific structural types for which tubes could be suitable for architectural and aesthetic reasons: i) slender foot- and cycle-bridges; ii) arches and truss elements of railway bridges, under extreme natural and anthropic repeated loadings, some of which were measured in situ. Necessary tools were the use of tests at the material, member and connection level, in structural labs and both identification and monitoring in situ, of finite element-based tools, of reliability assessment of a realistic case study. The project reported relevant behaviour of members, welded and bolted connections under monotonic, low-cycle fatigue and high-cycle fatigue loading, weights reduction and reliability analysis results.

List of deliverables of the project:

Information about deliverables is listed in Table 1.

Table 1 List of deliverables

Deliverables and Milestones	**Due date**	**Finalisation date**	**Form**	**Location**	**Partner- in-charge**
D1 (D1.1, D1.2, D1.3, D1.4)	December 2008	March 2010	Mid-term report	CIRCA	KIMAB,ISQ, UNITN,UNITH
D2 (D2.1, D2.2)	December 2008	March 2010	Mid-term report	CIRCA	UNITN,UNILG, UNITH
D3 (D3.1)	March 2010	September 2011	Six-monthly report	CIRCA	KIMAB,ISQ, ITMA
D3 (D3.2, D3.3)	March 2010	March 2012	Deliverable report	CIRCA	CSM
D4 (D4.3)	September 2009	March 2011	Six-monthly report	CIRCA	UNITH,ISQ, ITMA
D4 (D4.1, D4.4)	March 2010	September 2011	Six-monthly report	CIRCA	ISQ,KIMAB, ITMA,UNILG
D4 (D4.2)	March 2010	March 2012	Deliverable report	CIRCA	UNITH
D5 (D5.1)	June 2010	September 2011	Six-monthly report	CIRCA	UNITH,UNILG
D5 (D5.2)	June 2010	March 2012	Deliverable report	CIRCA	UNITH
D5 (D5.3)	June 2010	September 2011	Six-monthly report	CIRCA	UNILG
D6 (D6.1, D6.2)	December 2010	March 2012	Deliverable report	CIRCA	CSM,UNITH, UNITN,UNILG
D6 (D6.3)	December 2010	September 2011	Six-monthly report	CIRCA	UNITN
D7 (D7.1, D7.2, D7.3)	December 2011	March 2012	Deliverable report	CIRCA	ITMA,KIMAB, CSM,ISQ,UNILG, UNTH,UNITN
D8 (D8.1, D8.2)	December 2009	March 2010	Mid-term report	CIRCA	UNITN

Scientific and technical description of the results

In the following main aims, activities and results of the project are described. Additional details are reported in the enclosed appendices.

Objectives of the project

High strength steel (HSS) has been available for many years. However, its use in onshore engineering is quite restrictive. One reason is that structural codes and Eurocodes have covered steels with yield strength up to 460MPa; the other reason is higher costs than regular steel. Nonetheless very recently, there has been a growing trend for the use of high strength steel in tubular structures thanks to Eurocode 3 Part 1-12 (2006) that has extended its scope to steel grades up to S690/S700MC.

The HITUBES project intends to develop performance-based designs and assessment procedures to make full use of HSS tubes up to S700MC for structures subjected also to extreme repeated loads; in fact Eurocode 3 Part 1-12 imposes many limitations at the material, structural and design level. The ambitious targets are to increase the performance of tubular structures, reduce weights, construction and operating costs.

In particular in order to achieve the above mentioned goal the work was mainly focussed on:
→ literature survey and selection of case studies;
→ selection of FE codes, simulations and investigations on case studies;
→ structural identification and monitoring of footbridges;
→ tests on HSS materials and welds also considering post-weld treatment;
→ tests on HSS tubular members and bolted and welded connections;
→ simulations on HSS tubular members and bolted and welded connections;
→ simulation on footbridges and fatigue check;
→ development of design guidelines;
→ standard protocols, SWOT analysis and monitoring of project activities.

Comparison of initially planned activities and work accomplished

The initial Technical Annex 1 was amended due to the difficulty in realizing the wind turbines of varying tubular sections. The aims and objectives of the project have been accomplished without any substantial changes from that mentioned in the Amended Technical Annex 1. A considerable number of tests have been performed allowing to cover the main aims of the project.
Some modifications to the testing program reported in the Technical Annex were agreed during the project, in Table 2 a comparison between the Technical Annex and actual testing program is reported:

Table 2 Testing program changes with respect to the Technical Annex

	Technical Annex	Actual testing program
Task 3.2	3 cyclic tests under axial and bending	5 full scale cyclic tests under bending (symmetric and asymmetric)
Task 3.3	9 cyclic tests under axial and bending	10 full scale monotonic tests under axial and bending

Description of activities and discussion

WP1: Review on test data and design procedures on tubular members and connections and Bayesian approaches for probabilistic risk assessment

Objectives of the WP1 (Tasks 1.1, 1.2 & 1.3)
Main aims of this work package were as follows:

- Collection and evaluation of test data and design procedures on tubular members relevant to the investigated structures
- Collection and evaluation of test data and design procedures on tubular joints under fatigue loading
- Corrosion aspects of HSS material
- Collection of literature on foot/cycle/rail/road bridges made of HSS and/or tubular sections
- Evaluation of Bayesian approaches for probabilistic reliability assessment
- Choice of output-only identification techniques

Activities and results obtained

Task 1.1: Collection and evaluation of experimental test data on tubular members and joints relevant to the investigated structures under extreme repeated loadings

Test data and design procedures on tubular members and joints under monotonic loading

The classification of cross sections is closely related to the ductility of the material, the ductility of the element section and local buckling phenomena. An important problem of HSS section, owing to the high yield strength, consists of respecting the classification limits imposed by Eurocode 3-1-1. The classification of cross sections is function of the factor $\varepsilon = \sqrt{235/f_y}$, so that HSS is penalized. In addition the classification is function of the D/t ratio that is often high with use of HSS sections. Several studies and tests have shown that the slenderness limits in EC3-1-1 are probably too conservative both for mild steel up to grade S460 and for HSS, and in particular for circular hollow section [31] [32].

The main actions of concern in this project in monotonic loading of tubular members are: (1) axial compression loading; and/or (2) bending moment loading. The design procedures on tubular members are given in EN 1993-1-1 [33], CIDECT No. 2 [34] and API PR 2A – LRFD [35]. Moreover, the design procedures on tubular joints under monotonic loading are given in EN 1993-1-8, CIDECT No.1 [24] and API PR 2A – LRFD [35]. Details can be found in *Appendix A*.

Task 1.2: Evaluation of design procedures and techniques for welded/bolted HSS members and joints for low-cycle and high-cycle fatigue

<u>Test data and design procedures on tubular members and joints under fatigue</u>

There are two methods for fatigue design of structural details: the classification method and the hot spot stress method. The design procedures on tubular joints under fatigue are given in EN 1993-1-9 [16], CIDECT No.8 [17] and API PR 2A – LRFD [35]. Details can be found in *Appendix A*.

<u>Corrosion aspects of HSS material</u>

The literature survey showed that there are a lot of corrosion and stress corrosion cracking studies related to the oil and gas industry where the pipelines are made of medium or high strength steels. However, there is limited information of the long-term use of high strength steels in sea water and under severe conditions where the structures are subjected.

The corrosion forms that has to be considered in offshore environments are; pitting and crevice corrosion and stress corrosion cracking (SCC). Similar to SCC is another common failure, the hydrogen related stress corrosion cracking, sometime also called hydrogen embrittlement. There are three conditions that are important for SCC and hydrogen embrittlement to occur; the material should be susceptible to these types of corrosion, the environment should be corrosive e.g. hydrogen containing environment, and there should be a sufficient stress intensity. In offshore environments, chloride, CO_2 and H_2S play an important role as well as hydrogen formed at cathodic protection for the corrosion process. Another important source of hydrogen is from welding if not sufficient care is taken.

Furthermore, the literature review showed that the materials resistance to hydrogen embrittlement depends strongly on the microstructure. The susceptibility for hydrogen embrittlement is ranked in the order: tempered martensitic < tempered bainite < spheroid ferrite and pearlite < coarse ferrite and pearlite. In some papers it is declared that the strength or hardness of specific steel usually can give a first indication of its hydrogen embrittlement susceptibility. However, in most cases all the parameters as environment, microstructure and the level of strength have a great influence of appearance of hydrogen embrittlement. It is also stated that it is of great importance that each steel quality should be considered individually and should be subjected for testing before being accepted for use, especially in critical conditions. Recommendations, given in the literature, to control the cracking are: (i) emphasis on material selection, for example by use of slow strain rate testing (SSRT); (ii) high control over welding procedures; (iii) avoidance of anaerobic condition (e.g. hydrogen evolution corrosion in the absence of oxygen); and (iv) limiting the potentials of cathodic protection to minimize the generation of hydrogen.

Task 1.3: Collection of literature on foot-cycle bridges. Evaluation of Bayesian approaches for time dependent formulations in order to perform probabilistic risk assessment and carry out fatigue reliability. Choice of output-only identification techniques.

<u>Collection of literature on bridges-</u> The collected bridges are organized with relevant information as follows:

Foot/cycle/rail/road bridges made of HSS and/or tubular sections:

i) Bridges made of tubular sections

- Forth Rail Bridge in Scotland
- Eads Bridge in St Louis (road and railway) USA
- Tempe town lake light rail bridge Tempe, Arizona, USA
- St. Kilian viaduct, Germany [36]: tubular trusses in deck, see Figure 1a
- St. Luitpold Bridge, Bamberg, Germany [36]: tubular arches, see Figure 1b
- Weil am Rhein footbridge, Germany, [36]: tubular arches
- Dattwill Bridge, Swiss [36]: tubular trusses in deck
- Nesenbachtal, Stuttgart, Germany [36]: tubular trusses
- Landegem railway bridge, Belgium: RHS arches
- Ponte del Mare foot-cycle-bridge, Pescara, Italy: tubular mast
- San-Michele footbridge, Trento, Italy: tubular arch with S460
- Nomi footbridge, Trento, Italy: tilted RHS arch

Figure 1 a) St. Kilian viaduct, Germany b) Luitpold bridge, Germany

ii) Bridges used high strength steel sections

- Verrieres Viaduct, France [37]: S460 in deck
- Prince Claus Bridge, Holland [37]: S460 ML in pylon
- Ilverich Bridge, Germany [37]: S460 TM in pylon
- Rion Antirion, Greece [37]: S460 TM in composite girder and pylon
- Millau Viaduct, France [37]: 40% steel used S460 TM in deck and pylon
- Jassanas-Riottier Bridge [37]: 20% steel used S460 TM in deck
- Garrigues viaduct [37]: S460 in deck
- Messina Bridge [38]: S420 and S460 at some length of deck, pylon
- Bayerstrasse, Munich, Germany [36]: S690 in tubular arches, see Figure 2

Figure 2 Bayerstrasse, Munich, Germany

iii) Bridges experienced extreme events

- Golden Gate Bridge, San Francisco: 112 km/hr wind in 1951
- London Millennium Bridge [39]: 7 cm deck vibration amplitude due to pedestrians in 2001
- Tsing Ma Bridge [40]: 28 m/s wind typhoon

Figure 3 Millennium bridge, London

<u>Bayesian approaches for probabilistic reliability assessment</u>

Structural aging may cause the integrity of structures to evolve over time (e.g., a hostile service environment may cause structural strength and stiffness to degrade). Uncertainties that complicate the evaluation of aging effects arise from a number of sources. Any evaluation of the reliability or safety margin of a structure during its service life must take into account the uncertainties. Time-dependent reliability analysis methods provide the framework for dealing with uncertainties in performing condition assessment of existing and aging structures, and for determining whether in-service inspection and maintenance is required to maintain their performance at the desired level [41]. Bayesian updating techniques are very useful when faced with two sets of uncertain information and a planner needs to know which to believe. Bayesian updating uses both the prior information and new inspection information to account for the relative uncertainty associated with each [42].

Several studies in the past mainly focused on reinforced concrete bridge superstructures, showed that the reliability of the bridge decks depends significantly on the rate of corrosion of the steel [42] [43] [44]. Monte Carlo simulation is an iterative simulation technique used to evaluate functions of random variables. For every simulation, each random variable is assigned a deterministic value based upon the descriptor parameters of the distribution and a random number generator. The function is evaluated using the input parameter values for every simulation. The results are then treated as a distribution, and the descriptor parameters are determined. Figure 4 shows an example of the original and updated reliability indices using Bayesian theory [45].

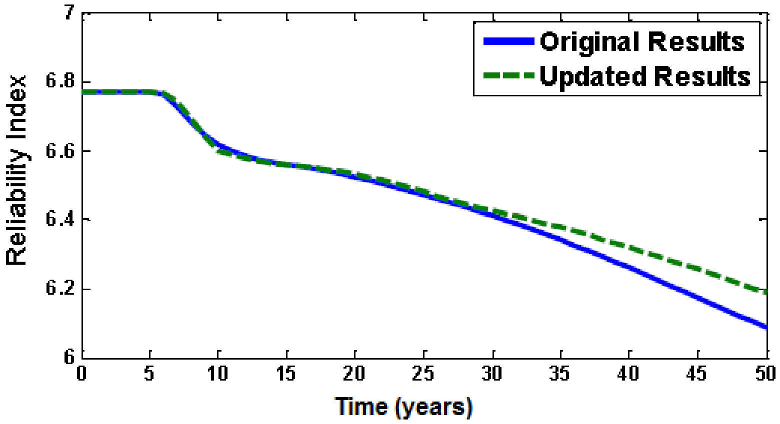

Figure 4 Original and updated reliability indices using Bayesian theory, after **[45]**

Output-only identification techniques

Output-only measurements present a challenge that requires the use of special modal identification technique, which can deal with very small magnitude of ambient vibration contaminated by noise. The following techniques are useful for the identification of structures such as footbridges:

- Peak Picking (PP) in frequency domain
- Stochastic Subspace Identification (SSI) in time domain
- Eigenvalue Realization Algorithm (ERA) in time domain
- Time-frequency (TF) instantaneous estimators

The SSI technique can detect frequencies that may possibly be missed by the PP method and gives a more reasonable mode shapes in most cases. To be able to trace non-linear phenomena that change with time, also short-time Fourier transform techniques can be used. The choice of a time-frequency (TF) technique is made because of its robustness, i.e. its capability to clearly identify: signal events which manifest during a short time interval (time localization); signal components which are concentrated at particular Fourier frequencies, such as sinusoids (frequency localization).

WP2: Extreme forces and stresses on foot- cycle-bridges, railway bridges and monitoring

Objectives of the WP2 (Tasks 2.1, 2.2, 2.3 & 2.4)

The main objectives of the WP 2 were to select the FE codes and to perform analyses on foot-cycle-bridge and railway bridge case studies to obtain the extreme forces and relevant stresses, to perform the system identification and structural health monitoring on footbridges.

Activities and results obtained

Task 2.1: Selection of MultiBody, Finite Element (FE) and identification codes

In order to re-design the “Ponte del mare” footbridge with circular hollow sections (CHS) and to evaluate both internal actions and stresses, the SAP 2000 [3] non-linear software code was chosen. Successively, in order to perform the FE analysis on the footbridge aiming at observing the effect of wind and pedestrians, the ANSYS-11 software (2008) [4] code was selected. This software was also used for the analysis of the “S. Michele” footbridge. In order to find modal parameters, i.e. natural frequencies, mode shapes and damping, the ARTeMIS-Extractor software code (2008) [5] and some in-house software developed by Politecnico of Torino was chosen. In order to perform the numerical simulation analysis on welded joints ABAQUS-STANDARD (2000) [6] software code was selected. In order to perform the numerical simulation analysis on flange bolted joints the LAGAMINE software code, developed by University of Liege (ULGG), was used.

Task 2.2: Evaluation of actions and stresses on foot-cycle bridges

In order to investigate and evaluate the implementation of HSS tubular members and connections under extreme loadings as well as to extract realistic specimens to be tested, the following two case studies were selected-

1. Footbridge “Ponte del Mare” Pescara, Italy, see Figure 5a ;
2. Landegem Railway Bridge, Belgium, see Figure 5b.

The footbridge is mainly subjected to the low cycle fatigue loading due to wind and pedestrians, whereas the railway bridge is subjected to the high cycle fatigue loading owing to the fast passage of trains.

Figure 5 a) The Footbridge “Ponte del Mare” in Pescara and b) Landegem railway bridge

The "Ponte del Mare" footbridge is located at the mouth of the Pescara river and is part of a programme for the rehabilitation of the urban area. The footbridge is a cable-stayed structure and it consists of two curved decks sustained by cables connected to a tilted mast, as illustrated in Figure 5a. The outer deck is dedicated to pedestrians, whilst the inner deck is for cyclists; both decks have constant radius, approximately 80 m and 100 m and their length is 173 m and 148 m, respectively. The two decks are constituted by a spatial steel-concrete composite truss connected to two prestressed concrete access ramps. The two sections of the bridge are reported in Figure 6. The tubular mast is made of steel filled with concrete and its inclination is about 11° with respect to the vertical axis. Two anchorage cables connect the top of the mast to the ground in order to reduce the displacements. In sum, the complexity of the structure is evident. Just note that the bottom chord of the foot-track deck (FTD) is in tension, whilst the chord of the cycle-track deck (CTD) is conversely in compression because of the eccentricity of the cable attachments and of the curve orientation with respect to the mast position.

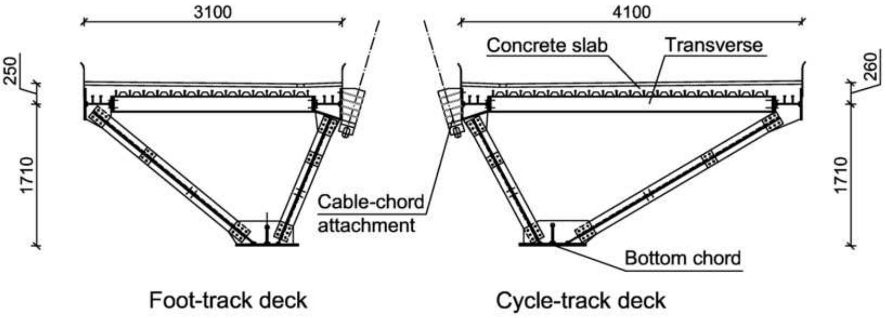

Figure 6 Sections of the two decks of the 'Ponte del Mare' footbridge

The footbridge was re-designed using the circular hollow sections made of HSS TS 590, see Figure 7. During the re-design of the bridge, the actions on the bridge structure were considered from the Eurocode 3, part 2 [46]. From the analysis it resulted that the possibility of exploitation of the high strength steel is remarkably limited from the problem of deformability of the structure. In summary, the employment of CHS provides the following advantages:

- More transparency of the bridge through the use of smaller sections with smaller inertia.
- Possibility to take away the hull, for aesthetic reasons, that covered the original deck of the bridge. This should also reduce aerodynamic problems; in fact the actual footbridge is endowed with elastic-viscous-fluid dampers connected through cables to the two decks in order to avoid flutter and galloping phenomena.
-The bridge entails a lower visual impact.
- A reduction of weight.

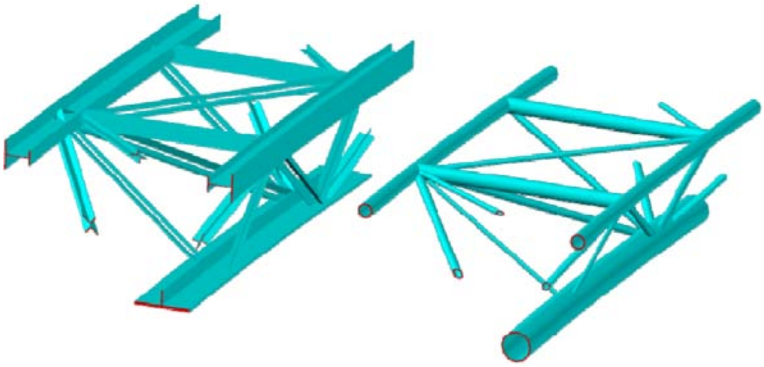

Figure 7 Deck with open and circular sections

Out of welded and bolted connections, welded joints are aesthetically more appealing for tubular sections, see Figure 8.

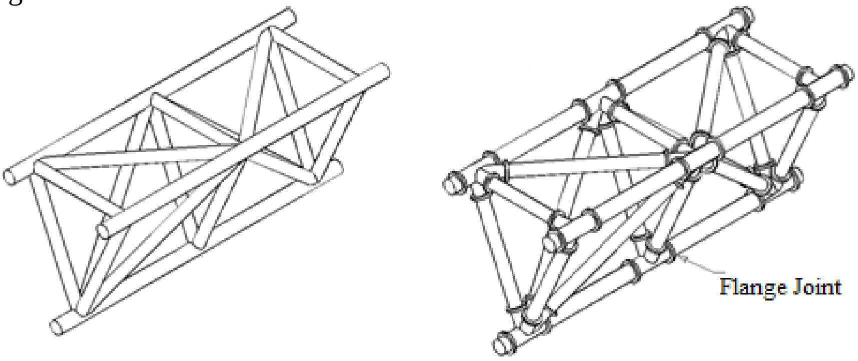

Figure 8 Welded and bolted connections for CHS sections of a deck

Cost analysis of the footbridge 'Ponte del Mare' of Pescara

Cost of the footbridge made with open sections is reported in the following Table 3.

Table 3 Major costs of the footbridge construction

	Component	Cost (Euro)
1	Piers, Deck, Cables, Mast	6300000
2	Metallic net	124000

3	Dampers	46000
4	Painting	121000

Cost of the decks made with open sections is reported in the following Table 4.

Table 4 Major costs of the footbridge decks and mast

	Component	Cost (Euro)
1	Material	620000
2	Production	450000
3	Bolts	115000
4	Transportation	82000
	Total deck cost	*1267000*
	Cost/ton	*2436.54*

Total steel needed= 520 ton
Reduction of cost after using the circular hollow sections (CHS)
Reduction in steel= 60.89 ton
Steel saving in percentage= 60.89/520= 11.7 per cent.
Cost of worked regular open section steel/ton= 2436.54 Euro/ton
Cost of worked CHS section steel/ton (15% higher) = 2436.54*1.15= 2802.02 Euro/ton
Reduction in steel cost w.r.t open section = 60.89*2436.54= 148360.83 Euro
Reduction in steel cost w.r.t CHS section = 60.89*2802.02= 170614.95 Euro

Net reduction due to worked steel= 148360.83-170614.95= -22254.12 Euro
Reduction in painting area/m= 35.8%
Reduction in painting cost= 121000*35.8%= 43318 Euro
Reduction in the cost of dampers (removed)= 46000 Euro
Reduction in the cost of the net (removed)= 124000 Euro

Total reduction = -22254.12+43318+46000+124000 = **191063.88** Euro

Therefore, the employment of CHS members in both decks provided a steel savings for the replacement of open sections with CHS of about 60.89 tons. The feasible cost savings relevant to decks was estimated to be 191063 Euro.

The footbridge was checked for fatigue due to wind and pedestrian loadings and it was satisfied. Simulations were performed in ANSYS on the finite element model of the footbridge shown in Figure 9.

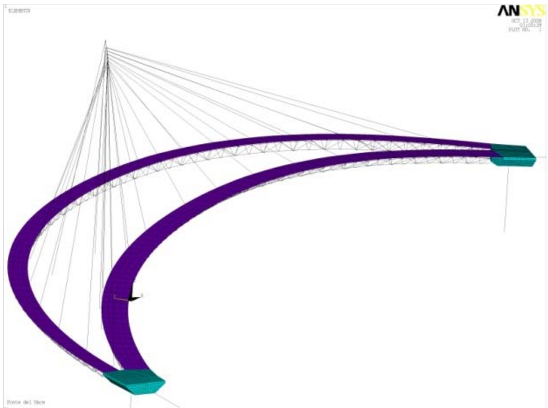

Figure 9 FE model of the footbridge ‘Ponte del Mare’ in ANSYS

A graphic representation of the stress history due to wind load at the most stressed detail is shown in Figure 10 for bottom chord. For the pedestrian load is shown in Figure 11.

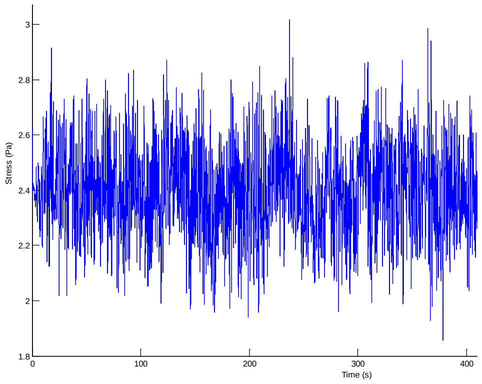

Figure 10 Stress (MPa) history of the most stressed structural element of the bottom chord

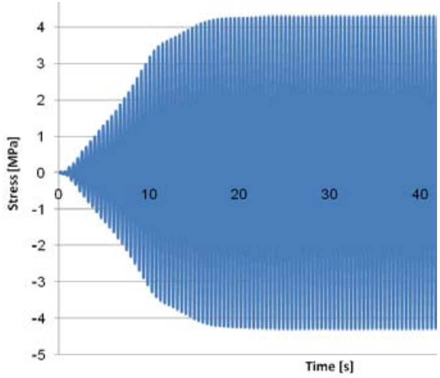

Figure 11 Stress (MPa) history of the most stressed structural element of bottom chord (mode 11 pedestrian deck)

Task 2.3: Redesign and analysis of the railway-bridge case study

Landegem Bridge (Figure 5b) built up in Landegem (Belgium) during 1980’s, is chosen as “case study 2” in the framework of the present project. This is a steel railway bridge designed by Greisch’s office [47] located in Liege (Belgium). The bowstring bridge is composed of an 86 meter long and 5.4 meter wide deck and 14.6 meter high twin arches (Figure 12). The load is directly applied on the deck, and transferred to the parabolic arches through the hangers. To ensure the transversal stability, the arches are joined by two transversal members. A rectangular hollow section was used for the arches and circular tubes were chosen for the hangers; the deck was fabricated from steel plates. Normal steels (AE235D and AE295D according to the Belgium national code at that time) were used for the bridge structure.

The scope of the study is to investigate the interest of using high strength steel (HSS) for components of such configuration of railway bridges, instead of using normal steel. As HITUBES project is dedicated to HSS circular tubes, the possibilities of using such HSS tubes for the arches and the hangers are examined in the present work. On the other hand, the deck is normally made of the steel plates; so, the possibilities for using HSS in this structural element is not considered herein (information on this last point can be found in literature, e.g. [48]).

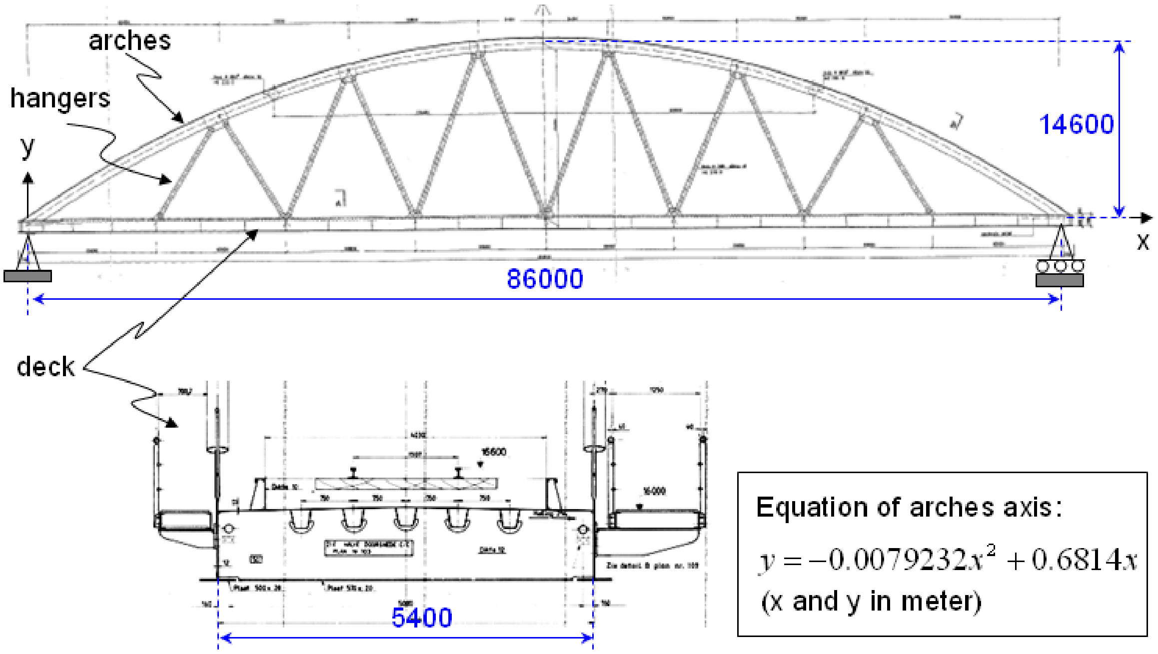

Equation of arches axis:

$$y = -0.0079232x^2 + 0.6814x$$

(x and y in meter)

Figure 12 Main dimensions and structural solution of Landegem bridge

As mentioned previously, the main objective is to compare the interest of using HSS in railway bridges (in comparison with normal steel). In order to make the comparison, optimal designs with the cost as objective function had to be performed for solutions using normal steels and HSS for the arches and the hangers. For the design, the safety requirements related to local buckling, member buckling and fatigue resistance were taken into account. The outside diameter (D) and the thickness (t) of the tubes were considered as variables (unknowns) to be optimised. By the way, the optimization problem can be mathematically written under the form:

$$\text{Find} \quad x=[D,t] \quad \text{such that} \quad \mathrm{C(x)} \rightarrow \min, \quad \text{but} \quad g_j(x) \le 0,\ j=1 \div n,$$

where C(**x**) is the cost function; $g_j(x)$ are the safety requirements. The detail description of the optimal problem can be found in Appendix B. Some main remarks are reported here below:

- The same cross-section is used all along the arches and all the hangers use the same section.

- The internal forces in the arches and in the hangers are assumed to be constant during the optimization procedure. The imprecision due to this assumption are negligible as the redistribution of internal forces associated to a modification of component rigidities is not significant. The axial forces and the bending moments in the arches and the hangers given in the computation note from Greisch's office [47] are used; the main values can be found in Appendix B.

- The steel grade S355 is considered as "normal" steel, while the steel grades TS500, TS550, TS620 and TS690 will be considered for the HSS (yielding strength of 500 N/mm^2, 550 N/ mm^2, 620 N/ mm^2 and 690 N/ mm^2 respectively).

- Eurocode 3, part 1-1 [33] rules are adopted for checking the resistance of the arches and the hangers. For the tubes, Section of class 1, 2 and 3 are considered while class 4 cross-sections are not dealt with. Eurocode 3, part 1-9 [16] rules are applied for the fatigue calculations.

- For the fatigue checks, the detail category 90 (detail number 4 in Table 8.6 of Reference [16]) is used for the arches in the case of normal steel (S355). For the fatigue resistance of HSS, another approach will be used. The admissible stress range will be varied from 90 N/mm² to 220 N/mm² in order to see if, with an improvement of the fatigue resistance using HSS, more economical solutions can be obtained.

- After having the optimal solution for each steel grade with each stress range, the comparison procedure on the weight and on the cost is carried out. The obtained results and discussions are summarized in the next section.

Results and discussions

With respect to the arches

In the case of S355 steel, yield strength of 355 N/mm^2 and the admissible stress range of 90 N/mm^2, an optimal section has been found: D=124.8 cm, t=2.09 cm, area= 807.5 cm^2 for a total weight for the two arches of 117 t. By varying the admissible stress ranges from 90 N/ mm^2 to 220 N/ mm^2, optimal sections for the arches using HSS are also obtained, and the corresponding weights are compared with the one of S355, as presented in Figure 13a. Using the steel prices (per tonne) presented in [7], the ratio of the arches cost using HSS to the arches cost using S355 can be obtained (Figure 13b) (in [7], in comparison with S355, the prices of TS500, TS550, TS620 and TS690 increase of 14%, 26%, 34% and 38%, respectively).

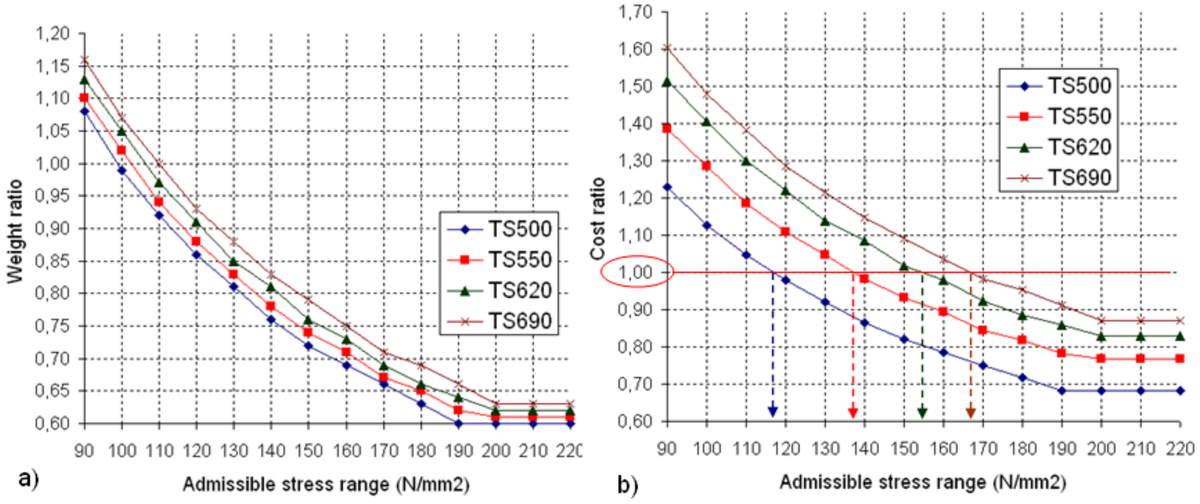

Figure 13 Comparison between HSS and S355 for the arches

Some remarks can be drawn:

- The weight decreases when the admissible stress range increases, which means that the fatigue requirement is decisive. For admissible stress range higher than 190 N/mm2, the weight remains constant demonstrating that the resistance conditions become decisive.
- With an admissible stress range of 90 N/mm^2 (as recommended in the Eurocodes for the considered detail), there is no interest of using HSS instead of S355.
- If the admissible stress range can exceed a value of about 120 N/ mm^2, the use of HSS could have an economical interest (depending of the material price). If the steel price proposed in [7] is used, the TS 500, TS 550, TS 620 and TS690 give an economical interest for stress ranges of 117 N/ mm^2, 137 N/ mm^2, 155N/mm^2 and 167 N/mm^2, respectively (Figure 13b).

In the framework of the present project, fatigue tests on TS590 tubes were performed. If the characterised admissible stress range of 126 N/mm² is used for TS590 (see Table 17 in WP4), the optimal section of the arches is: D=90.4 cm, t=2.5 cm, area=696.3 cm^2, leading to a total weight for the two arches of 100.8 tonnes. If compared to the 117 t for the S355 arches, the weight ratio is 0.86, meaning that TS590 is economically interesting if its price doesn't exceed 116% of the S355 one.

With respect to the hangers

There is no interest in using HSS for the hangers structural elements, even if the admissible stress range increases until 300 N/ mm^2.

According to the presented investigations, it has been demonstrated that, for the considered railway bridge, there is no interest in using HSS, if the rules as presently given in the Eurocodes have to be respected. However, if an improvement for the fatigue resistance can be demonstrated (see Table 17 in WP4), some interests in using HSS for the arches may be benefited. Accordingly, more investigations on the fatigue resistance of tubes made of HSS should be performed to confirm these observations.

Task 2.4: Structural identification and condition monitoring of two foot-cycle bridges

Structural identification of the 'Ponte del Mare' footbridge

The complex dynamic behavior and the uncertainties related to the numerical modeling led to a modal testing campaign of the bridge without and with dampers in two phases in the month of October and December 2009. The positioning of the sensors was decided from the modal analyses of the FE model. A typical record of the acceleration data is shown in Figure 14.

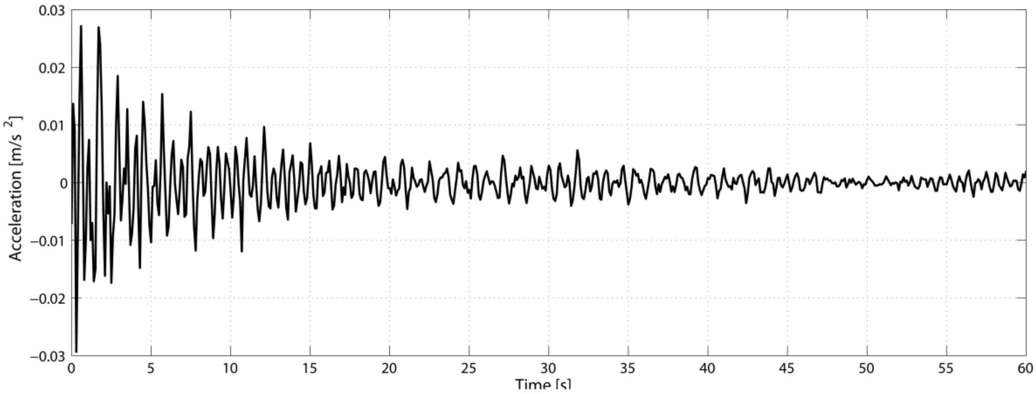

Figure 14 Vertical acceleration time-history associated to free vibrations

The identified frequencies and damping evaluated by different techniques are reported in Figure 15 and Figure 16, respectively. Moreover, Figure 17 shows 3-D graphical view of the first mode shape. This part is more described in *Appendix B*. Moreover, the results related to the identification of cables, damper behaviour and pedestrian excitation are reported in *Appendix B.*

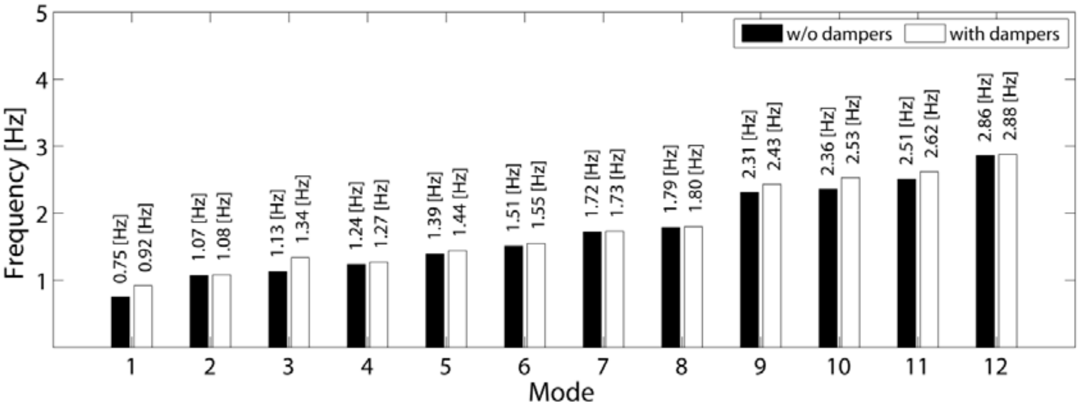

Figure 15 Identified modal frequencies w/o and with dampers

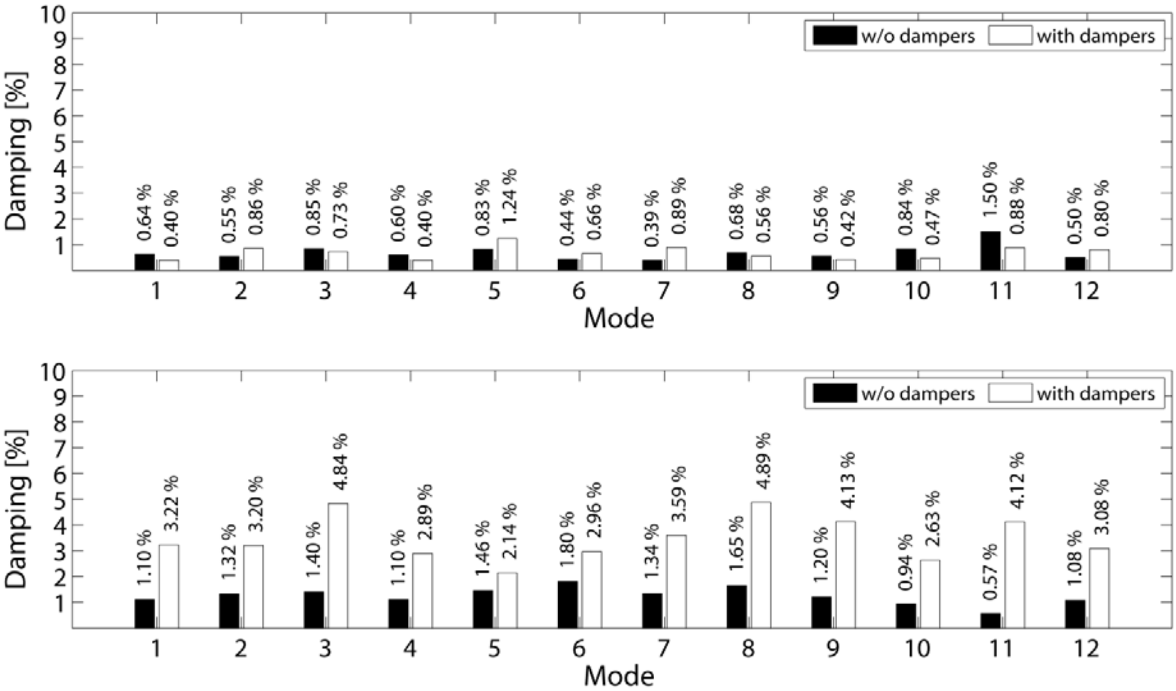

Figure 16 Modal damping estimates: above) ambient vibration data (from SSI method); below) free decay data (from ERA)

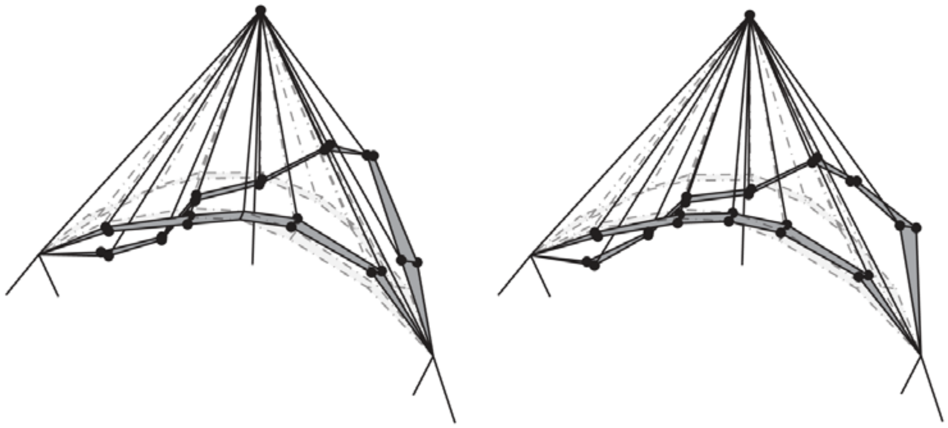

Mode 1 w/o dampers – f = 0.75 Hz Mode 1 with dampers – f = 0.92 Hz

Figure 17 3D views of the first identified mode w/o and with dampers

<u>Monitoring on site of the “Ponte del Mare” footbridge</u>

In order to know the response of the structure during use, the ‘Ponte del Mare’ footbridge was monitored during Dec 2009- Dec 2010, i.e. for about one year.

The whole monitoring system, as shown in Figure 18, is composed of 8 accelerometers, 4 thermo-resistances and 2 anemometers. Each of the anemometers gives two kinds of acquisition, that is, the wind speed and the wind direction. Three kinds of data are being acquired- continuous acquisition, at a fixed time every day and at the commencement of trigger events. A trigger event is defined for the wind and pedestrian actions according to the Table 5 and Table 6 respectively.

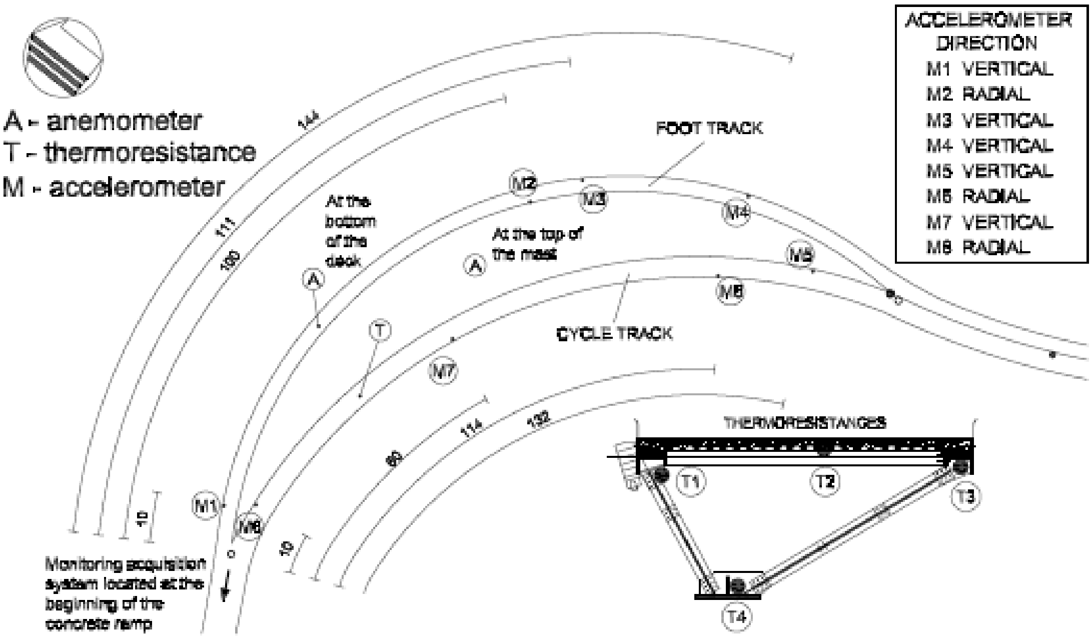

Figure 18 Monitoring system

Table 5 ULS and SLS for the design wind

Limit State	Return Period	Wind Direction	Wind Speed
SLS	1 Year	Sea to Earth	25.12 m/s
SLS		Earth to Sea	20.25 m/s
ULS (static)	50 Year	Sea to Earth	33.5 m/s
ULS (static)		Earth to Sea	27 m/s
ULS (dynamic)	500 Year	Sea to Earth	40.4 m/s
ULS (dynamic)		Earth to Sea	32.6 m/s

Table 6 SLS for the design pedestrian

Vertical Direction	0.7 m/s^2 (for 400 persons on the each deck- crowd density- 0.8 p/s^2)
Horizontal (Lateral) Direction	0.4 m/s^2 (for 400 persons on the each deck- crowd density- 0.8 p/s^2) 0.2 m/s^2 (for 200 persons on the bridge)

Figure 19, Figure 20 and Figure 21 show the time variation of wind speed, direction and temperature for the week 36 of the year 2010. It can be noticed that the anemometer at the mast approaches to the wind speed about 25.3 m/s and direction 200 degrees (from north direction) on 29 Aug 2010. This wind speed approaches to that of the design serviceability limit state (SLS) for 1 year return period, i.e. 25.12 m/s, see Table 5. Moreover, it should be noted that on the Christmas day (25/12/2009), there was a large wind trigger with a wind speed of 28.02 m/s. Please see Table 33 and Table 34 for the mean, minimum and maximum values of temperature and wind velocity for each months of the year 2010 in *Appendix B.*

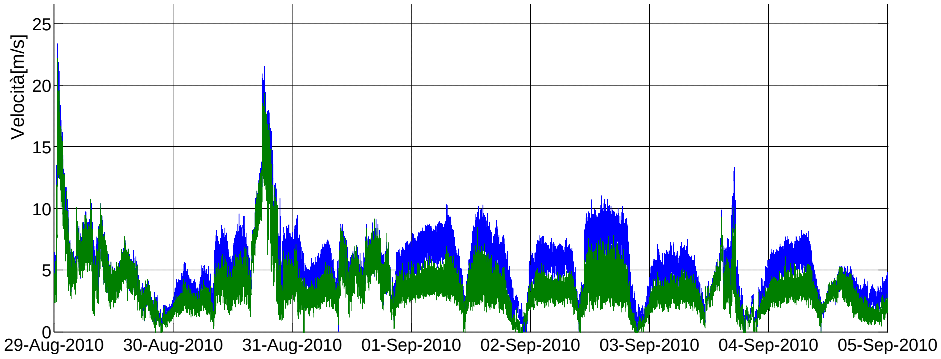

Figure 19 Wind speed-Week 36/2010

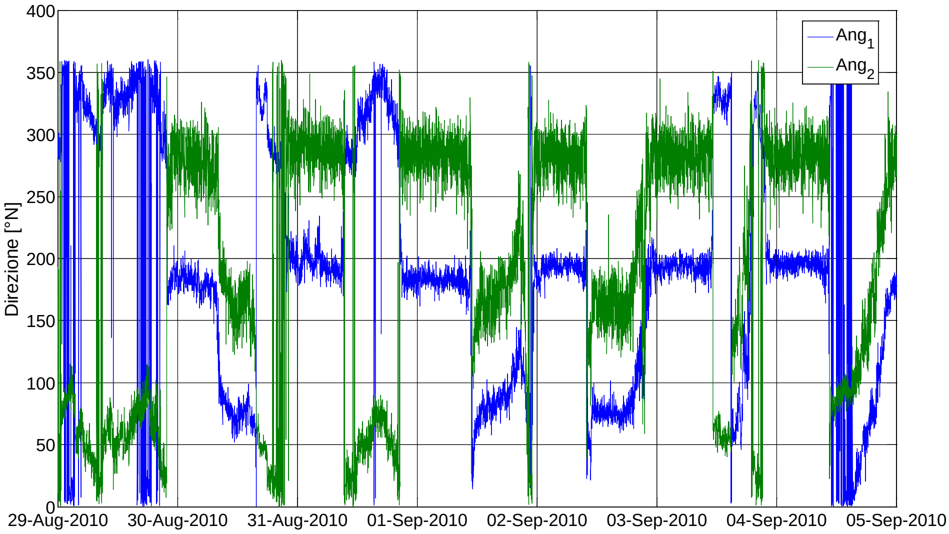

Figure 20 Wind direction- Week 36/2010

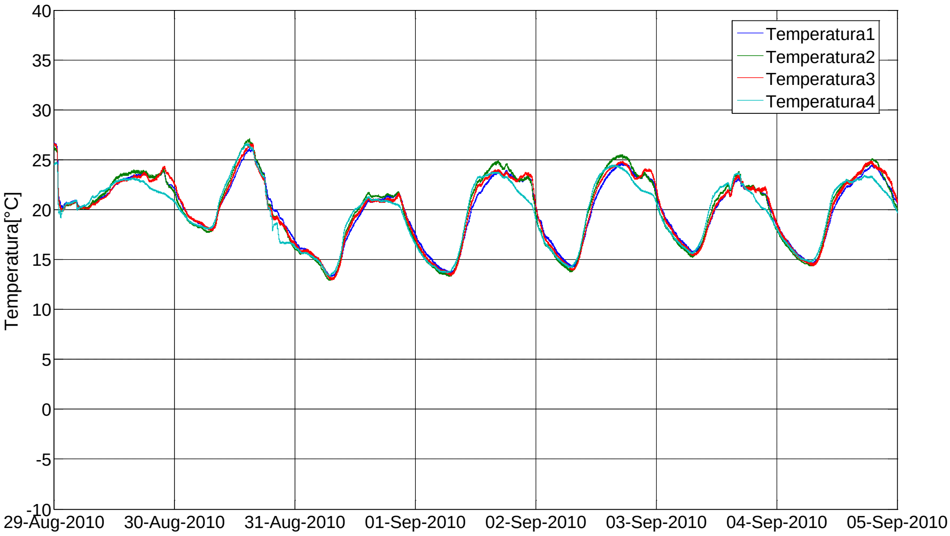

Figure 21 Temperature variation during 29 Aug-05 Sep 2010

The structural health monitoring was operational on the footbridge during Dec 2009- Dec 2010, i.e. for one year. The maximum wind speed of 28.02 m/s was recorded at the mast. The maximum acceleration reached up to 0.703 m/s^2 above the comfort level of pedestrians. After the FFT analysis and investigations, it was found that there was a running competition on 17 Oct 2010 that led to this peak acceleration level. Several normal pedestrian activities like walking, running and jumping were detected on other days too. Channels 4 and 7 were subject to the maximum number of triggers as well as most of the triggers occurred on weekends and at evening. It was also derived that the footbridge resulted to be more sensitive to pedestrian-induced excitations than to that of wind.

Identification and monitoring of S. Michele footbridge

S. Michele footbridge is situated in the town of San Michele in the province of Trento, Italy, see Figure 22a. FE model is shown in Figure 22b. Structural identification tests were performed on the footbridge to identify the modal properties such as natural frequencies, mode shapes and damping of the structure.

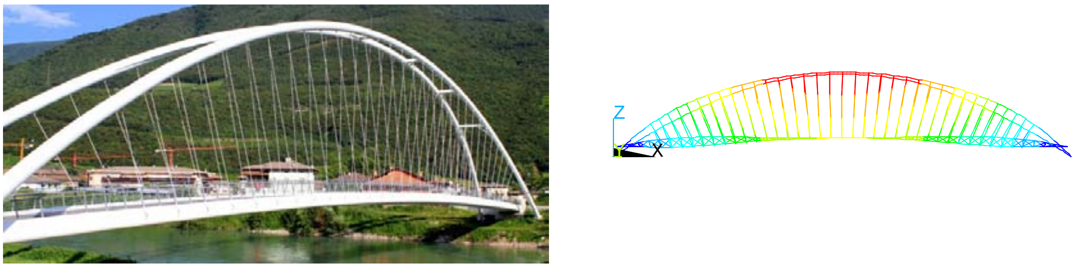

Figure 22 a) Footbridge of 'S. Michele' and b) FE model in ANSYS

Three types of excitations were used- released mass of 27.5 kN weight, impact hammer and ambient vibration. A total number of 23 accelerometers were employed to capture the response of the structure. Figure 23 shows a typical recorded acceleration data.

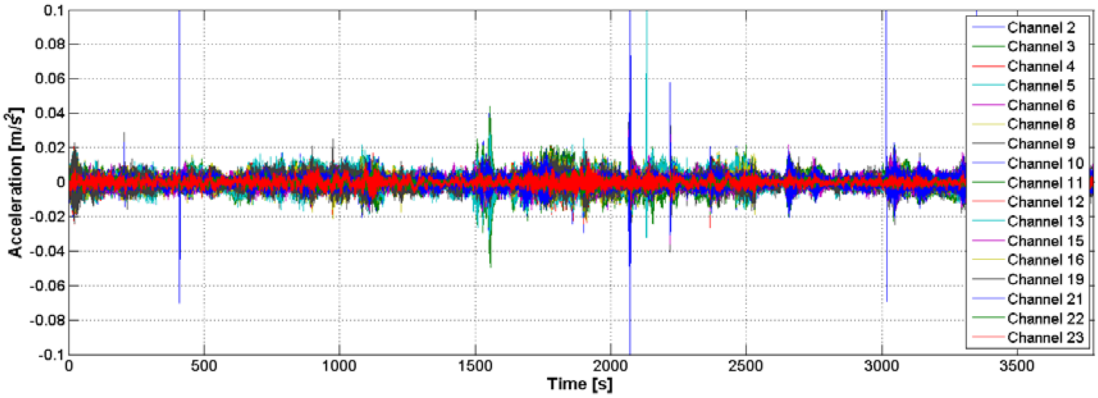

Figure 23 Acceleration signals captured in 23 channels

The Welch transform was used to identify the frequencies from the test data. The identified frequencies can be seen in Table 7.

Table 7 Identified modal frequencies

Mode [n°]	**Frequency [Hz]**	**Period [s]**
1	0.66	1.515
2	0.88	1.136
3	1.13	0.885
4	1.37	0.730
5	1.41	0.709
6	1.88	0.532
7	2.46	0.407
8	2.71	0.369

Several modern footbridges have shown the phenomenon of vibration induced by pedestrians. The vibration levels reach above the comfort level of pedestrians. Therefore, it is advised to monitor the footbridge after its construction.

In this regard, the monitoring tests were performed on S. Michele footbridge. Pedestrians were allowed to walk in a group of 11 at a known walking frequency produced by a metronome. The following frequencies were considered.

Table 8 Frequencies considered for the monitoring

Mode	**Component**	**Frequency**	**Walking Frequency**
2	Horizontal	0.90 Hz	1.80 Hz
3	Horizontal	1.21 Hz	2.42 Hz
7	Vertical	2.42 Hz	2.42 Hz

A typical record of the data and its FFT are shown in Figure 24a and Figure 24b, respectively. Here, one can notice that the main frequency is about f=1.84 Hz and other frequencies are an integral multiple (2f, 3f, 4f, 5f, etc.) of this frequency.

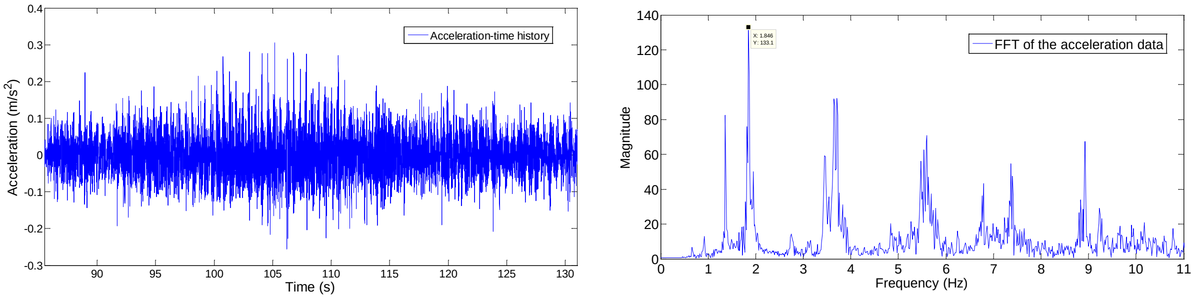

Figure 24 (a) Acceleration data recorded during monitoring of pedestrians; (b) FFT of the data

The footbridge frequencies and damping were identified. Moreover, the bridge was monitored for some pedestrian excitations. It was found that the acceleration obtained at each channel was within the maximum comfort range of pedestrians.

WP3: Inelastic behaviour and buckling performance of HSS tubular members

Objectives of the WP3 (Tasks 3.1, 3.2 & 3.3)

The main objectives of WP 3 are the mechanical characterization of HSS base material, the evaluation of the inelastic cyclic flexural behavior of HSS tubes and the evaluation of the buckling performance of HSS tubes. In order to facilitate the test program understanding, the number of tests performed for each task and partner is presented in Table 9 and relevant sketches of specimens are shown in Figure 25.

Table 9 Number of tests performed per partner and per Work Task

	KIMAB	**ISQ**	**ITMA**	**UTHESSA**	**CSM**	**ULGG**	**Total**
Task 3.1	30	25	18				**73**
Task 3.2					3 (+2)*		**3(+2)***
Task 3.3					9 (+1)*		**9(+1)***
Task 4.1	30	30	52				**112**
Task 4.2				10			**10**
Task 4.3			2				**2**
Task 4.4						6	**6**
Total	**60**	**55**	**72**	**10**	**12(+3)**	**6**	

*Note. Due to premature failure of 193.7x10 mm tube, some of these tests were performed with 323x10mm and 355x12mm tubes.

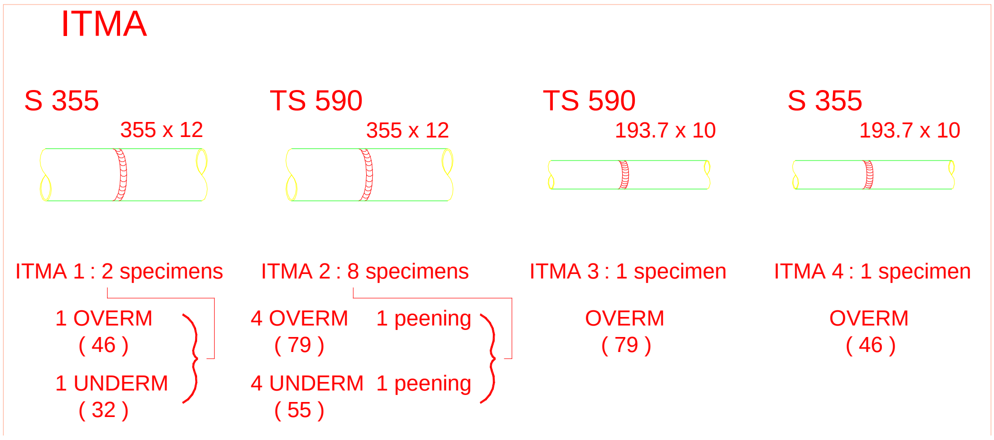

CSM

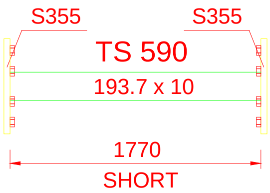

CSM 1*: 5 specimens

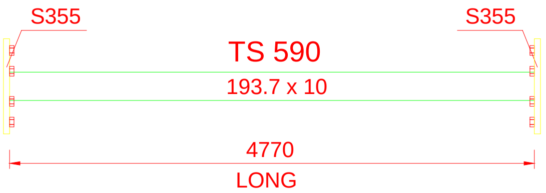

CSM 2*: 9 specimens

* UNDERM to TUBE & OVERM to PLATE (46)

ISQ

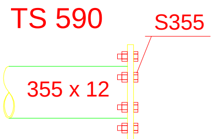

ISQ 1 : 1 specimen

UNDERM to TUBE
OVERM to PLATE
(46)

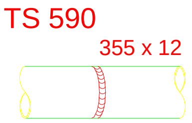

ISQ 2 : 4 specimens

2 OVERM
(79)

2 UNDERM
(55)

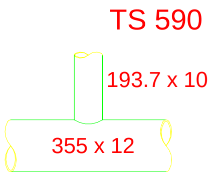

ISQ 3 : 1 specimen

OVERM
(79)

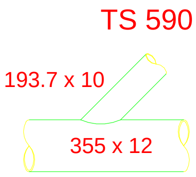

ISQ 4 : 1 specimen

OVERM
(79)

KIMAB

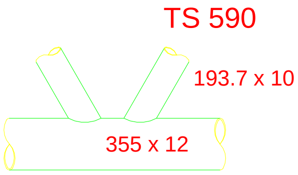

KIMAB 1 : 1 specimen

OVERM
(79)

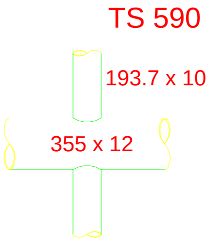

KIMAB 2 : 1 specimen
OVERM (79)

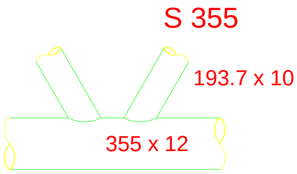

KIMAB 3 : 1 specimen

OVERM
(46)

*

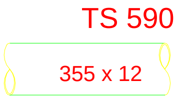

120 mm

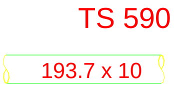

120 mm

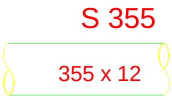

120 mm

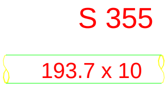

120 mm

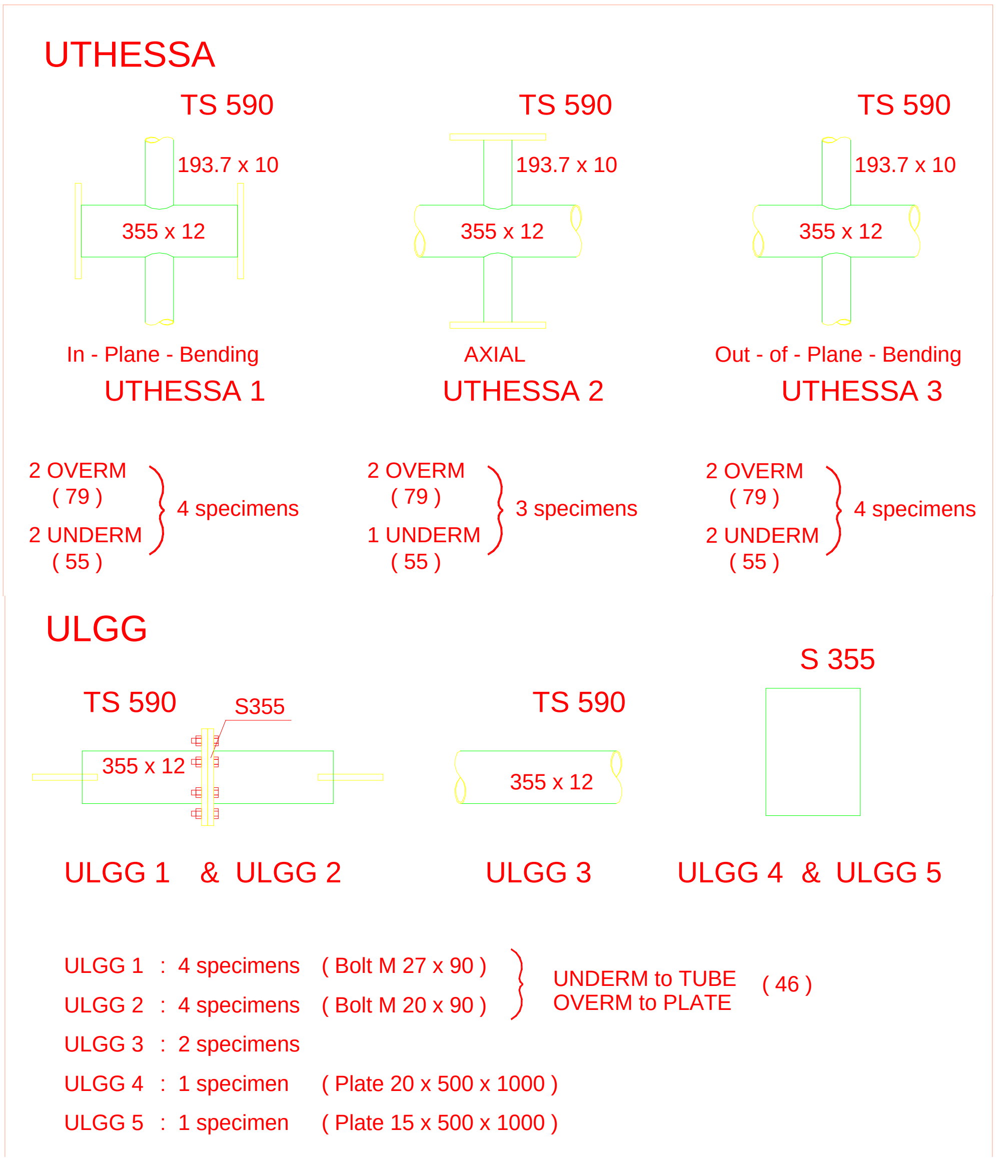

Figure 25 Sketch of specimens for different partners

Activities and results obtained

Activities and results are reported on a Task per Task basis for WP3 as follows.

Task 3.1 - Mechanical characterization of HSS and toughness also considering a corrosive environment

Tensile tests on HSS material

Tensile tests were performed on the coupon specimens extracted from 193.7x10 tubes. The mean yield strength is 694 MPa and ductility 19.67%, see Table 10. Moreover, the mean yield strength and tensile strength of specimens from 355.6x12.5 tube resulted to be 756 MPa and 817 MPa, respectively.

Table 10 Tensile test results on TS590 HSS material

No. of samples	YS [MPa]	TS [MPa]	Elongation [%]
1	621	706	22
1	616	702	22.1
1	704	778	19.2
1	741	807	17.7
1	765	822	20
1	717	783	18.8

Mean	**694**	**766.33**	**19.67**

Corrosion rate measurements and Slow Strain Rate Tests (SSRT)

Corrosion rate measurements and slow strain rate tests (SSRT) were performed on two different materials, TS590 and S355.Uniform corrosion rate of the base metal was measured in two different solutions, 1 wt% and 3.5 wt% NaCl, in order to simulate the offshore and seawater environments, respectively. The tests were carried out at ambient temperature. The linear polarization resistance technique, based on the change in potential and record of the polarization was used to measure the corrosion rate.

The SSRT testing was performed in order to evaluate the susceptibility of materials towards stress corrosion cracking and hydrogen embrittlement. The tests were performed in air, 1 wt% and 3.5 wt% NaCl solutions at ambient temperature. A strain rate of 10^{-6} s^{-1} was applied throughout the experiments. In order to simulate cathodic protection, cathodic polarisation with the magnitude of 40 mA was applied throughout the test of some of the samples in order to enable diffusion of hydrogen into the specimens. The elongation EL%, yield stress (YS) and ultimate tensile strength (UTS) were calculated from the stress vs. strain curves. The time to failure (TTF) was determined during the SSRT. Furthermore the Reduction of Area, (RA) (%) was measured on the samples after cracking.

The average of the corrosion rates are presented in Figure 26a. The corrosion rates of TS590 are slightly lower compared to S355 in all tested environmental conditions.

The reduction in area determined by the SSRT measurement is presented in Figure 26b. The RA determinations show a drastically lower RA for material TS590 with application of cathodic polarization. The measurement in 1 wt% NaCl with applied cathodic polarisation of 4 mA/cm², showed that TS590 had a lower RA than S355. Measurements in air and in 3.5 wt% NaCl without cathodic polarization gave no significant difference in RA for TS590 and S355.

- The electrochemical general corrosion rate measurements showed that steel TS590 had the same corrosion resistance or slightly better than the reference material S355.
- The SSRT-measurements showed that TS590 and S355 were sensitive towards stress corrosion cracking in presence of cathodic polarisation.

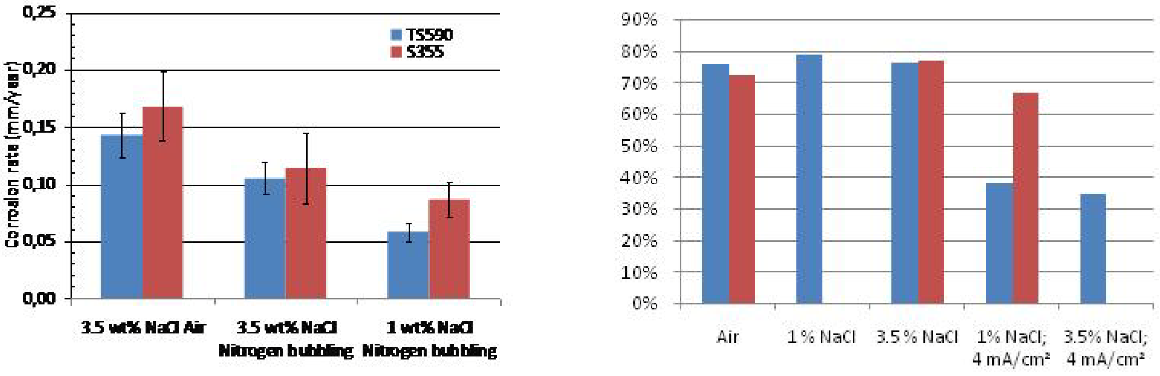

Figure 26 a) Corrosion rate of base metal of TS590 and S355 in various corrosive environments; b) Reduction in area, RA%, for base metal of TS590 and S355 in various corrosive environments with and without cathodic polarization

High-cycle Fatigue strength on base material

The fatigue characterization has been performed by means of the determination of an entire S-N curve. A set of ten specimens for the base material TS590 and a set of twelve specimens for the base material S355 were extracted from the tubes with an outer diameter of 355 mm and a thickness of 12 mm. Cylindrical specimens of 6mm of diameter in the minimum section and a shape with continuous radius between ends were machined following the requirements of the fatigue ASTM standard [8]. A complete S-N curve was constructed by means of the results of axial fatigue tests to the specimens with a load ratio of R=0.1. The points were fitted to a potential regression. The curve (Δσ – Log N) is depicted in Figure 27. The fatigue limit (stress level for 2×10^6 cycles) has been calculated for each base material. The fatigue limit values are 432 MPa and 690 MPa for the S355 and TS590 base materials respectively. The fatigue limit to tensile strength ratio is 0.82 for the TS590 material and 0.73 for the S355 base material, see Table 11.

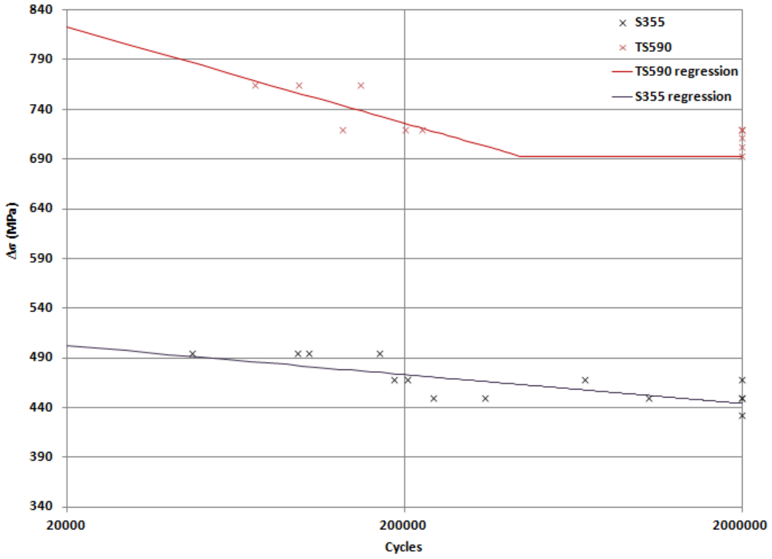

Figure 27 S-N curves of the base material S355 and TS590

Table 11 Fatigue limit and fatigue to tensile ratio

Base Material	Fatigue limit $\Delta\sigma$ (2×10^6 cycles) [MPa]	Tensile Strength [MPa]	Fatigue limit to Tensile strength ratio
S355	432	590	0.73
TS590	690	840	0.82

Fracture toughness

The fracture toughness characterization has been performed by means of the determination of the J-R curve of each base material. The specimens were extracted from the tubes with an outer diameter of 355 mm and a thickness of 12 mm. The dimensions of the specimens were 11x11x60 mm, having a standard notch from the inner side of the tube. The test procedure followed the requirements of the ASTM standard [9]. The tests were performed at ambient temperature. In *Appendix C* the mean J-R curve of three tests has been depicted and the value for the intersection of this curve with the 0.2 mm blunting line is shown. This value, that represents the energy for the onset of the stable crack growth, has resulted in 620 kJ/m^2 for the S355 and 440 kJ/m^2 for the TS590.

Task 3.2: Moment-curvature tests under flexural and axial loads in order to evaluate the inelastic cyclic flexural behaviour of HSS tubes

Five full scale bending cyclic tests have been performed on three (3) different CHS columns as reported in Table 12. The specimens have all the same length equal to 4850 mm; they are delivered with welded flanges so as to allow the connection to the testing machine. Dedicated testing grips have been designed and fabricated for this purpose. Tests have been performed under rotation control applying reverse bending load conditions. In particular two different load scenarios have been applied:

1. symmetric cyclic bending test: rotation-controlled load between + 8.5° and - 8.5° constant rotation rate of 0.1°/sec up to failure;
2. non-symmetric cyclic bending test: non-symmetric rotation-controlled load scenario between + 8.5° and - 6° at constant rotation rate of 0.1°/sec up to failure.

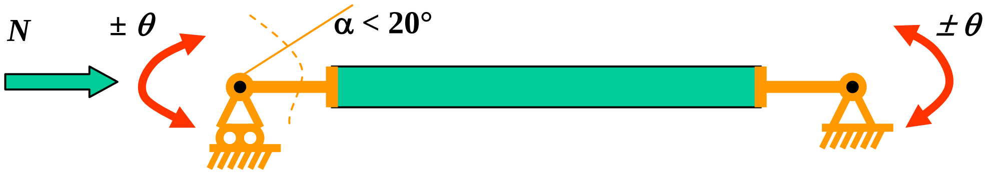

Figure 28 Full scale cyclic column tests- boundary condition and load configuration

Table 12 Full scale cyclic tests: testing program and specimens dimensions

Load scenario	ID	Diameter D [mm]	Thickness t [mm]	D/t	Nominal S590 Class	Actual S690 Class	Slenderness	θ range [degrees]
Symmetric cyclic bending test	Al-c1	355	12	29.6	3	3	40	(+ 8.5°; - 8.5°)
	Bl-c1	323.9	10	32.4	3	4	44	(+ 8.5° ; - 8.5°)
	Cl-c0	193.7	10	19.4	1	2	75	(+ 9.5° ; - 9.5°)
Non-symmetric cyclic bending test	Al-c2	355	12	29.6	3	3	40	(+ 8.5° ; - 6°)
	Bl-c2	323.9	10	32.4	3	4	44	(+ 8.5° ; - 6°)

Geometrical measurements and instrumentation can be found in *Appendix C.* Moreover, experimental results are reported in the following Table 13.

Table 13. Full scale cyclic tests results

ID	Description	Pictures
Al-c1	At the beginning of cycle 20th specimen failed. A crack starting from the base column stiffeners was detected. Some very light bulging is also observed at pipe ends, indicating plastic strain accumulation in those positions. The central section did not show significant ratcheting or ovalization. Recorded cycles are stable during all sequence.	
Bl-c1	At the beginning of cycle 11th the specimen buckled close to a column end. Trough wall crack also started to develop at the base column stiffeners but failure mode was actually buckling. Ovalization evolution measurements are available.	
Al-c2	Nr. 4 extra strain gages are placed close to the pipe ends. At 15th cycle severe cracking was observed. No buckling has been observed while a certain ovalization was measured.	
Bl-c2	From 5th cycle some cracks start to develop at the base column stiffeners. The test is finished at the 12th cycle when buckling occurred at one column end.	

Cl-c0	A tentative test was performed in the rotation range of (+ 9.2°; - 9.2°). Since it was not possible to reach stable cycles the test was interrupted. No Buckling was observed.	

The moment vs. rotation diagram and ovalization evolution of B1-c1 cyclic test is shown in Figure 29 and Figure 30, respectively. Moreover, additional results are presented in *Appendix C*.

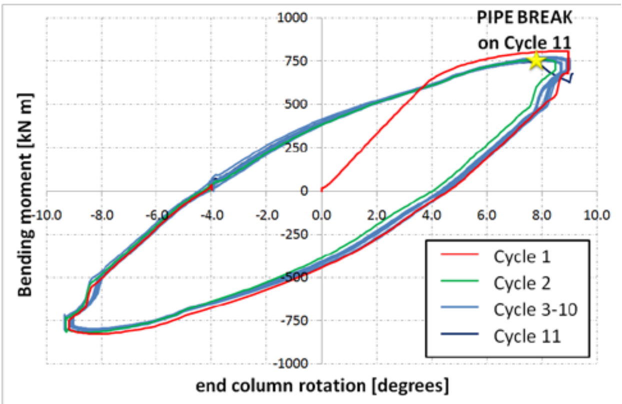

Figure 29 Full scale cyclic tests Bl-c1: bending moment vs. end column rotation records

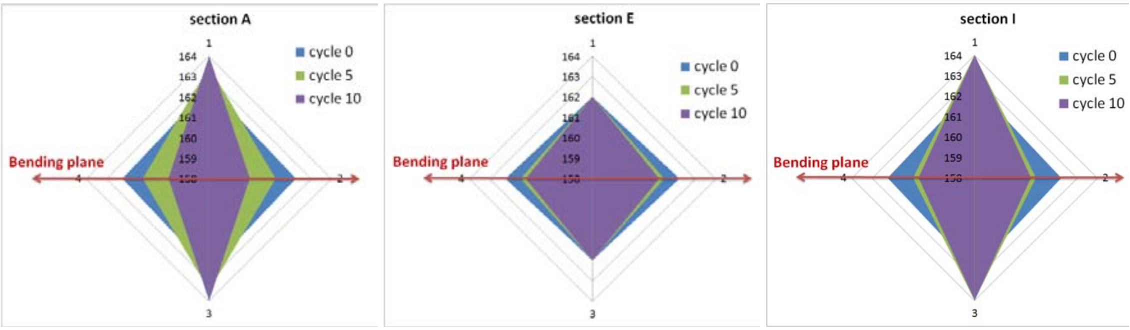

Figure 30 Full scale cyclic tests Bl-c1: ovalization evolution measurements

Task 3.3: Axial and bending tests in order to evaluate the buckling performance of tubes

Ten full scale monotonic tests have been performed on HSS CHS columns. Considering actual mechanical properties of columns (f_y = 694 MPa; D/t = 19.4) the cross section is classified as Class 2 in accordance with EN 1993-1-1 while considering nominal strength (f_y = 590 MPa) a Class 1 is obtained. In the following calculations actual yield stress is considered.

Two different column lengths have been tested:

- Short column (1850 mm from flange to flange) relevant for cross sectional behavior
- Long column (4850 mm from flange to flange) relevant for member behavior

Loading conditions applied are:

- Axial compressive load
- Combined load: bending moment in presence of constant axial compressive load (each test with different value of axial load)

Type 1: stub column test (axial compression with rotation fixed)

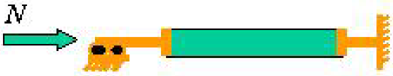

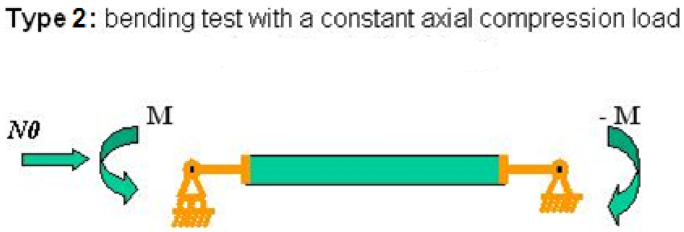

Figure 31 Test on column specimens in Task 3.3

Testing program is summarized in Table 14 together with column slenderness calculated on the basis of actual yield stress.

Table 14 Testing program for monotonic full scale tests

	Axial compressive test (fixed ends) Type 1			**Beam-column test (pin ends) Type 2**		
	slenderness	**Nr. test**	**ID**	**slenderness**	**Nr. test**	**ID**
Column short (Cs)	14.2	2	Cs1	28.4	3	Cs3
Column long (Cl)	37.3	1	Cl1	74.6	4	Cl3

Measurements of geometrical imperfections and residual stresses are reported in *Appendix C*.

Axial compression tests

Three full scale tests were conducted in pure axial compression and fixed ends conditions, see Table 15. Loading at a constant displacement rate of 1.7mm/min was applied.

Columns were instrumented as listed below:

- nr. 12 strain gauges at three different cross sections (L/4, L/2 and 3/4L where L is the column span net of ends stiffeners) on opposite circumferential positions 0°-180° (out-of-bending) and 90°-270° (in-bending plane);
- nr. 4 LVDT displacement transducers in axial direction on circumferential positions 0°, 90°, 180° and 270°
- specimens were grid marked with a 50mm edge square grid
- evolution of global deformation process by video-recording.

Load vs displacement curves are reported in Figure 32. The initial linear behavior is followed by a plateau at the maximum load for Cs1 columns and a development of an hinge at one column end; at the end a diffuse distortion of the column is observed. Columns Cs1-bis and Cl1 after the maximum load is reached had an immediate load drop down due to loss of stiffness at boundaries.

Table 15 Results of axial compression tests

ID	**Maximum load N_u [kN]**	**Axial shortening [mm]**	**Nominal strength [kN]**
Cs1	4414 kN	11.6	3972
Cs1-b	4682 kN	12.0	3972
Cl1	3956 kN	17.3	3614

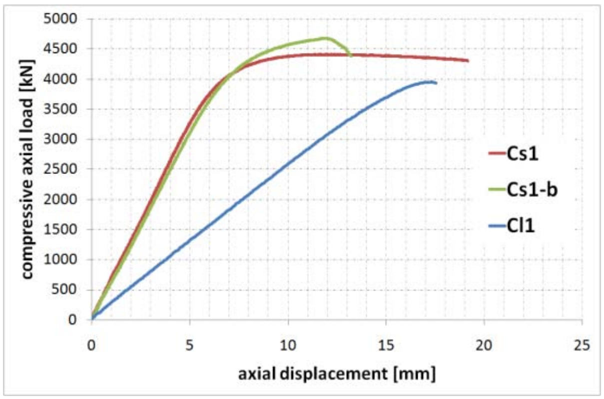

Figure 32. Axial compression tests: load vs. shortening diagram.

Combined axial and bending tests

Seven columns have been tested under combined axial and bending load and free end rotations (Table 16). The following testing procedure was followed:

- increase of axial load at a constant rate up to the desired value;

- while axial load is hold fixed, slowly increase of the bending moment.

The columns were instrumented as listed below:

- nr. 4 strain gauges at mid span on opposite circumferential positions 0°-180° (out-of-bending) and 90°-270° (in-bending plane);
- nr. 2 LVDT displacement transducers in axial direction in in-plane positions 90° - 180°;
- nr. 2 LVDT to measure column lateral displacement;
- Evolution of global deformation process by video-recording.
- Hinge rotation.

Testing conditions and results obtained are summarized In Table 16 in terms of compressive axial load applied (N_{apply}), maximum bending moment detected (M_u) and rotation at maximum bending moment (Φ_u).

Table 16 Results of combined axial and bending tests

ID	**N_{apply} [kN]**	**M_u [kN m]**	**Φ_u [degrees]**
Cs3-13	720	118	2.8
Cs3-25	1104	73	1.9
Cs3-50	2100	27	not available
Cl3-50	470	65	4.0
Cl3-50bis	450	80	6.5
Cl3-75	620	31	4.4
Cl3-80	720	15	3.5

Some pictures of the specimen after testing are reported in *Appendix C*. Complete moment vs. rotation diagrams are reported in Figure 33.

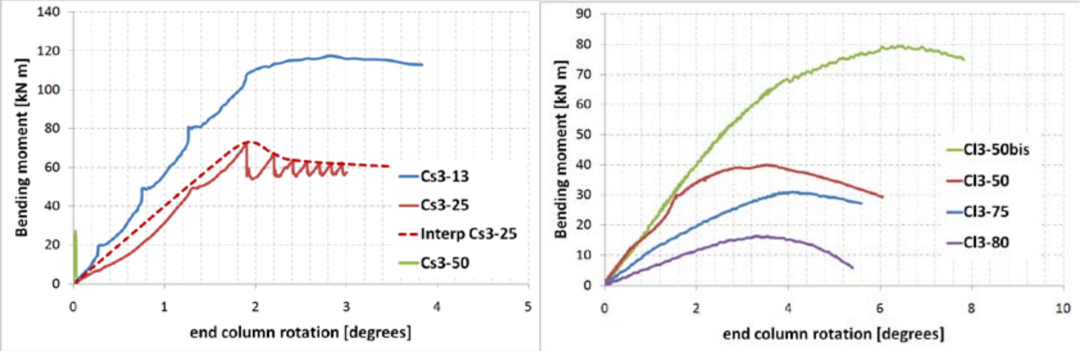

Figure 33 Full scale combined load tests: moment vs. rotation diagrams.

It has to be noted that test Cs3-25 was performed applying a stewise procedure where some test pauses are present as it can be seen in Figure 33, where also an interpretation of experimental curve is reported. The M-N diagram is shown in Figure 34.

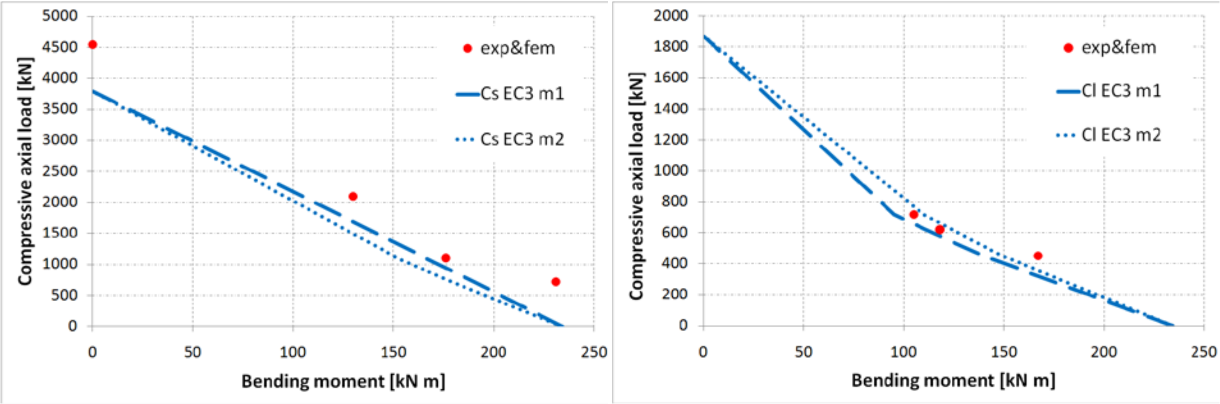

Figure 34 HSS CHS interaction M-N diagram: comparison between Eurocode 3 design recommendations and experimental results

WP4: Performance of HSS welded and bolted connections

Objectives of the WP4 (Tasks 4.1, 4.2, 4.3 & 4.4)

The main objectives of WP4 are as follows:

- tests on HSS base material and welds for elastic and elastic-plastic fracture characterization including loading rate and corrosion
- Tests on welded K,T,Y or X tubular connections with axial, in plane and out of plane loading
- Realization of advanced post-treatment welding techniques
- Tests on bolted connections

Activities and results obtained

Task4.1 Fatigue and fractures toughness tests on HSS welds

High-cycle fatigue characterization of welded sample coupon

The fatigue characterization consisted on axial tests performed on strip specimens machined from butt welds extracted from HSS tubes 355x12 and 193.7x10. The study included the evaluation of the mismatching behaviour as welds were made both in the overmatching and in the undermatching condition. The characterization consisted on the determination of an entire S-N curve with a run-out of 2·106 cycles as the maximum fatigue life and the tests followed the stair-case methodology. The results were fitted to a $\Delta\sigma/2$ - Log N linear curve following the instructions of the ASTM E739 standard for the evaluation of fatigue data.

Taking into account a value of 96 MPa of fatigue life for a conventional steel (S355) at about 300000 cycles, the overmatching condition for the weld seems to have better fatigue performance than the undermatching condition, as the fatigue life is 126 MPa for the overmatching curve and is 105 MPa for the undermatching curve, see Table 17 and Figure 35, respectively. The initiation of the crack that originates the fatigue is always located in the inner surface of the tube and the crack path goes through the thickness to the outer surface.

Table 17 Results of the fatigue tests

Codification	Equation	Fatigue life at $2E^6$ $\Delta\sigma$ (MPa)
TS590 Overmatching	$(\Delta\sigma/2)=10^{3.59}\cdot(N)^{-0.27}$	126
TS590 Undermatching	$(\Delta\sigma/2)=10^{3.99}\cdot(N)^{-0.38}$	105
S355 Undermatching	$(\Delta\sigma/2)=10^{4.08}\cdot(N)^{-0.38}$	96

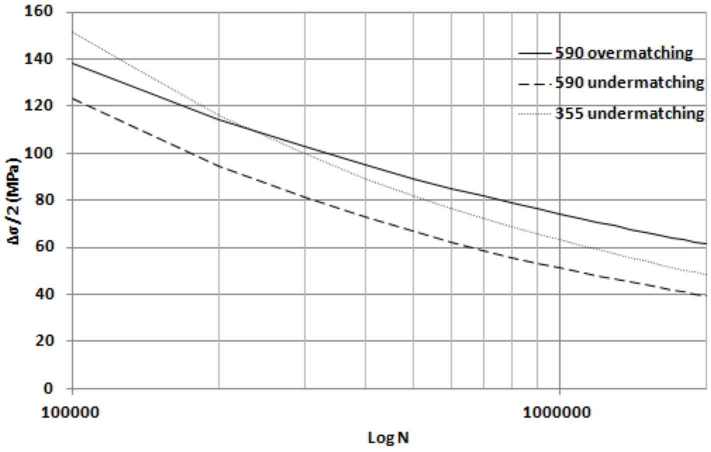

Figure 35 Fatigue curves of TS590 in the mismatching conditions and S355 undermatching

Fracture toughness characterization

The Fracture toughness characterization consisted on the determination of the J-R curve in the HSS steel in the mismatching conditions. The test procedure and the specimens dimensions are described in the Appendix D. The notch has been performed in the weld metal, so this is the zone submitted to the test. The fracture toughness, defined as the onset of the stable crack growth, is 440 kJ/m2 in the case of the TS590 base metal and decreases to 132 kJ/m2 and to 90 kJ/m2 for the undermatching and overmatching conditions, respectively; see Table 18 and Figure 36.

Table 18 Results of the fracture toughness tests

Codification	Fracture Toughness (kJ/m^2)

TS590 Base metal	440
TS590 Undermatching	132
TS590 Overmatching	90

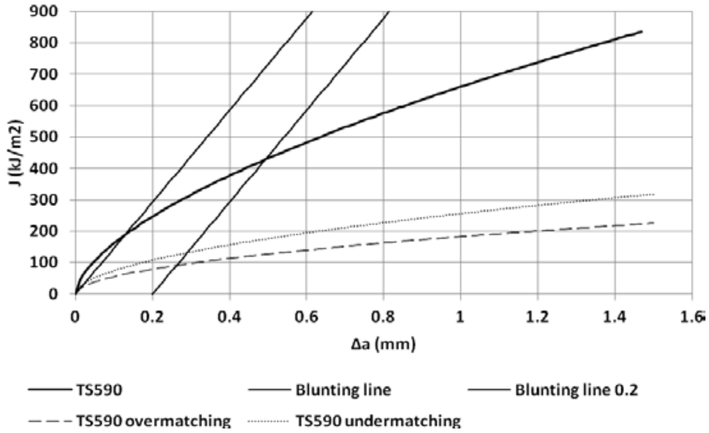

Figure 36 Comparison of J-R curves of TS590 base metal and TS590 in the mismatching conditions

Corrosion tests on HSS welds

Corrosion rate measurements and Slow Strain Rate Tests (SSRT) were performed on material from K- and X-joints and the heat affected zones of two different steel grades, TS590J2H and S355J2, respectively.

Uniform corrosion rate was determined in two different solutions, 1 wt% and 3.5 wt% NaCl, in order to simulate the offshore and seawater environments, respectively. The tests were carried out at ambient temperature. The linear polarisation resistance technique, based on the change in potential and record of the polarisation was used to measure the corrosion rate.

The SSRT testing was performed in order to evaluate the susceptibility of materials towards stress corrosion cracking and hydrogen embrittlement. The tests were performed in air, 1 wt% and 3.5 wt% NaCl solutions at ambient temperature. A strain rate of 10^{-6} s^{-1} was applied throughout the experiments. In order to simulate cathodic protection, cathodic polarisation with the magnitude of 40 mA was applied throughout the test of some of the samples in order to enable diffusion of hydrogen into the specimens. The elongation EL%, yield stress (YS) and ultimate tensile strength (UTS) were calculated from the stress vs. strain curves. The time to failure (TTF) was determined during the SSRT. Furthermore the Reduction of Area, RA (%) was measured on the samples after cracking.

The average of the corrosion rates for the weld metals of TS590 and S355 are presented in Figure 37. Higher corrosion rate was achieved in 3.5 wt% NaCl compared to 1 wt% NaCl for all tested samples. Steel TS590 had lower corrosion rate than S355 in the more aggressive solutions with 3.5 wt% NaCl, while it was slightly higher for the weld metal of TS590 in 1 wt% NaCl solution.

The SSRT-measurements at open circuit potential in air, 1 wt% and 3.5 wt% NaCl gave no significant difference in RA between base, weld metal and HAZ for TS590 with K-joint. Results from tests where cathodic polarisation was applied showed that the RA-values decreased for base, weld metal and HAZ for TS590 and S355 and K-joint as well as X-joint. The weld metal achieved the lowest RA and thereafter the HAZ. This is also visible from Figure 38, where the reduction in area in 1 wt% NaCl with applied cathodic polarization of 4 mA/cm² for TS590 and S355, base, weld and HAZ is presented. The measurements showed that TS590 had a lower RA than S355.

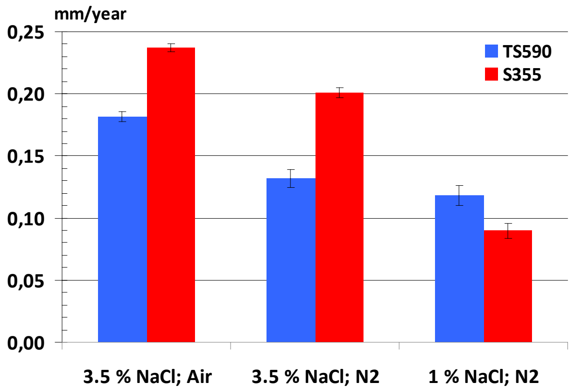

Figure 37 Corrosion rate of weld metal of TS590 and S355 in various corrosive environments

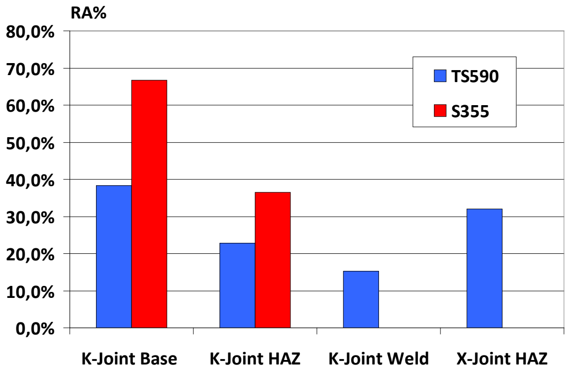

Figure 38 Reduction in area, RA%, for weld metal of TS590 and S355 in 1wt% NaClwith 4 mA/cm².

From results, it is obvious that the cathodic polarisation drastically decrease the reduction in area of all tested samples prepared from base metal, welds and HAZ. The obtained results also indicate that the susceptibility to stress corrosion cracking increases in the following order: base, HAZ and weld metal. The corrosion rate measurements in the most aggressive solution showed a higher corrosion rate for S355 and then for TS590. Furthermore the weld metal had higher corrosion rate than the base metal for both S355 and TS590.

Characterization of HSS weld joints

The partners were involved in the definition of the test pieces configuration for various tests along the project. As a result the configurations were grouped in butt welds, X and K joints, and flanged bolted joints. The variety of joint configurations is shown in Figure 39.

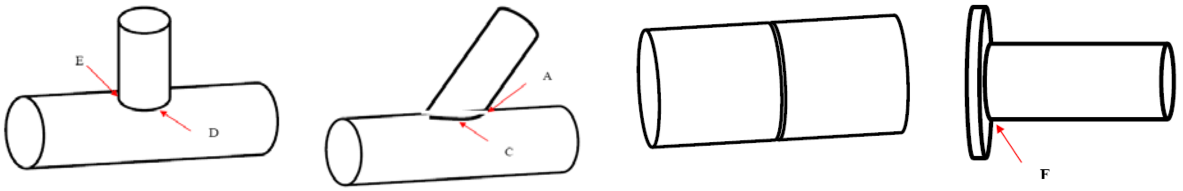

(a) (b) (c) (d)

Figure 39 Weld specimens: a) X-joint, b) K-joint, c) butt joint and d) flange joint

The criteria for the characterization of the above joint configurations was based on European standard providing the type and amount of tests, the test specimens configurations, methods of tests, and acceptance criteria The reference standard is EN ISO 15614-1:2004 – Specification and qualification of welding procedures for metallic materials – Welding procedure test. An initial set of welded joints was produced and evaluated to a European standard, and are *Appendix D* for type of tests and location of specimens.

The two butt joints were radio-graphed (procedure/acceptance criteria: EN 1435:1997/A1:2002/A2:2003/ EN 12517-1:2006) and controlled by magnetic particles (procedure / acceptance criteria: NP EN 1290:98 + A1:2002 + A2:2002/NPEN 1291:2000-level 2X) before mechanical tests. In radiographic tests isolated spherical pores were detected, within the acceptable range.

Transverse tensile test

Transverse tensile coupons are obtained in accordance with EN 895. They are cut out from butt welds perpendicularly to the weld, so the coupon contains a cross section of the weld in its middle. All the results of transverse tensile coupons were higher than the specified minimum value of 700 MPa (referred on TENARIS product TS590's specification PSP00148 rev 2). The rupture occurred in the parent metal (MB zone) in all cases evidencing no weak of the weld, even when undermaching consumable was used. The individual results for both transverse and all weld tensile tests are presented in Table 19.

Table 19 Transverse tensile test result

Reference	Thickness	Width/ diameter	section	Gauge length	Test temp	Tensile strength	Average tensile strength

	mm	mm	mm^2	mm	°C	MPa	MPa
OT1*	10.6	25.0	264.8	----	21	833	838
OT2	10.6	25.0	266.0	----	21	843	
UT1*	11.4	24.9	283.4	----	21	841	843
UT2	11.4	24.8	283.3	----	21	846	

*OT- overmatching tensile with G79 electrode, *UT- undermatching tensile with G55 electrode.

According to the test results shown in Table 19, the T590 steel shows nearly the same transverse tensile strength in undermatching (G55) and overmatching (G79) weld conditions.

Tensile Tests

These tests were performed on the test pieces extracted from the butt weld specimens, both in the undermatching as well as overmatching weld conditions. The specimen geometry and the test result are shown in Table 20. The relevant stress-strain diagram is shown in Figure 40.

Table 20 Tensile test result

reference	Thickness	Width/ diameter	section	Gauge length	Test temp	Yield strength	Tensile strength	Elongation after fracture
	mm	mm	mm^2	mm	°C	MPa	MPa	%
OT1	----	5.0	19.6	----	21	1011	1116	15.9
OT2	----	5.0	19.6	----	21	911	1040	17.5
UT1	----	5.0	19.2	----	21	908	945	14.9
UT2	----	5.0	19.5	----	21	823	855	16.5

All weld tension test coupons are cylindrical, and entirely constituted of weld metal. These tests were performed on butt welded specimens, both in the undermatching and overmatching conditions. All weld specimens provide information on how much the overmatching and undermatching is achieved.

- Average Yield strength for overmatching weld metal: 0.5x (911+1011) =961 MPa
- Average Yield strength for undermatching weld metal : 0.5x (823+908) =866 MPa

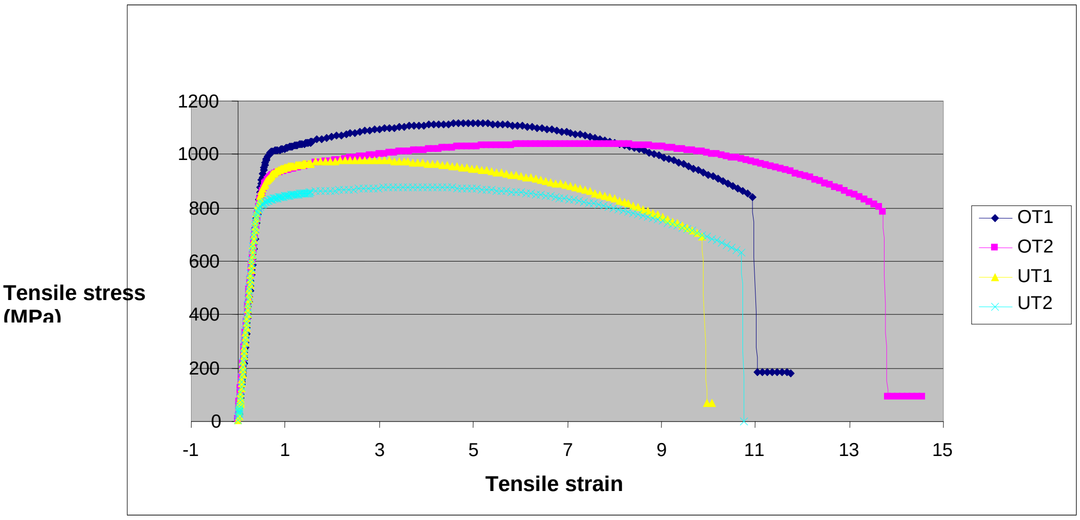

Figure 40 Stress-strain diagram

Taking the yield strength as reference for over and undermatching condition, it can be observed that actual values for wires G55 and G79 overmatches T590 yield strength. Nevertheless the usual definition of over and undermatching is the specified minimum yield strength value. Hence wire G79 can be considered as overmatching T590 steel as well as G55 wire is undermatching T590 steel; see Figure 41 in this respect.

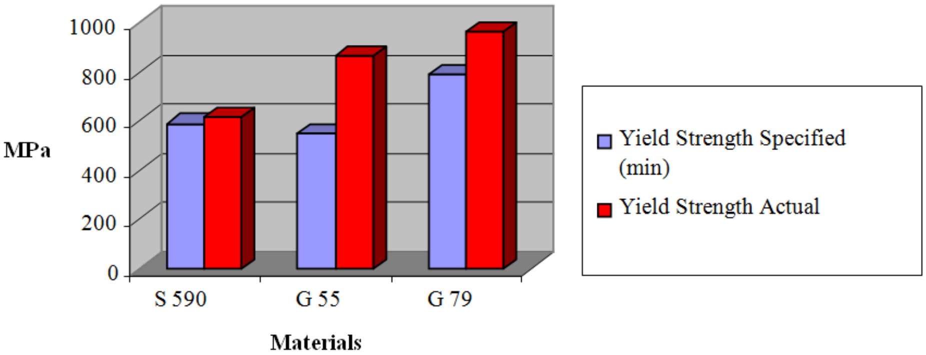

Figure 41 Yield strength matching of filler metals

Bending test

Bending test specimens have been taken from butt welds, and tests have been performed according to EN 910:1996. As widths are greater than 12mm, four side bend specimens have been tested for each matching condition. In the side bend specimens the surface in tension is a cross section of the weld. Acceptance criteria is that test specimen shall not reveal any one single flaw > 3mm in any direction. No flaws were detected in any specimens.

To evaluate the tenacity of the weld metal and the heat affected zones, three sets of three specimens were defined and tested. Because of unexpected low values at -40ºC, additional impact tests, on weld metal, were performed on the butt weld specimens for both the overmatching and undermatching weld conditions at four different temperatures, i.e.-40, -30, -20 and 0ºC, as shown in Table 21. From this table it can be observed that the weld region shows toughness value of 17 J at – 40ºC. According to ISO 16834, G55 only guarantees 47J at – 30ºC. Hence the toughness is lower in the weld metal. Nonetheless, from structural point of view the weld should satisfy 27 J at design temperature. Hence, the toughness of 29 J at -20ºC is acceptable for structural application.

The overall impact test results are plotted in a single graph, for comparison of both welding wires used in butt welds, as shown in Figure 42).

Table 21 Charpy V Impact test results for: undermatching (G55) / Overmatching (G79)

	Test temperature (ºC)			
test specimen nº	**-40**	**-30**	**-20**	**0**
1	14 / 30	29 / 35	33 / 41	40 / 70
2	14 / 16	18 / 41	27 / 52	39 / 59
3	22 / 37	22 / 18	26 / 37	42 / 49
Mean value (J)	**17 / 28**	**23 / 31**	**29 / 43**	**40 / 59**

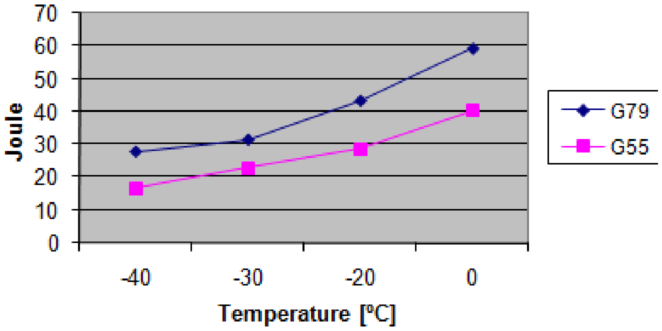

Figure 42 Charpy- V impact test result for under- and over- matching welds

Both macroscopic examination and hardness test are performed on the same specimen.

Macroscopic examination is used to reveal the macroscopic features of a welded joint, usually by examination of transverse sections. This is done by visual/optical examination of the prepared surface, after etching. The test specimens were prepared and etched in accordance with EN 1321 on one side, to clearly reveal the fusion line, the heat affected zone (HAZ) and the build-up of the runs. The macroscopic examination included the unaffected parent metal and a macro-reproduction picture was taken per procedure test.

Hardness tests are used to define hardened or softened regions due to welding. Vickers hardness testing with a load of HV10 was performed in accordance with EN 1043-1. Hardness measurements were taken in the weld, the heat affected zones and the parent metal in order to evaluate the range of hardness values across the welded joint.

The acceptance levels of hardness are given in EN 15614-1: TS 590 steel is quenched and tempered steel in group 3 according to technical report ISO/TR 15608, so the maximum acceptable hardness value is 450 HV10, in the non-heat treated condition. S355 used in flange connection is a material group 1, so the maximum acceptable value is 380 HV10, in the non-heat treated condition. It can be observed that values in base metal (BM) are in the same range (around 300 HV) except for the case were the flange was S355 steel (F) and filler metal (G46) are in lower grade. There is a slight variation in the heat affected zones of TS590 steel, nevertheless in the acceptable range of hardness's as shown in Figure 43.

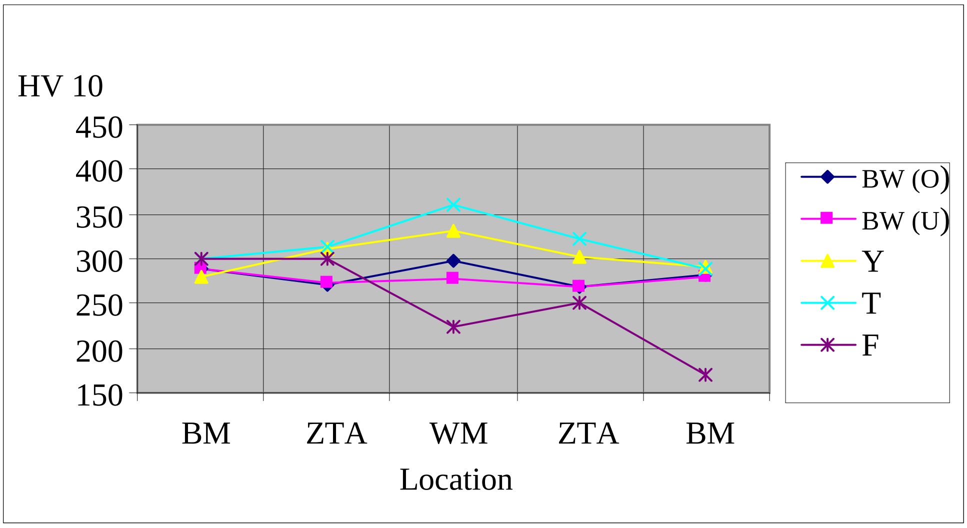

Legend of Figure 43
BW – Butt weld;
(O) – Overmatching;
(U) – Undermatching
Y – Y branch;
T – T branch;
F – flange connection
BM – Base metal ;
ZTA – Heat affected zone ;
WM – Weld metal

Figure 43 Hardness results

Both macroscopic examination and hardness tests have been found to comply with the requirements of EN 15614-1. The welding procedure specifications (WPS) used for the welding of samples for further tests by the project partners can be considered as qualified according to EN 15614-1:2004 plus additional project requirement for impacts (at least 27J at - 20ºC). Being that standard widely used in European industry we can also affirm that the weldments tested in HITUBES's project have enough quality as industrial welds should have for fabrication purposes.

WP4.2 Tests on welded connections

This experimental investigation consists of ten tests on welded tubular connections. The base material is HSS TS590) with nominal yield stress of 735 MPa. Two types of weld conditions are considered: weld A (lower weld yield strength, undermatching) and weld B (higher weld yield strength, overmatching). The specimens have been subjected to monotonic and cyclic in-plane bending (IPB), out-of-plane bending (OPB) and axial loading (AF), well beyond the elastic range. Test results are presented in Table 22. The brace has a nominal cross-section CHS 193.7x10 and the chord CHS 355x12. For the OPB tests, 4-point bending was applied to the brace through a steel cross-beam with two special ball-joint hinges and appropriate wooden grip assemblies, as shown in Figure 44a. Both ends of the specimens were supported on a double-hinge 'roller' system. For the IPB tests, 3-point bending was applied to the brace through a concentrated load at mid-span by attaching the actuator to the top of the chord, as shown in Figure 44b. Both ends of the specimens were supported by a double-hinge 'roller' system. For the axial tests, one end of the specimens' brace has been hinged to the bottom beam of the testing frame and the other end to a lever-arm steel beam. For the IPB and OPB tests strain gages were placed at critical locations to measure the specimens' strains. In addition, wire position transducers and DCDT's were used for load-point and support displacement measurements. Axial load is applied to the specimens through this lever-arm beam which is hinged to the actuator at one side of the reaction frame.

Table 22 Test results

Specimen and loading type	**Weld type**	**Type of loading**	**Applied moment M_{max} (kNm) or axial load (kN)**	**R**	**Loading cycles to failure, N_f**
OPB	A	monotonic	121.4	-	-
	B	monotonic	115.4	-	-
	A	cyclic	9.3 to 93.4	0.1	240
	B	cyclic	9.3 to 93.4	0.1	200
IPB	A	monotonic	267.8	-	-
	B	monotonic	251.5	-	-
	A	cyclic	21.3 to 213.1	0.1	976
	B	cyclic	21.3 to 213.1	0.1	669
Axial	A	cyclic	75 to 750	0.1	1000 (*)
	B	cyclic	75 to 750	0.1	750 (*)

(*) approximate values, corresponding to loss of axial stiffness.


(a) (b)

Figure 44 Test setup for tests: (a) out-of-plane bending, (b) in-plane bending

OPB tests: two specimens were subjected to monotonic loading, one for each weld type. The bending moment capacity Mmax of the specimen with weld type A and that with weld type B was 121.4 kNm at a load-point displacement (LPD) of 107.5 mm and 115.4 kNm at a LPD=78.5 mm, respectively. Both specimens failed at the chord saddle region of the weld toe of the joint (see deformed specimen in Figure 45a). The other two of the OPB specimens were tested under low-cycle fatigue, one with weld type A and one with weld type B. After an initial applied bending moment of 100 kNm to both specimens, they were subjected to fatigue loading with a Mmin=9.3 kNm and Mmax=93.4 kNm (load ratio, R=Mmin/Mmax=0.1) at a frequency of 0.1 Hz. The specimen with weld type A and that with weld type B failed after 240 and 200 cycles, respectively. Both failed due to low-cycle fatigue, at the same location as in the tests under monotonic loading.

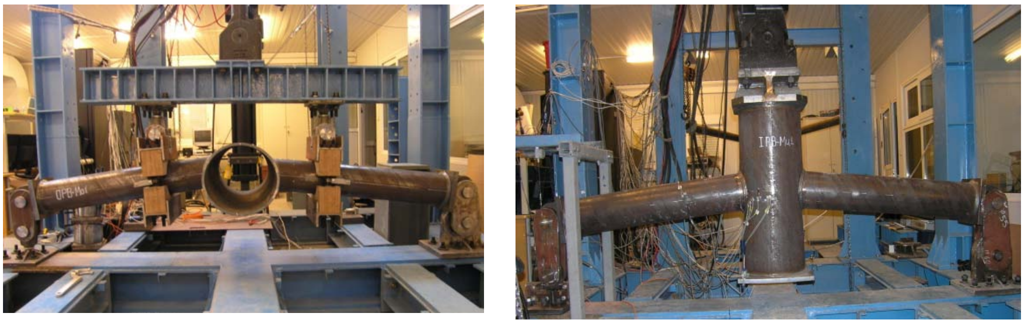
(a) (b)

Figure 45 Deformed specimen (a) OPB, (b) IPB

(b) IPB tests: two specimens were subjected to monotonic loading, one for each weld type. The specimen with weld type A and weld type B failed under a M_{max}=267.8 kNm with a LPD=159.3 mm and a M_{max}=251.5 kNm with a LPD=111.5 mm, respectively. Failure occurred at the chord crown location of the weld toe of the joint (see deformed specimen in Figure 45b). The other two IPB specimens were tested under low-cycle fatigue, one with weld type A and one with weld type B. After an initial applied bending moment of 213.1 kNm to both IPB specimens, they were subjected to fatigue loading with a M_{min}=21.3 kNm and M_{max}=213.1 kNm (load ratio, R=M_{min}/M_{max}=0.1) at a frequency of 0.2 Hz. The specimen with weld type failed after 976 loading cycles and that with weld type B after 669 cycles. Both specimens failed due to fatigue at the chord crown region of the joint, at the same location as in the tests under monotonic loading.

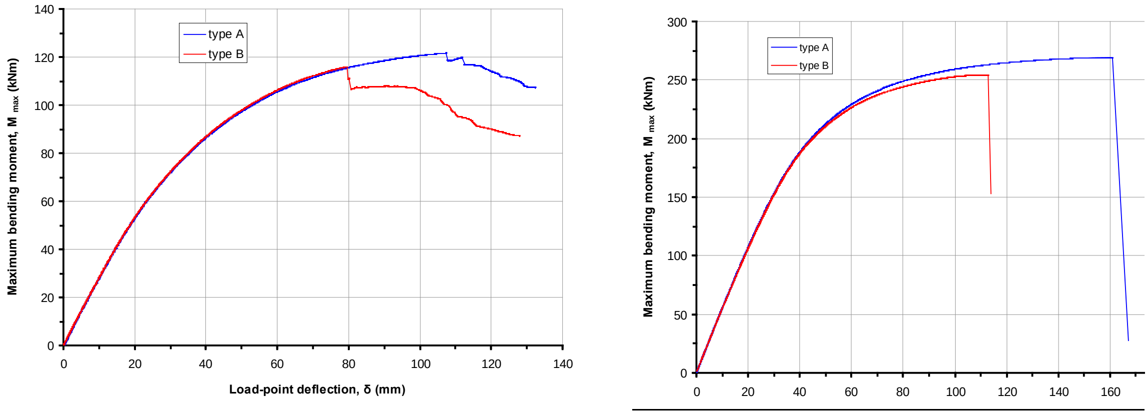

Figure 46 Load vs. displacement curves for the (a) OPB and (b) IPB specimens under monotonic loading

(c) Axial load tests: two X-joint specimens were subjected to low-cycle fatigue under cycling axial loading, one with weld type A and one with weld type B. Both specimens were subjected to fatigue loading with a Fmin=75 kN and Fmax=750 kN (load ratio, R=Fmin/Fmax=0.1) at a low frequency, ranging between 0.01 and 0.03 Hz. Both specimens failed due to through-thickness fatigue cracking at the chord saddle, see Figure 47b, but were able to sustain the applied load for more than 1000 cycles. In the specimen with weld type B, after about 750 loading cycles the rate of increase of overall axial deformation (axial stiffness loss) became quite significant and this could be considered as “structural failure”. The weld type A specimen had much better performance in terms of axial stiffness loss.

(a) (b)

Figure 47 Tested specimen under axial cyclic loading; (a) general set-up , (b) fatigue crack at weld toe (chord saddle location)

WP4.3 Advanced welding techniques and post-treatments

The welded tubes were conditioned by means of an ultrasonic treatment that consists on the cleaning of the weld toe area (outer surface) and the creation of a weld toe groove. The root (inner surface) was not treated by means of the ultrasonic equipment, both for costs and tool access reasons; see the size of the peening tool in Figure 48. As it was stated before, all the high-cycle fatigue failures initiate from the inner surface of the tube (root) and progress to the outer surface of the tube (weld toe), that is just the peened surface. Therefore after testing, it was discovered that the peening treatment did not affect the fatigue performance as it was performed in the opposite surface to crack initiation.

Figure 48 Ultrasonic generator and peening tool

Task 4.4 Tests on bolted connections

This task aims at characterising the behaviour of bolted joints through experimental evidences:

- under monotonic loading - initial stiffness, ultimate capacity, ductility and failure modes;
- under repeated loading - energy dissipation and failure modes;
- under fatigue loading - critical zones, hot-spot stress distribution and fatigue strength.

Tests were carried out on two joint configurations -configurations 1 and 2- having different flange thicknesses -15 mm and 20 mm respectively- and bolt sizes -M27 8.8 and M20 8.8 respectively-; see Figure 49. The configurations to be tested were designed so as to exhibit two different collapse modes – Mode 1 and Mode 2 predicted through an analytical approach funded on the T-Stub concept-:

- Configuration 1: collapse mode 1 corresponding to the development of a plastic mechanism in the flange
- Configuration 2 : collapse mode 2 associating the development of plastic yield lines in the flange and the failure of the bolts in tension

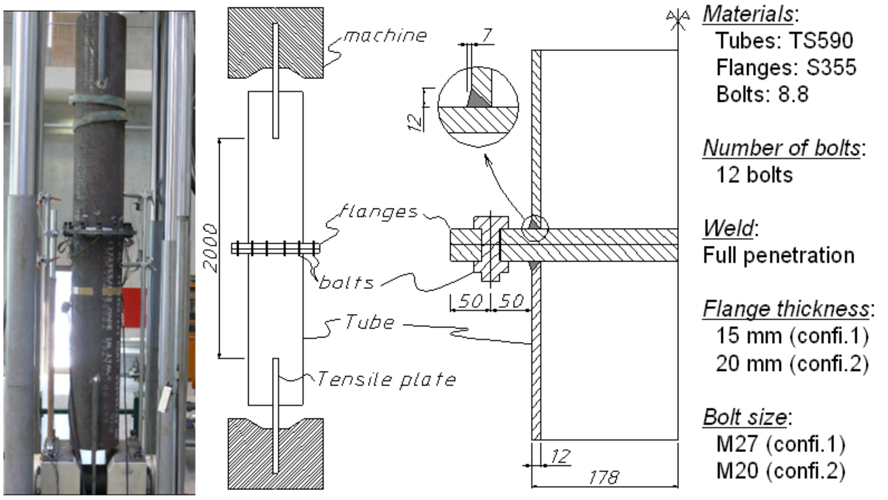

Specimen in the machine Set-up Detail of geometries and materials

Figure 49 Description of the bolted joint specimens

Configuration 1 and configuration 2 were tested under three types of loading: monotonic (tests M1 and M2 respectively), high cycle fatigue (HCF) (tests H1 and H2 respectively) and low cycle fatigue (LCF) (tests L1 and L2 respectively). Therefore, six specimens were tested.

Beside the above-mentioned tests, four supplementary tests were performed on the specimens with the objective to obtain more information about the hot-spot stress distribution in critical zones. These tests were performed by applying some load cycles, keeping the connection in the elastic domain. The tests were successful. The load-displacement curves for the monotonic and LCF tests are presented in Figure 50 and Figure 51, respectively. From the obtained results, it was possible to characterise the behaviour of the investigated joint configurations, as expected, highlighting their global behaviour and failure modes. Also, the obtained results were used for the numerical investigations -see WP5-Task 5.3- and for the derivation of design guidelines for bolted joints for column splices -see WP7- Task 7.3-.

Table 23 Description of tested specimens

Specimen	Load type	Component states		
		Tubes	Flanges	Bolt shanks
M1	Monotonic	No problem	Plastic deformation at weld toe	Plastic deformation
M2	Monotone	No problem	Almost no problem	Failures
H1	HCF	Crack at the weld toe	No problem	No problem
H2	HCF	Crack at the weld toe	No problem	A bolt are cracked
L1	LCF	No problem	Crack at the weld toe	Plastic deformation
L2	LCF	No problem	Almost no problem	Plastic deformation

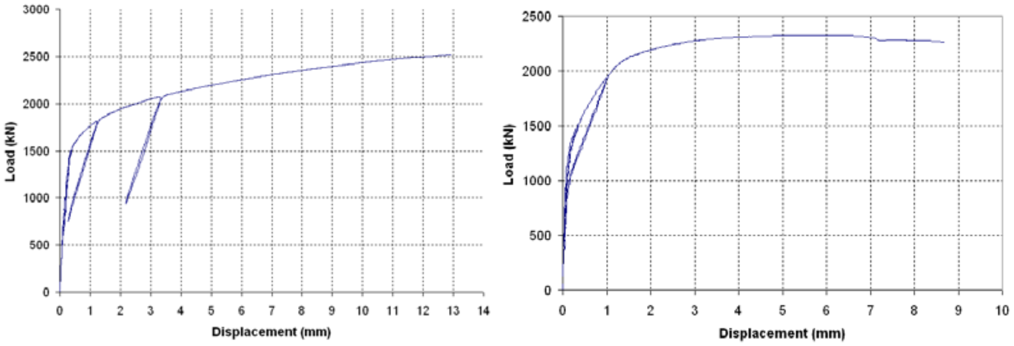

Specimen M1

Specimen M2

Figure 50 Load-displacement curve for specimens M1 & M2 (monotonic loading)

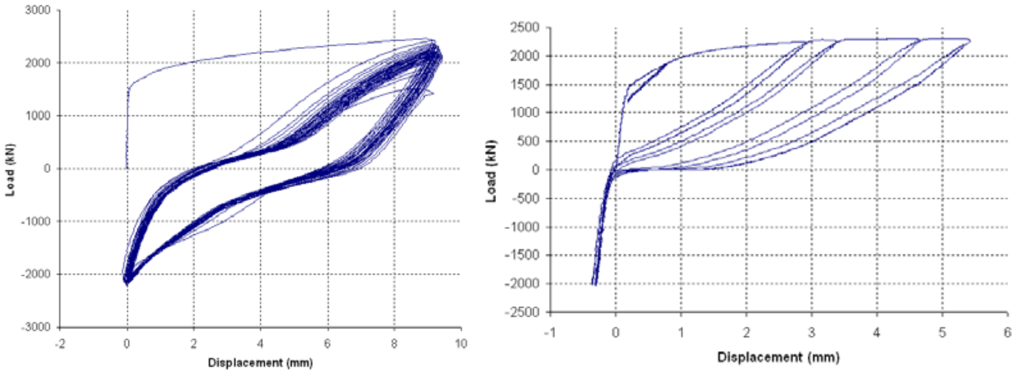

Specimen L1

Specimen L2

Figure 51 Load-displacement curve for specimens L1 & L2 (low cycle fatigue)

The behaviour of the joints under HCF load is reported in *Appendix D*. Moreover, details related to instrumentation, loading program for fatigue tests, hot-spot distribution at the critical zones and failure modes are reported in *Appendix D* too. Mechanical characteristics of the base materials: tubes, bolts, flanges is reported in Deliverable D4.4.

WP5: Numerical simulations of tubular connections and parametric study

Objectives of the WP5 (Tasks 5.1, 5.2 & 5.3)

The main objectives of WP5 regard Refined material parameter formula depending upon fast loading, Simulation of Welded Connections and Joints Under Strong Repeated Loading and Simulation of bolted connections and joints under strong repeated loading

Activities and results obtained

Task 5.1 Refined material parameter formula depending upon fast loading

On one hand, it is recognized that the rate of loading has an effect on material properties. On the other hand, flexible structures like slender foot- and cycle-bridges can be sensitive to extreme winds owing to typhoons [40] or anthropic actions, e.g. human beings walking. Similar effects can happen in the case of high-speed trains [49]. Even though strain-rate effects influence the yield stress, the tensile stress and the elongation of the material, see Figure 52, these affects are usually not taken into account, unless impact or blast is considered [50]. These effects were not explored for TS590J2H. As a result in order to investigate such phenomena, tests under low-cycle fatigue loading were performed up to 1/s strain rate (10 % deformation * 10 Hz).

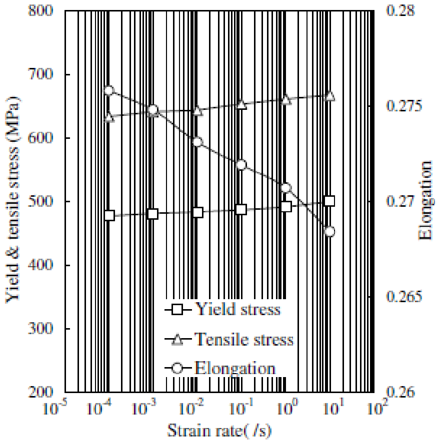

Figure 52 Distribution of mechanical properties for strain rate, after Chang Kyong-Ho et al. **[51]**

In order to reproduce these effects, some formula was reviewed and reported here. Previous works by Rao and recalled by Lamarche [52] indicated that the dynamic yield stress, σ_{yd}, can be expressed as a function of the strain rate as follows:

$$\frac{\sigma_{yd}}{\sigma_{ys}} = 1 + c\left(\dot{\varepsilon}\right)^{n}$$

where σ_{ys} is the yield stress under static loading, and C, n are constants to be determined experimentally. For a regular -strength steel A36 -equivalent to S235-, the following formula was proposed:

$$\frac{\sigma_{yd}}{\sigma_{ys}} = 1 + 0.021\dot{\varepsilon}^{0.26}$$

Alternatively, the following formula can be used:

$$\sigma_{yd} - \sigma_{ys} = 3.2 + 0.001\dot{\varepsilon} \quad \text{for } 200 < \dot{\varepsilon} < 1000$$

Based on tests performed in Task 4.1, Figure 53 and Figure 54 are plotted for S590J2H and S355J2, respectively, on the logarithmic scale for four values of strain rates, i.e. 0.001, 0.01, 0.1 and 1/s. The maximum value of strain rate, i.e. 1/s derived from the analysis of 'structures under typhoon [40]. One can notice that Figure 53 shows an increasing YS and TS similar to the one in Figure 52.

Eq.(1) was fitted with test data both for TS590 and S355 and the coefficients c and n were evaluated. The values presented in Table 24 show that the TS590 steel examined exhibits lower value of c and n than S355 steel. As a result, the HSS examined appears to be less sensitive than regular structural steel.

Table 24 Coefficients of the material parameter formula for TS590 and S355

	σ_{ys} (MPa)	*c*	*n*
TS590	745	0.085	0.19
S355	425	0.137	0.22

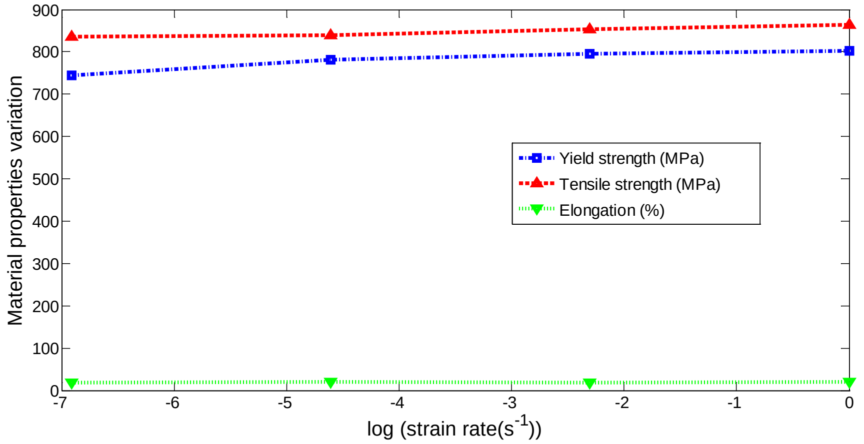

Figure 53 Distribution of mechanical properties of TS590 for four (log) strain rates

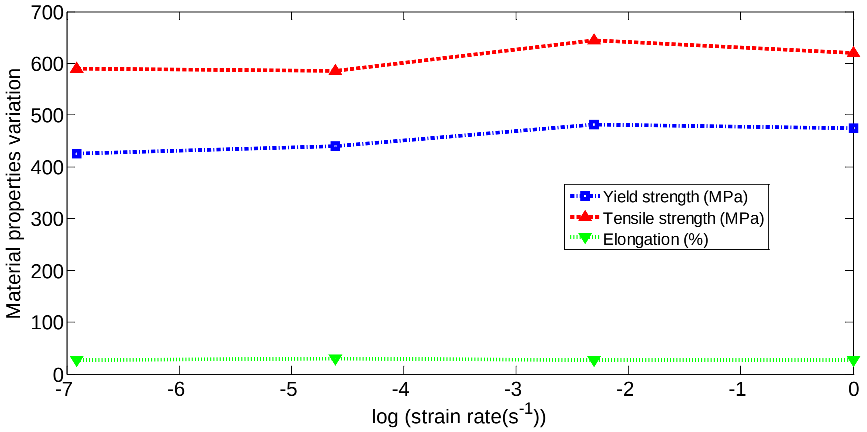

Figure 54 Distribution of mechanical properties of S355 for four (log) strain rates

Task 5.2 Simulation of welded connections and joints under strong repeated loading

Detailed numerical simulations of X-joint tests were conducted, considering the actual dimensions of each welded joint. The weld geometry has been modeled in detail, according to Eurocode 1993 Part 1-8 and AWS D1.1 [15] provisions, and the mesh size is denser near the weld region, as shown in Figure 55a. The steel material is modeled through J_2 flow plasticity, accounting for large strains, with linear kinematic hardening.

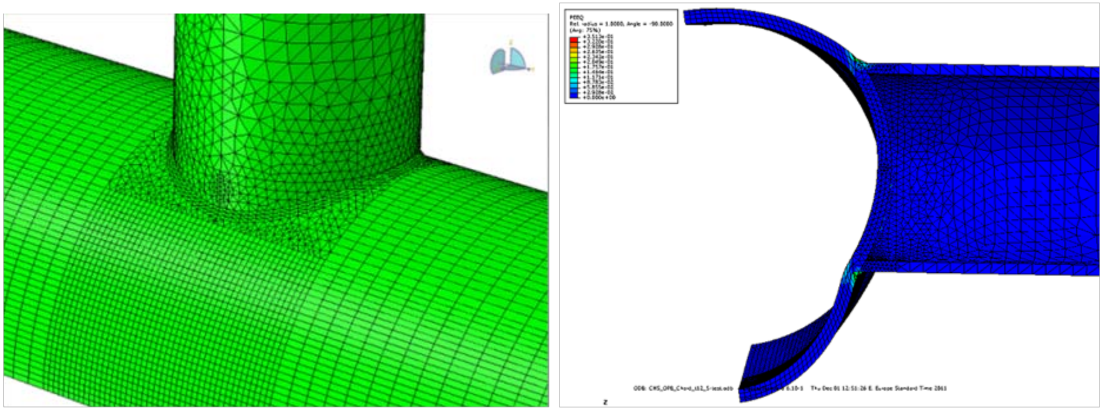

(a) (b)

Figure 55 Numerical model for welded joints: (a) Finite element mesh (b) Deformed shape under out-of-plane bending.

Simulation of out-of-plane bending response

In Figure 56, the experimental measurements are compared with the numerical results. It can be concluded that the numerical model can reproduce quite accurately for monotonic and cyclic loading conditions. Figure 55b shows the deformed shape of the joint.

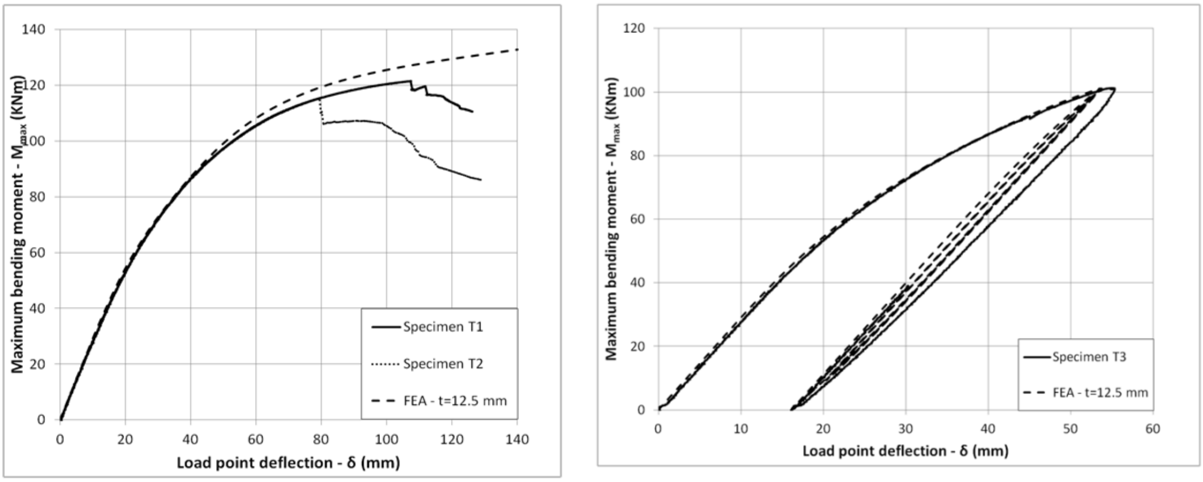

Figure 56 Analysis of welded tubular joints under out-of-plane bending moments - Comparison of the numerical and experimental load vs. displacement curves: (a) Monotonic loading, (b) Cyclic loading.

The corresponding strain concentration factor (SNCF) and the stress concentration factor (SCF) has been computed and compared fairly well with the experimental data and values from CIDECT guidelines (2001). The differences in the comparison are attributed to the notch effect.

Finally, local strain measurements from experimental data have been compared with numerical results, in an attempt to illustrate the deformed geometry of the chord member.

Simulation of in-plane bending

The same FE model has been used for the simulation of welded tubular joints under in-plane bending (monotonic and cyclic). The predictions of the model are in good agreement with the experimental measurements for both types of loading, as presented in Figure 57. Furthermore, the stress concentration factor has been evaluated and compared with the provisions of CIDECT No. 8 [17]. It is observed that the distribution of plastic deformations under this type of loading is widely spread along the circumference of the weld, which justifies the punching-shear failure observed in the experiments.

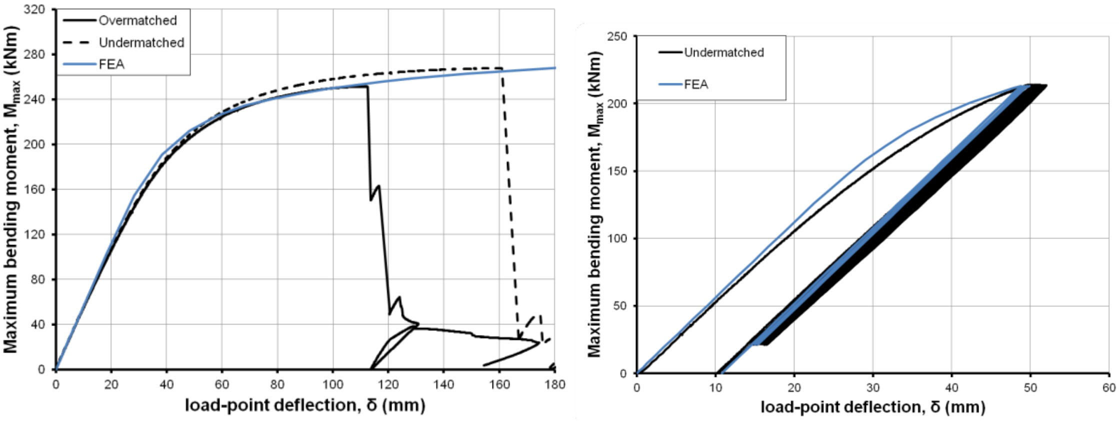

Figure 57 Analysis of welded tubular joints under in-plane bending moments - Comparison of the numerical and experimental load vs. displacement curves: (a) Monotonic loading, (b) Cyclic loading.

Simulation of axial loading tests

The predictions of the numerical model for axial loading of the joint are presented in Figure 58a. The most important observation is that the joint exhibits different behavior when subjected to axial compression or axial tension loads, as shown in the load-displacement curves. The deformed geometry of the joint under compressive loading is presented in Figure 58b.

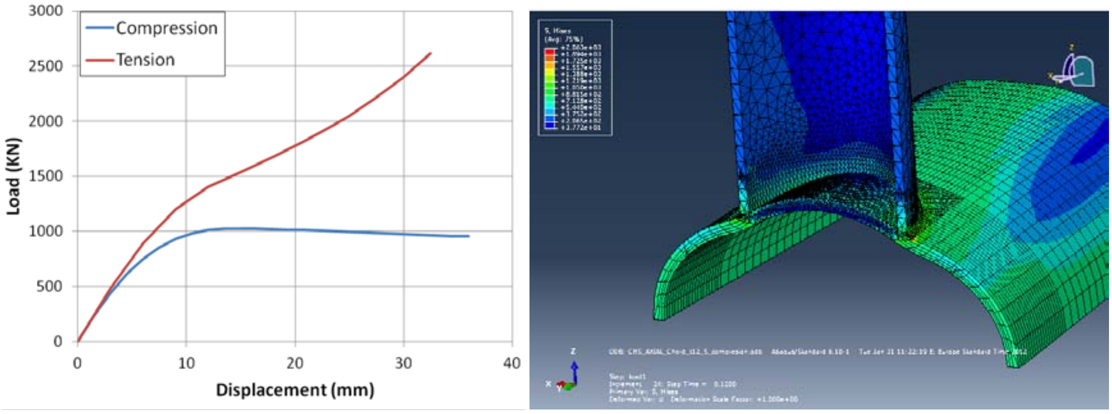

Figure 58 Numerical simulation of the X-joint subjected to axial compression and tension loading (a) Load-displacement curves and (b) deflected shape under axial compression.

With regard to definition of nominal, geometric and hot spot stresses used for low-, high-cycle fatigue loading, the reader can look at Figure 59.

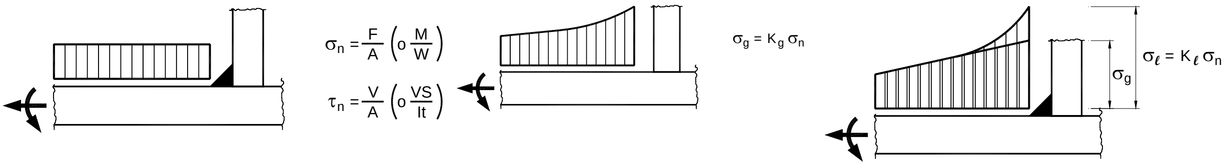

Figure 59 Stress near weld region-Eurocode 1993 Part 1-8 [14]

Relevant SNCF and SCF were computed according to indications shown in Figure 60 suggested in CIDECT Manual N. 8 [17].

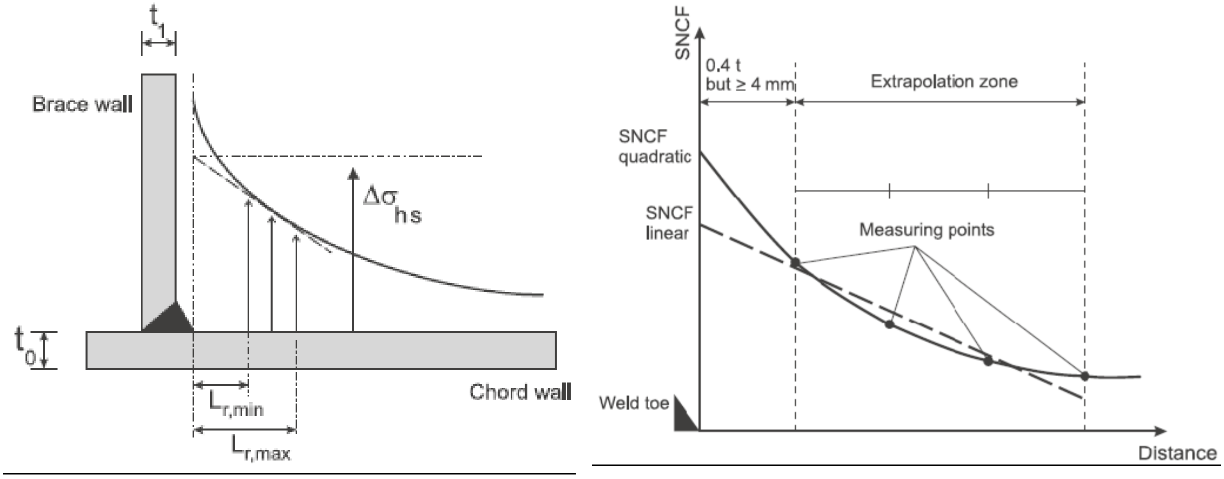

(a) (b)

Figure 60 Definition of extrapolation region and (b) Methods of extrapolation, after **[17]**

Task 5.3 Simulation of bolted connections and joints under strong repeated loading

This task aims to simulate the behaviour of the bolted joints under monotonic loading (load-displacement curves and failure modes), to simulate the hot-spot stress in critical zones (change of geometry) of the bolted joints and to simulate the behaviour of the bolted joints under repeated loading (hysteresis loops). The investigated joints were tested at Liège University and some experimental results is reported in WP4, Task 4.4.

A FE model is developed in LAGAMINE [53] software capable to reflect the full non-linear behaviour of elements subjected to great deformations, in order to simulate the behaviour of the joints. The main features of the proposed numerical model may be summarized as follows (see Figure 61):

- 3D solid element are used;
- Agerskov's conception for the bolt shank length [54] is adopted (see *Appendix E*);
- Plastic nonlinear material is introduced (natural ε-σ curves are used, see *Appendix E*);

- Geometrical nonlinearities (large deformation) are taken into account;
- Contact between the joint components (bolts-flanges, flange-flange) is modelled;
- Initial deformation of the flanges is included (see *Appendix E*);
- Geometry of the weld is introduced (but the weld material is assumed to have the same properties as the tube steel);
- Pre-stress in the bolts is considered;
- Monotonic and repeated loadings are simulated (see *Appendix E*).

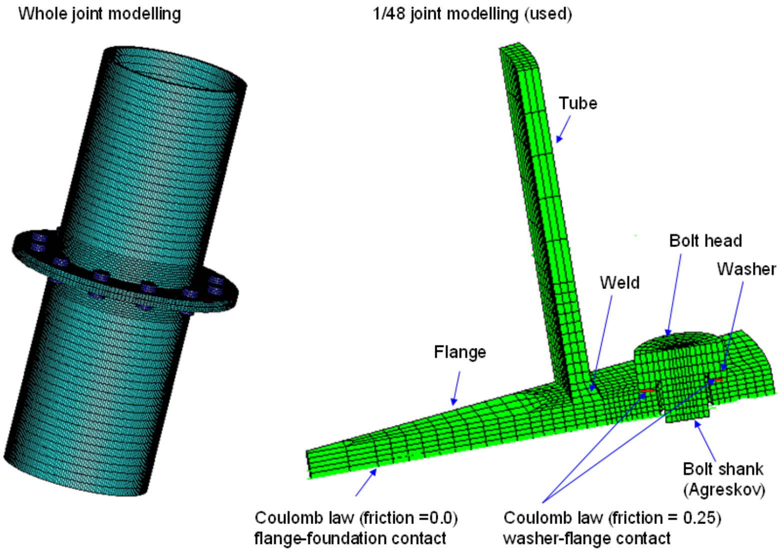

Figure 61 FE modelling for bolted joints

Concerning hot-spot stress studies, three different methods have been applied and compared; they are (more details can be found in Appendix E):

- Linear surface extrapolation method (LSE) [19]
- Through thickness at the weld toe method (TTWT) [20]
- Structural stress from the distance method (Dong's method) [21]

Numerical results have been compared with the test ones as shown in Figure 62, Figure 63 and Figure 64. It can be seen that a good agreement is obtained between numerical predictions and test results, in terms of: load-displacement curves, deformation/failure modes and hot-spot stress developments. Some differences for the value of stresses in bolts and on flanges (see Figure 64b and Figure 64c) are observed but with a limited impact as absolute values of these stresses are very small.

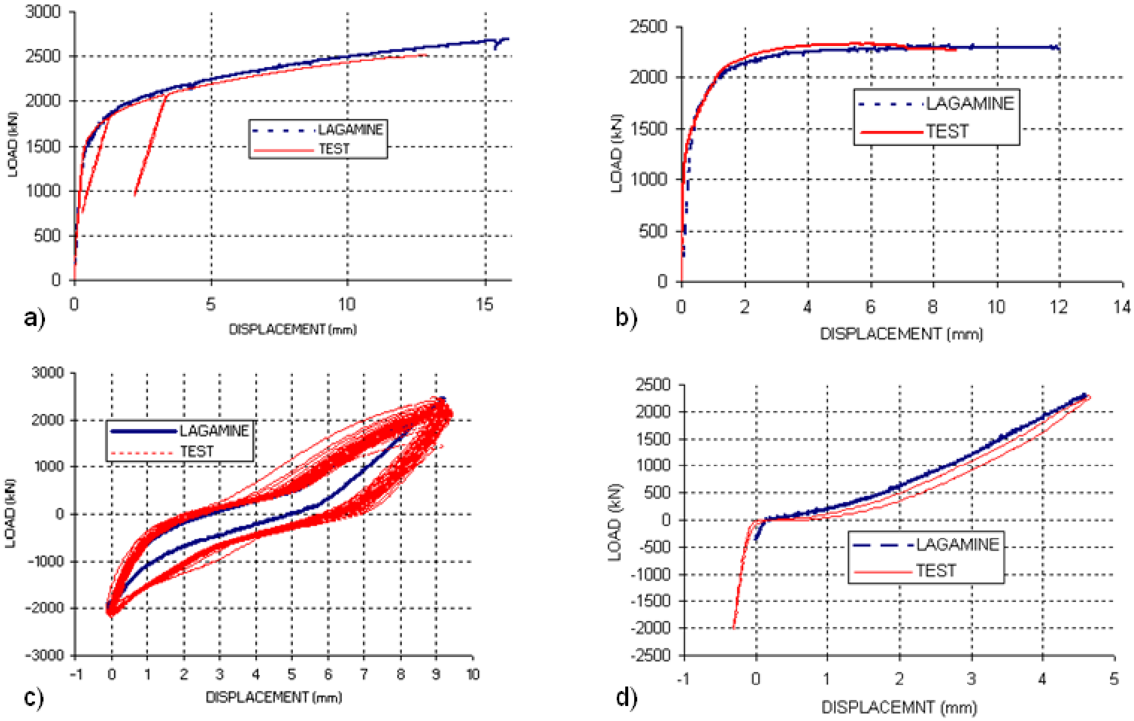

Figure 62 Comparison of the load-displacement curves for specimens M1 (a), M2 (b), L1 (c), L2 (d) respectively

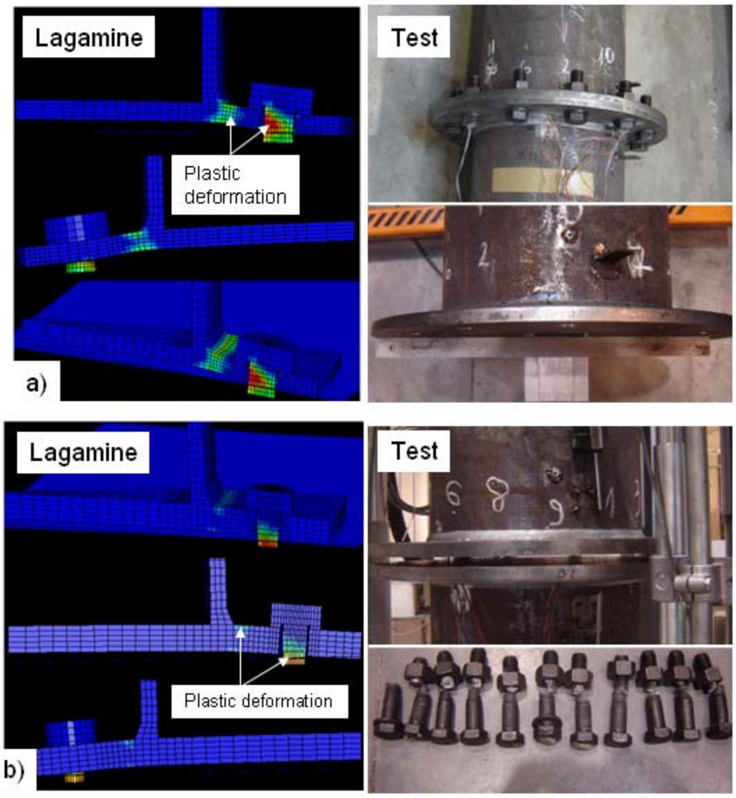

Figure 63 Comparison of the deformation for specimens M1 (a) and M2 (b) respectively

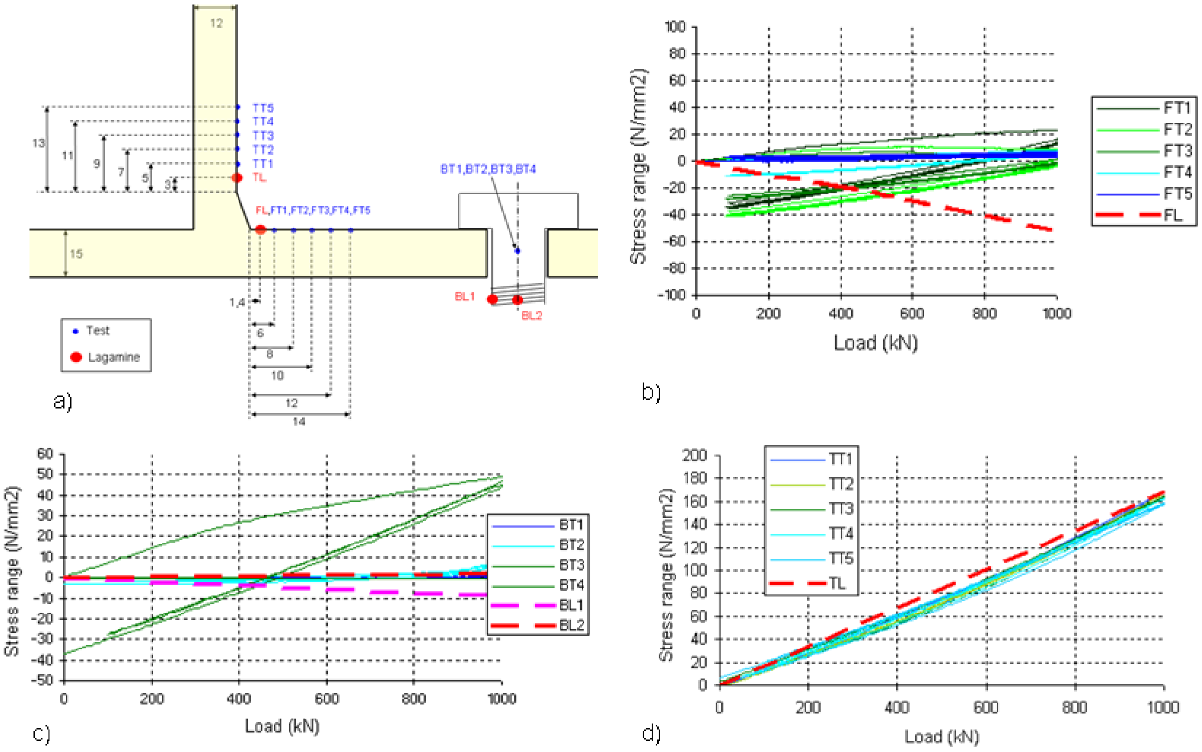

Figure 64 Comparison of the hot-spot stress: measured points (a) and stress development at the flange (b), the bolt (c) and the tube (d)

WP6: Numerical simulations of tubular members; parametric study

Objectives of the WP6 (Tasks 6.1, 6.2 & 6.3)

The main objectives of WP6 refer to Determination of S-N data for welded and bolted connections and refinement of the component method, Simulations of the behaviour of tubular members under strong repeated loading with FE codes and Simulation data on case studies and similar structural types

Activities and results obtained

Task 6.1 Determination of S-N data for welded and bolted connections and refinement of the component method

This task focuses on S-N curves and data for welded and bolted tubular connections under fatigue loading (low-cycle and high-cycle). The design of welded tubular connections can be conducted either with the “classification of details” method, as described in EN 1993-1-9 [16], section 8 (referring to a limited number of joint geometries), or with the “hot spot stress” method. It has been widely recognized that the use of the former method (classification of details) is rather inappropriate for the fatigue design of welded tubular connections. It is noticed that EN 1993-1-9 covers only a small range of possible joint geometries. On the other hand, the latter method (hot spot stress) is by far the most efficient method for the fatigue design of such joints. The hot spot method requires the calculation of the hot spot stress method, which is the maximum geometric stress at the vicinity of the weld. Subsequently, the fatigue design life is calculated though an appropriate fatigue S-N curve. CIDECT guidelines [17] present a complete procedure for hot spot stress fatigue design, and propose a concise methodology for the calculation of the hot spot stress at a specific welded tubular joint, either through special-purpose parametric equations for stress concentration factors (SCF) or a finite element analysis. Furthermore, they propose a fatigue curve, expressed as follows:

$$\log\left(N_f\right) = \frac{12.476 - 3\cdot\log\left(S_{rhs}\right)}{1 - 0.18\cdot\log\left(\frac{16}{t}\right)},\ \text{for } 10^3 < N_f < 5\cdot 10^6$$

$$\log\left(N_f\right) = 16.327 - 5\cdot\log\left(S_{rhs}\right) + 2.01\cdot\log\left(\frac{16}{t}\right),\ \text{for } 5\cdot 10^6 < N_f < 10^8$$

The above fatigue curve is applicable for high-cycle fatigue, i.e. for number of cycles greater than 1,000. In addition, all fatigue curves available in various specifications refer to high-cycle fatigue, whereas there is a lack of provisions for low-cycle fatigue design, where the structural component is loaded with repeated excursions well into the inelastic rage of material behavior. One simple way to extend the high-cycle fatigue curves to the low-cycle regime has been proposed by Ballio et al. [22], where an “equivalent elastic stress range” is introduced and a linear extension of the S-N curves in the log-log scale is proposed. Using this approach, the predicted number of cycles for the X-joints under consideration under out-of-plane bending is equal to $N_f = 69$, whereas the corresponding experimental results for the two tested joints are equal to 240 and 200 cycles for weld conditions A and B respectively (the weld metal of weld A has a lower ultimate strength). Furthermore, the predicted number of cycles for the same X-joints under in-plane bending is equal to $N_f = 128$, whereas the experimental results are equal to 976 and 669 cycles for weld conditions A and B respectively, as reported earlier [55].

In Figure 65 and Figure **66**, the experimental results are plotted in a fatigue graph together with the design fatigue curve proposed by CIDECT 8 and shifted for low-cycle fatigue. In the same graph the linear extension of the proposed curve in the low-cycle-fatigue range is presented with dashed line type.

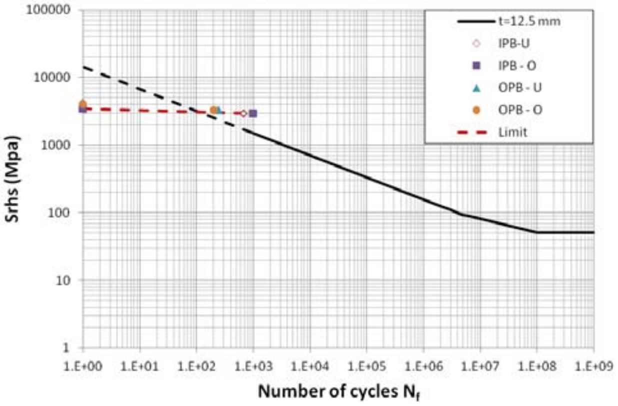

Figure 65: Hot-spot-stress method fatigue curve and experimental data

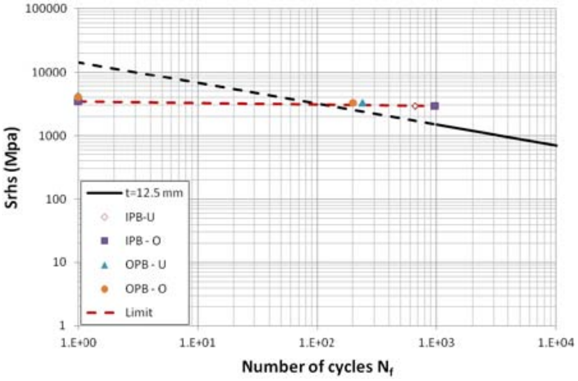

Figure 66: Fatigue curve and test data in the low-cycle regime.

The graphs above shows that the “equivalent elastic stress range” methodology provides reasonable, yet conservative predictions for the fatigue life of the specimens, compared with the experimental fatigue life for a number of cycles not less than 100. Taking into consideration the inherited safety margins in the design specifications, it can be concluded that the use of this design methodology in the low-cycle

fatigue range for a number of cycles not less than 100 results in safe predictions and can be adopted for design purposes [55].
The experimental results from monotonic tests indicate that in the fatigue area of 100 cycles and less, a nearly horizontal cut-off limit for the hot-spot stress needs to be considered (as shown in Figure 65 and Figure **66**). The development of such a curve at this very-low-cycle fatigue regime requires to be verified by more tests. In the absence of those tests, a proposal is presented in the development of design guidelines, in a subsequent section of the report. However, the cut-off effect owing to experimental monotonic data can be observed.

In the frame of HITUBES project a large set of high cycle fatigue data have been produced on tensile samples machined from girth welded HSS joints. Those tests have been performed in Task 4.1 with the aim to compare different possible joint conditions, in particular the following set of data have been produced:

- Overmatching (O) joint, where S590 columns are butt welded using a G79 consumable.
- Undermatching (U) joint, where S590 columns are butt welded using a G55 consumable.

A statistical analysis of fatigue data in terms of nominal stress ranges has been performed in order to compare the experimental S-N curves with the design S-N curve reported in the Eurocode 1993 Part 1-9 [16]. Fatigue mean S-N curves have been evaluated by a regression analysis in accordance with the ASTM standard [12]. Statistical analysis of fatigue data has been carried out according to the IIW recommendations [56]. The value of stress range corresponding to 2 million of cycles has been calculated with a 75% confidence level and a survival probability (P_s) of 95% (failure probability of 5%) as recommended in the Eurocode 1993 Part 1-9 [16]. Fatigue curve slope has been imposed to the constant value m equal to 3 as recommended by Eurocode 1993 Part 1-9 [16] for welded details subjected to axial loading. Main results are reported in Table 25. Both fatigue S-N curves with P_s = 50% and P_s = 95% and confidence level (CL) of 75% have been drawn in Figure 67.

Table 25 statistical analysis of fatigue data

Welded joint	constant slope (m = 3)		Standard deviation of log Δσ
	Δσ(2e6 cycles) [MPa]		
	P_s = 50%	P_s = 95%	
O	111	71	0.081
U	118	47	0.171

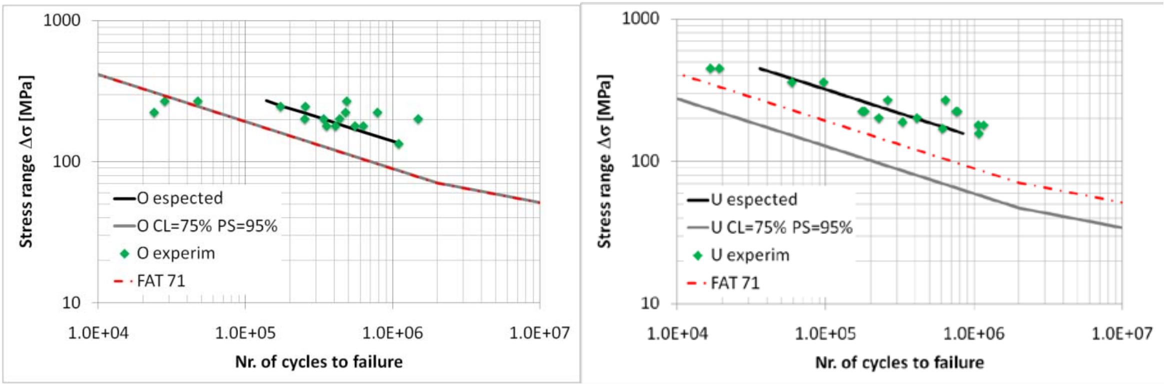

Figure 67 Overmatching (left) and Undermatching (right) joint fatigue curves

Main results of statistical analysis of fatigue data are reported herein.

- Fatigue strengths at 2 million cycles for a P_s= 50% highlight similar mean fatigue performance.
- Standard deviations both of Overmatching and Undermatching joint data differ; as a result, Undermatched joints exhibit a less favourable performance owing to larger dispersions.

- As a consequence of standard deviation fatigue strengths at 2 million cycles for a P_s = 95% (CL=75%) are quite different: fatigue strengths are 71 MPa and 47 MPa for O and U welded joints, respectively.
- Overmatched welding seems to give better fatigue performance.
- Category detail FAT 71 proposed in the Eurocode 3 (detail no. 13 of Table 8.3 in [16]) is consistent (Figure 67) with experimental data of O welded joints.

Bolted tubular connections with circular end-plate under fatigue

With regard to bolted connections two high-cycle fatigue tests were performed on specimens with flange thickness of 15 and 20 mm, respectively. Cracks happened always at the weld toe of tubes, and only for the ticker flange a bolt cracked too. FE simulations and the evaluation structural stresses based on the Dong's method, allow hot spot stress to be correctly evaluated in tubes, flanges and bolts; with regard to tubes, using "detail number 11" of Table 8.5 (full penetration, no request on Non Destructive Testing), detail 71 is adopted. Δσ (nominal stress) = Delta_load/tube area = 69,5 MPa. We can obtain the number of cycles = 2,1x10E6 cycles >> 0,96E6 cycles. It shows that "detail number 11" of Table 8.5 is overestimated by Eurocode 1993 Part 1-9 [16].

We used also "hot spot stress" and Detail 100 was adopted (full penetration weld); Δσ from the test = Δσ from numerical calculation = 140 MPa. We have number of cycles = 0,73E6 cycles < 0,96E6 cycles. We can say "hot spot stress" is on the safe side. The same situation is shown in the second test (configuration 2, M20). The concentration factor K_1 for the tube at the weld toe (in the two bolted joints of HITUBES) is about 2.0. This factor is about 3.0-4.0 in some other researches where the initial imperfection of the flanges was neglected. Note that many reseaches in the literatures propose to use the "hot spot tress" for the tube of flange bolted joints. With regard to bolts, from the tests, the stress ranges is not the same for bolts in each joint; bolt "BT3" completely failed – see Deliverable D4-. From these data, with Delta_force =600 kN, Δσ in the bolt (threaded portion) = 61 MPa. Using detail 50MPa, we have the number of cycles = 1,1E6 cycles. In fact, this bolt can resist more than 2,0E6 cycles. However, other methods to determine the stress in the bolts of bolted joints taking into account the prying effect, bending stresses, etc. are not yet available. With reference to flanges, Detail Category 100 is recommended for flange at the weld toe (full penetration weld). In tested joints, both experimental and numerical investigation show that stresses on flanges at the weld toe are very small owing to initial imperfection of flanges.

With regard to the analysis of the behaviour of flange bolted joints under low-cycle fatigue, the component method should be applied. For the case of monotonic loading, the application of the component methods for bolted joints has been developed [57] through the T-Stub approach – a basic component in Eurocode 3, part 1-8 [14]. In the case of repeated loading, from the test results (Task 4.4), it can be observed that the hysteretic loops of bolted joints are similar to the ones of T-Stub. Therefore, the T-Stub development can be again extended to the bolted joints. An analytical model for the T-stub under cyclic loading has been developed by Piluso et al [58], in which the cyclic behaviour of Tee-Stub is simulated from its geometrical and material characteristics. Therefore, it is suggested to extend the Piluso's model to bolted joints in the case of low-cycle fatigue loading. All formulas in [22] remain valid, the main difference is that the effective length of the yield lines in the failure modes should be introduced, in order to take into account the actual geometric shape of the bolted joints. With the circular flange bolted joints, the effective length $l_{eff} = \pi r_p$ (with r_p is the radius of bolt pitch circle) is proposed for both Mechanism 1 (i.e. full yielding of the circular plate) and Mechanism 2 (i.e. partial yielding of the circular plate and failure of the bolts).

Task 6.2 Simulations of the behaviour of tubular members under strong repeated loading with FE codes

Simulation of beam-column behaviour under monotonic loading

The simulation of CSM experiments on monotonic loading of CHS beam-columns has been performed with nonlinear FE models. The tube cross-section is denoted as type C, with nominal diameter and thickness equal to 193.7 mm and 10 mm respectively. The FE models employ shell elements, which are capable of describing rigorously the behavior of the CHS member, and account for nonlinear deformation and plasticity of the steel, through a linear kinematic hardening model (LKH). The material of the tubes is HSS, with a stress-strain curve measured experimentally from appropriate uniaxial tests, described in previous sections. Imperfections and residual stresses have been taken into account, based on the initial imperfection measurements that have been reported by CSM. Furthermore, an extensive parametric study on beam-columns with the above cross-sectional dimensions has been conducted. Representative results from the simulation of test data and from the parametric study are depicted in the *Appendix F*.

Simulation of CHS member behavior under cyclic loading

The four cyclic bending tests, conducted by CSM on specimens type A and type B, have also been simulated with finite element models, and focus on tests on CHS members of two cross-sections, namely cross-section A (∅355.6/12.5) and cross-section B (∅323.9/10). The measured cross-sectional characteristics of specimen type A and B are reported in Table 26, together with the actual geometric characteristics (mean values) are also reported, and have been used in the numerical simulations.

The specimens have been subjected to rotation-controlled bending loads (symmetric and non-symmetric) exceeding the elastic limit for each cross-section type. The two type A specimens failed after several loading cycles due to fracture near the connection of the specimen. The two type B specimens (thinner specimens) sustained a few cycles until local buckling took place.

Table 26 Summary of specimens with cyclic bending; measured dimensions

Test No.	Specimen	Cross-section	Measured diameter (mm)	Measured thickness (mm)	Loading type – Magnitude	Failure
1	AL	A	356.27	12.83	Symm. ± 8.3°	Fracture at the end
2	BL3-0	B	323.36	10.89	Symm. ± 9°	Buckling
3	AL3 -25	A	355.52	12.79	Non Symm. +8.6°/-6.2°	Fracture at the end
4	BL	B	324.75	10.88	Non Symm. +8.5°/-6.5°	Buckling

For the simulation of the conducted cyclic bending tests, detailed numerical models have been developed using 8-node solid elements with linear-hybrid formulation (C3D8H) and the mean measured geometrical characteristics presented in Table 26. The stiff connectors to hinges have also been simulated, and cyclic bending has been introduced by controlling end-rotations of each specimen. A key issue is the hardening of the cyclic plasticity model, so that the cyclic plasticity phenomena and the change of the cross-sectional geometry (ovalization) are captured. Herein, two von-Mises plasticity models have been used, the linear kinematic hardening (LKH) and the more advanced Tseng – Lee model (TL), which adopts the “bounding surface” concept and was implemented into ABAQUS through a developed user-subroutine (UMAT). The material model parameters have been properly calibrated based on the material cyclic-testing data, provided by CSM.

The comparison between the experimental and numerical results for Test No.2 is presented in Figure 68 for the moment-rotation relationship. In addition, the evolution of ovalization of the tube is also reported for both models adopted. The fitting between experimental and the numerical load-displacement loops is considered satisfactory for the both models, however, the predictions of the TL model are superior. The LKH model overestimates the range of the elastic behavior of the tube under reverse bending. Moreover, the evolution of ovalization according to the LKH model is also underestimated compared to the predictions of the TL model.

The analysis shows that all tubes, under cyclic bending with controlled curvature conditions develop an increasing ovalization pattern, which eventually may result in local buckling of the tube wall, as shown in Figure 69, for Test No.2. In the case of more thin-walled tubes of section B (i.e. Tests No.2 and No.4), the local buckling occurs in both analyses and tests. Nevertheless, if the tube is thick enough, then buckling might not occur and, instead, the accumulation of plastic deformation at the two tube ends may result in the development of low-cycle fatigue cracking near a weld connection, as occurred in both specimens of type A cross-section (i.e. Tests No.1 and No.3).

Simulation results for tubes with cross-section B have also been reported, considering symmetrical and not symmetrical moment-controlled cyclic bending in a moment level exceeding the elastic limit (yield moment) of the member. First, the specimen has been subjected to moment-controlled non-symmetric cyclic bending at the level +730/-600 KNm. The moment-rotation curves, and the evolution of ovalization evolution are presented in Figure 70, and indicate accumulation of plastic deformations, increase of cross-section ovalization, and – most importantly – a translation of the moment-rotation hysteresis loops, so that, after a sufficient number of cycles, buckling of the specimen takes place, in a form similar to the one presented in Figure 69. Finally, the case of not symmetrical moment-controlled cyclic bending has been also examined, with moment-controlled symmetric cyclic bending at ±730 KNm. Again, after a certain number of cycles, local buckling of the specimen occurs.

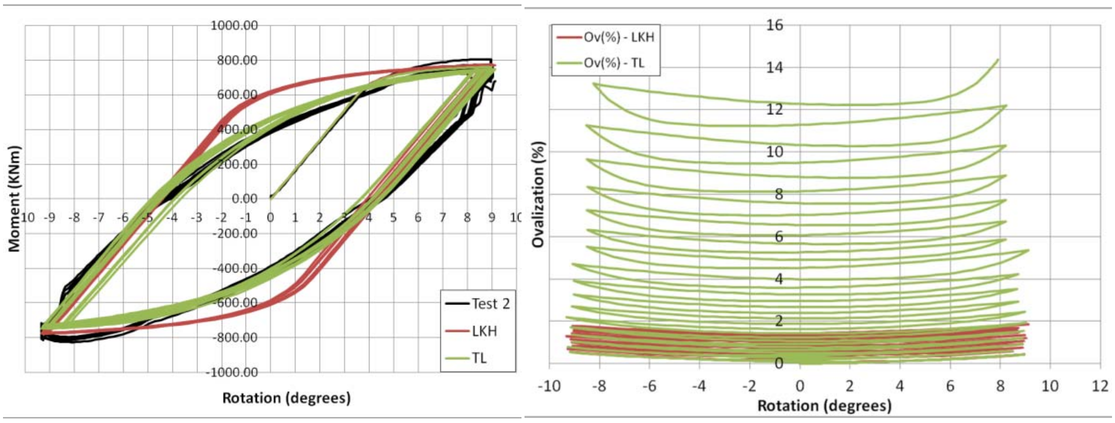

Figure 68: Test No. 2 – Cyclic moment-rotation loops and evolution of cross-sectional ovalization.

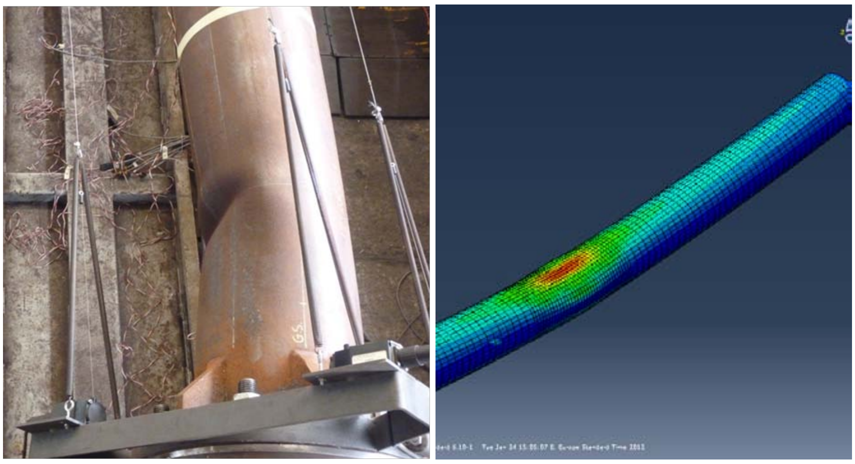

Figure 69: Local buckling shapes of Test No.2 (experimental and numerical) under strong cyclic loading.

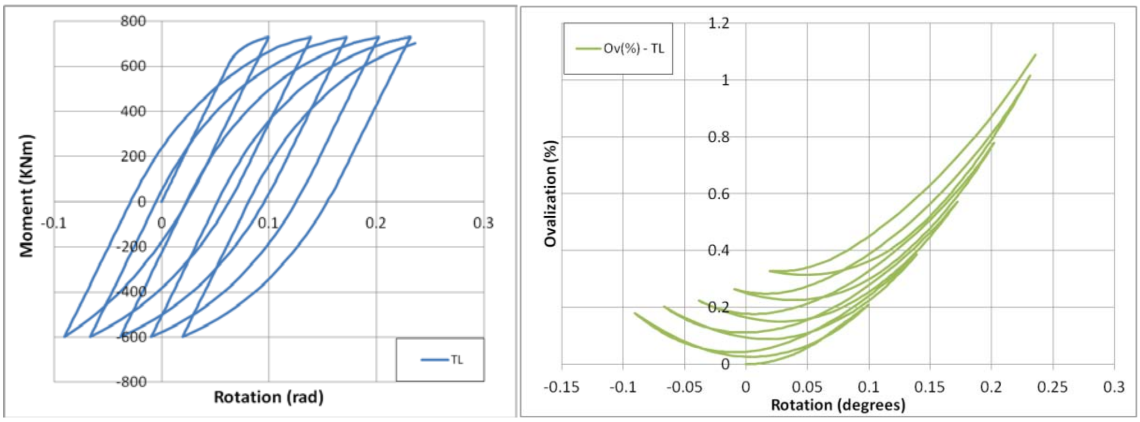

Figure 70: Cyclic moment-rotation loops under non-symmetric and evolution of cross-sectional ovalization

T6.3 Simulation data on case studies and similar structural types

Simulation on ‘Ponte del Mare’ footbridge

The modal properties estimated from the modal testing campaign of the ‘Ponte del Mare’ of Pescara footbridge did not match to that of the numerical model. In order to get a robust FE model capable to simulate the actual behaviour of the footbridge, the initial FE model was updated in the light of the experimental data obtained from the identification of the bridge. The sensitivity based model updating techniques and Powell’s Dog-Leg method of optimisation based on the Trust-Region approach were used. The sensitivity matrix was calculated and the 9 most sensitive parameters were selected. The final updated model showed a considerable reduction of errors relevant to frequencies. Figure 71 gives a visual representation of the first updated mode shape with MAC value 98.6.

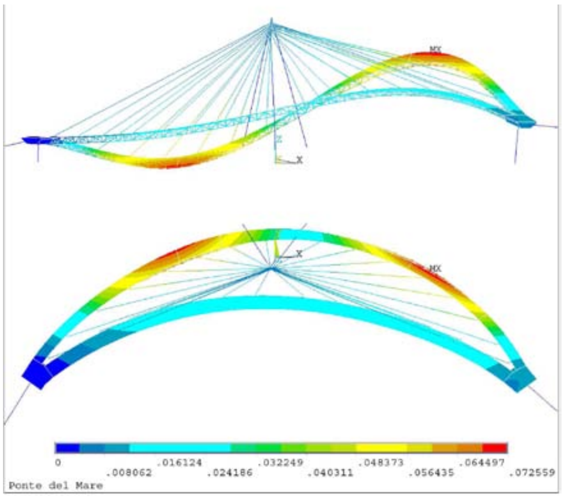

Figure 71 First mode of ANSYS correlated with 1st mode of experiment with MAC=98.6 of the ‘Ponte del Mare’ of Pescara footbridge

The updated FE model was used to reproduce the acceleration response under the actual wind recorded on 25/12/2009 to check the applicability of the model. The mean wind speed near the deck was considered 16.19 m/s, i.e. an average of the measurement obtained from the two anemometers one below the deck and other on the top of the mast. Figure 72 presents the acceleration response obtained after the execution of the analysis on the model without the dampers while that with the connected dampers is shown in Figure 73. From the figures it can be concluded that the updated model well reproduced the response of the footbridge under an actual wind loading condition characterized by an average velocity of 16.19 m/s. Moreover and in the case of dampers, it underestimated the acceleration response with respect to the one obtained from measurements. This was due to the fact that, in reality, dampers are characterized by slack up to displacements of 4 mm.

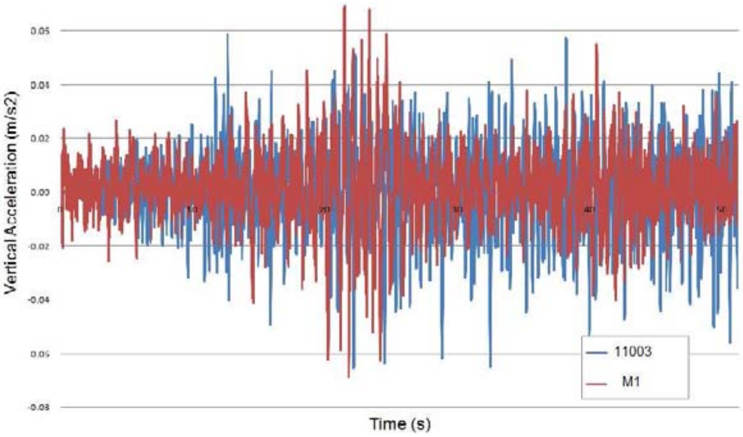

Figure 72 Comparison between the acceleration recorded at M1 with the vertical acceleration at node 11003 of ANSYS model without dampers

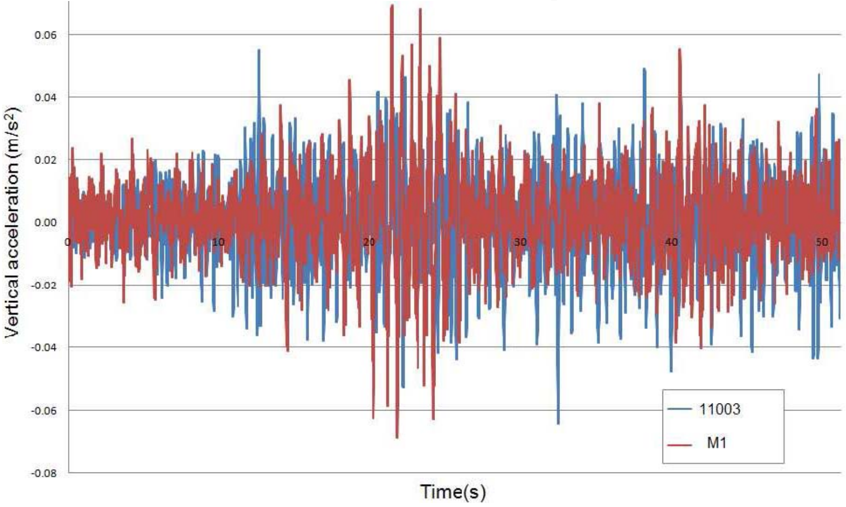

Figure 73 Comparison between the acceleration recorded at M1 with the vertical acceleration at node 11003 of ANSYS model with dampers

Fatigue due to pedestrian loads on footbridges

Footbridges are subjected to vibrations caused by the human walking, which is mainly a dynamic load and may induce relevant oscillations which may compromise the functionality of the structure. This dynamic nature of the load might cause fatigue damage to steel structural members. Safety problems due to overstressing or high-cycle fatigue may also occur and should also be considered in the design of footbridges, see HIVOSS 2008 [2]. In this respect, high-cycle fatigue checks with respect to pedestrian loadings on three footbridges were performed. For high-cycle fatigue analysis, EN 1993-1-9 [16] and for pedestrian loading the ‘Technical Guide Setrà’ [23] were used. In the ‘Technical Guide Setrà’ it is possible to find information about the pedestrian load model and a methodology for dynamic analysis for vibrations due to human walking. For fatigue analysis we adopted this formulation of pedestrian load, because in the EN 1991-2 [46] is explicitly said that the load model given in that section are not applicable for fatigue limit state. The general steps for the fatigue check were followed in the following order: (i) determination of loading events, (ii) stress history at details, (iii) cycle counting, and (iv) fatigue life verification. The simulations and fatigue checks were performed on three case studies, i.e. Ponte del Mare of Pescara, S. Michele and Nomi footbridges, shown in Figure 5a, Figure 74a and Figure 74b respectively.

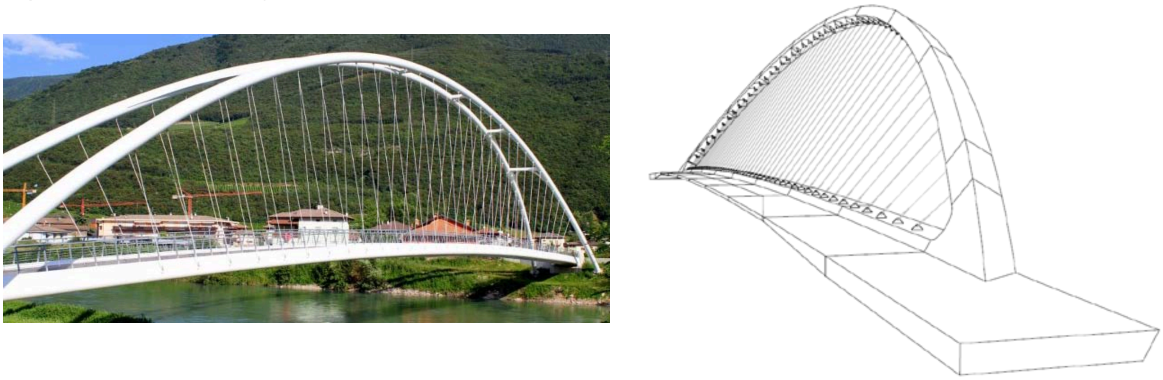

Figure 74 a) Footbridge ‘S. Michele’ and b) Footbridge ‘Nomi’

A stress history at one of the arch-arch welded joint mode 2VH of the ‘Nomi’ footbridge is shown in Figure 75.

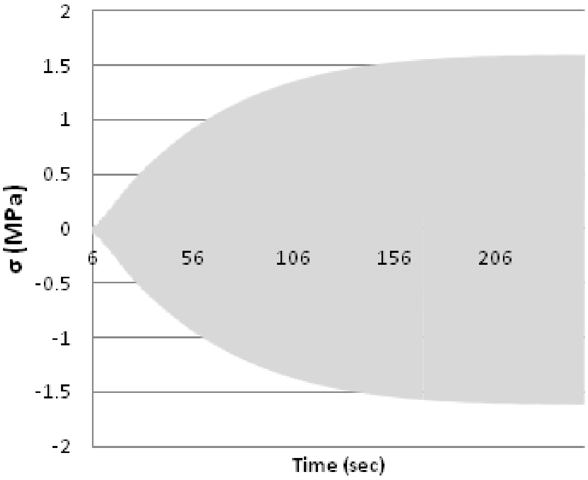

Figure 75 Stress history of the arch-arch welded joint Mode 2VH of the ‘Nomi’ footbridge

The endurance number of cycles (N_R) can be calculated on the basis of the Wöhler curves, given in the UNI EN 1993-1-9 [16] where:
$\Delta\sigma_C$ is the fatigue strength at 2 million cycles for the detail category considered
$\Delta\sigma_R$ is the stress range in the detail
m is the slope of the Wöhler curve

If a structural detail entails stress range values smaller than the cut- off limit, i.e. it is found that $\Delta\sigma_{dyn} < \Delta\sigma_L$ and $\Delta\sigma_{stat} < \Delta\sigma_L$, this is not sensitive to the fatigue.. The fatigue assessment is made through damage verification according to the Palmgren-Miner formula:

$$D = \sum_i \frac{n_i}{N_i} < 1$$

where n_i, is the number of cycles for each $\Delta\sigma_i$ and N_i is the endurance (in cycles) obtained from the S-N curve for a defined stress range $\Delta\sigma_i$. Moreover, UNI EN 1993-1-9 states that below the cut off limit N_i is equal to 10^{20}. Therefore, if all stress ranges for footbridge details show that $\Delta\sigma_E < \Delta\sigma_L$, so they do not give a relevant contribution to the damage of details. The simulations and fatigue checks performed on three case studies, i.e. Ponte del Mare of Pescara, S. Michele and Nomi footbridges resulted that none of the footbridge was prone to fatigue problems owing to pedestrians. Therefore, we can conclude that in general, footbridges don’t exhibit fatigue problems due to pedestrians loading. Hence, fatigue checks due to pedestrians are not needed.

WP7: Development of design guidelines and recommendations for high strength tubular structures

Objectives of the WP7 (Tasks 7.1, 7.2, 7.3, 7.4 & 7.5)

The main objectives of WP7 refer to: Development of design guidelines for High Strength Steel for onshore structures under extreme loadings; Development of design guidelines and recommendations for welded connections of onshore structures; Development of design guidelines and recommendations for bolted connections of onshore structures; Development of design guidelines and recommendations of onshore tubular structures under extreme loadings; Time dependent reliability assessment and Bayesian estimate.

Activities and results obtained

7.1. Development of design guidelines for High Strength Steel for onshore structures under extreme loadings

The part 9 of the “EN 1993-1-9: Eurocode 3. Design of Steel Structures” [16] defines fatigue strength curves for design based on experimental testing performed in accordance to EN 1990. The Standard uses the concept of “Reference fatigue strength” as the constant amplitude nominal stress range ($\Delta\sigma_c$), for particular details of joints, that corresponds to an endurance of $N=2\cdot10^6$ cycles. In the case of the HITUBES project, the constructional detail of hollow sections and transverse butt welds are in accordance with the geometry of the specimen tested. With reference to transverse butt welds of sample coupons extracted by CHS subject to fatigue and considering a 75 per cent confidence level with survival probability of 95 per cent -typical reliability values used in Eurocode 1993 part 1-9- details categories with nominal stresses are 71 MPa and 47 MPa for Overmatching and Undermatching weldments, respectively. Because the Detail Category suggested by Eurocode 1993 Part 1-9 is 71 MPa, overmatched welds provide better fatigue performance. Nonetheless, we have to note that only nominal stresses were considered here. Moreover, it must be noted that Eurocode 1993 part 1-9 confuses hot spot stresses with geometrical stresses and tends to underestimate Stress Concentration Factors.

In terms of toughness, there are other variables to consider apart from the mismatch effect as for example the weld width, the crack length and the plate thickness. As it is demonstrated in Appendix G for this WP7, for a long crack (a/W=0.5) and WPS defined in this project, the variable to consider for toughness evaluation is just the mismatching effect and not the geometry. The fracture toughness results for TS590J2H provide a sharp decrease of the value from 440 KJ/m2 in the base metal to 136 KJ/m2 in the case of more ductile undermatching condition and to 90 KJ/m2 in the case of the overmatching condition. In both cases, there is a stable crack growth and no critical propagation is achieved. It is concluded that in terms of toughness, undermatching condition is preferred although overmatching is not excluded.

Besides beneficial physical and mechanical properties, the corrosion resistance of the selected HSS grade is of essential importance also in onshore applications. It is stated in WP4 that HSS steel materials TS590J2H and S355J2 are sensitive towards stress corrosion cracking in presence of cathodic polarisation. Furthermore it is also stated that the susceptible to stress corrosion cracking is higher for the weld metal than the base metal. The heat affected zone that arises during welding is also more susceptible to stress corrosion cracking than the base metal but lower than the weld metal.

Task 7.2: Development of design guidelines and recommendations for welded connections of onshore structures

In welded tubular connections, failure usually occurs in the form of cracks at a discontinuity or stress raiser, associated with a microscopic defect at the weld toe. As a result, the cracks (under monotonic or fatigue loading) initiate at these locations irrespective of the steel grade. Higher grades of steel can be used, they improve the static strength of the joints, but do not necessarily improve the deformation capacity or the fatigue strength. CIDECT Design Guides No. 1 [] and 8 [17] present typical weld details at the main locations of welded tubular connections constructed with circular hollow sections. More extensive information on the detailing of those joints can be found in the AWS Welding Code [15] that was used too. Weld start/stop positions for non-continuous welds should not be located at points of high stress concentration (crown and saddle points), since these can themselves cause stress concentrations. Various methods of improving the fatigue resistance of welded connections are available. They result in a change in the weld geometry to minimize weld defects and stress concentrations, or to reduce the tensile residual stresses in the joint.

Welding results in residual stresses due to material cooling which value is about the same of the yield strength of the weld metal. In the toe of the weld there are three discontinuities present at the same time and local. There is a metallurgical discontinuity between parent metal and weld metal structures, discontinuity in stress levels and geometrical discontinuity. This combination affects the local fatigue behavior. Various methods of improving the fatigue resistance of welded connections are available. Mechanical peening mainly introduces compression stresses in the toe of the weld that will reduce the balance of tensile stresses resulting from external actions. Mechanical peening can be applied by using sand blasting, hammer needle and Ultrasonic Impact Treatment). UIT, used in the project, introduces both compressive stresses and also increases the toe radius). The application of a rotating burin is also used to obtain a small rounded groove in the weld toe Also Laser re-melting or TIG dressing of the weld toe are available and are proficient in smothering the transition of the weld to parent metal.

As far as toughness is concerned, it was observed lower impact values for electrode G79 (overmatching base material) than expected for that wire although the actual values were accepted from a structural point of view. These impact values could be higher, if necessary, by increasing the content of CO_2 % in the shielding gas.

With regard to static strength the design provisions of EN 1993-1-8 (2002) [14], which are identical to those proposed by the CIDECT Manual [17] for plastic resistance, are used for predicting the joint capacity under axial load or bending loading. The results of the present study have demonstrated that the static strength equations in the above two specifications can be used for design purposes. Nonetheless, it should be noted that EN 1993-1-12 (2009) [29] introduces a reduction factor equal to 0.8 for the steel grade under consideration. Experimental results from the present study indicate that for overmatched welds in the range considered the use of this reduction factor is not necessary. The present results indicate that – for overmatched welds within the range considered in the present investigation – the increase of the grade of the weld metal, results in a reduction of the deformation capacity of tubular joints under monotonic loading conditions.

Existing high-cycle fatigue design tools for welded tubular connections have been developed for ordinary steel grades up to 460 MPa, whereas tubular joints made of HSS are not covered by any international design code. Furthermore, EN 1993-1-9 (2002) [16] provisions for welded tubular joints adopt the "classification of details" method, which is not applicable to the majority of tubular X-joints because the nominal stress is not accurate. For out-of-plane bending low-cycle fatigue tests of X connections carried out in Task 4.2, the Strain Concentration Factor (SNCF) numerically estimated was equal to 7.18, higher than the experimentally evaluated value. According to CIDECT guidelines [17], the corresponding Stress Concentration Factor (SCF) for the connection under exam was equal to 9.82, whereas the numerical model entailed a SCF value equal to 6.16 using a linear extrapolation and 8.19 using a quadratic extrapolation suggested by Romeijn [18]. The above differences are attributed to the sensitivity of the strain/stress field near the weld toe owing to local conditions (notch effect).

The fatigue design of welded tubular connections in the low-cycle fatigue regime is an area not considered in current design practice. We extended high-cycle fatigue curves to low-cycle regime by a method proposed by Ballio et al. [22]; an equivalent elastic stress range was introduced and a linear extension of the S-N curves in the log-log scale was made. Using this approach, the experimental number of cycles for the X-joints under consideration both for out-of-plane bending and in-plane bending endowed with overmatching and undermatching welds were beyond S-N data suggested by CIDECT manual [17]. A large set of high cycle fatigue data were produced on tensile sample coupons machined from girth welded CHS connections. Those tests were performed in Task 4.1 both with Overmatching where TS590J2H elements were butt welded using a G79 consumable and with Undermatching (U) where TS590J2H elements were butt welded using a G55 consumable. Values of stress range corresponding to 2 million of cycles were calculated with a 75% confidence level and a survival probability of 95% as recommended in Eurocode 1993 Part 1-9 [16]. Both Overmatching and Undermatching specimens satisfy the Detail Category 71 of Detail 3 of Table 8.6 – or Detail 13 of Table 8.3 - and Overmatched weldments provide a better fatigue performance.

Task 7.3: Development of design guidelines and recommendations for bolted joints of onshore structures

Combining the literature review and the experimental and numerical results of the present project the following conclusions can be drawn for the design guidelines to be recommended for bolted joints with circular flanges. With reference to monotonic loading the following methods have been considered: Igarashi method [59], Cao and Belle method [60] [61], Eurocode method [62] and Couchaux method [63]. With regard to the estimation of the plastic failure capacity of the considered joints, all above-mentioned methods are conservative; the observed differences between the method predictions and the experimental results are in a range of 4%-40%. The predictions given by Eurocode method are the most accurate one.

With reference to high-cycle fatigue loading, through the preformed investigations it has been demonstrated that the use of "detail number 11" of Table 8.5 in Eurocode 3, part 1-9 (calculating the fatigue strength of the tube at the weld toe) [16] leads to an overestimation of the fatigue strength, which is unconservative. Therefore, it is suggested to use the hot-spot stress concept for this detail. The latter can be estimated through finite element analyses or through analytical methods using stress concentration factors to take into account stress concentration. With this method, it has been demonstrated that a conservative prediction of the fatigue strength can be obtained. The detail number 14 in Table 8.1 of Eurocode 3, part 1-9 [16] may be used to calculate the fatigue strength of the bolts, but the stress range in bolts should be estimated in two steps: (i) using finite element method to computer the stress in the bolts and (ii) applying the "Through thickness at the weld toe" method (see Deliverable 5.3) to calculate the structural stress that may be considered as the "nominal" stress, taking into account the bending and pre-stress effects as requested in Eurocode 3, part 1-9. Detail category 100 as proposed in Eurocode 3, part 1-9 [16] can be applied to estimate the fatigue strength of the flanges at the weld toe. The "Through thickness at the weld toe" method (see Deliverable 5.3) or "Structural stress from the distance" method (i.e. Dong method, see Deliverable D5.3) should be adopted to capture the stress ranges from the stress given by finite element models. The initial deformation of the flanges due to the heat-affect during the weld procedure significantly influences to the stress range on the tubes and on the flange. Therefore, the initial deformation should be taken into account in the finite element modelling if an economic design is needed. As far as low-cycle fatigue loading is concerned, for bolted joints with circular flanges, it is suggested to extend the model of Piluso [64] initially developed for the modelling of T-stubs.

Task 7.4: Development of design guidelines and recommendations of onshore tubular structures under extreme loadings

The behavior of tubular members under extreme cyclic loading conditions, with emphasis on bending, has several particularities that should be recognized by the design engineers. Nevertheless, modeling of those particularities is a demanding topic that requires high-performance computations with advanced numerical tools. The main characteristic of the structural behavior of tubular members under strong cyclic loading, associated with significant inelastic deformations of alternative sign, is the accumulation of plastic deformation. More specifically, the response of a steel tube under monotonic loading defines the maximum bending moment of the tube, and the corresponding deformation capacity. If one considers cyclic bending of the tube in the inelastic range, but within the load and deformation limits defined for monotonic conditions, the tube might not be safe. Under this repeated loading, accumulation of deformation occurs, resulting in excessive strains and eventually in the formation of local buckling of the tube wall or – in a few cases – fracture of the tube near the two ends. To investigate the above structural behavior, it is important for the designer to identify whether the tubular member is subjected to load-controlled or deformation-controlled action. Experimental data and numerical results have shown that in both cases, the accumulation of deformation in the tubular member may result in failure in the form of bucking or fracture. Nevertheless, it has been recognized that cyclic load-controlled conditions about a non-zero mean load value is the most dangerous case, where maximum curvature may increase rapidly resulting in significant strain amplification and member failure, together with a progressive increase of cross-sectional ovalization [65].

Members under axial compression plus bending develop specific load-carrying behaviour in the different ranges of slenderness. Depending on the emphasis given to the different ranges, different concepts of interaction formulae have been proposed in the past. The present approach of EN1993-1-1 [30] is based on the linear-additive form of interaction formula derived from linear-elastic buckling response, where the effect of the axial force and the bending moments are linearly summed and the nonlinear effects are accounted for by specific interaction factors. Latest version of the Eurocode 1993 Part 1-1 has incorporated some new design formulae that enable a more economic design. This is particularly the case for the rules for the verification of members subjected to combined bending and compression. Moreover Part 1-12 of Eurocode 3 has been recently published that extends its scope to strength grades up to S700. Part 1-12 gives a few changes and some additional rules to the already existing parts of Eurocode 3 in order to make them applicable to steel grades up to S700.

In the frame of this project an HSS CHS is studied which nominal dimensions are 193.7mm in diameter and 10mm in thickness. Considering actual mechanical properties of columns (f_y = 694 MPa; D/t = 19.4) the cross section is classified as Class 2 in accordance with EN 1993-1-1 [30] while considering nominal strength (f_y = 590 MPa) a Class 1 is concerned.

Full-scale tests have been performed at two different column lengths

- Short (member slenderness 28.4) relevant for cross sectional behaviour
- Long (member slenderness 74.6) relevant for member behaviour

The outcome of experimental data (Task 3.3) are compared with Eurocode 3 predictions in the N-M interaction diagrams in Figure 76. The EC3 predictions are calculated following both methods presently reported in the standard, namely Method 1 (m1) and Method 2 (m2). The experimental results are on the boundary safe side of the interaction diagrams indicating that recommended formulae are consistently extended to HSS members for the slenderness range investigated.

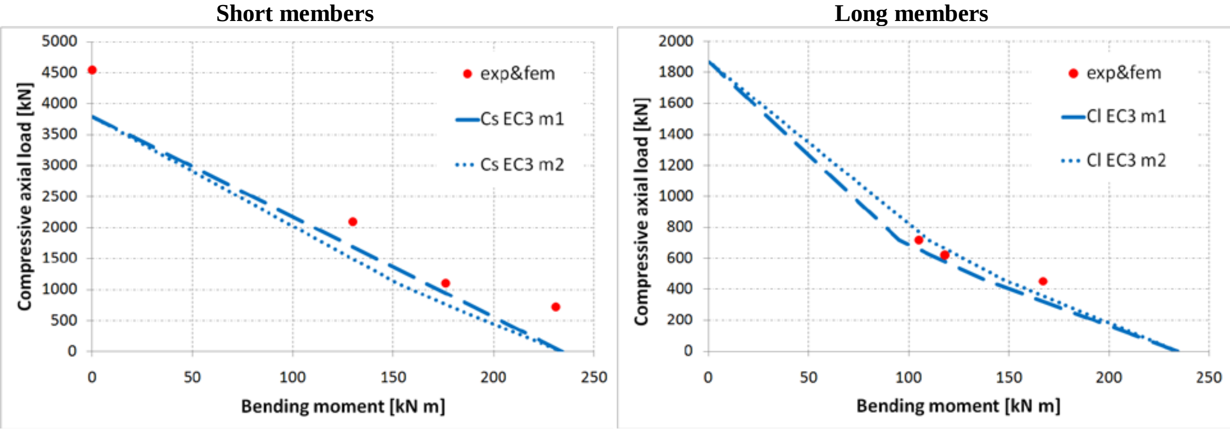

Figure 76 HSS CHS interaction M-N diagram: comparison between Eurocode 3 design recommendations and experimental results

Experimental data and FE analyses outcomes are in this section presented in a form to make it consistent with Eurocode 1993 part 1-1 interaction formulae. In particular second order moment imposed by extensions of the testing machine are explicitly reported.

Task 7.5 Time dependent reliability assessment and Bayesian estimate

The Ponte del mare of Pescara redesigned with tubular sections offered us two possibilities: on one hand both with identification and numerical data, we had the possibility to check and employ several indications provided by Eurocode 1993 Part 2 for steel decks and Eurocode 1991 Part 1-4 and Eurocode 1993 Part 3-1 for masts of Ponte del Mare with reference to along-wind and vortex-shedding wind loadings; on the other hand, we estimated the safety of the footbridge decks by means of the calculation of the reliability index β -or the probability of failure P_f-, followed by Bayesian updating techniques that use both prior information and new inspection information to account for the relative uncertainty associated with each.

Structural aging may cause the integrity of structures to evolve over time (e.g., a hostile service environment may cause structural strength and stiffness to degrade). Any evaluation of the reliability or safety margin of a structure during its service life must take into account the uncertainties. Time-dependent reliability analysis methods provide the framework for dealing with uncertainties in performing condition assessment of existing and aging structures, and for determining whether in-service inspection and maintenance is required to maintain their performance at the desired level [41]. Bayesian updating techniques are very useful when faced with two sets of uncertain information and a planner needs to know which to believe. Bayesian updating uses both the prior information and new inspection information to account for the relative uncertainty associated with each [42].

Several studies in the past have shown that the reliability of the bridge decks depends significantly on the rate of corrosion of the steel [42] [43] [44]. The safety of the system as a whole can be defined by the safety of each component, deck, girders, piers, etc, and how each component interacts within the system. The safety of the deck components, such as tubular truss sections and connections of the footbridge Ponte del Mare of Pescara, are the focus of this investigation.

Fig.2 3D section of the deck of the footbridge with CHS trusses.

Limit states for the reliability of the footbridge

The performance or reliability of a structural system can be evaluated based on different limit states, most notably safety and serviceability limits. Both the safety and serviceability can play a significant role in determining the reliability of a structure; this investigation considers both limit states.

Ultimate/Safety Limit State

Safety margin, $SM = R - S \geq 0$

where R= capacity or strength, S= demand or stress.

Serviceability Limit State

Deflection, $\delta \leq L/500$

Deck Rotation, $\theta \leq 5.48\% \rightarrow$ corresponding to 21 cm of lateral deck deflection

General corrosion model

The resistance of the structure changes due to the reduction of cross-sectional area of tubular steel trusses under corrosion assumed at the outer surface. At any time t, the reduced section area A(t) of a tube truss is given by the following Equation

$$A(t) = \frac{\pi}{4} \cdot \left[[D_0 - 2 \cdot r_{corr} \cdot W \cdot N \cdot (t - T_{corr})]^2 - {D_i}^2\right] \qquad \text{Eq(1)}$$

where A(t)= area of a truss at time t (mm^2), t= time (years), D_o and D_i = outer and inner diameter of tube under corrosion (mm), T_{corr}= corrosion initiation time (years) – 10 years, r_{corr}=corrosion rate (mm/year) – 0.058 mm/year -, W= a weight coefficient taking into account the global positioning of the trusses w.r.t the sea canal; and N is a random number between 0 and 1 to consider the spreading of corrosion along each member – 0 implies no corrosion; 1 implies complete corrosion along a member -.

Simulations in ANSYS and main results

Simulations were performed for 5 to 50 years on the numerical model in ANSYS using Monte Carlo Simulation (MCS) technique and Latin hypercube sampling to accelerate convergence. Two hundred (200) iterations were run for each analysis. The input and output parameters used as random variables are given in Table 27. Two types of loading conditions were considered, i.e. with the wind and without the wind.

Table 27 Random parameters and chosen distributions

Type of parameters	**Name of the parameter**	**Type of random distribution**
Input parameters	Corrosion start time, T_{corr}	Lognormal (Type1)
	Corrosion rate, r_{corr}	Gaussian
	Yield strength of steel, f_{ys}	Gaussian
	Pedestrian load (live), A0	Weibull
	Wind speed (live), U	Weibull
	Local variability, N	Uniform
Output parameters	Safety margin, SM	Gaussian
	Deflection, δ	Gaussian
	Rotation, θ	Gaussian

The time dependent variation (reduction) of the safety margin is shown in Figure 77. The time dependent behavior of displacement and rotation is described in *Appendix G*.

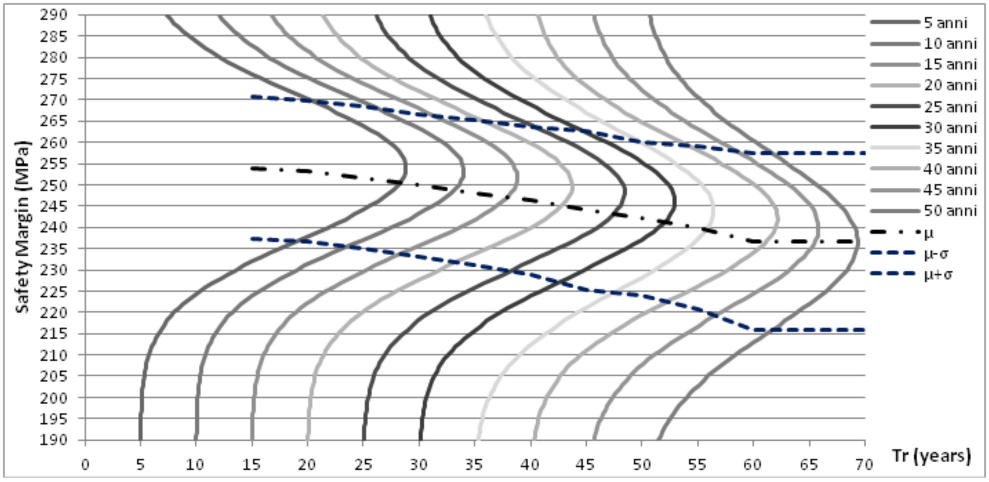

Figure 77 Safety margin (MPa) of the footbridge deck without wind

Reliability index and probability of failure

A convenient method for describing the safety of a structural component or system is with the reliability index β, or the probability of failure P_f. According to the Annex C of the Eurocode '0' [66], the β and the P_f are related as:

$$P_f = \Phi(-\beta) \qquad \text{Eq(2)}$$

where Φ is the cumulative distribution function of the standard normal distribution.

The limit states of the maximum deflection- that should be less than L/500, and the limit state of the safety margin- that should be greater than 0, are satisfied. However, the calculations and the graphs showed that the maximum rotation doesn't satisfy the limiting rotation value of 5.48%. Therefore, we shall calculate the time dependent reliability evolution for the maximum rotation limit state.

The P_f and β are plotted with time for the rotation limit state in Figure 78 and Figure 79, respectively for the live load with and without considering the wind. In Figure 79, the limiting value of β is drawn from the Annex C of the Eurocode '0' [66] that means that β should be greater than 1.5 at 50 years.

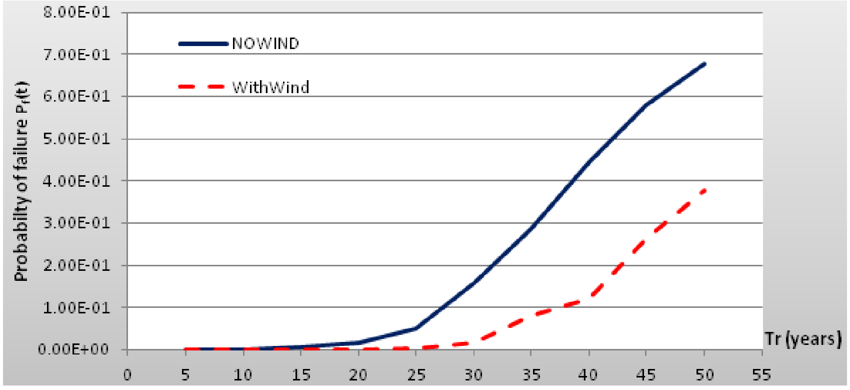

Figure 78 Time variation of probability of failure of the footbridge

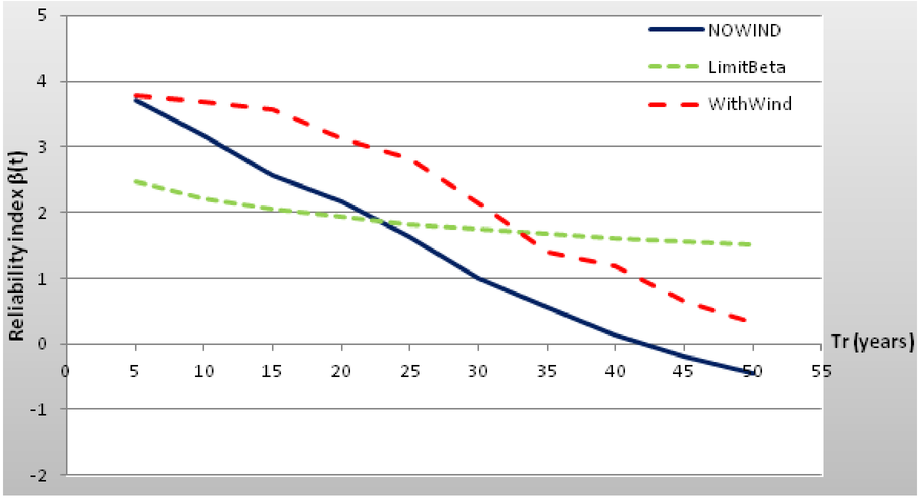

Figure 79 Time variation of reliability index of the footbridge deck

The value of β crosses the limiting value at about 23 years and 33 years for the case without and with wind. This shows that wind acts to increase the reliability of the footbridge structure owing to lifting effects. Moreover, the decision should be based on the critical case i.e. without wind. Therefore, the repair and/or retrofit plan should be activated before 23 years of the life of the footbridge to increase its reliability index.

Bayesian estimation

Bayesian updating techniques are very useful when faced with two sets of uncertain information and a planner needs to know which to believe. Bayesian updating uses both the prior information and new inspection information to account for the relative uncertainty associated with each.

$$f''(\Theta) = kL(\Theta) f'(\Theta) \qquad \text{Eq(3)}$$

where $L(\Theta)$= likelihood function; $f'(\Theta)$ is the prior distribution, and k= normalizing constant.
We used the distribution of input parameters r_{corr}, T_{corr}, N, W, U and A_0. Moreover, if the new data would arrive, the posterior distributions of these inputs would provide $L(\Theta)$ and so $f''(\Theta)$ will change according to Eq. (3). Footbridge of 'Ponte del Mare' entered in operation in December 2009. Therefore, we don't have data for Bayesian update, because corrosion and other critical quantities are under warranty and control. However, by measurement data of wind speed, pedestrian loads, local and global distribution of corrosion, PDF distributions could be updated. The new distribution values could be used in the FE model to provide an updated reliability of the footbridge.

WP8 Project coordination

Objectives of the WP8 (Tasks 8.1, 8.2, 8.3 & 8.4)
The main objectives of the WP8 were to establish an efficient management process, to define standard protocols, to carry out both a SWOT evaluation and the monitoring of activities of the project.

Activities and results obtained

Task 8.1 Efficient management process

HITUBES project comprises several partners and specific objectives. The co-ordinator (University of Trento) is responsible to manage the project activities to complete successfully on time. In order to manage the project work certain necessary steps were taken.
(i) The representatives of each partner meet once in every six month for work-progress. The work finished was evaluated and the next task was planned. This kind of meeting provided an opportunity for formal discussion in detail among partners. Seven meetings were held among partners of the project during the period of concern, i.e. 01 July 2008-31 Dec 2011.
(ii) FTP server directory was created by the University of Liege. Each partner could access this directory and it could download and upload necessary information and documents related to the project. The documents related to the project work, i.e. research papers, thesis report etc., the agenda and minutes of the meeting, experimental as well as simulation data and reports were uploaded on the server. This provided an efficient distribution of the urgent and necessary information helpful to the progress of the project.
(iii) The co-ordinator and all the partners were in regular contact via e-mail. The necessary issues were also discussed by phone. E-mail was the communications medium that was used at the large and preliminary scale. If more than two partners weer involved in discussion, teleconferencing was used. Partners who were doing tests on base materials and welds, for example ISQ, ITMA and KIMAB, discussed together certain issues by teleconference. This helped for the smooth progress of the work. For very critical and urgent issues two partners for example University of Trento and Stahlbau Pichler, met together in Trento in order to discuss the production of specimens.

Task 8.2 Definition of the standard protocols

A protocol is a written set of technical rules describing a detailed plan for the scientific experiment or trial. It is a document that describes the objective(s), design, methodology, statistical considerations and organization of a trial. In the course of HITUBES project, we set standard protocols for the tests at the following levels: (i) test planning and (ii) test performance.

Tests planning

HITUBES project involved several types and number of laboratory tests to be performed by the different partners. It is necessary, in this situation to follow a common set of procedures to prepare the tests. This reduces the discrepancy in the test results as well as increases the efficiency. The following steps have been taken in this respect:

- The HSS tube materials was decided to be supplied by the only one steel manufacturer (i.e. Tenaris Dalmine).
- All the specimens were produced by the only one manufacturer (i.e. Stahlbau Pichler).
- The final drawings of the specimens were made by the Stahlbau Pichler after the initial drawings provided and verified by the different partners. This ensured the compatibility between the users and the manufacturer.

- The welding electrodes and welding procedure specifications (WPS) were chosen for the entire set of specimens following the same selection criteria.

Tests performance

The test protocols regarding performance of tests were made and the information in detail about the types of tests, loadings, number of cycles, strain rate and instrumentation were described in WP3 & WP4. The preliminary numerical simulations have been performed to understand the load-deflection (or stress-strain) behavior of the members and connections in order to prepare the test set-up. The standards followed for tests are reported in *Appendix H.*

Task 8.3 SWOT evaluation of the project

SWOT is a strategic planning method used to evaluate the Strengths, Weaknesses, Opportunities, and Threats involved in a project or in a business venture. It involves specifying the objective of the business venture or project and identifying the internal and external factors that are favorable and unfavorable to achieving that objective. The concept of SWOT can be understood from the SWOT matrix shown in Figure 80.

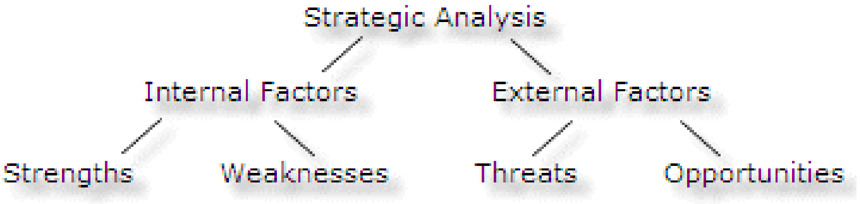

Figure 80 SWOT Matrix

The initial SWOT analysis of the HITUBES project was as follows. More details are available in *Appendix H.*

Strengths

i) University-Industry partnership, (ii) Earlier experience on similar (European) projects, (iii) All partners located in Europe, (iv) Partners specialized in their work area, (v) Manufactures (S. Pichler) and Co-ordinator (UNITN) situated nearby, (vi) Innovation, and (vii) Selection of Case-studies.

Weaknesses

i) Many-Partners, (ii) Limitation of Eurocodes- need of AWS, (iii) HSS un-explored, (iv) Limited HSS-CHS manufacturers, (v) Small amount of HSS - CHS need.

Opportunities

i) Finding HSS tube producer (T. Dalmine) in Italy, (ii) Gain in experience, (iii) Monetary Gain.

Threats

i) Pescara Bridge case study (under construction) – Delay of the project objectives, (ii) Dependency on Tenaris Dalmine (a mass producer) for small amount of TS590 tubes demand – Uncertain delay, (iii) Mixing of Euro codes & AWS.

Task 8.4 Monitoring of activities of each research unit

The monitoring of activities of each research unit was regularly performed through the co-ordination meetings in every six month period. Seven meetings were held among partners of the project during the period of concern, i.e. 01 July 2008-31 Dec 2011.

In the kick-off meeting held in Liege, Belgium, on 29-30 September 2008, the objectives of the project was recalled together with the distribution and content of the work in different WPs related to the concerned period. The two case studies were chosen. In the second meeting held in Moena, Italy, on 22-23 January 2009, the design and analysis of the two case studies were discussed and the tubular connections extracted from case studies were finalized. The issues related to both the design of welded joints and welding of high strength steel circular hollow sections were discussed. The need of the American Welding Society code was realized for detailing of weld profile of tubular welded connections. The representative of tube manufacturer Tenaris Dalmine was invited in the meeting to finalize the tube dimensions in order to comply with production. The partners were directed to make a primary sketch of test specimens according to their test requirements in order to calculate the total length of tubes to be ordered to Tenaris Dalmine. In the third meeting held in Volos, Greece, on 17-18 September 2009, the drawings of the specimens were finalized. Welding procedure specifications were presented. The issue of undermatching and overmatching was discussed. In the fourth project meeting, held in Bolzano, Italy, on 11-12 February 2010, the results of structural identification and monitoring activities on the footbridge of Pescara were presented. The test plan, i.e. loadings, number and type of tests to be performed by each partner was presented and discussed. The initial simulation model of welded and bolted connections were presented and discussed. In the fifth project meeting, held in Pula, Italy, on 23-24 September 2010, the results of structural identification and monitoring activities on the footbridge of Pescara were presented. The test plan, i.e. loadings, number and type of tests to be performed by each partner was presented and discussed. The improved simulation model of welded and bolted connections were presented and discussed. In the sixth project meeting, held in Asturias, Spain, on 01-02 March 2011, the experiments performed on the base materials and welds were presented and the results were discussed. The remaining tests on the base materials, welds as well as tubular connections and members were recalled and discussed. The improved simulation model of welded and bolted connections were presented and discussed. In the last project meeting, held in Rome, Italy, on 12-13 October 2011, the experimental results were discussed and the remaining tests were recalled and discussed. The simulation results were discussed. The format of the draft final report and contents of the design guidelines were presented and discussed.

Conclusions

New steel production processes have led to a remarkable improvement in steel products within the last few years, and now they allow steels to be produced according to the desired mechanical and chemical properties. High Strength Steel (HSS) or High Performance Steel is the designation given to this new generation of steels that offer higher performance, especially in the case of tubular members produced for offshore applications, not only in terms of strength but also toughness, weldability, cold formability and corrosion resistance, compared to traditionally used mild steel grades. The development of HSS goes with today’s increased demand for slender lightweight structures, as for instance in footbridge and bridge design. However, on the structural engineering side there is a need for knowledge of these new steel grades combined to proper conceptual designs. Nonetheless quite often, recent design codes like Eurocode 3-1-12 do not provide sufficient information to fully exploit the advantageous properties of HSS. In this respect the HITUBES project showed new conceptual designs and assessment procedures in order to make full use of HSS TS590 for onshore structures that employed tubes 355/12 with $D/t > 29$ and 193.7/10 with $D/t > 19$. In particular, we analysed in depth two specific structural types for which tubes could be suitable for architectural and aesthetic reasons: i) slender foot- and cycle-bridges; ii) arches and hanger elements of railway bridges, under extreme natural and anthropic repeated loadings, some of which we measured in situ. Necessary tools were the use of tests at the material, member and connection level in structural labs and both identification and monitoring in situ, of finite element (FE)-based tools, of reliability assessment of a realistic case study. The project reported relevant behaviour of members, welded and bolted connections under monotonic, low-cycle fatigue and high-cycle fatigue loading, weights reduction and reliability analysis results. We believe that several information and benefits at the material, member, connection and structural level when using HSS in comparison with mild steel were provided.

Exploitation and impact of the research results

The outcomes of HITUBES were obtained through a sound process of conceptual design of Case Studies made of tubular structures under extreme repeated loadings; characterization of unknown extreme forces of case studies via structural identification and health monitoring; tests on mild and HSS steel, tubular members; tests on welded and bolted connections; numerical simulations of tubular connections and structures; reliability analysis of some case studies; development of design guidelines and recommendations for HSS tubular structures. Technical assistance by Tenaris Dalmine, world-class producer of seamless pipes and accurate steel fabricators, like Stahlbau Pichler, contributed a lot.

As a result, we believe that we contributed to the exploitation of research results, because:

- Case Studies were redesigned in the realm of footbridges and bridges and were based on innovative conceptual design that entailed, safety, robustness and reliability from a technical point of view;

- Case Studies based on HSS entailed also economical savings in decks for the analysed footbridge and arches for the studied railway bridge that went with today's increased demand for slender lightweight structures.

It is evident that the aforementioned advantages come mainly from technical considerations and actual impact depends on several factors, governed mainly by commercial policies. Moreover, conceptual design and experimental data could be extended to other types of structures not tacked by the project, like lattice structures of telescopic cranes and tower cranes and some type of offshore structures.

With regard to publications/conference presentations resulting from the project, 10 papers and 1 book – in Italian for the time being - were issued; in greated detail, 2 papers published on international journals; 3 papers under preparation; 5 papers presented on international conferences. For the benefit of the reviewer, they are listed below.

List of Publications

(1) Zanon G., Kumar A., Bursi O.S., Ferrario F., Giacobbe A. (2011), "High strength tubular columns and connections under earthquake, fire loading and fatigue", Metallurgia Italiana , 3, 2011, 25-31.

(2) Ceravolo R., Tondini N., Abbiati G., Kumar A. (2011), "Dynamic characterization of complex bridge structures with passive control systems", Struct. Control Health Monit., Published online in Wiley Online Library (wileyonlinelibrary.com). DOI: 10.1002/stc.450.

(3) Papatheoharis C., Varelis G.E., Perdikaris P., Karamanos S. A. (2011) "High-strength steel welded tubular connections under monotonic and cyclic loading ", EUROSTEEL 2011 conference, Budapest, Hungary.

(4) Varelis G.E., Pournara A., Karamanos S. A. (2011) "Strength and stability of high-strength steel tubular beam-columns under static and cyclic loads", EUROSTEEL 2011 conference, Budapest, Hungary.

(5) Bonelli A., Bursi O.S., Ceravolo R., Santini S., Tondini N. and Zasso A. (2010) "Dynamic Identification and Structural Health Monitoring of a Twin Deck Curved Cable-Stayed Footbridge: The "Ponte del Mare" of Pescara in Italy", Fifth European Workshop on Structural Health Monitoring, Sorrento, Italy, 29 June-2 July 2010.

(6) Bursi O.S., Bonelli A., Ceravolo R., Tondini N., Ussia A. (2011) " Dynamic and aeroelastic behaviour of a twin deck curved cable-stayed footbridge equipped with passive devices", EMI 2011 conference Boston, USA.

(7) Tondini N., Bursi, O.S. , Bonelli A., Francescotti S. (2011) "Dynamic and Aeroelastic Behavior of a Twin Deck Curved Cable-Stayed Footbridge Equipped with Passive Devices", Proceedings of the 8th International Conference on Structural Dynamics, EURODYN 2011, Leuven, B, July 4-6, 2011, 1829-1835.

(8) Bursi O.S., Pucinotti R., Zanon G., "Design of hollow steel joints and structures", Flaccovio, 2012. Sponsored by Italian Foundation for Steel Promotion

(9) Long H.V., Demonceau J.-F., Jaspart J.-P., "Behaviour of flange bolted joints under monotonic, high cycle fatigue and low cycle fatigue loadings, I: Experimental investigation". In preparation to be submitted to the *Journal of Constructional Steel Research.*

(10) Long H.V., Demonceau J.-F., Jaspart J.-P., "Behaviour of flange bolted joints under monotonic, high cycle fatigue and low cycle fatigue loadings, II: Numerical investigation". In preparation to be submitted to the *Journal of Constructional Steel Research.*

(11) Bursi O.S., Ceravolo R. and Kumar A. (2012), "Software for dynamic characterization and reliability of complex footbridge structures", in preparation to be submitted to *Computer-Aided Civil and Infrastructure Engineering.*

List of figures

List of tables

List of acronyms and abbreviations

AF	Axial Force
APDL	Ansys Parametric Design Language
ASTM	American Society for Testing and Materials
AWS	American Welding Society
CHS	Circular Hollow Section
CP	Check Point
EDM	Electric Discharge Machining
EL	Elongation
EN	Element Number
FE	Finite Element
FEM	Finite Element Method
FFT	Fast Fourier Transform
FTP	File Transfer Protocol
HAZ	Heat Affected Zone
HCF	High Cycle Fatigue
HSS	High Strength Steel
IPB	In-Plane Bending
ISO	International Organization for Standardization
LCF	Low Cycle Fatigue
LSE	Linear Surface Extrapolation
LVDT	Linear Variable Differential Transformer
MAC	Modal Assurance Criteria
M-N	Moment Normal-load
MU	Model Updating
MVC	Micro Voids Coalescence
OCP	Open Circuit Potential
OP	Overmatching Peening
OPB	Out-of-Plane Bending
PDF	Probability Density Function
PM	Parent Metal
RA	Reduction in Area
RMS	Root Mean Square
SCC	Stress Corrosion Cracking
SCF	Stress Concentration Factor
SLS	Serviceability Limit State
S-N	Stress Number of cycle
SSRT	Slow Strain Rate Tests
SWOT	Strength Weakness Opportunity Threat
TTF	Time To Failure
TS	Tensile Strength
TTWT	Through Thickness at the Weld Toe
ULS	Ultimate Limit State
UP	Undermatching Peening
US	Ultra Sonic
UTS	Ultimate Tensile Strength
VH	Vertical Horizontal
WM	Weld Metal
YS	Yield Strength
w.r.t	With respect to

List of References

[1] Gunther Hans-Peter et al., "SED 8: Use and application of high-performance steels for steel structures," IABSE, 2005.

[2] "Design of footbridges guidelines, Human induced vibrations of steel structures," HIVOSS-RFS2-CT-2007-00033.

[3] CSI, Computers and Structures Incorporated, "SAP2000 NL,v15," Berkeley, CA, USA, 2010.

[4] ANSYS-11, "Ansys structural," ANSYS, Inc. Software Products, 2008.

[5] ARTeMIS-Extractor, "Structural Vibration Solutions A/S," Aalborg East, Denmark, 2008.

[6] Hibbitt, Karlsson and Sorensen, "ABAQUS user's manuals," Pawtucket (RI), 1080 Main Street. 02860, 2000.

[7] Johansson Bernt, Collin Peter, "Eurocode for high strength steel and applications in construction," Lulea University of Technology, Sweden, 2006.

[8] "ASTM E466-07. Standard Practice for Conducting Force Controlled Constant Amplitude Axial Fatigue Tests of Metallic Materials".

[9] "ASTM E1820 – 11 Standard Test Method for Measurement of Fracture Toughnes".

[10] "EN ISO 15609-1 "Specification and qualification of welding procedures for metallic materials -- Welding procedure specification -- Part 1: Arc welding"".

[11] "EN 10210-2:2006. Hot finished structural hollow sections of non-alloy and fine grain steels Part 2: Tolerances, dimensions and sectional properties.".

[12] ASTM E739 – 10 Standard Practice for Statistical Analysis of Linear or Linearized Stress-Life (S-N) and Strain-Life (ϵ-N) Fatigue Data.

[13] "EN 15614-1:2004 Specification and qualification of welding procedures for metallic materials — Welding procedure test: Part 1: Arc and gas welding of steels and arc welding of nickel and nickel alloys".

[14] "Eurocode 3: Design of steel structures - Part 1-8: Design of joints. EN-2005".

[15] "AWS D1.1/D1.1 M:2004, Structural Welding Code – Steel".

[16] "Eurocode 3: Design of steel structures - Part 1-9: Fatigue strength of steel structures. EN-2005.," 2005.

[17] Zhao X.-L., Herion S., Packer J.A., Puthli R.S., Sedlacek G., Wardenier J., Weynand K., van Wingerde A.M., Yeomans N.F., "Design Guide for Circular and Rectangular Hollow Section Welded Joints under Fatigue Loading," Design Guide 8, TUV-Verlag, 2001.

[18] Romeijn A., "Stress and strain concentration factors of welded multiplanar tubular joints," PhD Thesis, Delft, The Netherlands, 1994.

[19] Hobbacher A., "Recommandations for fatigue design of welded joints and components," 2005.

[20] Radaj D., Design and analysis of fatigue resistant welded structures, Abington Publishing, 1990.

[21] Dong P. , "A structural stress definition and numerical implementation for fatigue analysis of weld joints," *International Journal of Fatigue*, vol. 23, pp. 865-876, 2001.

[22] Ballio G., Castiglioni C.A., "A Unified Approach for the Design of Steel Structures under Low and/or High cycle Fatigue," *Journal of Construction Steel Research*, vol. 34, pp. 75-101, 1995.

[23] SETRA, "Assessment of vibrational behaviour of footbridges under pedestrian loading," Technical Guide Setrà, 2006.

[24] "CIDECT No. 1. 1991. Design Guide for Circular hollow Sections (CHS) under Predominantly Static Loading".

[25] "CIDECT No. 8. 2001. Design Guide for Circular and Rectangular Hollow Section Welded Joints under Fatigue Loading".

[26] "AWS D1.1/D1.1 M:2004, Structural Welding Code – Steel".

[27] "Eurocode 3: Design of steel structures - Part 1-8: Design of joints. EN-2005".

[28] Wardenier J., Packer J.A., Zhao X.-L., van der Vegte G.J, "Hollow sections in structural applications," CIDECT, 2010.

[29] "EN 1993-1-12. Eurocode 3: Design of steel structures – Part 1-12: Additional rules for the extension of EN 1993 up to steel grades S 700, European Committee for Standardization".

[30] ""Eurocode3: Design of steel structures, part 1-1, EN 1993-1-1, General rules and rules for buildings," Brussels, Belgium.".

[31] Elchalakani M., Zhao X.L., Grzebieta R., "Bending tests to determine slenderness limits for cold-formed circular hollow sections," *Journal of Constructional Steel Research*, vol. 58, no. 11, pp. 1407-1430, 2002.

[32] Beg D.,Hladnik L., "Slenderness limit of Class 3 I cross-sections made of high strength steel," *Journal of Constructional Steel Research*, vol. 38, no. 3, pp. 201-217, 1996.

[33] "Eurocode 3: Design of steel structures - Part 1-1: General rules and rules for buildings. CEN-2005.," 2005.

[34] "CIDECT No. 2. 1991. Design Guide for structural stability of hollow Sections".

[35] American Petroleum Institute, "Recommended practice for planning designing and constructing fixed offshore platforms- LRFD design," API RP 2A-WSD, 20th Edition, 1993.

[36] Josat O., "Sustainable bridge constructions- elegant arches- filigree structrues- cost effective design," pp. 584-596.

[37] Hoorpah W., Vigo J.M., "Innovative design of bridges with high strength steel," in *7th International Conference on Steel Bridges*, 2008.

[38] Jensen L., Bloomstine M.L., "Application of high strength steel in super long span modern suspension bridge design," *NSCC2009*, pp. 494-501, 2009.

[39] Dallard P. et. al., "The London Millennium Footbridge," *The Structure Engineer,* vol. 79, no. 22.

[40] Li Z.X., Chan T.H.T., Ko J.M., "Evaluation of typhoon induced fatigue damage for Tsing Ma Bridge," *Engineering Structures,* vol. 24, pp. 1035-1047, 2002.

[41] Melchers R.E., Hough R., Modeling complex engineering structures, Reston, Virginia: ASCE.

[42] Estes A.C., Frangopol D.M., "Updating bridge reliability based on bridge management".

[43] Marsh P.S., Frangopol D.M., "Reinforced concrete bridge deck reliability model incorporating temporal and spatial variations of probabilistic corrosion rate sensor data," *Reliability Engineering and System Safety,* vol. 93 , p. 394–409, 2008.

[44] Decò A., Frangopol D.M. , "Risk assessment of highway bridges under multiple hazards," *Journal of Risk Research,* no. DOI:10.1080/13669877.2011.571789, 2011.

[45] Wang, Ruizi, Ma, Lin, Yan, Cheng, & Matthews, Joseph, "Structural reliability prediction of a steel bridge element using Dynamic Object Oriented Bayesian Network (DOOBN)," in *Proceedings of International Conference on Quality, Reliability, Risk, Maintenance, and Safety Engineering, IEEE,* Xi'an International Conference Center, Xi'An, China, 2011.

[46] "EN 1991-2, (2005), "Actions on structures – Part 1-2 : Traffic loads on bridges.".

[47] Greisch's office, "Calculation notes for the design of the rail-way Landegem bridge," Internal report, 1987.

[48] Veljkovic M., Johansson B., "Design of hybrid steel girders," *Journal of Constructional Steel Research,* vol. 60, pp. 535-547, 2004.

[49] Castellani A., "Vibrations generated by rail vehicles: a mathematical model in the frequency domain," *Vehicle System Dynamics,* vol. 34, no. 3, pp. 153-173, 2000.

[50] Xiuhua Z, et al., "Numerical simulation of dynamic response and collapse for steel frame structures subjected to blast load," *Transaction of Tianjin University,* vol. 14, pp. 523-529, 2008.

[51] Chang Kyong-Ho et al., "Strain-rate dependence of mechanical behavior and hysteretic characteristics of TMCP steel (SM570-TMC) and its modeling," *Computational Materials Science,* vol. 45, pp. 669-673, 2009.

[52] Lamarche C-P., *Development of real-time dynamic substructuring procedures for the seismic testing of steel structures,* PhD Thesis, Ecole Polithecnique de Montreal, 2009.

[53] "LAGAMINE: User's manual, University of Liege, 2010".

[54] Agreskov H., "High strength bolted connections subject to prying," *J. Struc Div,* 1976.

[55] Varelis G. E., et al., "Structural performance of TS590 high-strength steel welded tubular joints under extreme bending loading," in *ISTS 14,* London, UK, 2012.

[56] Hobbacher, " IIW Recommendations on fatigue XIII-1539-95/XV-845-95".

[57] Jaspart J.P. et al., "Development of a full consistent design approach for bolted and welded joints in building frames and trusses between steel members made of hollow and/or open sections: application of the component method. Volume 1: practical guidelines," CIDECT research project 5BP, 2005.

[58] Piluso V., Rizzano G., "Experimental analysis and modelling of bolted T-stub under cyclic loads," *Journal of Constructional Steel Research,* vol. 64, pp. 655-669, 2008.

[59] Igarashi S. et al. , "Limit design of high strength bolted tube flange joint, Part 1 and 2.," *Journal of Structural and construction engineering transactions of AIJ, Department of Architecture reports, Osaka University, Japan,* 1985.

[60] Cao J.J. & Bell A. J. , "Determination of bolt forces in a circular flange joint under tension force," *Int. J. Press. & Piping,* vol. 68, pp. 63-71, 1996.

[61] Cao J.J. & Bell A. J. , "Design of Tension Circular Flange Joints in Tubular Structures," *Engineering*

Journal, pp. 17-25, 1997.

[62] Jaspart J.P. et al., "Development of a full consistent design approach for bolted and welded joints in building frames and trusses between steel members made of hollow and/or open sections: application of the component method. Volume 1: practical guidelines," CIDECT research project 5BP, 2005.

[63] Couchaux M., "Comportement des assemblages par brides circulaires boulonnés," PhD thesis, INSA of Rennes, France., 2010.

[64] Piluso V., Rizzano G., "Experimental analysis and modelling of bolted T-stub under cyclic loads," *Journal of Constructional Steel Research,* vol. 64, pp. 655-669, 2008.

[65] Shaw P.K. & Kyriakides S., "Inelastic analysis of thin-walled tubes under cyclic bending," *Int. Journal of Solids and Structures,* vol. 21, pp. 1073-1100, 1985.

[66] "UNI EN 1990, 2002 Annex B Management of Structural Reliability for Construction Works and Annex C Basis for Partial Factor Design and Reliability Analysis".

[67] Sivakumaran, Yuan, "Slenderness limit and ductility of high strength steel sections," *J. Construct Steel Research,* vol. 46, pp. 149-151, 1998.

[68] Rasmussen, Hancock, "Test of High Strength Steel Columns," *Journal of Constructional Steel Research,* vol. 34, pp. 27-52, 1995.

[69] Richter, Hanus, Wolf , "Structural Steels of 690 MPa Yield Strength – a State of Art".

[70] Al-Shawi, FAN, "On the rotation capacity of structural steel circular hollow sections in plastic analysis," *Sheffield Hallam University,* 2000.

[71] Billingham J., "Steel - a versatile advanced material in marine environments," *Iron making and Steelmaking,* vol. 21, no. 6, 1994.

[72] Billingham J., Healy J., Spurrier J., Current and potential use of high strength steels in offshore structures, MTD Publication 95/102, ISBN 1-870-533-24-1, 1995.

[73] Billingham J., Sharp J.V., Spurrier J, Kilgallon P.J., Review of the performance of high strength steels used offshore, HSE Books, ISBN 0-7176-2205-3, 2003.

[74] Zimmer P., Seeger D.M., Boellinghaus Th., "Hydrogen permeation and related material properties of high strength structural steels," in *Proceedings of High Strength Steels for Hydropower Plants*, paper no. 17, Graz, 5-6 July, 2005.

[75] Muraki T., Tsuru E., Asahi H., "Sulfide stress cracking resistance of post expanded low alloy steel," *Corrosion NACExpo,* p. Paper No. 06153, 2006.

[76] Malina J., Samardži I., Gliha V., "Susceptibility to hydrogen-induced cracking of weld beads on high-strength structural steel," *Material science,* vol. 41, no. 2, 2005.

[77] Ronald D. Ziemian, Guide to Stability design criteria for Metal Structures, Jhon Wiley & Sons, inc., 2010.

[78] Batista E.de M., Rodriguez F.C. , "Residual Stress Measurements on Cold-formed profiles," *Experimental Techniques* , vol. 16, no. 5, pp. 25-29, 1992.

[79] "ASTM E1928 – 99. Standard Practice for Estimating the Approximate Residual Circumferential Stress in Straight Thin-walled Tubing".

[80] "ATTEL project: "Performance-based approaches for high-strength tubular columns and connections under earthquake and fire loadings". Grant Agreement Number: RFSR-CT-2008-00037. Deliverable Report D.4: Fire test data, 9-2011.".

[81] Fricke W., Kahl A., "Comparison of different structural stress approaches for fatigue assessement of welded ship structures," *Marine Structures,* vol. 18, p. 437 – 488, 2005.

[82] Kim M.H. et al., "A comparative study for the fatigue assessment of a ship structure by use of hot spot stress and structural stress approaches," *Ocean Engineering* , vol. 36, pp. 1067-1072, 2009.

[83] Poutiainen I. et al., "Finite element methods for structural hot spot stress determination – a comparison of procedures," *International Journal of Fatigue,* vol. 26, pp. 1147-1157, 2004.

[84] Boothman D.P., Lee M.M.K., Luxmore A.R., "The effects of weld mismatch on J-integrals and Q-values for semi-elliptical surface flaws," *Engineering Fracture Mechanics,* vol. 64, pp. 433-458, 1999.

[85] Koçak M., "Structural Integrity of welded structures: Process – Property – Performance (3P) Relationship," in *63rd annual assembly and international conference of the international institute of welding,* Istambul, Turkey, 11-17 July 2010.

[86] Anderson T.L., Fracture Mechanics. Fundamentals and applications, Second edition.

[87] Davis J.R., "Corrosion : understanding the basics.," in *ASM International,* Materials Park, Ohio, 2000.

[88] Cwiek J., "Hydrogen assisted cracking of high-strength weldable steels in sea-water," *Journal of Materials Processing Technology,* Vols. 164-165, pp. 1007-1013, 2005.

[89] Chawla K., Rigsbee J., Woodhouse J., "Hydrogen-induced cracking in two linepipe steels," *Journal of Materials Science,* vol. 21, no. 11, pp. 3777-3782, 1986.

[90] Hardie D., Charles E.A., Lopez A.H., "Hydrogen embrittlement of high strength pipeline steels," *Corrosion Science,* vol. 48, no. 12, pp. 4378-4385, 2006.

[91] Dong C.F. et al. , "Effects of hydrogen-charging on the susceptibility of X100 pipeline steel to hydrogen-induced cracking," *International Journal of Hydrogen Energy,* vol. 34, no. 24, pp. 9879-9884, 2009.

[92] Eliaz N. et al., "Characteristics of hydrogen embrittlement, stress corrosion cracking and tempered martensite embrittlement in high-strength steels," *Engineering Failure Analysis,* vol. 9, no. 2, pp. 167-184, 2002.

[93] Sastri V.S., Ghali E., M. Elboujdaini M. , "Corrosion prevention and protection : practical solutions," *Chichester: Wiley. xiv,* vol. 4, p. 557, 2007.

[94] Hassan T. & Kyriakides, S., "., (1992). “Ratcheting in cyclic plasticity, Part I:Uniaxial behavior," *Int. Journal of Plasticity,* vol. 8, pp. 91-116, 1992.

[95] Hassan T., Corona E., Kyriakides S., "Ratcheting in cyclic plasticity, Part II: Multiaxial behavior," *Int. Journal of Plasticity,* vol. 8, pp. 117-146, 1992.

[96] Chaboche J.L., "Time-independed constitutive theories for cyclic plasticity," *Int. Journal of Plasticity,* vol. 2, pp. 149-188, 1986.

[97] C. J. Lemaitre J., Mechanics of solid materials, Cambridge University Press, 1990.

[98] Simiu E., Heckert N.A., Filliben J.J., Johnson S.K., "Extreme wind load estimates based on Gumbel distribution of dynamic pressures: an assessment," *Structural Safety,* vol. 23, pp. 221-229, 2001.

[99] "CNR DT207-2008 Istruzioni per la valutazione delle azioni e degli effetti del vento sulle costruzioni, ROMA – 17 gennaio 2008".

[100] Chiodi R., Ricciardelli F., Pelino V., Prota A.,, "Updated statistical analysis of Italian extreme wind speeds".

Appendices

Appendices A, B, C, D, E, F, G and H are reported herein.

Appendix A: Literature review

This literature survey investigates the characteristics of HSS required in structural applications. The summary of this study is given below.

1. Current Design Procedures for Welded/Bolted High Strength Steel (HSS) Materials

1.1 Mechanical Characteristic of HSS

The stress-strain $(\sigma - \varepsilon)$ behaviour of HSS is considerably different from that of mild steel, exhibiting considerably lower material ductility. Strain at rupture ε_{rp} of HSS range from 10% to 15%, strain at ultimate load level ε_u is about 10% [67] [68]. EN 1993-1-12 (2006) [29] is issued to develop rules to make EN 1993 applicable to High Strength Steel. EN 1993-1-12 covers steels according to EN 10025-6 and EN 10149-2. The former deals with quenched and tempered steels delivered as flat plates and those included in EC3-1-12 range from S500 to S690. EN 10149-2 deals with TM- steels for cold forming and the grades included in EN 1993-1-12 range from S500 to S700 [7]. The requirements on material ductility are stated in 3.2.2(1) of EN 1993-1-1 with recommended values as follows:
In EN 1993-1-12, three requirements on material behaviour and ductility are stated. These are a little different than that stated in EN 1993-1-1, i.e.

- $\frac{f_u}{f_y} \geq 1.05$
- Elongation at failure not less than 10%
- $\varepsilon_u \geq 15\frac{f_y}{E}$.

The restrictions on structures made of steels fulfilling those relaxed requirements are mainly that plastic analysis and semi rigid joints should not be used. The structural analysis should either be elastic or made by non-linear FE analysis. It should be noted that the plastic resistance may still be used for cross sections in Class 1 and 2 [7].

1.2 Weldability of HSS

It is more difficult to weld quenched and tempered HSS and thermo-mechanically rolled HSS than mild steel. The more difficult weldability results from the increasing of the Carbon Equivalent (CE) parameter. However, these difficulties must be overcome by precautions in welding. This means higher preheat, and interpass temperature, the application of low hydrogen consumables and possibly soaking after welding for a removal of residual hydrogen [69] [67]. Moreover it is known that nickel improves consistently the low temperature toughness in parent material and heat affected zone for QT and normalized steels. If Nickel is added, it can replace carbon, manganese and other alloying elements that are less favourable for the *Heat Affected Zone* (HAZ) [69] [67].

One way of simplifying the welding of HSS is to use undermatched electrodes, which makes the welds more ductile and less prone to crack. Undermatched electrodes are not allowed in EN 1993-1-8 but they are allowed in EN 1993-1-12. The design of such undermatched welds should be based on the electrode strength rather than the base material strength [7]. The results come out from some test to be a modification of the design formula (4.1) of EN 1993-1-8, which reads:

$$\sqrt{\sigma_{\perp}^2 + 2\tau_{\perp}^2 + 3\tau_{//}^2} \leq \frac{f_u + f_{eu}}{2\gamma_{M2}|}$$

The notations are the same as in EN 1993-1-8 with the additional symbol f_{eu} meaning the characteristic ultimate strength of electrodes [7].

1.3 Ductility of HSS elements and sections

Several studies have verified the difficulty of using plastic analysis for HSS elements due to the reduced ductility parameters of the material [67]. The ratio between the tensile strength (f_u) and the yield strength (f_y) is considerably lower than that of mild steel; the ratio between the strain at hardening (ε_{st}

), and the strain at yielding (ε_y) is about 1, so that there isn’t a horizontal plateau after the yield strength; the ratio between the strain at ultimate load level (ε_u), and the strain at yielding (ε_y) is considerably lower than that of mild steel [67]. However these studies were carried out on a H section and are not directly extensible to circular sections.

In conclusion, we can say that the ductility of materials and sections for HSS elements can be considered lower than that of ordinary steel; hence, one needs to pay particular attention to use plastic analysis, particularly in seismic conditions.

1.4 Classification of cross section for CHS made of HSS

The classification of cross sections is closely related to the ductility of the material, the ductility of the element section and local buckling phenomena. An important problem of HSS section, owing to the high yield strength, consists of respecting the classification limits imposed by Eurocode 3-1-1. The classification of cross sections is function of the factor $\varepsilon = \sqrt{235/f_y}$, so that HSS is penalized. In addition the classification is function of the D/t ratio that is often high with use of HSS sections. Several studies and tests have shown that the slenderness limits in EC3-1-1 are probably too conservative both for mild steel up to grade S460 and for HSS, and in particular for circular hollow section [31] [32]. There are significant differences in slenderness limits (shown in Table **29**) recommended in various codes for circular hollow sections (CHS) under bending [31].

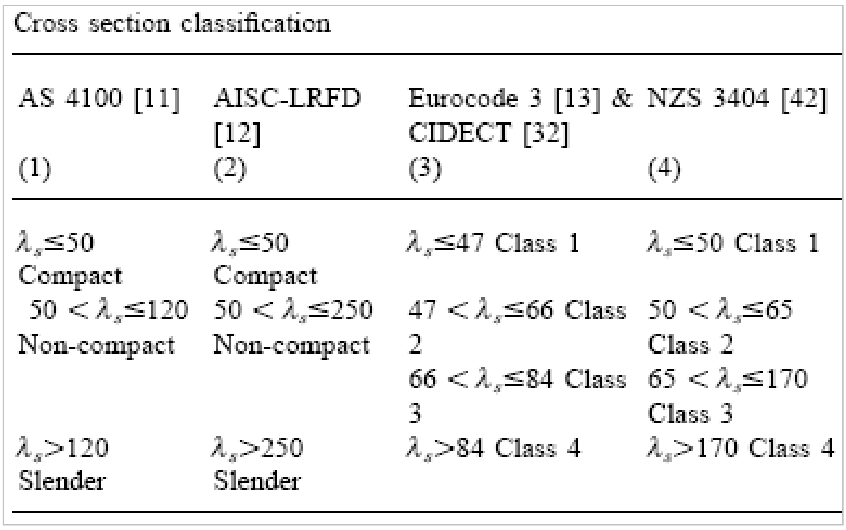

Cross section classification

AS 4100 [11] (1)	AISC-LRFD [12] (2)	Eurocode 3 [13] & CIDECT [32] (3)	NZS 3404 [42] (4)
$\lambda_s \le 50$ Compact	$\lambda_s \le 50$ Compact	$\lambda_s \le 47$ Class 1	$\lambda_s \le 50$ Class 1
$50 < \lambda_s \le 120$ Non-compact	$50 < \lambda_s \le 250$ Non-compact	$47 < \lambda_s \le 66$ Class 2	$50 < \lambda_s \le 65$ Class 2
		$66 < \lambda_s \le 84$ Class 3	$65 < \lambda_s \le 170$ Class 3
$\lambda_s > 120$ Slender	$\lambda_s > 250$ Slender	$\lambda_s > 84$ Class 4	$\lambda_s > 170$ Class 4

$$\lambda_s = \frac{D/t}{\varepsilon^2} \qquad \varepsilon^2 = \frac{250}{f_y}$$

Table 28– Cross section classification for different standards

Major differences concern slenderness limit between Classes 3 and 4 (i.e. non-compact and slender sections), and the EC3-1-1 is particularly conservative compared to other international standards. Several studies have been carried out attempting to define new limits for classification of sections CHS [31] [32] [68]. Other researches [70] have been aimed at studying the behaviour and the rotational capacity of CHS in the plastic range in order to investigate the behaviour of circular hollow sections beyond the stage of development of the plastic moment . In the standards, the possibility to develop a plastic moment M_p is fitted in the classification of cross sections. But in this way it does not take into account the secondary *P*–d effect which takes place in the plane of the cross section of the tube. This effect will reduce the plastic section (ovalisation) modulus due to the deformation in the form of flattening of the cross section [70]. It is therefore necessary to perform experiments and tests with regard to these issues, mainly investigating the behaviour of circular sections in HSS.

1.5 Corrosion aspects of HSS material

In offshore engineering, high strength steels (HSS) are, in general, susceptible to hydrogen embrittlement which could lead to cracking problem or accelerated corrosion fatigue crack propagation. The allowable stress in design is often restricted to 60-80% of the yield strength. In the case of tubular joints the situation is more restrictive [71] [72] [73]. Therefore, high strength steels (YS>650MPa) should be examined for possibility of hydrogen damage in service, both in the base material and in the weldments [73].

In recent year, the proportion of high strength steels used in offshore structures like topsides, jackets, jack-up and moorings has been increased. Some researches have been taken on high strength steels in order to provide data to support offshore applications [74] [75] [76]. However, there is limited information of the long-term use of high strength steels in sea water and under severe conditions where the structures are subjected.

Pipeline steel developments have been concerned more with obtaining a better balance in the overall steel properties than only increasing strength. The most commonly used pipeline steel is X70 grade with yield strength of 482Mpa. However, up to X100 grade (yield strength of 689Mpa) pipeline steels are available and there is a growing trend to use such steels. Quite a lot corrosion and stress corrosion cracking studies were related to the oil and gas industry where the pipelines are made of medium or high strength steels with diameters from 8 in to 30 in.

Drilling jack-ups have suffered many accidents over the years due to damage and cracking. About 2000 individual survey reports show that many defects were found at the spud cans or on the leg connection to the can [71] [72] [73]. The reasons of the defects were mainly due to the rig design and fabrication; however, some of the defects were due to extreme load, cyclic load and hydrogen cracking. Most of the cracks were found in the Q&T low alloy high strength steels, especially in the HAZ. This problem led to a lot of researches. The main conclusions are that the cracking was due to the presence of H_2S in the spud can, too negative cathodic protection and poor material selection. Therefore, a number of recommendations to control the cracking were made as follows: i) Emphasis on material selection, for example by use of slow strain rate testing (SSRT); ii) Welding procedures; iii) Avoidance of anaerobic condition (e.g. hydrogen evolution corrosion in the absence of oxygen); iv) Limiting the potentials of cathodic protection to minimize the generation of hydrogen.

High strength steels are being used more and more in the construction of offshore platforms and other structures like slender foot- and cycle-bridges. From a view of corrosion aspect, one big drawback of using HSS is the increased risk of hydrogen related stress corrosion cracking. The literature review show that the materials resistance to hydrogen embrittlement depends strongly on the microstructure [73]. The hydrogen embrittlement susceptibility of different microstructure is ranked in the order: tempered martensite < tempered bainite < spheroid ferrite and pearlite < coarse ferrite and pearlite.

The strength or hardness of specific steel usually can give a first indication of its hydrogen embrittlement susceptibility. However, it is not always true. Hydrogen embrittlement susceptibility is more sensitive to the specific environment, microstructure and the level of strength. It is important that each steel should be considered individually and should be subjected for testing before being accepted for use, especially in critical conditions.

The conventional steels usually exhibit uniform corrosion, pitting attack, crevice corrosion and stress corrosion cracking (SCC) in offshore environment. The uniform corrosion is relatively easy to protect by use coating or painting at the metal surface. However, pitting and crevice corrosion as well as stress corrosion cracking are considered to be more dangerous than uniform corrosion damage because it is more difficult to detect, predict and design against. Similar to SCC, another common failure is the hydrogen related stress corrosion cracking, sometime also called hydrogen embrittlement. The requirements for SCC and hydrogen embrittlement are threefold, as shown in Figure 92. First of all, the material should be susceptible to SCC and hydrogen embrittlement. Secondly, there should be a suitable corrosive environment (for SCC) or a source of hydrogen which leads to a sufficient distribution of atomic hydrogen in the material (for hydrogen embrittlement). Lastly, it requires sufficient stress intensity to cause sub-critical fracture.

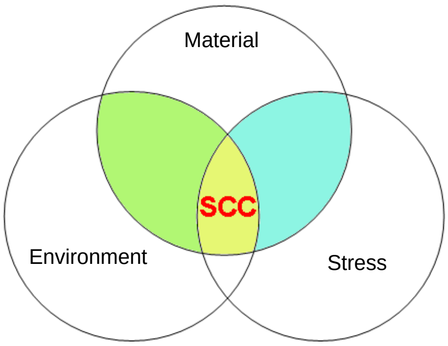

Figure 81 Threefold requirement for stress corrosion cracking

In offshore environments, the main sources of hydrogen in high strength steels are from corrosion and cathodic protection. The presence of corrosive species such as chlorides, CO_2 and H_2S in offshore environment has an increased effect on corrosion of materials. Furthermore, a sulphide layer formed at the steel surface enhances hydrogen uptake into the material. Another important source of hydrogen is from welding if not sufficient care is taken during welding.

Current Design Procedures for Tubular Members

The main actions of concern in this project in monotonic loading of tubular members are: (1) axial compression loading; and/or (2) bending moment loading.

a. EN 1993-1-1 Comité Européen de Normalisation (CEN). Eurocode 3: Design of Steel Structures, part 1-1, EN 1993-1-1, General Rules and Rules for Buildings. Brussels, Belgium

The design of beams and columns is based on the classification of the cross-section as stated in Paragraph 5.5, Table 5.2 (sheet 3 of 3) of the specification, Table **30**. Furthermore, Chapter 6 is used for the verification of members under axial compression and bending. More specifically,

- Paragraph 6.2.4 concerns cross-sectional strength under axial compression
- Paragraph 6.2.5 concerns cross-sectional strength under bending
- Paragraph 6.2.9 concerns cross-sectional strength under combined action of axial compression and bending
- Paragraph 6.3.1 concerns column strength under axial compression
- Paragraph 6.3.3 concerns column strength under axial compression and bending (beam-columns)

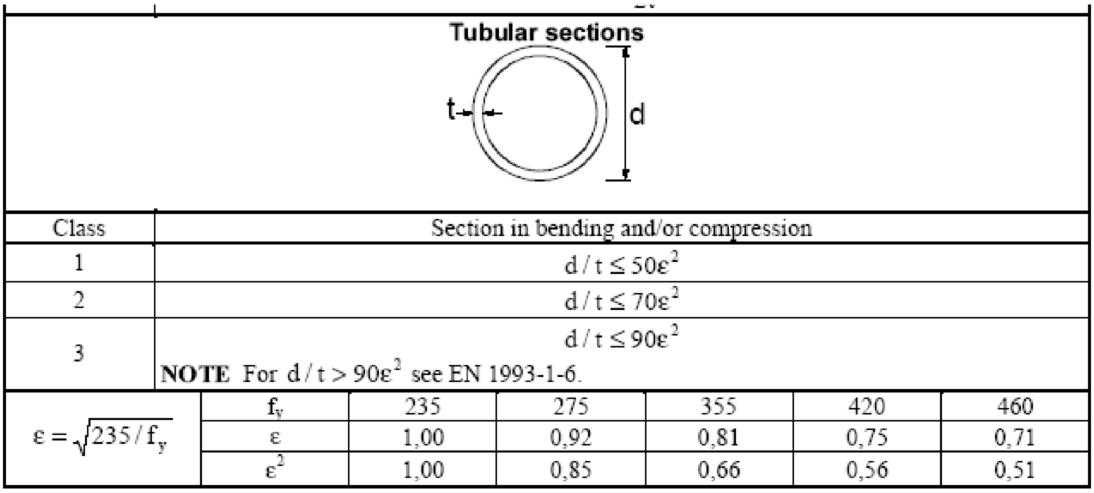

Tubular sections

Class	Section in bending and/or compression
1	$d/t \le 50\varepsilon^2$
2	$d/t \le 70\varepsilon^2$
3	$d/t \le 90\varepsilon^2$ **NOTE** For $d/t > 90\varepsilon^2$ see EN 1993-1-6.

$\varepsilon = \sqrt{235/f_y}$	f_y	235	275	355	420	460
	ε	1,00	0,92	0,81	0,75	0,71
	ε^2	1,00	0,85	0,66	0,56	0,51

Table 29 Classification of tubular sections after Eurocode 3-1-1 (2005)

b. CIDECT design guidelines – No.2 Rondal, J, Wulker, KG, Dutta, D, Wardenier, J, and Yeomans, N (1991). “Design Guide for Structural Stability of Hollow Sections”, Verlag TUV Rheinland GmbH, Köln, Germany.

The design of tubular members for stability under axial loads and bending is conducted in a manner similar to the one in EN 1993-1-1. More specifically,

- Chapter 2 concerns the classification of the CHS members
- Chapter 3 refers to design under axial compression
- Chapter 4 refers to design under bending moments
- Chapter 5 refers to design under combined action of axial compression and bending moments
- Chapter 6, Section 6.3, refers to special design rules for stability under axial compression. The guidelines state that for thin-walled members, a shell-type design should be conducted.

c. API PR 2A – LRFD

American Petroleum Institute (1993). “Recommended Practice for Planning Designing and Constructing Fixed Offshore Platforms - LRFD Design”, API RP 2A-WSD, 20th Edition.

Tubular members are designed according to Section D: “Cylindrical Member Design”. In particular,

- Paragraph D2.2.1 concerns column buckling
- Paragraph D2.2.2 refers to local buckling, elastic and inelastic
- Paragraph D2.3 refers to bending capacity of a tubular member

- Paragraph D3.2 concerns the combined action of axial force and bending.

3. Design procedures for tubular joints under monotonic loading

a. EN 1993-1-8
Comité Européen de Normalisation (CEN). Eurocode 3: Design of Steel Structures, part 1-8, EN 1993-1-8, Design of Joints, Brussels, Belgium
The static strength design of welded tubular connections in EN 1993-1-8 is performed through Chapter 7. In particular,

- Paragraph 7.2 refers to general behavior describing failure modes
- Paragraph 7.3 refers very briefly to welding
- Paragraph 7.4 contains all the necessary formulae for calculating the static strength of the CHS welded connections in terms of the geometric parameters of the joint.

b. CIDECT design guidelines – No.1 - Wardenier, J, Kurobane, Y, Packer, JA, Dutta, D and Yeomans, N (1991). "Design Guide for Circular Hollow Section (CHS) Joints under Predominantly Static Loading", Verlag TUV Rheinland GmbH, Köln, Germany, ISBN 3-88585-975-0.
The verification design of CHS joints under static loading is conducted through parametric design equations in chapter 4 of the design guide, which are very similar to the design formulae in EN 1993-1-8, section 7.4 (see above).
c. API PR 2A – LRFD - American Petroleum Institute (1993). "Recommended Practice for Planning Designing and Constructing Fixed Offshore Platforms - LRFD Design", API RP 2A-WSD, 20th Edition.
The design of welded tubular connections should be conducted according to Section E of the specification. The geometry/material of the joint should follow the effectiveness criterion strength of section E.1. The strength of the connection is calculated through Paragraph E.3. In particular, Paragraph E.3.1 refers to simple (gap) joints, whereas Paragraph E.3.2 refers to overlapping joints. Design equations are provided for both axial loading and bending moments (in-plane and out-of-plane). The failure mode is based on the excessive ovalization of the chord member. The design equations for both axial and bending loading indicate that the joint strength is analogous to $\sigma_y t^2 / \sin\theta$. Furthermore, some factors are included to account for the load in the chord member, and the geometry (type) of joint (T, Y, X or K joint).

4. Design procedures for tubular joints under repeated loading (fatigue)

A typical tubular joint weld detail consists of a main cylindrical member, called "chord", and two secondary members, referred to as "braces", which are welded to the chord, for e.g. see Figure **90**. The braces are loaded with cyclic axial load or bending moments. After a number of loading cycles, a crack starts at the vicinity of the weld. With increasing number of cycles the crack propagates, extending through the thickness and "destroying" the joint (loss of its structural integrity). In the absence of a major defect, the point at which the crack initiates is the point of maximum local stress, called "hot spot stress". The location of this point depends on the geometry of the connections and the loading condition. The local stress value depends mainly on the diameter and the thickness ratio of the two intersecting members. For the particular case of a tubular joint, such as the joint shown in the Figure **90**, the hot spot stress at the weld toe, at the chord and the brace side, can be estimated using appropriate formulae or linear elastic finite element analysis. There are two methods for fatigue design of structural details

- The classification method
- The hot spot stress method

Welded plated (not tubular) connections are usually designed using a classification method. According to this method, there exist in the relevant fatigue design specification (e.g. API, EN, DNV etc), a list of standard details and for each detail a distinct S-N curve is specified. In such a case, the designer has to pick the appropriate "class" for the detail under consideration and calculate the fatigue life in terms of the applied variation of stress. In this method, the nominal stress at the vicinity of the weldment is considered as input for the S-N curve. On the other hand, welded tubular connections have the particularity of having much more complex geometry than simple plated connections. When tubular joints are loaded under various loading conditions, high stress concentrations occur at the weld toe, which are responsible for a significant increase of the local stress with respect to the nominal stress. This high local stress is responsible for a remarkable decrease of the fatigue life of the joint. Due to the variety of geometries that tubular joint may have, the classification method is not very useful for the design of such connections. The method widely employed for their fatigue design is referred to as "hot spot stress" method and is based on the calculation of the maximum local geometric stress at the weld toe at the critical location called "hot spot". Upon calculation of the hot spot stress, a single S-N curve is used to obtain the fatigue design life of the joint. It should be noted that the hot spot stress does not comprise the "local notch effect" on the weld; the notch effect is not explicitly considered, and it is included in the S-N curve.

Hot-spot stress is calculated from the nominal stress range multiplied by a corresponding stress concentration factor (SCF). In other words, the SCF value is the local stress for unit nominal stress. An accurate estimate of the SCF value is crucial for the reliable prediction of the hot-spot stress. The SCF value depends mainly on the joint geometry (Figure 90) described through the following dimensionless parameters

- Brace-to-chord diameter ratio—beta, $\beta = d_1/d_0$
- Chord radius-to-thickness ratio—gamma, $\gamma = d_0/2t_0$
- Brace-to-chord thickness ratio—tau, $\tau = t_1/t_0$
- Brace-to-chord angle—theta, θ

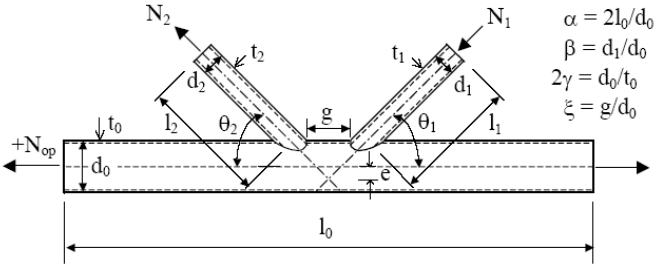

Figure 82 Design specifications of a K-joint

General references for SCF calculation

1. Efthymiou, M. and Durkin, S. (1985), "Stress Concentrations in T/Y and Gap/Overlap K-joints", *Behavior of Offshore Structures*, Delft, The Netherlands, July 85, pp. 429 – 440.
2. Kuang, J. G., Potvin, A. B. Leick, R. D. and Kahlich, J. L. (1977), "Stress concentration in Tubular Joints", *J. Soc. Petroleum Engineers*, Aug. 77

The fatigue design according to various specifications is described below:

a. EN 1993-1-9

Comité Européen de Normalisation (CEN). Eurocode 3: Design of Steel Structures, part 1-9, EN 1993-1-9, Fatigue. Brussels, Belgium

This specification follows the classification method, not the hot spot method. The design is conducted through tables 8.6 and (mainly) 8.7. For each connection type, a class is assigned so that the appropriate design S-N curve is used. Those curves are presented in Figures 7.1 and 7.2 of the specification.

b. CIDECT design guidelines – No.8

Zhao, X-L, Herion, S, Packer, JA, Puthli, RS, Sedlacek, G, Wardenier, J, Weynand, K, van Wingerde, AM, and Yeomans, N (1998). "Design Guide for Circular and Rectangular Hollow Section Welded Joints under fatigue Loading", Verlag TUV Rheinland GmbH, Köln, Germany.

The CIDECT guidelines allow the design of welded tubular connections using either the classification method or the hot spot stress method.

- The classification method is presented in Chapter 2, and the classification of details in Appendix B.
- The hot-spot stress method is presented in Chapter 3. The calculation of SCFs for CHS joints is stated in Chapter 4 and in Appendix D. Furthermore, guidelines for the numerical computational of SCFs through finite element modelling of the joint are presented in Appendix C.

c. API PR 2A – LRFD

American Petroleum Institute (1993). "Recommended Practice for Planning Designing and Constructing Fixed Offshore Platforms - LRFD Design", API RP 2A-WSD, 20th Edition.

Fatigue design of welded tubular connection is covered in Section F, and in particular in paragraphs F.4 and F.5. Tubular connections should be design through the design using the hot spot method. The method, described in a previous section, is based on the calculation of the maximum geometric stress in the vicinity of the weld, excluding the notch effect (which is incorporated in the fatigue curve), but including the “geometric” effects through appropriate SCFs. Suggested SCF values are given in the Commentary of section F. Upon calculation of the hot spot stress, the fatigue life is computed though an appropriate S-N fatigue curve. In API RP2A-LRFD, two curves are used, namely X and X′, shown in Figure 91. A thickness correction is also considered to take in to account the experimental observation that thin-walled members exhibit a better fatigue resistance.

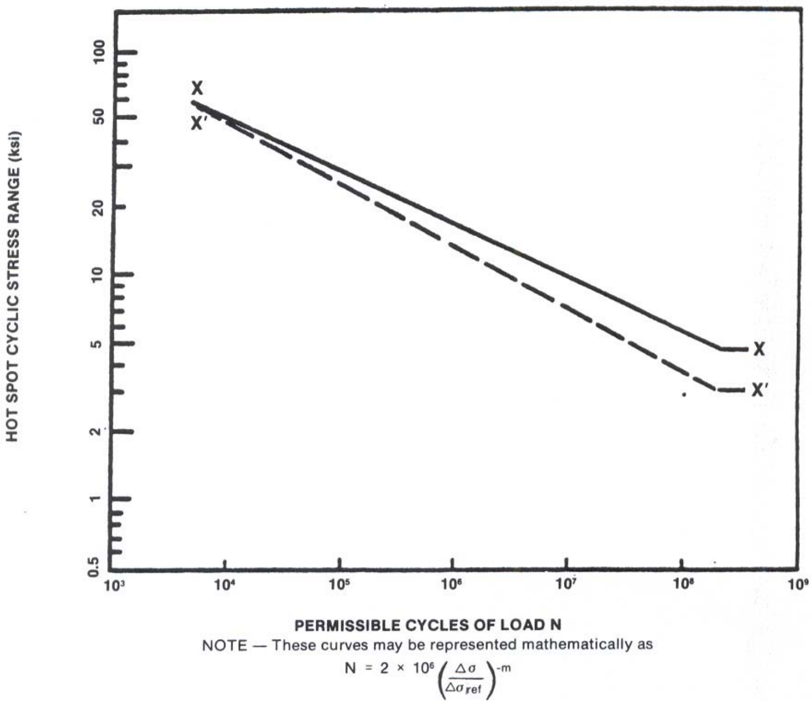

Figure 83 S-N curves based on hot-spot stresses

For welds without profile control, but conforming to a basic standard profile according to ANSI/AWS D.1.1-92) and a branch thickness less than 16 mm, the X′ curve should be used. For thicknesses greater than 16 mm, a thickness correction factor should be used as follows

$$S = S_0 \left(\frac{t}{t_0} \right)^{-0.25}$$

where S is the allowable stress that includes the thickness correction, S_0 is the allowable stress from the S-N curve, t in the actual branch member thickness ($t \le t_0$) and t_0 is the limiting branch thickness, herein equal to 16 mm. For welds with profile control and having a branch thickness less than 25 mm, curve X should be used. If the thickness is greater than 25 mm, the thickness correction t_0 should be considered, with the limiting reference thickness equal to 25 mm.

5. Bayesian evaluation in probabilistic reliability assessment

5.1 Time-dependent reliability analysis

Evaluation of structures for continued service should provide quantitative evidence that their capacity is sufficient to withstand future demands within the proposed service period with a level of reliability sufficient for public health and safety. Structural aging may cause the integrity of structures to evolve over time (e.g., a hostile service environment may cause structural strength and stiffness to degrade). Uncertainties that complicate the evaluation of aging effects arise from a number of sources: inherent randomness in structural loads, initial strength, and degradation mechanisms; lack of in-service inspection measurements and records; limitations in available models and supporting databases for quantifying time-dependent material changes and their contribution to reduce the capacity; inadequacies in nondestructive evaluation; and shortcomings in existing methods to account for repair. Any evaluation of the reliability or safety margin of a structure during its service life must take into account these effects, plus any previous challenges to the integrity that may have occurred. Time-dependent reliability analysis methods provide the framework for dealing with uncertainties in performing condition assessment of existing and aging structures, and for determining whether in-service inspection and maintenance is required to maintain their performance at the desired level.

5.2 Bayesian updating

Bayesian updating techniques are very useful when faced with two sets of uncertain information and a planner needs to know which to believe. Bayesian updating uses both the prior information and new inspection information to account for the relative uncertainty associated with each. Assume that prior to an inspection, a random variable Θ was believed to have a density function $f'(\Theta)$ where Θ is the parameter of that distribution, i.e. the deterioration model. During an inspection, a set of values $x_1,x_2,...,x_n$ representing a random sample from a population X with underlying density function f(x) are observed and are fit to a new density function $f(x_i)$, i.e., the visual inspection results. The updated or posterior density function $f''(\Theta)$ which uses both sets of information and provides the best use of both can be expressed as [42]:

$$f''(\Theta) = kL(\Theta) f'(\Theta)$$

where $L(\Theta)$= likelihood function; and k= normalizing constant. For the case where both $f'(\Theta)$ and $f(x)$ are normally distributed, the posterior function $f''(\Theta)$ is also normally distributed and has the mean value and standard deviation, respectively, as

$$\mu'' = \frac{\mu(\sigma')^2 + \mu'(\sigma)^2}{(\sigma')^2 + (\sigma)^2}, \sigma'' = \sqrt{\frac{(\sigma')^2(\sigma)^2}{(\sigma')^2 + (\sigma)^2}}$$

where μ, μ', and μ'' = mean values of the inspection results, the prior distribution, and the posterior distribution, respectively, and σ, σ', and σ'' = standard deviations of those same distributions.

6. Design of bridges with high strength steel [37]

Bridge design with S460 and S690 steel is not fundamentally different with the conventional steel (S355) commonly used nowadays. Design methods are identical as well as the various calculation checks. If some special bridges: mobile, temporary or pedestrian can be built completely with S460 steel or even S690, things are different for road bridges where the technical options chosen by designers for fatigue justifications are a combination of two steel grades S355 and S460.

Many modern bridges built in France and Germany have been designed with these particularities. However in rail bridges, these high grade steels are completely absent, because these bridges are designed for stiffness.

Design detailing can be classified in two main groups:

- Main structural elements
- Structural detail elements

In the main structural design of decks, the different steel grades have to be distributed longitudinally and sometimes transversely. Structural detail points concern local elements with high stress values, for example supports elements, piers or pylons.

The opportunity to include high strength steel in conventional bridge design depends on the bridge structure: long pr small span decks, steelworks with plate girders, truss or hollow-tubular sections.

These steels allow a reduction of steel sections, hence smaller weights, reduction in thickness and in welds at end to end joints of continuous girders. This aspect tends to show that there are only advantages to use high strength steel for bridges; however attention should be paid to the following points:

- Maintain a minimal stiffness to respect the deflection limits under service conditions,
- Ensure buckling and other stability which are independent of the yield strength,
- Resistance to fatigue which is also independent of the yield strength,
- Toughness against brittle fracture.

Stiffness can be increased by increasing the composite action with concrete, for example double composite action with concrete at the lower flanges also.

In order to maintain a good resistance to buckling, it is often preferable to have thicker webs in a lower steel grade. The design of this type of hybrid girders is now well defined in different parts of EN 1993.

Fatigue resistance can be increased with post weld treatments like grinding, thermal dressing of the weld or peening.

7. High-strength high-performance steel for long span bridges [1]

The benefits and the limitations of the use of HPS steel for conventional bridge types are well documented. However, the use of higher strength HPS for cable supported long span steel bridges is still emerging. There are several key differences in the behavior of cable-supported long span structures that makes the design optimization of these quite different from those of girder and truss type bridges. These same differences make HPS an ideal material of application on these longer span structures. While these advantages make them even more suitable for long span applications, they are yet to be fully exploited for these types of signature large-scale structures.

For example, the traditional live load deflection control of conventional bridge types requires stiffer girders, or heavier sections. The uses of higher strength steels produce more flexible cross sections that produce higher live load deflections. While live load deflection as a design criterion is under review and may change in the future, this limits the realization of maximum potential benefits of the higher strength steels for conventional bridges. Higher strength HPS girders have higher strength to stiffness ratio (F/E) than the traditional grade 50 steels. While this can be a disadvantage in conventional bridge design due to deflection control, it is very desirable for cable-supported bridges due to the following two factors.

First, the stiffness of long span cable-supported structural systems is less dependent on the stiffness of the superstructure, especially for gravity type loading conditions. The controlling live load deflections of long span structures are produced by global loading conditions involving longer length lane loads. While these deflections are highly dependent on the tower stiffness and the stiffness of the supporting cable system, they can be shown to be practically independent of the superstructure stiffness in the range of girder depths used in typical applications.

Second, the internal moments produced in long span bridge superstructures are due to deformations produced by the global loading. Thus the stiffer girder produces higher demand leading to needing a larger girder that in turn increases the demand. The use of HPS provides a means of increasing capacity without increasing stiffness and can provide tremendous advantages for long span bridges. This is a factor not recognized widely at the present time and it is hoped that a discussion on this topic would bring it the attention it deserves.

Furthermore, as evident by the Charles River Bridge in Boston, MA, HPS can be the material of choice for special applications on long span bridges. This first time application took advantage of HPS for its steel composite tower and all of the cable anchorages. The design provided optimal solutions considering the complex design issues, improving constructability and the visual aspects of some key components. This proved to be, while a-typical, an interesting application of this material in its early stages of its availability in the US. Many of the fabrication aspects were first-time applications that required thorough investigation to establish the feasibility early in the design process.

Appendix B: Identification and monitoring of case studies

1. Structural identification of the ‘Ponte del Mare’ foot-cycle-bridge

The complex dynamic behavior and the uncertainties related to the numerical modeling led to a modal testing campaign of the bridge without and with dampers in two phases in the month of October and December 2009. The positioning of the sensors was decided from the modal analyses of the FE model.

1.1 Natural frequencies and mode shapes

The identified frequencies and 3-D graphical view of some mode shapes are reported in Figure 15 and Figure 83, respectively.

Mode 1 w/o dampers – f = 0.75 Hz

Mode 1 with dampers – f = 0.92 Hz

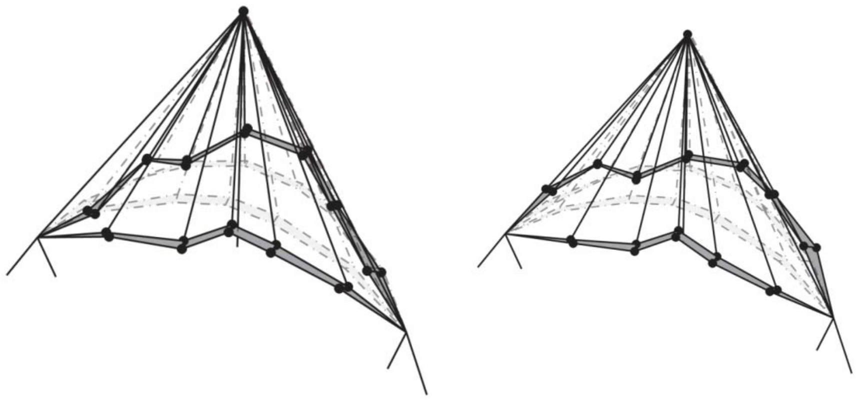

Mode 3 w/o dampers – f = 1.13 Hz Mode 3 with dampers – f = 1.34 Hz

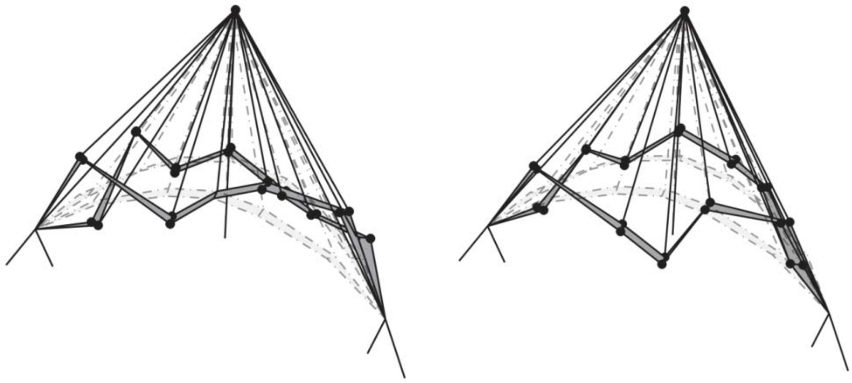

Mode 10 w/o dampers – f = 2.36 Hz Mode 10 with dampers – f = 2.53 Hz

Figure 84 - 3D views of three of the identified modes w/o and with dampers.

The identification process was able to identify the dual behaviour of dampers. From Figure 84 it can be observed that dampers are active only at large amplitude of vibrations, nonetheless, at the lower amplitude they caused stiffening and consequently an increase of the frequency.

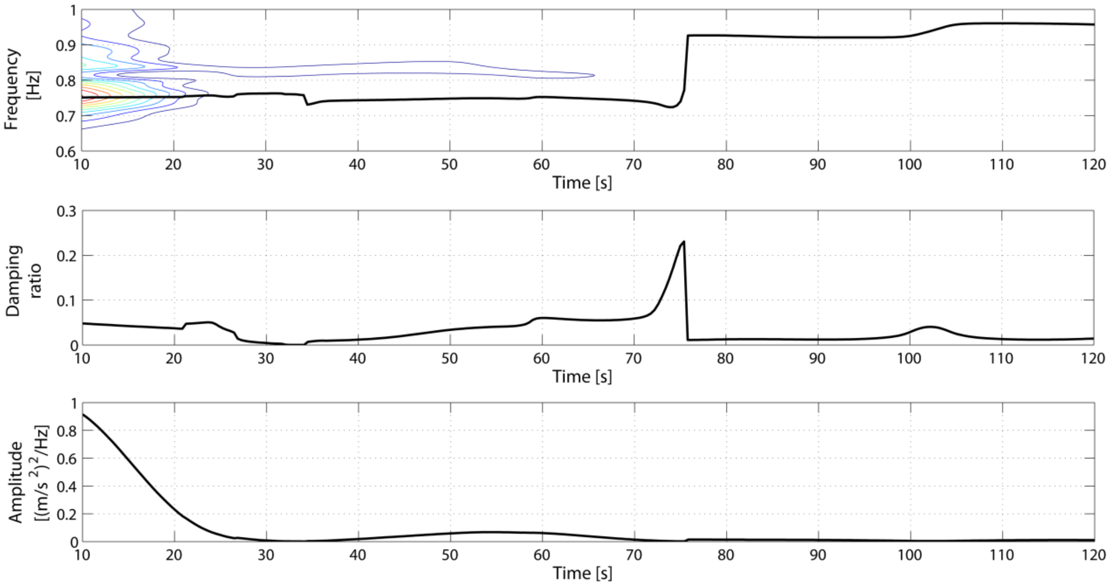

Figure 85 Instantaneous estimates of frequency, damping and amplitude of the first mode obtained from free decay tests (channel M1, ST1 set-up acquisition, structure with dampers)

1.2 Identification of some cables

The dynamic identification of some bridge cables was also performed. In detail, the NE8, NE7, NE5 and NW4 cables were instrumented and ambient vibration tests were carried out. Their position is reported in Figure 85. In the first phase the cables were identified without dampers, whereas in the second phase these were identified with anti-vandalism tubes provided with elastomeric cylinders installed on the cables, with the dampers connected to the structure. The corresponding modal frequencies and axial force estimates, assuming pinned boundary conditions, are reported in Table 30.

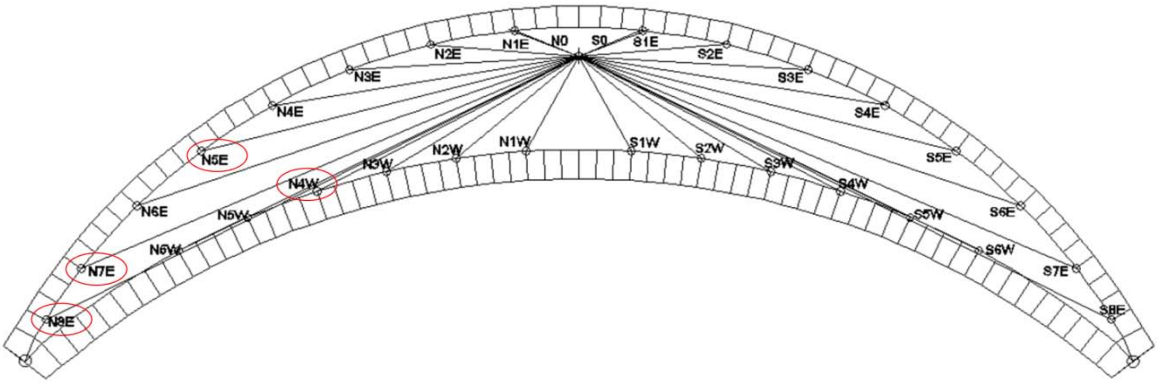

Figure 86 Cable locations

Table 30 Comparison between natural frequencies for the structure without dampers and for the structure with dampers and anti-vandalism tubes

STRUCTURE WITHOUT DAMPERS													
CABLE	L [m]	m [kg/m]	Frequency [Hz]					Axial force estimate [kN]					ξ [‰]
NE8	80	20.2	0.84	1.52	2.30	3.05	3.81	364.9	298.7	304.0	300.7	300.3	0.460
NE7	73.73	10.7	1.06	2.08	3.11	4.16	5.19	259.5	250.4	250.5	251.3	251.1	0.597
NE5	55.7	10.7	1.66	3.30	4.95	6.61	8.28	365.9	361.5	361.5	362.6	364.1	0.301
NW4	46.89	10.7	2.06	4.06	6.07	8.10	10.13	399.3	387.6	384.9	385.5	386.3	0.365
STRUCTURE WITH ANTI-VANDALISM TUBES													
CABLE	L [m]	m [kg/m]	Frequency [Hz]					Axial force estimate [kN]					ξ [‰]
NE8	80	20.2	0.86	1.56	2.30	3.02	3.78	378.0	313.0	302.6	295.2	295.6	0.871
NE7	73.73	10.7	1.13	2.21	3.31	4.41	5.52	297.1	283.8	283.6	283.2	283.4	0.966
NE5	55.7	10.7	1.72	3.45	5.15	6.89	8.59	393.7	394.7	390.9	393.6	392.1	0.253
NW4	46.89	10.7	2.09	4.04	5.91	7.75	9.80	412.6	383.8	365.2	353.3	361.3	0.310

From Table 30, one may notice that the first natural frequencies are slightly increased. This turns out in a stiffening of the cables. Furthermore, what we obtain results to be reasonable if we think that the presence of the anti-vandalism tube introduces a restraint. The damping values calculated according to the Half-bandwidth method highlights an increase of about 60% and 90% for the NE7 and NE8 cables, respectively; and a decrease of about 15% for the NE5 and NW4 cables.

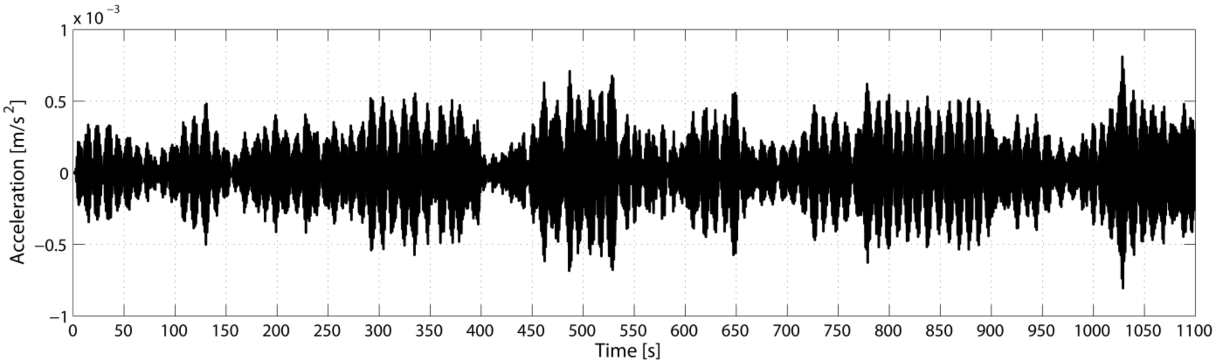

Figure 87 Vertical acceleration time-history from ambient excitation (channel M3, ST1 set-up, structure with dampers)

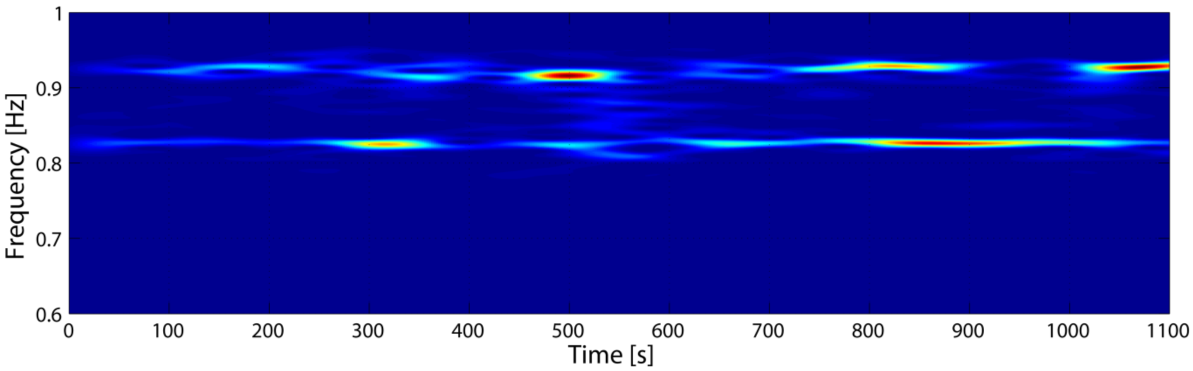

Figure 88 Spectrogram obtained from the signal of Figure 98

Spectrogram in Figure 87 shows clearly the presence of first modal frequency (at 0.93Hz) and the NE8 cable frequency (at 0.86 Hz). Therefore, it was identified a cable-deck interaction phenomenon.

1.3 Identification of the damper cables

The identification of the damper cables, according to the set-up reported in Figure 88, led to the results shown in Table 31.

Table 31 Natural frequencies of the damper cables

DAMPER CABLES													
CABLE	L [m]	m [kg/m]	Frequency [Hz]					Axial force estimate [kN]					ξ [‰]
B-South	14.03	2.90	2.82	5.32	7.98	10.72	12.81	18.2	16.2	16.1	16.4	15.0	0.191
B-North	13.27	2.90	2.86	5.88	8.68	11.28	14.18	16.7	17.6	17.1	16.2	16.4	0.218
A-South	12.98	2.90	2.95	5.93	8.93	12.10	15.47	17.0	17.2	17.3	17.9	18.7	0.160
A-North	11.31	2.90	3.33	6.64	9.79	13.05	16.72	16.4	16.3	15.8	15.8	16.6	0.139

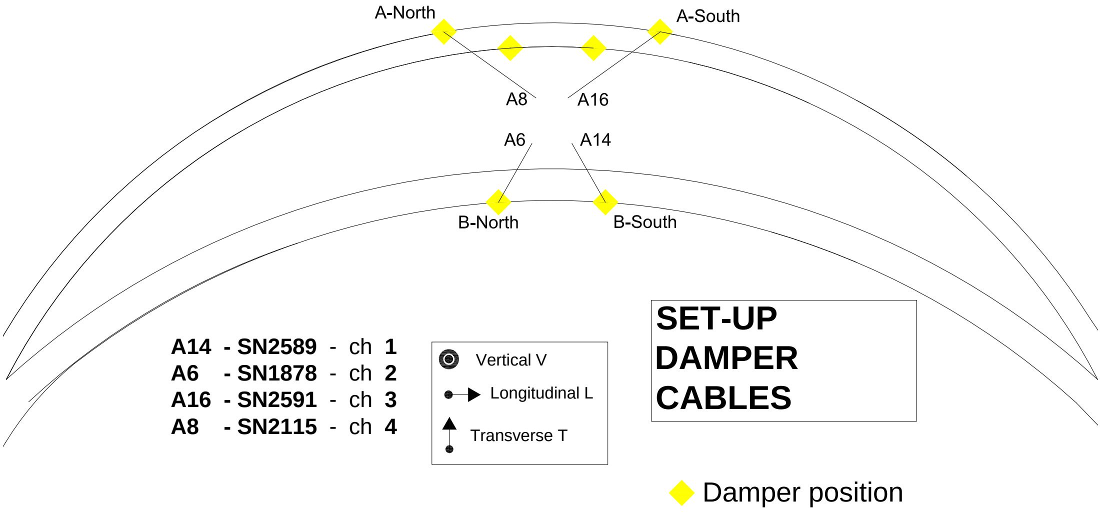

Figure 89 Set-up for the identification of the damper cable

1.4 Analysis of the pedestrian excitation

Due to the dynamic nature of the pedestrian actions, 9 tests with 27 synchronized pedestrians according to the exciting frequencies reported in Table 32 were carried out. The pedestrians, some of them are shown in Figure 89, advanced according to f_{vert}, so that the structure was also indirectly excited by $f_{rad} = f_{vert}/ 2$. One may note that the vertical exciting frequencies of P1 ÷ P4 tests correspond to the frequencies of modes 4 ÷ 7 that were identified for the structure with dampers; while P5 ÷ P9 correspond to the frequencies of modes 1 ÷ 4 for the radial frequencies. The P9 test represents the repetition of the P8 test that entails a pedestrian crossing located only on the foot-track deck, because the latter is more flexible and it is reserved to the pedestrians only. In particular, the P1 ÷ P7 tests are representative of walking frequencies, while the P8 ÷ P9 tests are associated to a running frequency.

Figure 90 Some pedestrians used in the tests

Table 32 Description of the tests with pedestrians

Test	f_{vert} [Hz]	f_{rad} [Hz]	# cycle-track pedestrians	# foot-track pedestrians
P1	1.54	0.77	13	14
P2	1.73	0.87	13	14
P3	1.79	0.90	13	14
P4	2.43	1.22	13	14
P5	1.84	0.92	13	14
P6	2.16	1.08	13	14
P7	2.54	1.27	13	14
P8	3.08	1.54	0	27
P9	3.08	1.54	0	27

A typical time history plot of the pedestrian excitation P9 is shown in Figure 90.

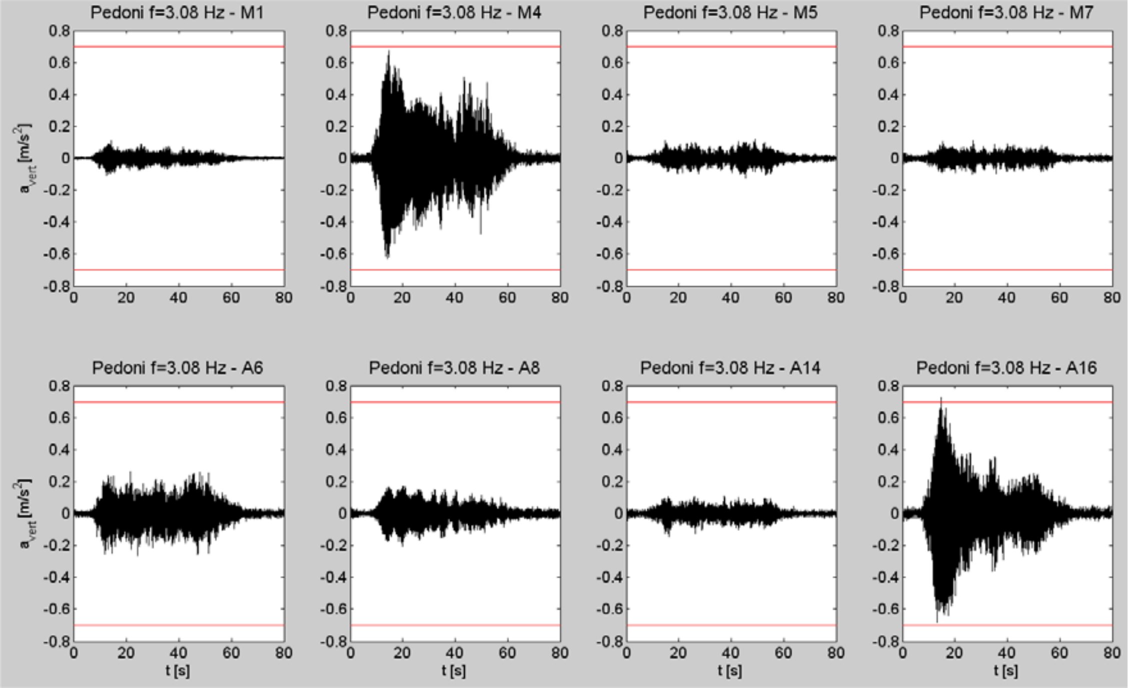

Figure 91 P9 - Vertical acceleration time-histories with exciting frequency fvert = 3.08 Hz

Figure 91 reports the spectrograms for a typical P1 test excitation. In particular, it is observed that the modes corresponding to the frequency range 1.50 Hz ÷ 1.90 Hz are well excited. Conversely, the first mode at 0.92 Hz is weakly excited; this means that the transverse forcing component, equal to half of the vertical exciting frequency, produces oscillations of small magnitude.

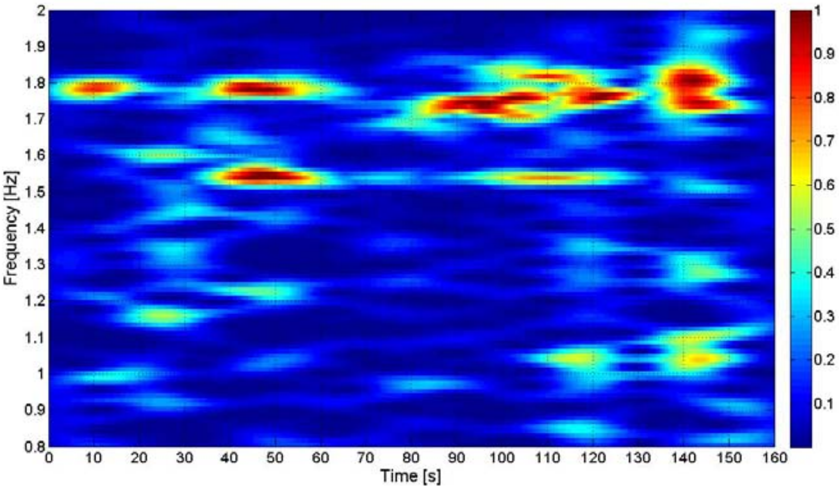

Figure 92 Spectrogram relative to P1 test- Excitation fvert = 1.54 Hz
(Freq. Range 0.80÷2.00 Hz, Filter order 5, subsampling 8)

The time-frequency analyses of the pedestrian excitation data give us the opportunity to check again the natural frequencies of the bridge, already identified in the first phase.

2. Monitoring on site of the “Ponte del Mare” foot-cycle bridge

2.1 Wind speed, wind direction and temperature

The two anemometers installed on the structure are shown in Figure 92.

(a) (b)

Figure 93 Anemometers: (a) 2 m below the foot deck (b) At the mast (height about 40 m)

Figure 93-Figure 95 show the time variation of wind speed, direction and temperature for the week 50 of the year 2010. It can be noticed that the anemometer at the mast approaches to the wind speed about 25.3 m/s and direction 200 degrees (from north direction) on 29 Aug 2010. This wind speed approaches to that of design serviceability state limit (SLS) for 1 year return period, i.e. 25.12 m/s, see Table 5. Please see Table 33 and Table 34 for the mean, minimum and maximum values of temperature and wind velocity for the year 2010.

Table 33 Year 2010: mean, minimum and maximum values of temperature from the four sensors

Value	**T1**		**T2**		**T3**		**T4**	
	(^{o}C)	Date	(^{o}C)	Date	(^{o}C)	Date	(^{o}C)	Date
mean	14.3		14.4		14.4		14.3	
min	-5.6	17/12/2010	-5.7	17/12/2010	-5.5	17/12/2010	-5.2	17/12/2010
max	32.3	16/7/2010	33.4	17/7/2010	33.1	17/7/2010	31.5	17/7/2010

Table 34 Year 2010: mean and maximum values of wind velocity from the two anemometers

Month	**day**	**Vel1**		**Vel2**	
		V_{mean} (m/s)	V_{max} (m/s)	V_{mean} (m/s)	V_{max} (m/s)
January	value	4.3	20.7	3	18.8
	date		3/1/2010		3/1/2010
February	value	4.4	21.5	3	14.7
	date		19/2/2010		7/2/2010
March	value	4	17.3	2.8	16.5
	date		31/3/2010		4/3/2010
April	value	4.1	20.4	2.8	18.2
	date		5/4/2010		5/4/2010
May	value	4.4	20	3	17.2
	date		5/5/2010		31/5/2010
June	value	4.4	22.5	3.2	18.7
	date		21/6/2010		21/6/2010
July	value	4	18.6	2.9	19.1
	date		30/7/2010		30/7/2010
August	value	3.9	25.3	2.7	23
	date		29/8/2010		29/8/2010

September	value	4.7	17.8	3.1	16.4
	date		27/9/2010		10/9/2010
October	value	4.7	18	3.2	17
	date		26/10/2010		26/10/2010
November	value	4	24.5	2.4	18
	date		1/11/2010		1/11/2010
December	value	5.2	24.3	3.4	22.5
	date		9/12/2010		9/12/2010
Annual	**value**	**4.3**	**25.3**	**2.9**	**23**

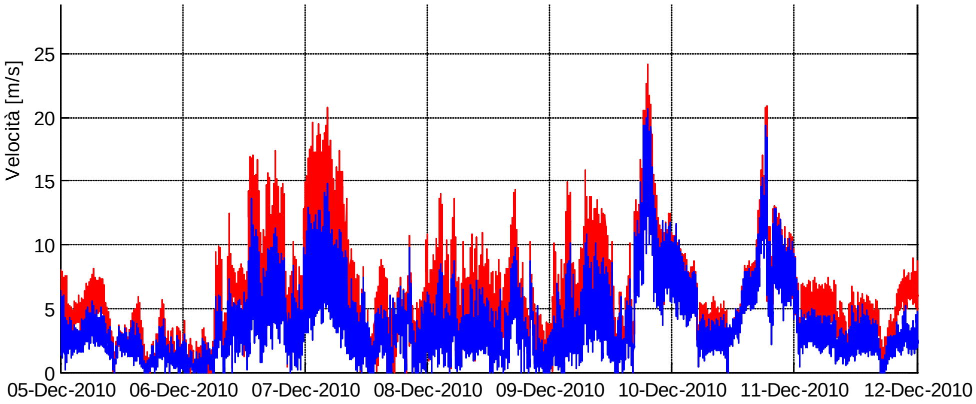

Figure 94 Wind speed , week 50, 2010

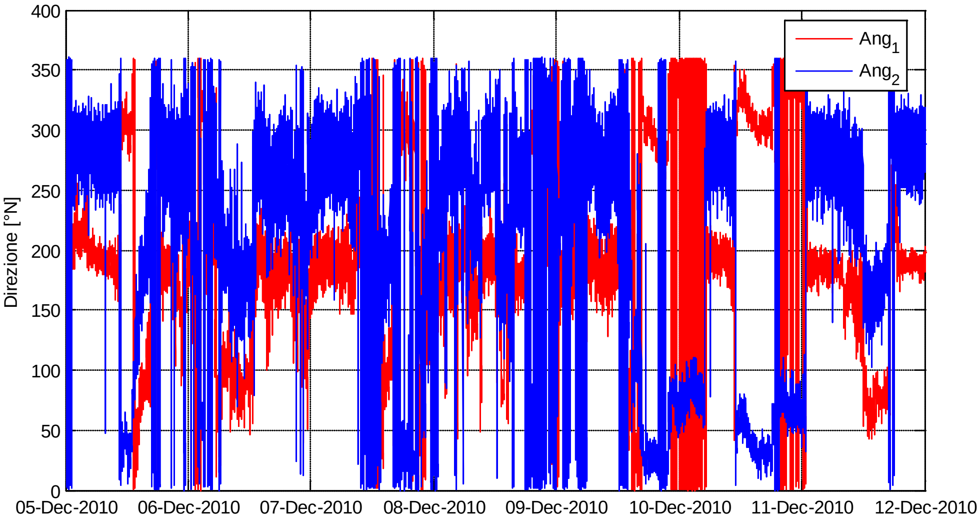

Figure 95 Wind direction, week 50, 2010

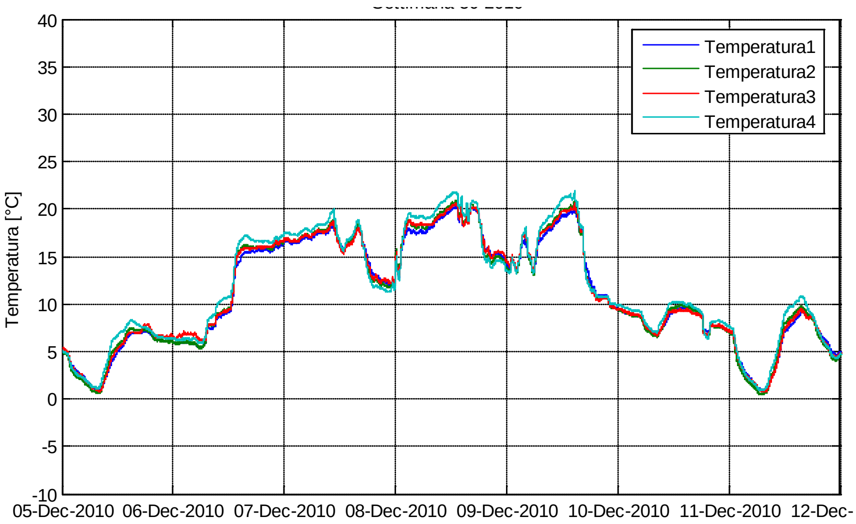

Figure 96 Temperature variation, week 50, 2010

2.2 Analysis of Trigger data: Dec 2009 – Dec 2010

There may be triggers due to wind, pedestrians or some unknown reasons. The number of trigger occurrence is distributed on a bar chart to extract important information, if any.

1. Distribution of triggers with clock hours- It is observed (from Figure 96) that there is the minimum trigger between 6 a.m. to 8 a.m. and the maximum about 6 p.m. This may be due to the presence of more pedestrians on the bridge at evening rather than at morning.

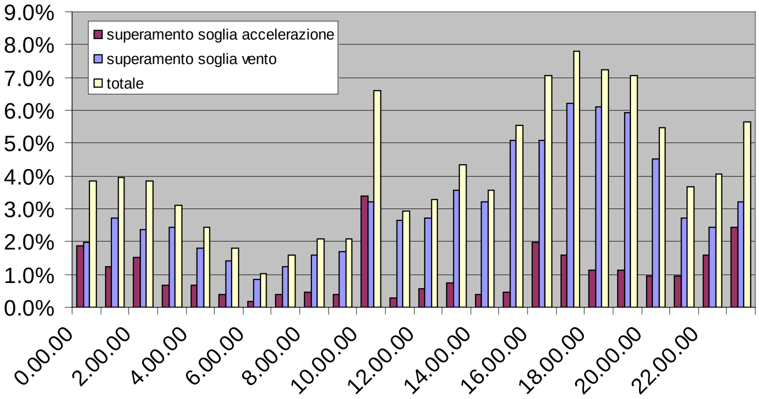

Figure 97 Distribution of triggers with clock hours

2. Distribution of triggers with week days- It is observed (from Figure 97) that the most of the triggers (about 60 %) occur on weekends (Friday-Saturday-Sunday) with maximum on Sunday, i.e. 30. This shows that the bridge is more sensitive to the pedestrian excitations than the wind excitation.

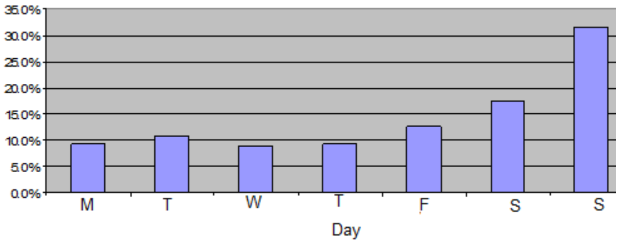

Figure 98 Distribution of triggers with week days

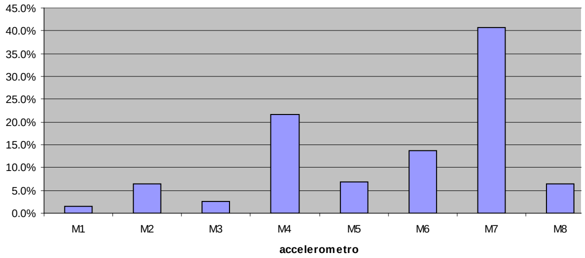

Figure 99 Distribution of triggers with accelerometer channels

3. Distribution of triggers with accelerometer channels- It is observed that (in Figure 98) that the channels 4 & 7 are the locations with the most of the triggers, i.e. about 60%. The channel 4 is located near the end of the foot deck, while channel 7 is located at the middle of the cycle deck. These are the locations more prone to damage due to the extreme events.

2.3 FFT of data

The Fast Fourier Transform (FFT) of some of the monitoring data is performed to reveal the information about the excitation frequencies. Figure 99-Figure 106 show the time history and the FFT of some acquisitions.

2.3.1 Data on 25 Dec 2009 at 12:49:16 (Wind Trigger)

On the Christmas day (25/12/2009), there was a large wind trigger (wind speed 28.02 m/s). The Fast Fourier Transform (FFT) of data reveals information about the excitation frequencies. In Figure 99 and Figure 100, the wind excitation and the corresponding excitation frequencies respectively that occurred on 25 December 2009 can be seen. It can be observed that frequencies below and near 1 Hz are well excited. This is because wind typically excites frequencies below 1 Hz.

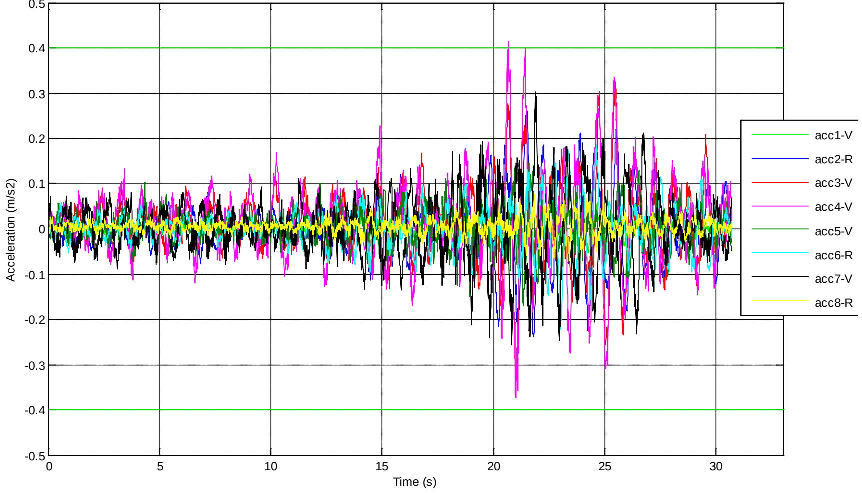

Figure 100 Time history of the wind excitation on 25 Dec 2009

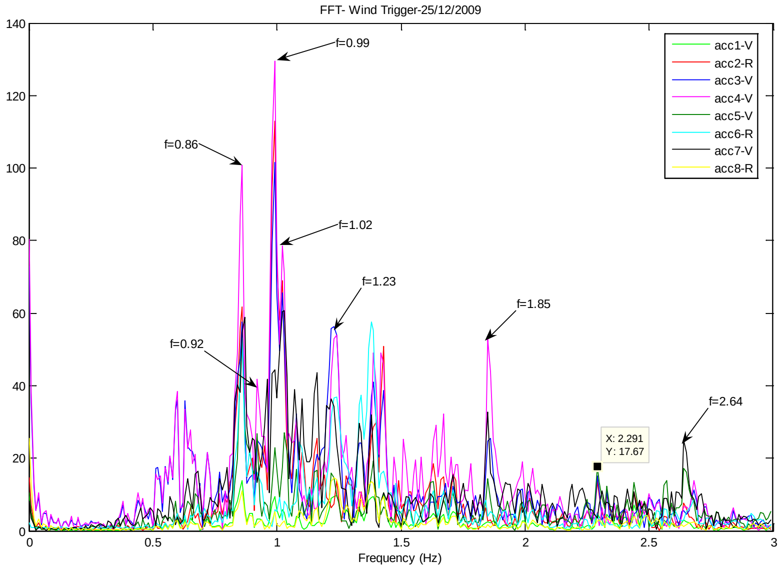

Figure 101 FFT of the wind excitation data on 25 Dec 2009

2.3.2 Data on 17 Oct 2010 at 10:15:47 (Pedestrians Trigger)

There was a running competition on 17 Oct 2010 about 10:00. About 800 persons passed via the bridge that time and the acceleration level reached above the comfort level (0.7 m/s2). In addition to the highest peak frequencies near 3 Hz, the FFT of the data in Figure 104 shows the presence of higher frequencies near 6 Hz and 9 Hz. These may be the higher harmonics of the main frequencies. According to the Fourier series higher harmonics are the integral multiple of the fundamental frequency, refer SETRA [23]. Similar event was observed on 11 April 2010 during the running competition.

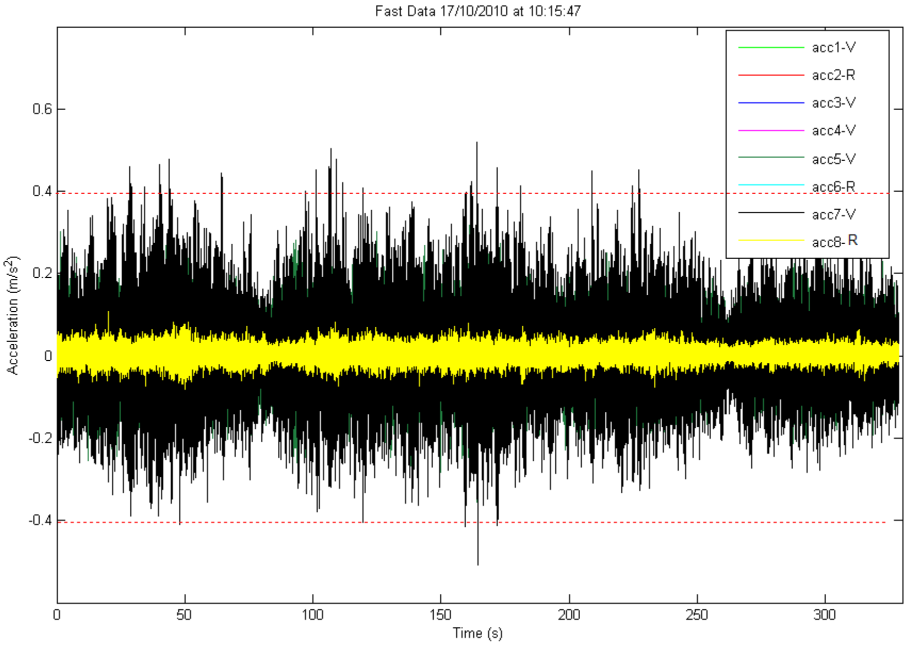

Figure 102 Time history of the data on 17 Oct 2010 at 10:15:47

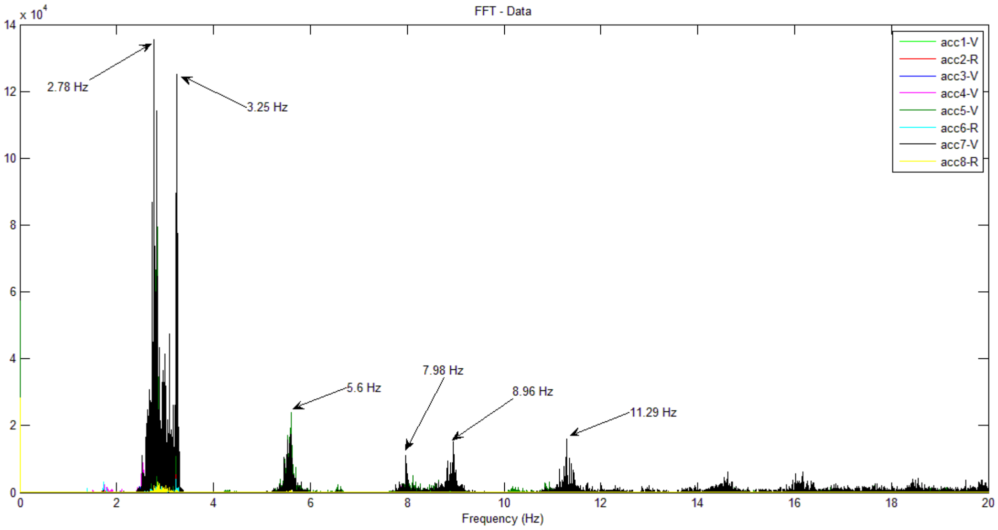

Figure 103 FFT of the data on 17 Oct 2010 at 10:15:47

2.3.3 Data on 01 Nov 2010 at 17:44:05 (Wind Trigger)

This shows a wind excitation as most of the frequencies are concentrated around 1 Hz. However, the damping effect is clearly visible. The decaying amplitude shows that the dampers are effective to mitigate the vibration. The wind speed was recorded 22.05 m/s at this time.

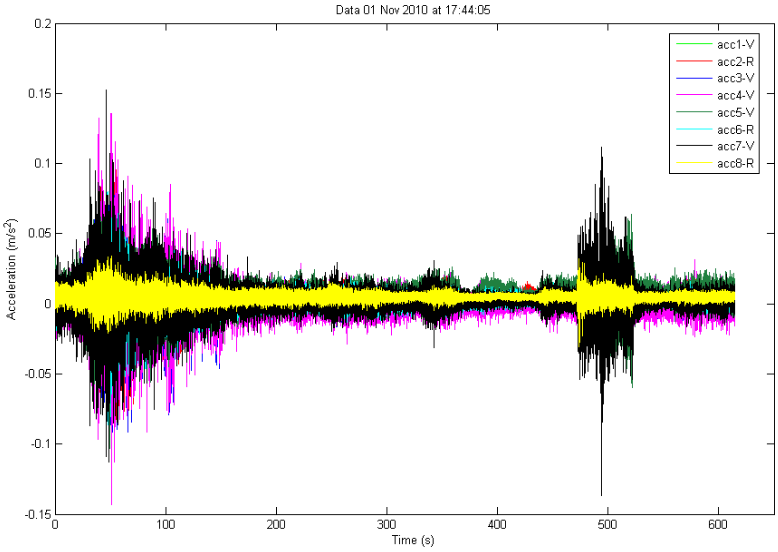

Figure 104 Time history of the data on 01 Nov 2010 at 17:44:05

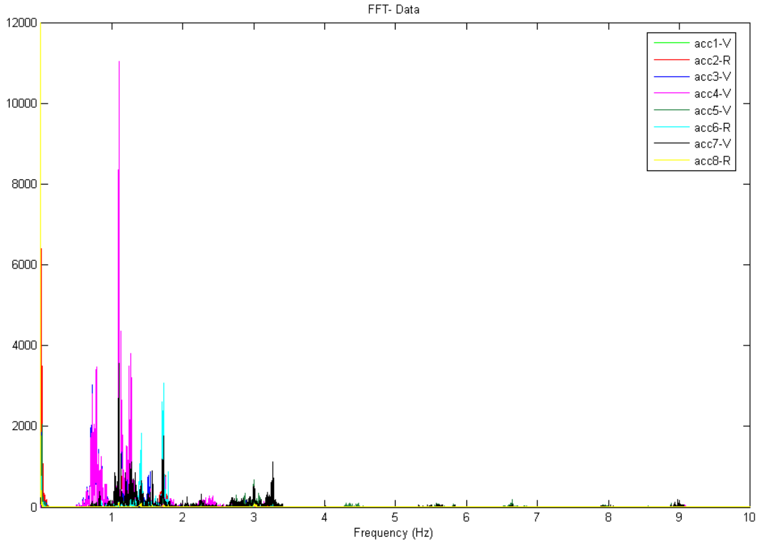

Figure 105 FFT of the data on 01 Nov 2010 at 17:44:05

The structural health monitoring was operational on the footbridge during Dec 2009- Dec 2010, i.e. for one year. The maximum wind speed of 28.02 m/s was recorded at the mast. The maximum acceleration reached up to 0.703 m/s^2 above the comfort level of pedestrians. After the FFT analysis and investigations, it was found that there was a running competition on 17 Oct 2010 that led to this peak acceleration level. Several normal pedestrian activities like walking, running and jumping were detected on other days too. Channels 4 and 7 were subject to the maximum number of triggers as well as most of the triggers occurred on weekends and at evening. It was also derived that the footbridge resulted to be more sensitive to pedestrian-induced excitations than to that of wind.

3. Landegem Railway Bridge

3.1 Geometries and characteristics of the arches and the hangers

In the original calculation note [47], the designed arches and hangers have the geometries and characteristics presented in Table 35 [47].

Table 35 Geometries and characteristics of the arches and the hangers **[47]**

Element	Section shape	A (cm^2)	I_z (cm^4)	I_y (cm^4)

Arches	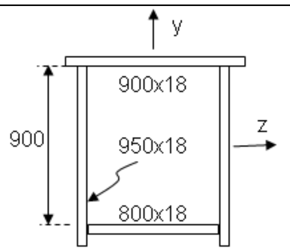	648	904033	758251
Hangers	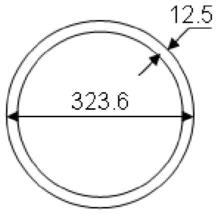	122	14803	14803

3.2 Internal forces in the arches and the hangers

The axial force and the bending moment reported in Table 36 were chosen to calculate the arches and the hangers [47].

Table 36 Internal forces in the arches and the hangers **[47]**

Element	Internal forces (in tonne and meter)			
	For the calculation of resistance		For the calculation of fatigue	
	N_{max}	M_{max}	ΔN_{max}	ΔM_{max}
Arches	-571	175	358	111
Hangers	115; -34	≈ 0	125	≈ 0

3.3 Structural analysis of the arches

3.3.1 Effective length

In the calculation note of Greisch's office [47], the slenderness (λ_{arches}) of the arches was computed as follows:

- the system of arches and the traverse members is simplified as a plane system with a length equal to the developed length of the arches. The effects of the hangers are modelled through equivalent spring supports (Figure 105).

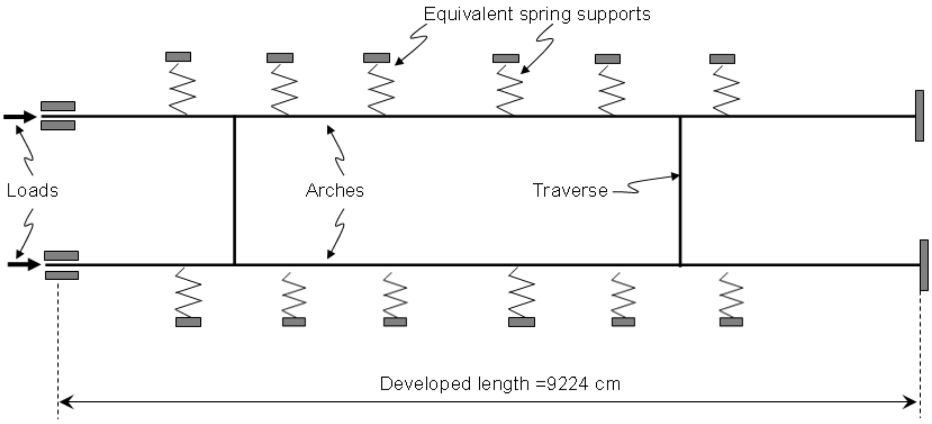

Figure 106 Arches modelling for the stability analysis

- An elastic buckling analysis for the system is carried out; the critical load is obtained and the associated critical stress (σ_{cr}) can be directly found. The first buckling mode is shown in Figure 106.

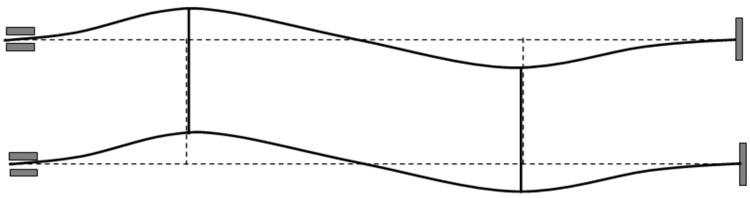

Figure 107 First buckling mode of the arches

- The slenderness of the arches can be computed through the formula:

$$\lambda_{arches} = \pi \sqrt{\frac{E}{\sigma_{cr}}}, \tag{B1}$$

with E, the Young modulus of steel.
Finally, according to [47], $\lambda_{arches}=75$ was obtained.
In the present work, an optimisation process is used, in which the arches section is varied. In this process, it would be very complicated to include the buckling analysis as the used procedure is iterative. Therefore, the simplified procedure as described here below has been adopted:

- From the slenderness of the aches ($\lambda_{arches}=75$), an effective length of 2566 cm is obtained. Also, for the buckling mode presented in Fig.B2, the effective length of the arches may be expressed as:

$$l_{eff,arches} = 0.7 k l_{dev,arches} / 2, \tag{B2}$$

where the coefficient of 0.7 takes into account of the support conditions of the arches; $l_{dev,arches}/2$ is due to the double wave buckling mode as presented in Figure 118 ($l_{dev,arches}$ = 9224 cm); and k is a coefficient taking into account the effects of the hangers.

- Substituting the value of 2566 cm for the effective length in Eq.(B2), a value of k equal to 1,25 is obtained. It is reasonable to see that the effective length is increased of about 25% due to the hanger effects.

- Accordingly, it is decided to fix the value of 2566 cm as the effective length for the arches.

After having the effective length, the arches can be considered as an isolated column subjected to compression and bending with an actual length equal to 2566 cm.
3.3.2 Member stability analysis
The rules from Eurocode 1993 Part 1-1 [33] are used; only essential information is reminded here below.

- *The input quantities are:*
  - f_y is the yield strength of the steel;
  - E is the modulus of elasticity of the steel ($E = 2{,}1x10^9$ kN/m^2);
  - D is the outside diameter of the tube;
  - t is the tube thickness;
  - l_{eff} is the buckling length of the arches.
  - N_{Ed} , M_{Ed} are the design values of the compression and the bending moment respectively (see Table 36).

- *Classification of sections*:

$$\left| \begin{array}{ll} D/t \le 50\varepsilon^2: & \text{Class 1;} \\ D/t \le 70\varepsilon^2: & \text{Class 2;} \\ D/t \le 90\varepsilon^2: & \text{Class 3;} \end{array} \right. \tag{B3}$$

where $\varepsilon = \sqrt{235/f_y}$ with f_y expressed in N/mm^2.

Class 4 is not considered in the present work.

- *Intermediate quantities*:
  - $A = \pi(t^2 + dt)$ is the cross-section area;
  - $W_{el} = \frac{\pi}{32d}[d^4 - (d-2t)^4]$ is the elastic bending modulus of the cross-section;
  - $W_{pl} = \frac{1}{6}[d^3 - (d-2t)^3]$ is the plastic bending modulus of the cross-section;

- $I = \frac{\pi}{64}[d^4 - (d-2t)^4]$ is the second moment of inertia of the cross-section;
- $N_p = f_y A$ is the design plastic compression resistance of the cross-section;
- $M_{el} = f_y W_{el}$ is the design elastic bending resistance of the cross-section;
- $M_{pl} = f_y W_{pl}$ is the design plastic bending resistance of the cross-section;
- $i = \sqrt{\frac{I}{A}}$ is the radius of gyration of the cross-section;
- $\overline{\lambda} = \sqrt{\frac{N_{pl}}{N_{cr}}} = \frac{l}{\pi i}\sqrt{\frac{f_y}{E}}$ is the non-dimensional slenderness of the arches with the elastic buckling force provided through Eq. (B4);

$$N_{cr} = \frac{\pi^2 EI}{l_{eff}} \tag{B4}$$

- $\Phi = 0,5[1 + \alpha(\overline{\lambda} - 0,2) + \overline{\lambda}^2]$ is used to determine the reduction factor χ, with: $\alpha = 0,21$ for S355 steel and $\alpha = 0,13$ for HSS (the tubes are assumed to be hot rolled). The reduction factor is calculated using Eq. (B5);

$$\chi = \frac{1}{\Phi + \sqrt{\Phi^2 - \overline{\lambda}^2}} \tag{B5}$$

- C_{yy} is the factor taking into account the reduction of the design plastic resistance due to bending moment:

$C_{yy} = 1$ for section of Class 3;

$$C_{yy} = \begin{vmatrix} 1,1 \quad \text{if} \quad \overline{\lambda} \le 1 \\ 1/[0,9 + 0,5(W_{pl}/W_{el} - 0,9)(\overline{\lambda} - 1) \quad \text{if} \quad 1 < \overline{\lambda} \le 3 \\ (W_{pl}/W_{el})^{-1} \quad \text{if} \quad \lambda > 3 \end{vmatrix} \quad \text{for section of Class 1 or 2.}$$

- M_{Rk} is the characteristic bending resistance of the critical cross-section: for sections of Class 1 and Class 2: $M_{Rk} = M_{pl}$; for sections of Class 3: $M_{Rk} = M_{el}$.

- *Member verification*:

$$\frac{N_{Ed}}{\chi N_p} + \frac{1}{1 - \frac{\chi N_{Ed}}{N_{cr}}} \frac{M_{Ed}}{C_{yy} M_{Rk}} \le 1 \tag{B6}$$

3.3.3 Fatigue verification for the arches

The stress range in the arches is calculated by:

$$\Delta\sigma = \frac{|\Delta N|}{A} + \frac{|\Delta M|}{W_{el}} \le [\Delta\sigma] \tag{B7}$$

with ΔN and ΔM the variations of internal forces (Table 37). [Δσ] is the admissible stress range.

3.3 Definition of the optimisation process for the arches

- *Cost function*

The following cost function is adopted:

$$C = lAc_a, \tag{B7}$$

with l the real length of the arches, A the area of the arches, c_a the price (per volume unit) of the steel.

- *Constraint condition*

- Requirement of *section classification*: Eq.(B3);
- Requirement for *member buckling resistance*: Eq.(B6)
- Requirement for *fatigue resistance*: Eq.(B7);
- *Constitutive* condition: $t \le D/2$.

The optimum research problem can be qualitatively interpreted as it is depicted in Figure 107.

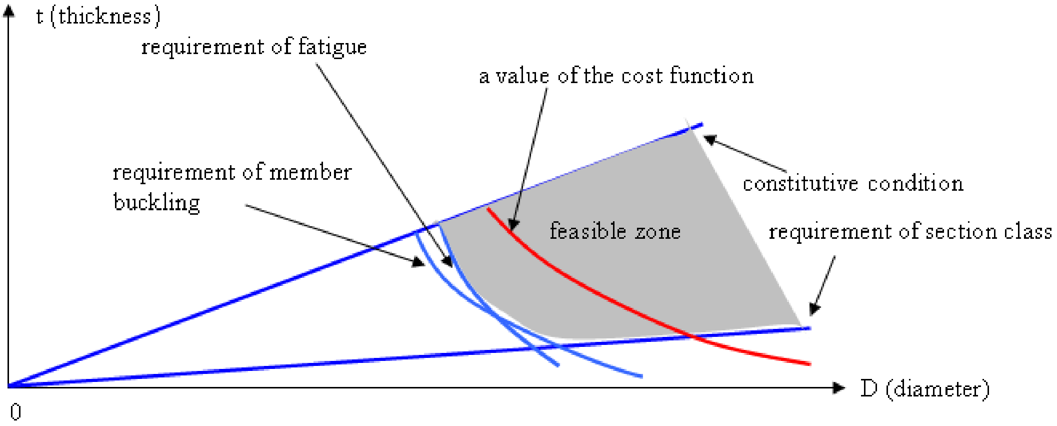

Figure 108 Graphical representation of the optimisation process

3.4 Structural analysis for the hangers

The behaviour of the hangers may be considered as element subjected to tension; rules from Eurocode 3, part 1-1 [33] are used. The calculation is quite simple and they are not presented herein.

4. Identification of S. Michele footbridge

Three types of excitations were used- released mass of 27.5 kN weight, impact hammer and ambient vibration, see Figure 108.

Figure 109 Type of excitations- released mass and impact hammer

A total number of 23 accelerometers were employed to capture the response of the structure. Figure 23 shows a typical recorded acceleration data.

The Welch transform was used to identify the frequencies from the test data. The identified frequencies can be seen in Figure 109 and Table 7. Moreover, Figure 110 shows the damping values corresponding to identified frequencies.

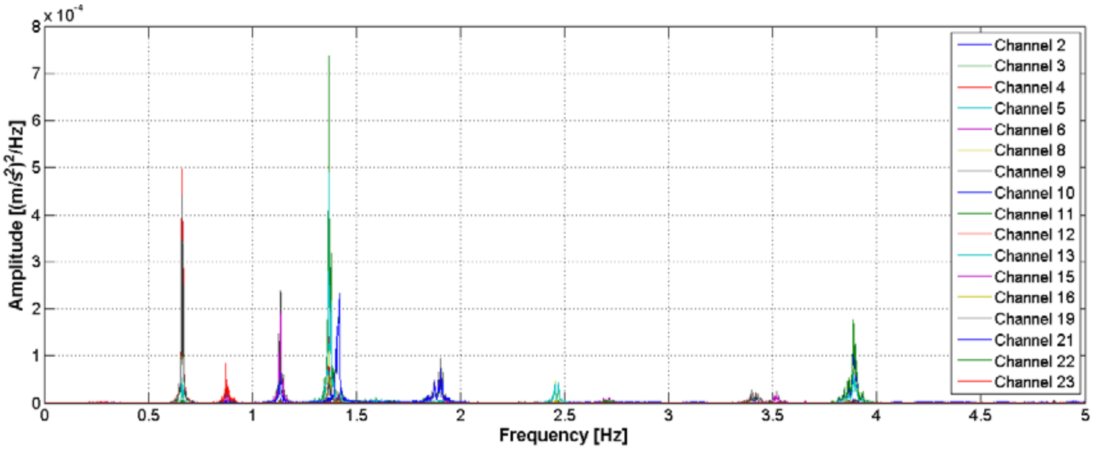

Figure 110 PSD of the data

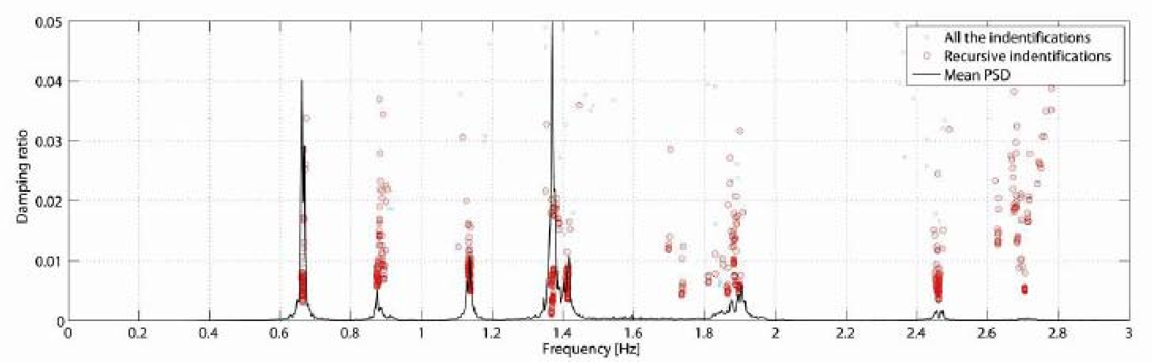

Figure 111 Identified frequencies and damping ratios

The first two mode shapes are shown in the following Figure 111.

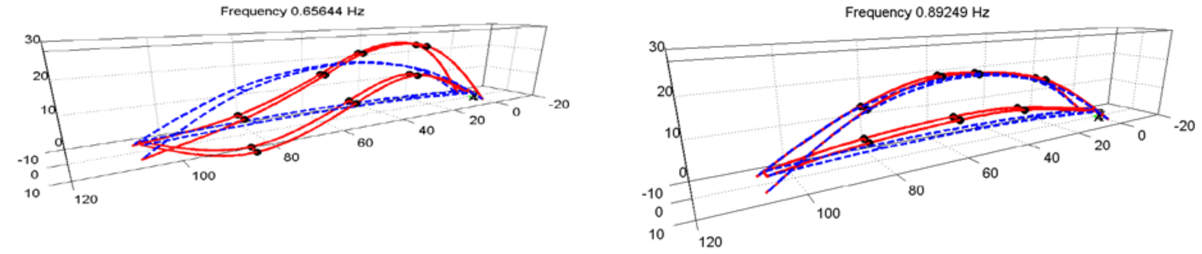

Figure 112 Mode shape (a) Ist mode (b) 2nd mode

5. Monitoring of S. Michele footbridge for pedestrian excitations

Several modern footbridges have shown the phenomenon of vibration induced by pedestrians. The vibration levels reach above the comfort level of pedestrians. Therefore, it is advised to monitor the footbridge after its construction.

In this regard, the monitoring tests were performed on S. Michele footbridge. Pedestrians were allowed to walk in a group of 11 at a known walking frequency produced by a metronome.

The following frequencies were considered.

Table 37 Frequencies considered for the monitoring

Mode	Component	Frequency	Walking Frequency
2	Horizontal	0.90 Hz	1.80 Hz
3	Horizontal	1.21 Hz	2.42 Hz
7	Vertical	2.42 Hz	2.42 Hz

The accelerometers location is shown in Figure 115.

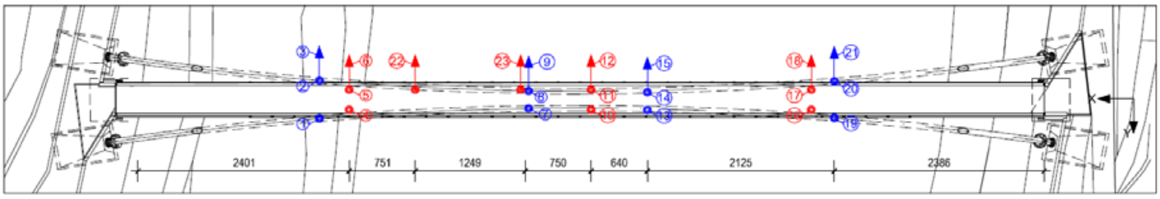

Figure 113 Top view of the acquisition setup

The RMS value of the acceleration records is reported in the following Figure 116.

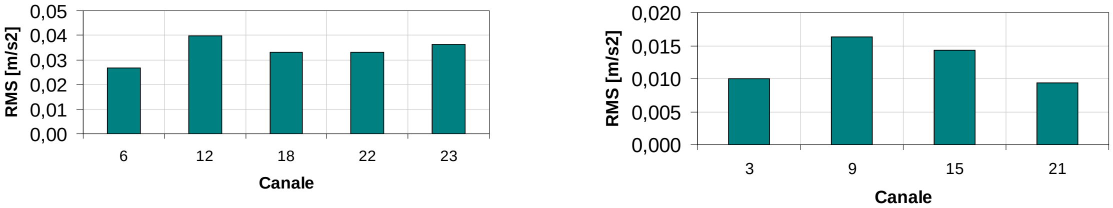

Horizontal acceleration in the bridge

Horizontal acceleration in the arch

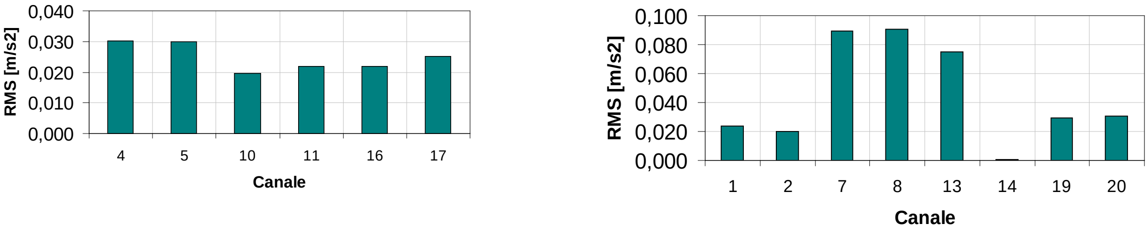

Vertical acceleration in the bridge

Vertical acceleration in the arch

Figure 114 Extreme RMS acceleration values in each channel with 7 acquisitions

The footbridge frequencies and damping were identified. Moreover, the bridge was monitored for some pedestrian excitations. It was found that accelerations obtained at each channel were within the maximum comfort range of pedestrians.

Appendix C: Tests on materials and members

1. Mechanical characterization of HSS (S500Q/ S500MC to S690Q/S700MC) and toughness also considering a corrosive environment

1.1 Corrosion rate measurements

Uniform corrosion rate of the base metal was measured in two different solutions, 1 wt% and 3.5 wt% NaCl. Test solutions were made from analytical grade reagent NaCl and deionized water in order to simulate the offshore and seawater environments, respectively. The tests were carried out at room temperature (~ 25 °C). The pH of the solution was 6.5 at the beginning of the experiments. The effect of oxygen concentration on uniform corrosion resistance in sodium chloride solution was investigated in aerated and de-aerated (N_2-bubbleing) conditions. In de-aerated condition, the solution was purified before running the experiment with dry nitrogen gas for 10 minutes to remove dissolved oxygen. The nitrogen bubbling was kept during the test. The linear polarization resistance technique, based on the change in potential and record of the polarization resistance (the slope of the linear polarization curve dE/di is termed the Rp) was used to measure the corrosion rate. The corrosion potential (E_{corr}) and current density (i_{corr}) were calculated from the data and obtained with the use of Tafel extrapolation technique. The corrosion rate was calculated from the current by using Faraday’s law. The experiments were performed in a three-electrode Avesta cell.

The average of the corrosion rates are summarized in Table 38. No apparent crevice or pitting corrosion was observed on the surface. The corrosion rate of S355 was slightly higher compared with the TS590 grade in all tested environmental conditions. Higher corrosion rate was achieved for both materials in 3.5 wt% NaCl compared to 1 wt% NaCl. Furthermore, maximum corrosion rates for both materials were obtained in the presence of the oxygen.

Table 38 Average of corrosion rates [mm/year] for TS590 and S355 base metal at room temperature

Steel grade	Environment	Air or N_2 bubble	Average corrosion rate **(mm/year)**	$\pm \frac{1}{n}\sum \left| x - \bar{x} \right|$
TS590	3.5 wt% NaCl	Air bubble	0.140	0.018
TS590	3.5 wt % NaCl	N_2 bubble	0.105	0.014
TS590	1wt % NaCl	N_2 bubble	0.058	0.008
S355	3.5 wt % NaCl	Air bubble	0.168	0.030
S355	3.5 wt % NaCl	N_2 bubble	0.114	0.031
S355	1 wt % NaCl	N_2 bubble	0.086	0.016

The electrochemical general corrosion rate measurements showed that steel TS590 had the same corrosion resistance or slightly better than the reference material S355.

1.2 Slow strain rate tests (SSRT)

The SSRT testing, combines slow strain rate in corrosive environment and is used to evaluate the susceptibility of materials to stress corrosion cracking and hydrogen embrittlement. The samples were longitudinally cut. The length direction of the tensile sample was parallel to the longitudinal of the pipe. The SSRT were performed in air, 1 wt% and 3.5 wt% NaCl solutions open in contact with air in ambient temperature (~ 25 °C). A strain rate of 10^{-6} s^{-1} was applied throughout the experiments. The test was performed at Open Circuit Potential (OCP), i.e. E_{corr}. In order to simulate cathodic protection, cathodic polarization with the magnitude of 40 mA was applied throughout the test of some of the samples in order to enable diffusion of hydrogen into the specimens. The elongation EL%, yield stress (YS) and ultimate tensile strength (UTS) were calculated from the stress vs. strain curves. The time to failure (TTF) was determined during the SSRT. Furthermore the Reduction of Area, RA (%) was measured on the samples after cracking.

The results from the SSRT measurements are presented in Table 39. The RA determinations show drastically lower RA for material TS590 with in presence of cathodic polarization. The measurement in 1 wt% NaCl with applied cathodic polarization of 4 mA/cm², showed that TS590 had a lower RA than S355. Measurements in air and in 3.5 wt% NaCl without cahodic polarization gave no significant difference in RA for TS590 and S355. The TTF in hours was significantly decreased when cathodic polarization was applied for the materials. No significant difference in TTF was measured for TS590 and S355. The elongation of TS590 and S355 steels was lower when cathodic polarization was applied. No significant differences were observed in YS and UTS for TS590 compared to S355.

Table 39 Mechanical properties of TS590 and S355 in different environments, with and without cathodic polarization.

	Air		**1 wt% NaCl**		**1 wt% NaCl at 4 mA/ cm²**		**3.5 wt% NaCl**		**3.5 wt% NaCl at 4 mA/ cm²**	
	TS590	**S355**	**TS590**	**S355**	**TS590**	**S355**	**TS590**	**S355**	**TS590**	**S355**
RA (%)	75.67	72.30	78.85	-	38.29	66.74	76.31	76.73	34.78	-
TTF(hr)	34.13	37.00	35.38	-	29.83	28.42	35.17	34.17	28.04	-
EL (%)	9.86	10.40	10.35	-	6.80	6.60	10.00	9.10	6.35	-
YS (MPa)	782	765	770	-	755	765	780	765	778	-
UTS (MPa)	818	803	812	-	804	803	822	807	822	-

The SSRT-measurements showed that TS590 and S355 were not susceptible to stress corrosion cracking (SCC) in 1 wt% and 3.5 wt% NaCl solutions where no cathodic polarization was applied. However, when applying cathodic polarization a significant effect on RA, TTF and EL were achieved for both of the materials. The RA-values as well as the TTF and EL-values were considerable lowered when cathodic polarization was applied. This reflects that both of the materials, TS590 and S355, are sensitive towards hydrogen assisted corrosion cracking in presence of cathodic polarization. It is not possible from the actual data to draw any conclusions concerning the ranking between TS590 and S355 in sensitivity towards stress corrosion cracking. Material S590 had a considerable lower RA than S355 in 1 wt% NaCl with 4 mA/cm², while it had a slightly longer TTF and higher EL.

Additional SSRT-measurements were performed on welds from the different materials within WP4. These results are presented separately in that working package. When putting these results together a better overview of the comparison of the sensitivity towards stress corrosion cracking of the different material is achieved.

1.3 Fracture toughness

The fracture toughness characterization has been performed by means of the determination of the J-R curve of each base material. The specimens were extracted from the tubes with an outer diameter of 355 mm and a thickness of 12 mm. The dimensions of the specimens were 11x11x60 mm, having a standard notch from the inner side of the tube. The test procedure followed the requirements of the standard [9]. The tests were performed at ambient temperature. In Figure 117 and Figure 118, the mean J-R curve of three tests has been depicted and the value for the intersection of this curve with the 0.2 mm blunting line is shown. This value, that represents the energy for the onset of the stable crack growth, has resulted in 620 kJ/m^2 for the S355 and 440 kJ/m^2 for the TS590.

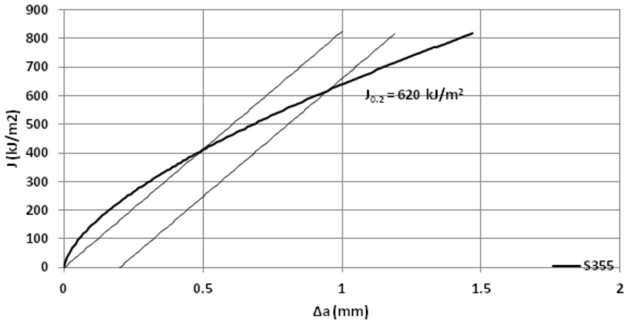

Figure 115 J-R curve of S355 base material. J0.2 = 620 kJ/m2

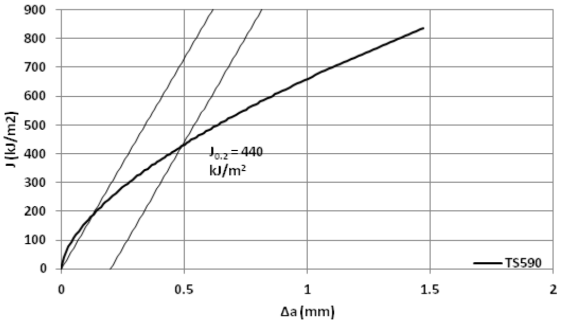

Figure 116 J-R curve of TS590 base material. J0.2 = 440 kJ/m2

2. Moment-curvature tests under flexural and axial loads in order to evaluate the inelastic cyclic flexural behavior of HSS tubes

2.1 Geometrical measurements and instrumentation

In Figure 119, a schematic of the specimen geometrical survey is reported. Thickness and diameters have been measured at 9 different cross sections at 8 measuring positions in each cross section. Analysis of geometrical imperfections is reported in the Section 3 of this appendix. Whole sets of measurements are reported in the relevant Deliverable 3.2.

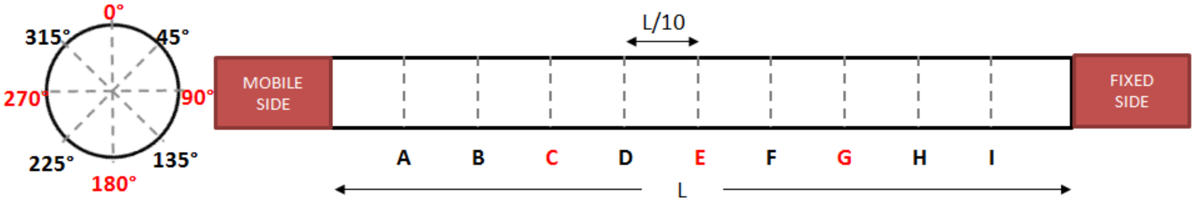

Figure 117 Sketch of the specimen geometrical survey and position of strain gages

Ovalization evolution was monitored via diameter measurements at cross sections A, B, E, H and I (Figure 119) at 2nd, 3rd, 5th, 10th and 15th cycles.

The strain gauges positions are listed below with reference to Figure 119:

- Nr. 4 strain gages in the middle section E: E0°, E90°, E180° and E270° to provide a measure of the axial strain (E90° and E270° are placed on the bending plane).
- Nr. 2 strain gages in section C on the bending plane (C90° and C270°).
- Nr. 2 strain gages in section G on the bending plane (G90° and G270°).
- Nr. 4 LVDT are placed in longitudinal directions in positions 0°, 90°, 180° and 270° providing axial shortening.

The strain gages in section C and G are connected in Wheatstone bridge in order to provide directly the bending contribution of strain without any axial contribution.

2.2 Experimental results

For test nomenclature look at Table 12.

Test Al-c1: The moment-rotation curve and the failure mode are shown in Figure 120 and Figure 122, respectively.

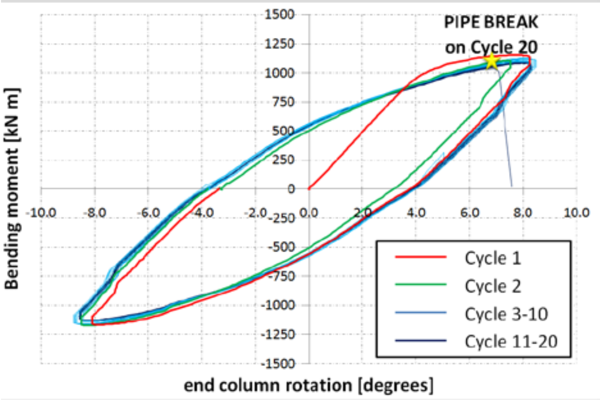

Figure 118 Full scale cyclic tests Al-c1: bending moment vs. end column rotation records

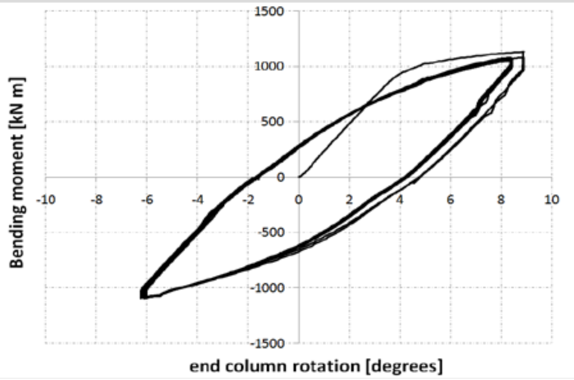

Figure 119 Full scale cyclic tests Al-c2: bending moment vs. end column rotation records

Figure 120 Specimen Al-c1 after testing

Test Bl-c1: The moment-rotation curve, ovalization evolution and the failure mode are shown in Figure 29, Figure 30 and Figure 123, respectively.

Figure 121 Specimen Bl-c1 after testing

Test Al-c2: The moment-rotation curve and the ovalization evolution are shown in Figure 121 and Figure 124, respectively.

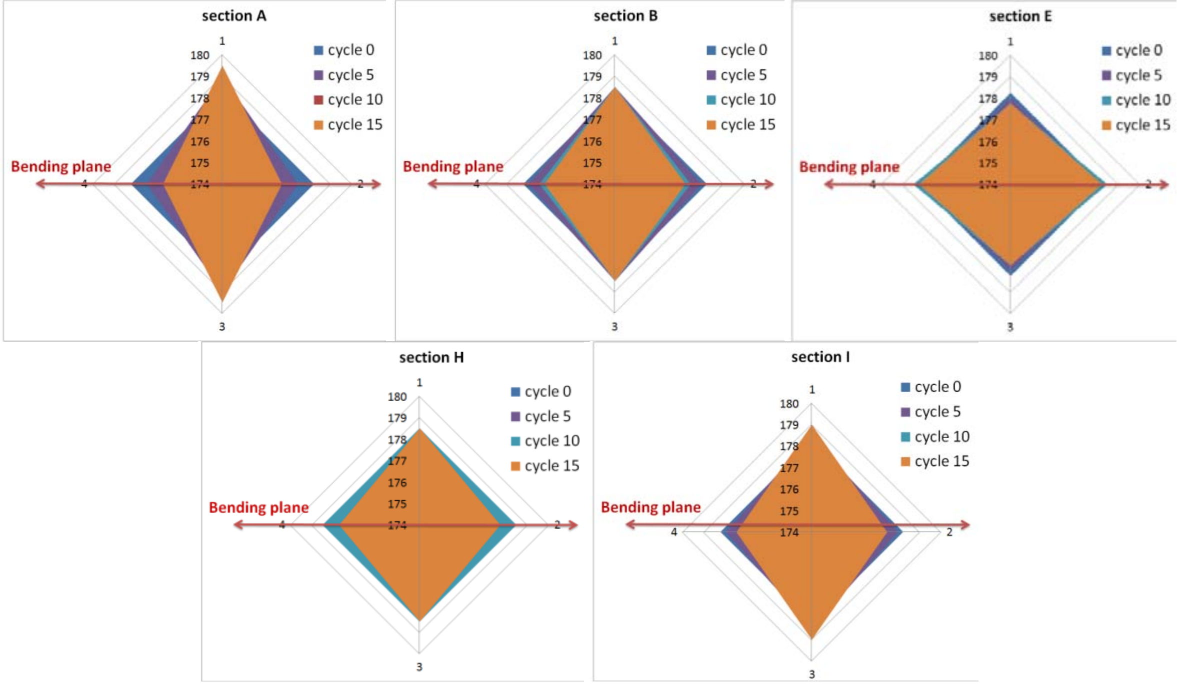

Figure 122 Full scale cyclic tests Al-c2: ovalization evolution measurements

Test Bl-c2: The moment-rotation curve and the failure mode are shown in Figure 125 and Figure 127, respectively.

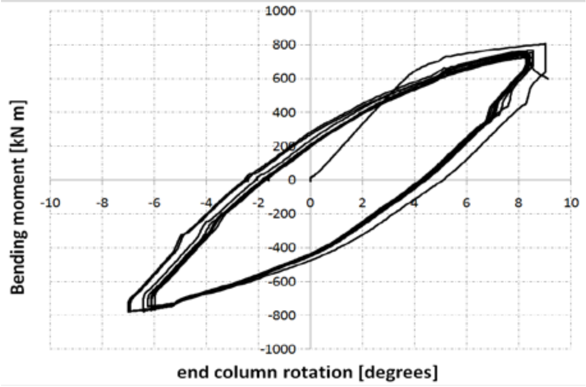

Figure 123 Full scale cyclic tests Bl-c2: bending moment vs. end column rotation records

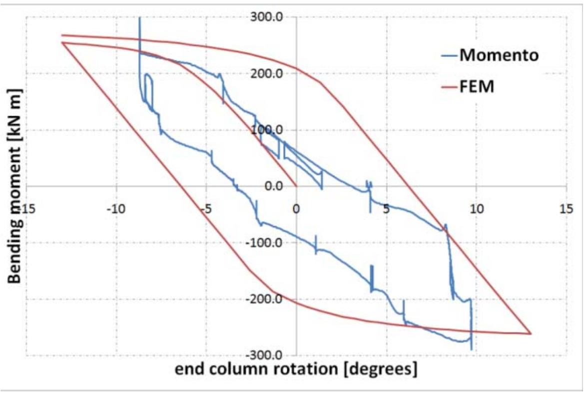

Figure 124 Full scale cyclic tests Cl-c0: bending moment vs. end column rotation records

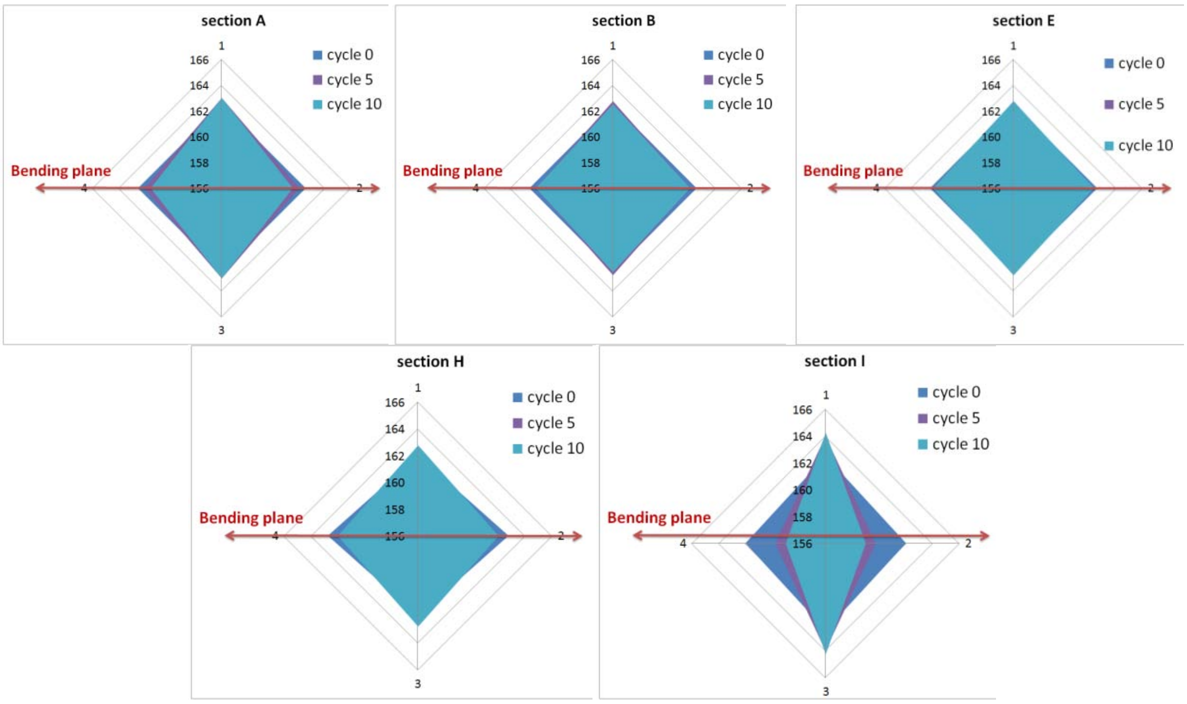

Figure 125 Full scale cyclic tests Bl-c2: ovalization evolution measurements

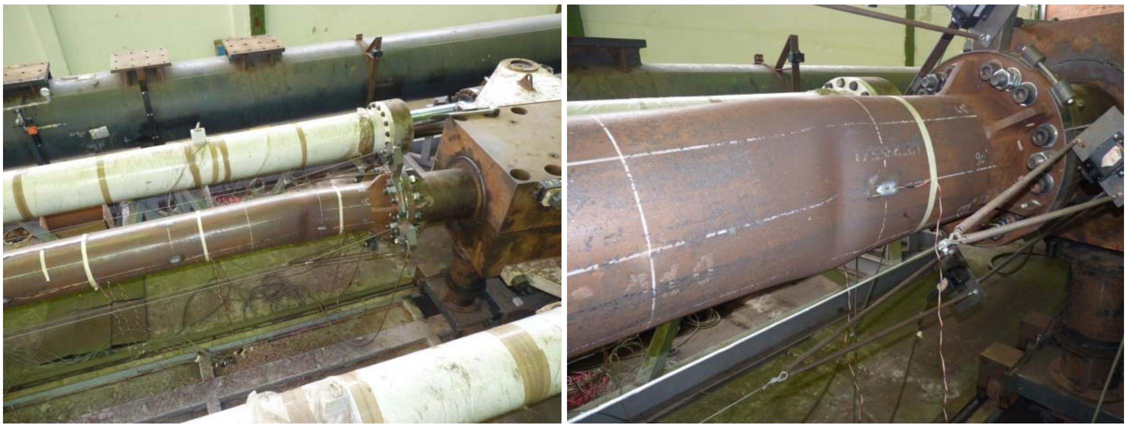

Figure 126 Specimen Bl-c2 after testing

Test Cl-c0: The moment-rotation curve is shown in Figure 126.

Tests and analyses data for specimens endowed with Section A and B are organized in M-N interaction diagrams in Figure 127, for short and long specimens, respectively.

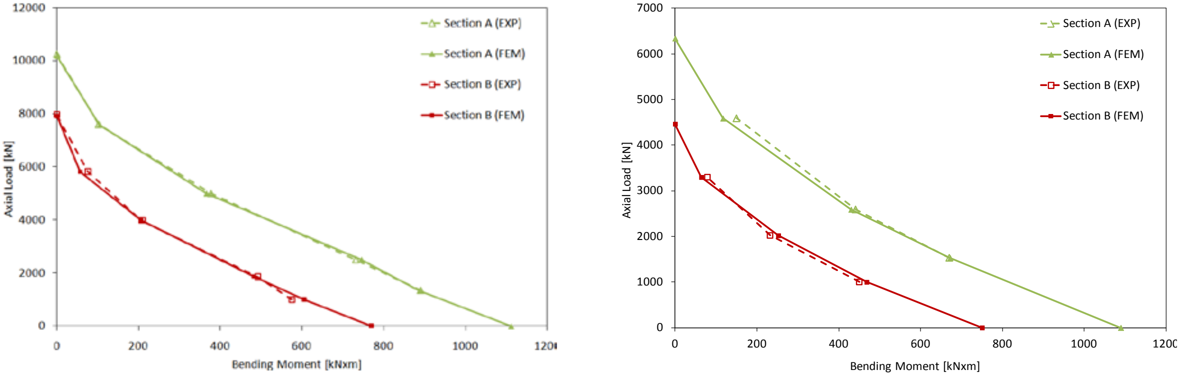

Figure 127 Experimental and numerical interaction diagrams for short and long specimens of section A and B, respectively.

3. Axial and bending tests in order to evaluate the buckling performance of tubes

The full scale testing arrangement is shown in Figure 128 where Cs specimen is ready to be tested. Bending moment is applied at column ends leading to uniform bending along the column. Columns are connected to the machine hinges via two symmetric extensions (1.5 m long for long specimens and 2.0 m for short specimens). With the scope of reducing time needed for the testing arrangement, dedicated testing grips have been designed and fabricated. Hence full scale column specimens have been delivered with base column flanges to be bolted on the dedicated frame grips (Figure 128).

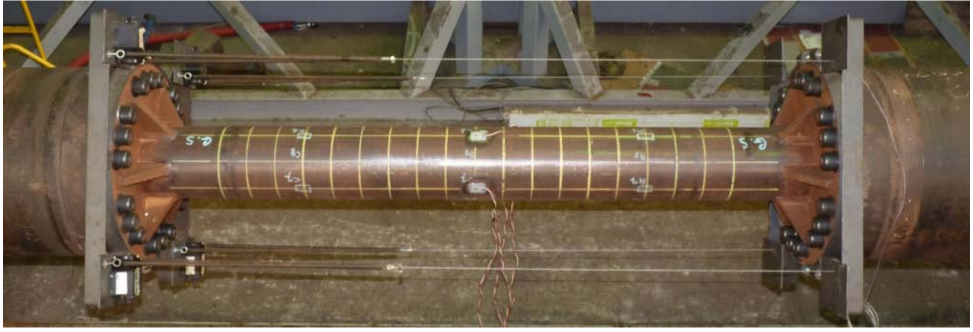

Figure 128 Full-scale column testing arrangement

3.1 Geometrical measurements

The geometrical survey of the outer profile was performed employing measuring equipment, developed and realized by CSM in the frame of ATTEL project composed by an aluminum stiff reference frame used as a sliding guide for a LVDT which is always in contact with the pipe body (Figure 129). It allows to obtain actual diameters (D), ovality imperfections (O) and dimples (wrinkling) imperfections (e).

Figure 129 Frame arranged on short specimen measuring phase on cross section of a short specimen

Thickness (t) distribution has been measured on the short column to be tested under combined loading. Three cross sections have been measured each column, using ultrasonic device for thickness for the diameters. The actual column dimensions such as diameters (D), Thickness (t) ovality imperfections (O = $(D_{max}-D_{min})/D_{nominal}$) and dimples (wrinkling) imperfections (e) have been measured before testing so as to characterize geometrical imperfections. Maximum measured deviations of the above dimensions (D, O, t and e) from the nominal value are summarized in Figure 130 while complete set of measurements are available on the relevant Deliverable 3.3. A comparison with tolerances reported in the relevant standard of products [11] was also performed. The admissible tolerances are reported in Figure 130 with dashed line with the relevant colors, it can be noted that columns actual dimensions are in accordance with and satisfy the admissible tolerances.

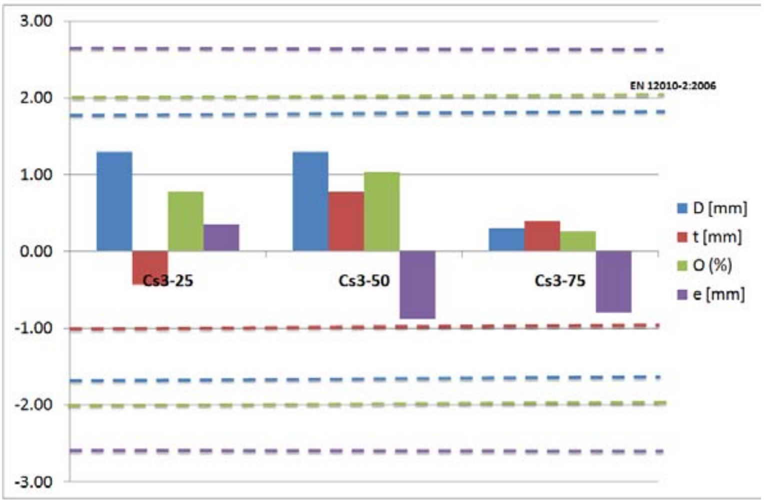

Figure 130 Measurement of geometrical imperfections: deviations from nominal dimensions of column specimens and admissible tolerances from **[11]**

3.2 Residual stresses measurements

Residual stresses of HSS CHS columns have been measured. As first attempt *hole drilling* technique have been applied for the scope. This technique is a semi-destructive one and measure via electrical strain gauges the evolution of residual strains relieved while removing by drilling a little quantity of material. It allows the measurements of residual stress (both longitudinal and circumferential) and its evolution from the external surface thorough the thickness up to 1mm depth. Four (4) measurements on two (2) different column samples have been performed producing a total of 8 measuring points. The application of this method resulted in a relative high value of residual stresses (about 400MPa).

As due to tempering process very low value of residual stresses were expected (about 5-15% f_y) extra investigations were needed. In particular:

- Material characterization to verify the effectiveness of tempering process
- Residual stress measurements applying another technique

3.2.1 Material characterization: when substantial variation of residual stresses is expected it should be coupled with variation of metallurgical quantities and material hardness.

Metallographic inspections and hardness HV10 measurements have been performed in 4 different points of a cross-section per 3 points through thickness. Moreover chemical composition and material toughness have performed.

The data obtained show no substantial variation of metallurgical quantities thorough thickness and in the different points analyzed. That is in accordance with the heat treatment performed on the material.

3.2.2 Longitudinal residual stresses: cross sectional distribution of longitudinal residual stress has been obtained using the “sectioning method” [77]. This method consists of the extraction of a cross-section and its sectioning in several strips. It is based on the principle that internal stresses are relieved by cold-cutting the specimen. The stress distribution over a cross section can be determined with reasonable accuracy by measuring the change in length of each strip and by applying Hooke’s Law. Substantial variation through thickness of longitudinal residual stress is detected via measuring eventual deflection of strips after cutting. While historically the change in length of the strips was measured by means of mechanical extensometers recently the application of electrical strain gauges has proved its benefits [78] and the present application refers to the latter (Figure 131 and Figure 132).

Each strip is instrumented with electrical strain gauges on the external surface allowing to the record of longitudinal strains relaxation during sectioning. Those strain gauges measurements coupled with flexural displacements of the strip allow to the evaluation of the residual stress through thickness variation

After sectioning the longitudinal residual stress measured on the external surface ranged between + 74 MPa and – 60 MPa. No flexural displacements are visible in the strips, also considering a 500mm long strip, hence bending component of longitudinal residual stress is evaluated to be negligible (less than ± 10 MPa).

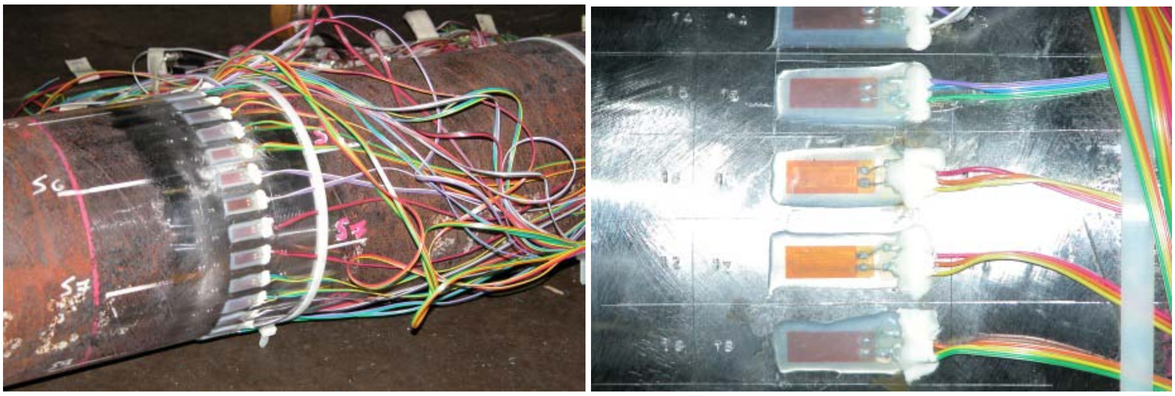

Figure 131 Instrumented specimen (left); Detail of instrumentation (right)

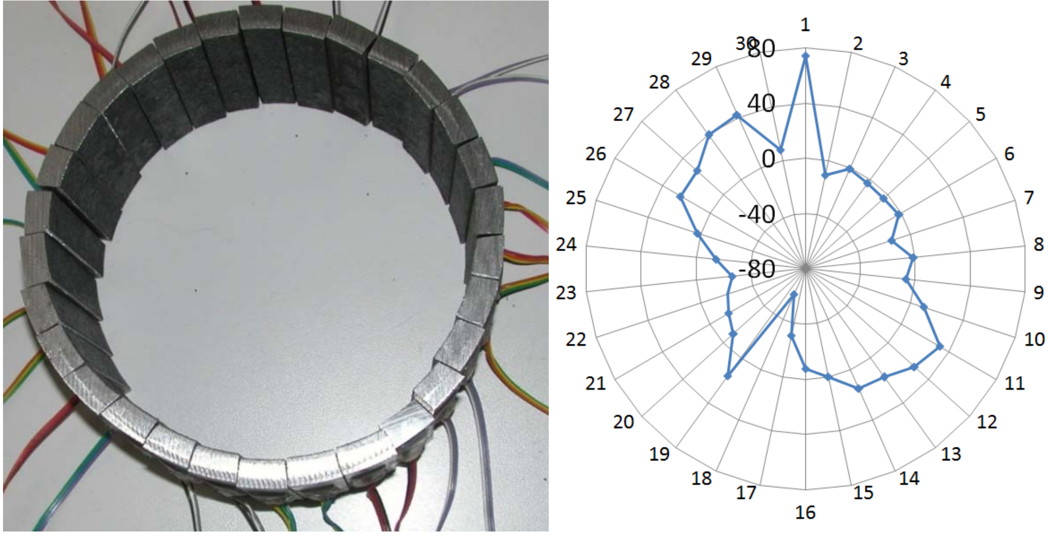

Figure 132 Sectioned cross section (left) and measured longitudinal residual stresses at the external surface (right)

<u>3.2.3 Circumferential residual stresses</u>: measurements of circumferential residual stress have been carried out according to the ASTM standard [79]. According to the standard outer diameters have been measured. The thickness of minimum diameter was considered for the longitudinal cut. A biaxial rosette has been installed at 180° from the cut section.

After cut a circumferential residual stress value of + 93 MPa on the external surface is measured. Under the hypothesis of butterfly distribution through thickness (as recommended by the procedure) a compressive residual stress of - 93 MPa is supposed to be on the internal surface.

3.3 Axial compression tests

In Figure 133 the columns after testing are shown. It is possible to observe that the column Cs1 underwent a combined in-plane and out-of-plane collapse. Local buckling it is observed both in the middle section (out-of-plane) and close to the stiffeners connecting the flange and the column (in-plane).

Figure 133 Columns after axial compression tests: column Cs1, Cs1-b and Cl1 (left to right)

3.4 Combined axial and bending tests

Some photographs of the specimen after testing are reported in Figure 134 where is possible to observe that the column underwent an in plane bending without severe collapse of the pipe body. This result is expected. In fact for Class 2 cross sections local buckling (total collapse of the section) is normally observed well beyond the load bearing capacity of the column, point at which the stiffness of the structure rapidly decrease.

Figure 134 Columns after combined load test: a) specimen Cs3-13; b) specimen Cl3-75

Appendix D: Tests on weld materials and connections

1. Test on HSS weld material

1.1 Fatigue test data on HSS weld and peening

The test conditions of the fatigue tests are presented in Table 40. The data of the fatigue tests performed on undermatching and overmatching weld specimens are given in Table 41 and Table 42, respectively. Moreover, results of peening conditions are reported in Table 43 and Table 44, respectively. Two examples of fracture surfaces are depicted in Figure 135 and Figure 136).

TEST, MACHINE AND SPECIMEN DATA	Material designation: TS590 overmatching, TS590 undermatching	
	Geometry: See the figure below	Surface treatment: as-cast

	Machining: Following annex I of testing standard ASTM E466. The specimen edges have been mechanically rounded by hand polishing to a radius of 3 mm.		
	Type of machine: Servo hydraulic testing machine INSTRON 8504.		
	Software: INSTRON FASTRACK 2 SAX Single Axis.		
	Waveform: Sine	Load ratio: R=0.1	Run-out: 2E^{6}cycles
	Test temperature: 23ºC	Specimens tested:	
	Failure criteria: Total rupture of the specimen		

Nominal dimensions of reduced sections (not considering weld over thickness)
Width – 25.00 mm
Thickness – 12.50 mm

Specimen Geometry

Table 40 Test conditions

Table 41 Test results – TS590 Undermatching

Nº	Specimen	Max Stress [Mpa]	Mean Stress [Mpa]	Stress Range [Mpa]	Freq [Hz]	Cycles
1	U1	200	110	180	25	1151578
2	U2	200	110	180	25	1066728
3	U3	175	96.25	157.5	25	1074859
4	U4	175	96.25	157.5	25	2000000
5	U5	250	137.5	225	25	175354
6	U6	250	137.5	225	25	181302
7	U7	225	123.75	202.5	25	408490
8	U8	175	96.25	157.5	25	869072
9	U9	175	96.25	157.5	25	2000000
10	U10	190	104.5	171	25	612243
11	U11	225	123.75	202.5	25	227546
12	U12	210	115.5	189	25	328886

Table 42 Test results – TS590 Overmatching

Specimen	Max Stress [Mpa]	Mean Stress [Mpa]	Stress Range [Mpa]	Freq [Hz]	Cycles
O1	200	110	180	25	553123
O2	150	82.5	135	25	1093649
O3	125	68.75	112.5	25	2000000

O4	150	82.5	135	25	2000000
O5	200	110	180	25	354775
O6	200	110	180	25	406638
O7	150	82.5	135	25	2000000
O8	225	123.75	202.5	25	433154
O9	225	123.75	202.5	25	1485436
O10	225	123.75	202.5	25	2000000
O11	300	165	270	25	483968

Table 43 Test results – TS590 Undermatching and peening

Nº	Specimen	Max Stress [Mpa]	Mean Stress [Mpa]	Stress Range [Mpa]	Freq [Hz]	Cycles
1	UP1	500	275	450	25	16659
2	UP2	400	220	360	25	59144
3	UP3	300	165	270	25	261336
4	UP4	200	110	180	25	2000000
5	UP5	100	55	90	25	538680
6	UP6	200	110	180	25	2000000
7	UP7	250	137.5	225	25	753125
8	UP8	300	165	270	25	640880
9	UP9	250	137.5	225	25	766225
10	UP10	400	220	360	25	96485
11	UP11	200	110	180	25	2000000
12	UP12	500	275	450	25	19070

Table 44 test results – TS590 Overmatching and peening

Nº	Specimen	Max Stress [Mpa]	Mean Stress [Mpa]	Stress Range [Mpa]	Freq [Hz]	Cycles
1	OP1	300	165	270	25	47138
2	OP2	200	110	180	25	2000000
3	OP3	300	165	270	25	28226
4	OP4	200	110	180	25	2000000
5	OP5	250	137.5	225	25	23890
6	OP6	250	137.5	225	25	477346
7	OP7	275	151.25	247.5	25	171490
8	OP8	275	151.25	247.5	25	253782
9	OP9	200	110	180	25	628646
10	OP10	225	123.75	202.5	25	252098
11	OP11	250	137.5	225	25	782897
12	OP12	225	123.75	202.5	25	337346

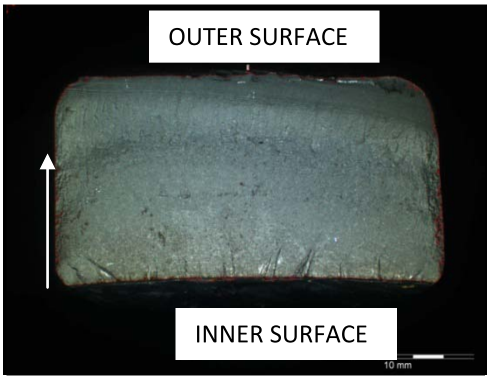

Figure 135 Fracture surface of undermatching and peening 4. White mark indicates the crack progress.

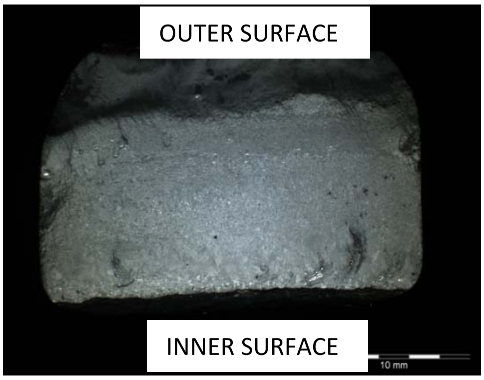

Figure 136 Fracture surface of overmatching and peening 1.

1.2 Fracture Toughness test conditions

The tests have been performed following the requirements of the ASTM E1820 standard. The specimens were extracted from the tubes in a longitudinal position. The nominal dimensions of the specimens were (W= 11 mm; B= 11 mm; L $\approx$ 60 mm). A notch was machined by EDM to a final length to width relation of 0.4 (a/W=0.4). A sharp crack was then originated by fatigue until a length to width relation of 0.6 was achieved. In this situation a complete J-R curve was obtained for each test. The tests were performed in an Instron universal testing machine with a load cell of 100 kN and an extensometer (COD type) was used to measure the crack growth by means of the elastic compliance technique.

(a) (b) (c)

Figure 137 Fracture surface of- a) base metal specimen, b) undermatching specimen, c) overmatching specimen

1.3 Corrosion tests on HSS welds

Corrosion rate measurements and slow strain rate tests (SSRT) have been performed on material from K- and X-joints and the heat affected zones of two different materials, TS590 and S355 in different environments.

1.3.1 Corrosion rate measurements

Uniform corrosion rate on samples from theweld metal were measured in two different solutions, 1 wt% and 3.5 wt% NaCl. Test solutions were made from analytical grade reagent NaCl and deionized water in order to simulate the offshore and seawater environments, respectively. The tests were carried out at ambient temperature, i.e~ 25 °C. The pH of the solution was 6.5 at the beginning of the experiments. The effect of oxygen concentration on uniform corrosion resistance in sodium chloride solution was investigated in aerated and de-aerated (N_2-bubbleing) conditions. In de-aerated condition, the solution was purified before running the experiment with dry nitrogen gas for 10 minutes to remove dissolved oxygen. The nitrogen bubbling was kept during the test. The linear polarisation resistance technique, based on the change in potential and record of the polarisation resistance (the slope of the linear polarisation curve dE/di is termed the Rp) was used to measure the corrosion rate. The corrosion potential (E_{corr}) and current density (i_{corr}) were calculated from the data and obtained with the use of Tafel extrapolation technique. The corrosion rate was calculated from the current by using Faraday’s law. The experiments were performed in a three-electrode Avesta cell.

Two different materials were tested, TS590 and S355. The specimens were cut from the weld metal,the heat affected zone (HAZ) and base metal (WP3.1). Prior to the tests, the samples were wet ground with 600-grade SiC paper and rinsed with de-ionized water and ethanol, dried and exposed to air for approximately 24 hours. The exposed surface area of each specimen was approximately 100 mm². The test was performed on duplicate samples.

1.3.2 Slow strain rate tests (SSRT)

The SSRT testing, combines slow strain rate in corrosive environment and is used to evaluate the susceptibility of materials to stress corrosion cracking and hydrogen embrittlement. The samples were longitudinally cut. The length direction of the tensile sample was parallel to the longitudinal of the pipe. The SSRT were performed in air, 1 wt% and 3.5 wt% NaCl solutions open in contact with air in ambient temperature (~ 25 °C). A strain rate of 10^{-6} s^{-1} was applied throughout the experiments. The test was performed at Open Circuit Potential (OCP), i.e. E_{corr}. In order to simulate cathodic protection, cathodic polarisation with the magnitude of 40 mA was applied throughout the test of some of the samples in order to enable diffusion of hydrogen into the specimens. Samples from TS590 and S355 were longitudinally cut from base metal (Task 3.1) welded metal and from the HAZ region of the welds. The SSRT specimens, with 3 mm in gauge diameter and 31 mm in gauge length (± 0.05) were machined from the two different kinds of weld configurations, i.e. K and X-joint. The length direction of the tensile sample was parallel to the longitudinal of the pipe. The samples' surfaces were abraded with 600-grith SiC abrasive paper.

The elongation EL%, yield stress (YS) and ultimate tensile strength (UTS) were calculated from the stress vs. strain curves. The time to failure (TTF) was determined during the SSRT. Furthermore the Reduction of Area, RA (%) was measured on the samples after cracking.

The corrosion rates for the weld metals of steel TS590 and S355 are given in Table 45.Ascomparison are given the corresponding values for the base metals.

Table 45 Average of corrosion rates [mm/year] for weld metal of TS590 and S355

Steel grade	Environment	Gas bubble	Average corrosion rate, mm/year weld metal;*(base metal)*	$\pm\frac{1}{n}\sum\left\|x-\bar{x}\right\|$ weld metal; *(base metal)*
TS590	3.5 wt % NaCl	Air bubble	0.180; *(0.140)*	0.004; *(0.018)*
TS590	3.5 wt % NaCl	N_2 bubble	0.130; *(0.105)*	0.007; *(0.014)*
TS590	1 wt % NaCl	N_2 bubble	0.120; *(0.058)*	0.008; *(0.008)*
S355	3.5 wt % NaCl	Air bubble	0.240; *(0.168)*	0.003; *(0.030)*
S355	3.5 wt % NaCl	N_2 bubble	0.200; *(0.114)*	0.004; *(0.031)*
S355	1 wt % NaCl	N_2 bubble	0.090; *(0.086)*	0.006; *(0.016)*

Higher corrosion rate was achieved in 3.5 wt% NaCl compared to 1 wt% NaCl for all tested samples. Furthermore, maximum corrosion rates for both materials were obtained in the presence of the oxygen. Steel S355 had higher corrosion rate than TS590 in the more aggressive solutions with 3.5 wt% NaCl, while it was slightly lower for the weld metal of S355 in 1 wt% NaCl solution. Higher corrosion rates were achieved for the welded metal of both TS590 and S355 in all tested environments.

The results from the SSRT measurements are given in Table 46. The SSRT-measurements at open circuit potential in air, 1 wt% and 3.5 wt% NaCl gave no significant difference in RA between base, weld metal and HAZ for TS590 with K-joint. The same was also achieved for X-joint except for tests in air where the RA decreased for the weld metal. Results from tests where cathodicpolarisation was applied showed that the RA-values decreased for base, weld metal and HAZ for TS590 and S355 and K-joint as well as X-joint. The weld metal achieved the lowest RA and thereafter the HAZ.

Comparing the RA-results for TS590 and S355 with cathodic polarization in 1.5 wt% NaCl shows that the HAZ for TS590 had a lower RA than corresponding for S355. The same relation was achieved for TTF, i.e. HAZ samples from TS590 had a shorter time to failure than corresponding from S355. No significant differences were achieved between the K-joints and X-joints for any of the measured mechanical parameters.

The results from the measurements of base material are part of the Task3.1 but are also presented in this WP. In order to draw any conclusions regarding the corrosion resistance of weld metal and heat affected zone, the results have to be put in relation to the corresponding achieved for the base metal.

From the results it is obvious that the cathodic polarisation drastically decrease the reduction in area of all tested samples prepared from base metal, welds and HAZ. The obtained results also indicate that the susceptible to stress corrosion cracking increase in following order: base, HAZ and weld metal.

The corrosion rate measurements in the most aggressive solution showed a higher corrosion rate for S355 than for TS590.Furthermore the weld metal had higher corrosion rate than the base metal for both S355 and TS590.

Table 46 Mechanical properties of TS590, S355 and their welded joints and HAZ.

Steel grade	Samples	RA (%)	TTF(hr)	EL (%)	YS (MPa)	UTS (MPa)
Air						
TS590 K-joint	Base metal	75.67	34.13	9.86	782	818
	HAZ	73.55	35.33	10.00	774	840
	Weld metal	70.57	36.33	10.00	820	893
TS590 X-joint	HAZ	78.38	38.92	11.60	740	806
	Weld metal	42.66	26.92	11.30	730	820
S355 K-joint	Base metal	72.30	37.00	10.40	765	803
	HAZ	78.78	50.58	15.30	470	564
	Weld metal	70.49	53.75	16.80	485	600
1 wt% NaCl						
TS590 K-joint	Base metal	78.85	35.38	10.35	770	812
	HAZ	75.45	32.08	9.40	740	804
	Weld metal	74.45	29.42	8.20	745	796
TS590 X-joint	HAZ	76.64	36.38	10.65	688	757
	Weld metal	73.40	35.58	10.50	700	765
S355 K-joint	Base metal	-	-	-	-	-
	HAZ	66.77	44.88	13.30	458	593
	Weld metal	75.10	43.50	13.50	455	653
1 wt% NaCl; 4 mA/cm^2						
TS590 K-joint	Base metal	38.29	29.83	6.80	755	804
	HAZ	22.81	30.50	7.80	760	834
	Weld metal	15.26	21.00	3.30	820	877
TS590 X-joint	HAZ	32.01	31.00	7.20	695	778
	Weld metal	*	*	*	*	*
S355 K-joint	Base metal	66.74	28.42	6.60	765	803
	HAZ	36.48	35.33	9.20	430	558
	Weld metal	*	*	*	*	*
3.5 wt% NaCl						
TS590 K-joint	Base metal	76.31	35.17	10.00	780	822
	HAZ	74.05	33.58	9.25	770	835
	Weld metal	72.23	35.42	10.30	690	780
TS590 X-joint	HAZ	77.40	36.75	10.80	710	784
	Weld metal	75.41	34.08	10.00	670	731
S355 K-joint	Base metal	76.73	34.17	9.10	765	807
	HAZ	72.98	44.17	13.20	465	568
	Weld metal	65.99	50.50	14.60	410	547
3.5 wt% NaCl 4 mA/cm^2						
TS590 K-joint	Base metal	34.78	28.04	6.35	778	822
	HAZ	28.41	28.42	5.90	775	838
	Weld metal	25.11	27.83	6.30	730	801
TS590 X-joint	HAZ	38.33	25.08	5.30	730	788
	Weld metal	26.09	25.67	5.10	775	849
S355 K-joint	Base metal	-	-	-	-	-
	HAZ	*	*	*	*	*
	Weld metal	*	*	*	*	*

**No measurements: Not possible to make specimens due to curvature of joints*

2. Tests on welded X tubular connections with axial, in-plane and out-of-plane loading

For the experimental study of the behavior of high-strength steel welded tubular connections under bending loading [out-of-plane (OPB) and in-plane (IPB) bending], eight (8) specimens were tested, four (4) for each type of loading. In addition, two (2) specimens have been tested under axial loading conditions. Two (2) weld types have been considered, denoted as weld type A (lower weld metal strength, undermatching) and weld type B (higher weld metal strength, overmatching). The joint welds have been performed according to the provisions of AWS D1.1/D1.1M:2004.

To conduct these tests special hinges and grips were manufactured in order to carry out 4-point bending tests for the OPB specimens and 3-point bending tests for the IPB specimens (see Figure 138). For the OPB tests, the specimens were supported using a double-hinge 'roller' system (see Figure 138) with ball joint hinges and the load was applied to the brace through a steel cross-beam with a system of two special ball-joint hinges and appropriate wooden grips (see Figure 139). For supporting the IPB specimens, the same double-hinge 'roller' system was used, while the load was applied through an actuator which was bolted to the top of the chord (see Figure 138). Regarding the instrumentation set-up for both types of tests, wire position transducers were used to measure load-point displacements, DCDT's for measuring support displacements and a number of strain gages were placed at critical locations. Especially, uniaxial 5-element strip strain gages were placed on the chord for measuring strains in the region near the weld toe. The gages were at a distance of 3 mm, with the first one being 5 mm away from the weld toe. For the OPB tests the gages were placed in the hoop direction of the chord (saddle) and for the IPB test in the meridional direction of the chord (crown) (see Figure 140).

2.1 OPB tests

Two (2) of the OPB specimens were subjected to monotonic and two (2) to low-cycle fatigue loading, one for each type of weld type (A and B). Under monotonic loading, the specimen with the lower strength of the weld (type A) showed about 5% higher flexural capacity and 37% higher load-point deflection than the one with the higher strength weld (type B) (see Figure 46a). According to CIDECT 8, the predicted moment capacity of the OPB specimen under monotonic loading is about 113 kNm. The measured values were 7% and 2% higher for weld type A and B, respectively.

Under low-cycle fatigue, a cyclic loading of 75% to 80% of the maximum monotonic load (R=0.1) up to failure was applied to the specimens with weld type A and B, respectively. The behavior of the specimens subjected to monotonic and cyclic loading was rather similar. The weld type A specimen failed after 240 loading cycles exhibiting a slightly higher fatigue resistance than the specimen with the weld type B which failed after 200 cycles (Figure 141). All specimens failed in the form of fracture at the chord saddle of the joint, near the weld toe (Figure 142).

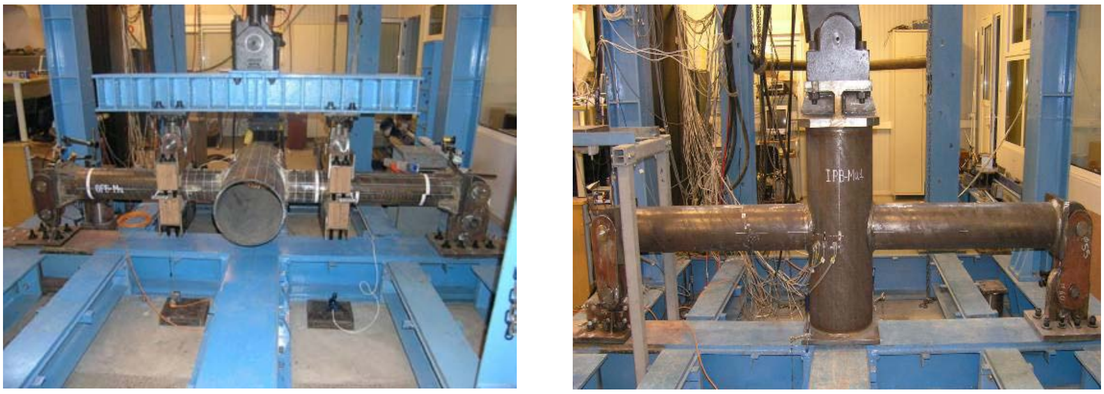

(a) (b)

Figure 138 General view of the test set-up with the specimens for: (a) out-of-plane bending tests, (b) in-plane bending tests.

(a) (b)

Figure 139 (a) Double-hinge ‘roller’ and (b) beam/wooden grips system.

(a) (b)

Figure 140 Uniaxial 5-element strip strain gages at: (a) the hoop direction of the chord, (b) the meridional direction of the chord

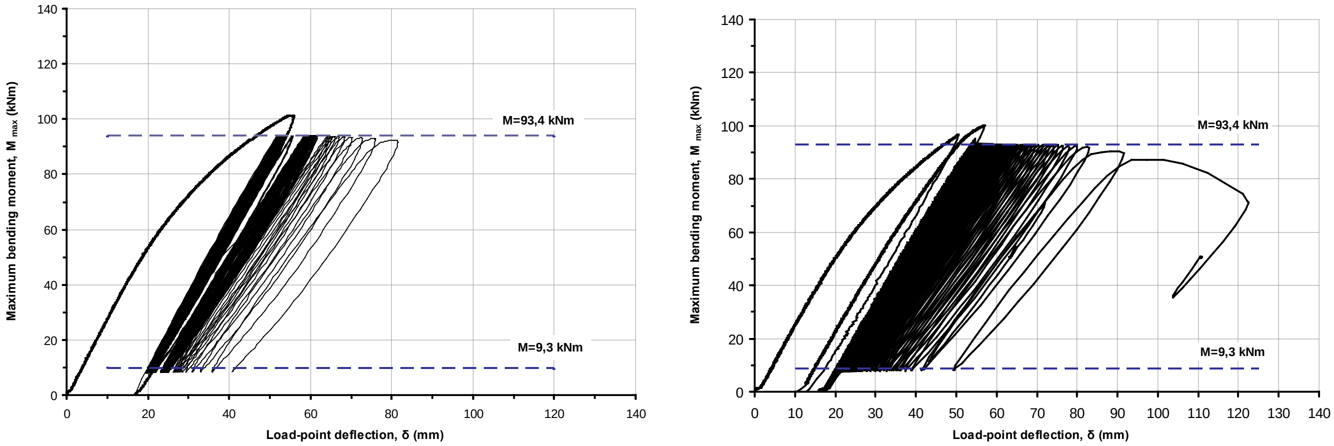

(a) (b)

(a) (b)

Figure 141 Load vs. displacement curves for OPB specimens under cyclic loading: (a) type A weld, (b) type B weld.

(a) (b)

Figure 142 (a) OPB specimen at failure, (b) failure crack of OPB specimen

2.2 IPB tests

Two (2) of the IPB specimens were subjected to monotonic loading, one for each weld type (A and B). The specimen with the lower strength weld (type A) exhibited about 6% higher flexural capacity and 43% higher load-point deflection than the one with the higher strength weld (type B) (see Figure 46b), values which are similar to those for the OPB monotonic tests. According to the provisions of EN 1993-1-8, the predicted bending moment capacity of the joint under monotonic loading is about 202 kNm. The measured capacity was about 33% and 25% higher for weld type A and B, respectively.

The other two (2) of the IPB specimens were tested under low-cycle fatigue, one for each weld type (A and B). The specimens were subjected to a cyclic loading of 80% and 85% of the maximum monotonically applied load (R=0.1) for the weld type A and B, respectively. The weld type A specimen resisted 44% more loading cycles than the weld type B one. The weld types A and B specimens failed after 974 cycles and 676 cycles, respectively (see Figure 143). All specimens failed after forming a through-thickness crack in the chord along the circumference of the weld, starting at

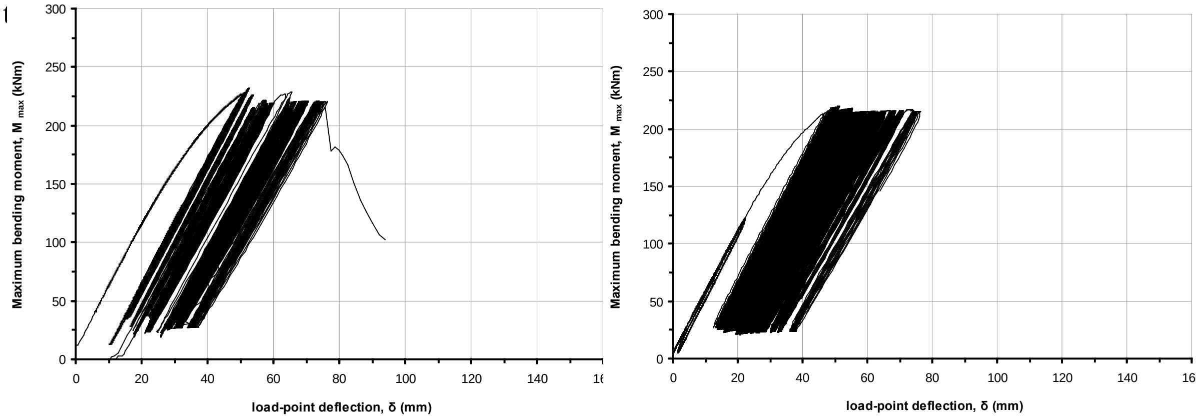

(a) (b)

Figure 143 Load vs. displacement curves for: (a) type A, (b) type B cyclic IPB tests

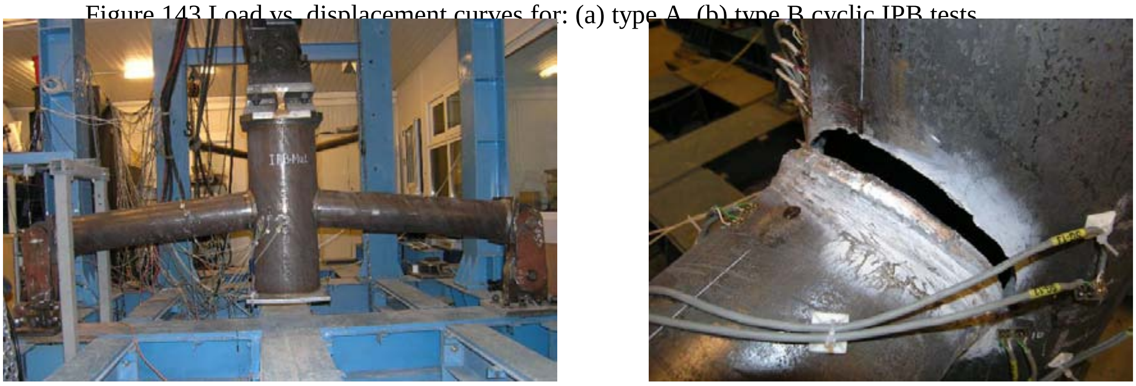

(a) (b)

Figure 144 (a) IPB specimen at failure, (b) failure crack of IPB specimen.

2.3 Axial loading tests

Two (2) X-type welded tubular joint specimens were tested under low-cycle fatigue, one for each weld type (A and B). The specimens were subjected to a cyclic tensile loading on the braces, with a maximum and minimum force equal to 750 kN and 75 kN respectively (R=0.1). The load was applied through a level-arm system, as shown in Figure 143a, at a low frequency ranging between 0.01 and 0.03 Hz.

Both specimens developed a fatigue crack through the thickness at the chord saddle location and were able to sustain the applied load for more than 1000 cycles. The initial range of axial deformation (elongation) of the specimens were measured equal to 7.3 mm and 7.6 mm (Figure 145b). Furthermore, the evolution of range of axial deformation with respect to the number of cycles indicated that after a certain number of cycles nf, the rate of increase becomes quite significant (Figure 145b), and this can be considered as structural failure. From Figure 145b, the value of N_f for weld type B can be considered approximately equal to 750 cycles, whereas weld type A had a better behavior and the corresponding value is equal to about 1000 cycles. The two curves of Figure 145b demonstrate clearly the superior behavior of weld type A. The response of the two specimens under cyclic loading is shown in Figure 146. Finally, the through-thickness crack is shown in detail in Figure 147a and Figure 147b.

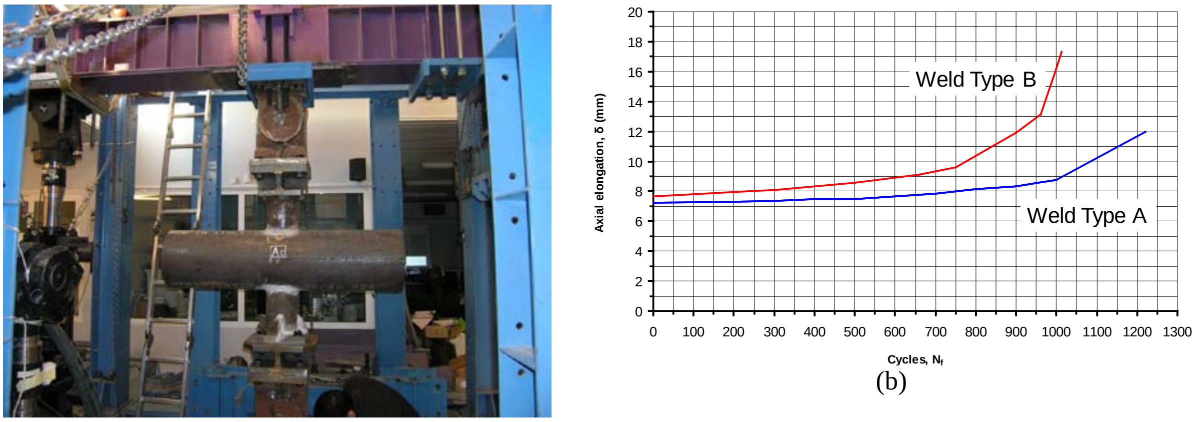

(b)

(a)

Figure 145 Axial loading specimen; (a) set-up, (b) load-deformation curve (weld type b)

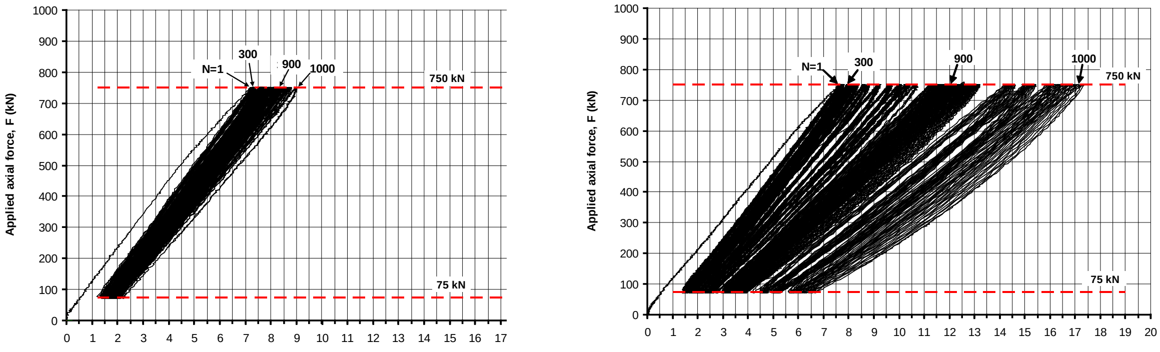

(a)

(b)

Figure 146 Axial loading specimen; load-deformation curve (a) weld-type A (b) weld type B


(a) (b)

Figure 147 Fatigue crack of axial loading specimen; (a) external view of crack at chord saddle, (b) internal view of through-thickness crack development.

3. Tests on bolted connections

Test instrumentation: all critical zones (in the bolt shanks, on the tube at the weld toe and on the flanges at the weld toe) were instrumented by a large number of strain gauges in order to record the hot-spot stress distribution. In all specimens, the tightening procedures were controlled by the strain gauges inside the bolt shank such that the pre-stress value given by Eurocode 3, part 1-8 is reached. SHENCK machine with capacity 2500 kN in both tensile and compression was used for the tests.

Loading sequences: the applied load may be considered as a perfect axial tensile force. Quasi-static loading was applied for the monotonic and low cycle fatigue tests while a loading with frequency of 1.4 Hz was adopted during the high cycle fatigue tests (see Figure 148).

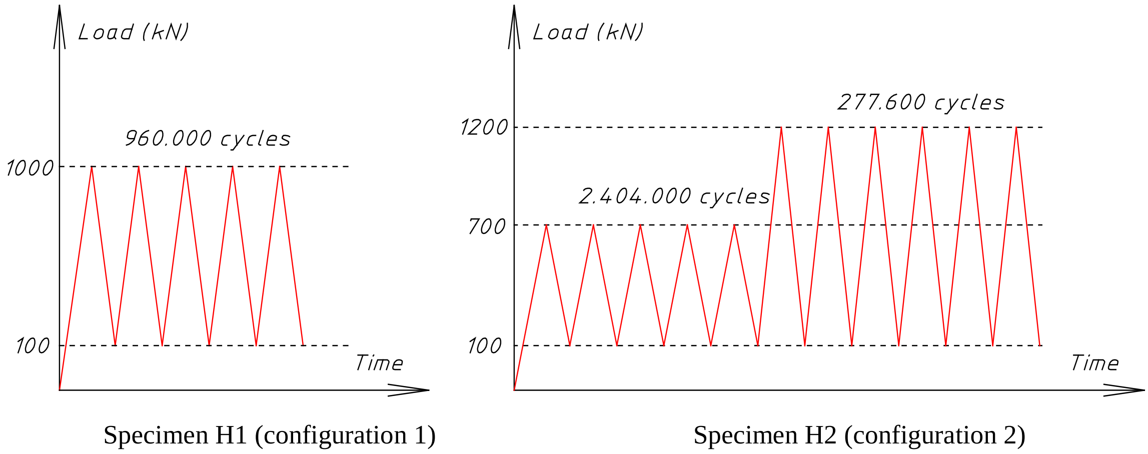

Specimen H1 (configuration 1) Specimen H2 (configuration 2)

Figure 148 Loading procedures for fatigue tests

Characterisation of the materials: tests on base materials were carried out for both steel plates and bolts (tensile tests and tightening tests); twenty-five (25) coupon tests were performed in total.

Geometrical imperfection: the global deformations of the specimens were recorded using four displacement transducers. The initial deformations of the flanges due to the heat-effect of the weld operation were also measured.

Table 47 and Figure 150 -Figure 152 describe the observed failure modes of different types of tests. Moreover, Figure 149 presents the evolution of hot-spot stress at critical zones of joints.

Table 47 Description of tested specimens

Specimens	Load type	Referent figures	Component states		
			Tubes	Flanges	Bolt shanks
M1	Monotonic	Figure 153	No problem	Plastic deformation at weld toe	Plastic deformation

M2	Monotone	Figure 153	No problem	Almost no problem	Failures
H1	HCF	Figure 154	Crack at the weld toe	No problem	No problem
H2	HCF	Figure 154	Crack at the weld toe	No problem	A bolt are cracked
L1	LCF	Figure 155	No problem	Crack at the weld toe	Plastic deformation
L2	LCF	Figure 155	No problem	Almost no problem	Plastic deformation

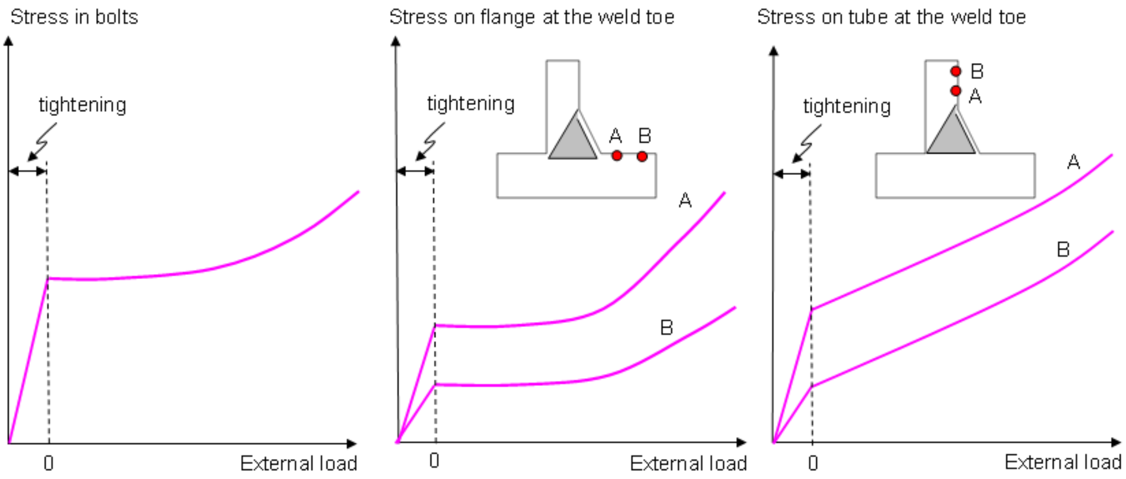

Figure 149 Evolution of stress in critical zones of joints

Specimen M1 Specimen M2

Figure 150 Specimens after monotonic tests

Specimen H1 Specimen H2

Figure 151 Specimens after HCF tests

Crack in flange of specimen L1 A bolt of specimen L2

Figure 152 Specimens after LCF tests

Appendix E: Numerical simulations of welded and bolted connections

1. Simulation of welded connections and joints under strong repeated loading

A detailed numerical model has been developed for the simulation of the tests on the X-joints. The numerical model represents the actual dimensions of each welded joint. The weld geometry has been modeled in detail, according to the provisions of the American Structural Welding Code AWS D1.1 [15].

The model is developed in ABAQUS and uses 8-node, quadratic, reduced integration solid elements (C3D8R) for most of the chord, whereas 4-noded solid elements (C3D4) are used in the brace part and the weld region of the joint on the chord. Moreover, the mesh size is denser near the weld region in order to provide accuracy in the simulation results and time-effective simulations. Only half of the joint is modeled, taking advantage of symmetry and applying the appropriate symmetry conditions. The model is shown in Figure 153.

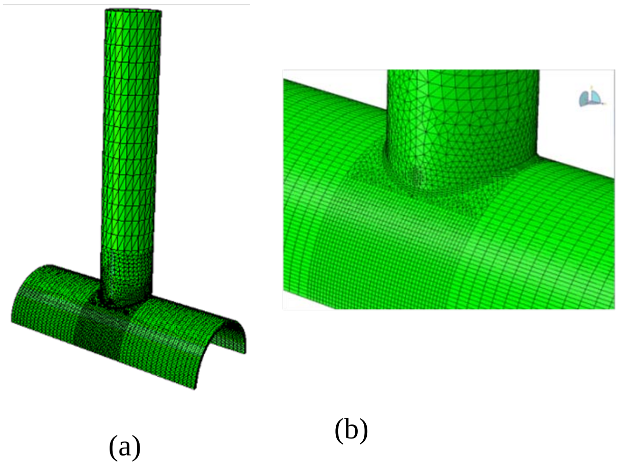

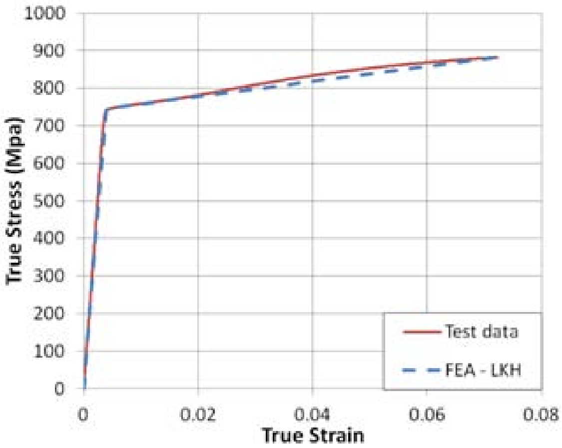

Figure 153 Numerical model developed: (a) general view (b) weld region

Figure 154 Uniaxial steel material stress-strain curve

The numerical results have been initially obtained using a material model of J_2 flow plasticity, accounting for large strains. For the purposes of the present analysis, linear kinematic hardening has been employed. A bilinear stress-strain curve which compares fairly well with the uniaxial tensile test data was used for the simulations (Figure 154).

1.1 Numerical results for joints under out-of-plane bending

For the simulation of the OPB tests, the joint geometry was modeled according to the measured dimensions of the tubular members, which are very close to the nominal ones, considering a uniform thickness of the chord and the brace. As displayed in Figure 155, the experimental measurements can be numerically reproduced quite accurately for monotonic and cyclic loading conditions.

It is worth noticing that the overall joint behavior is sensitive to rather small variations of the chord thickness value. This difference is attributed to the earlier initiation of inelastic behavior when the chord thickness becomes smaller, so that the joint resistance is significantly reduced. In all cases of applied loading type, the results show that the numerical model is capable of simulating accurately the experimental procedure and representing the experimental results.

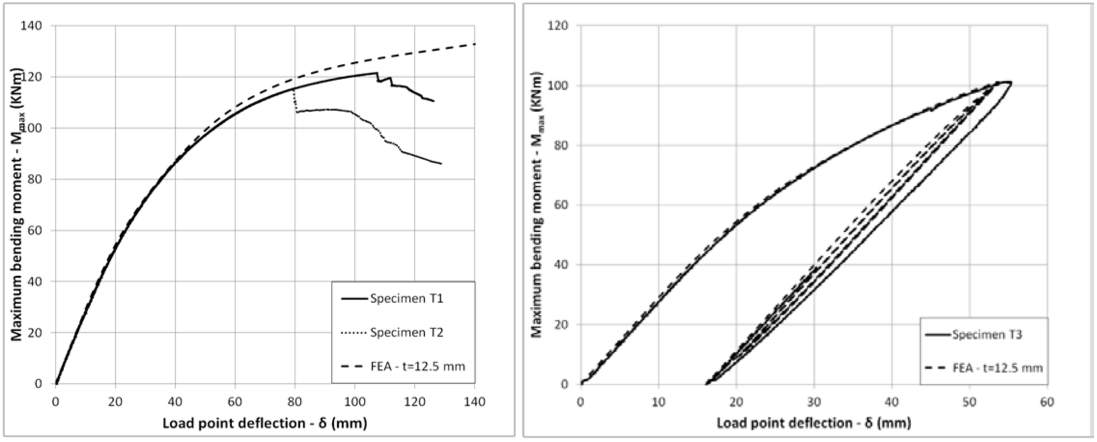

(a) (b)

Figure 155 Out-of-plane bending tests - comparison of the numerical and experimental load vs. displacement curves: (a) Monotonic, (b) Cyclic loading

The strain concentration factor (SNCF) and the stress concentration factor (SCF) has been also evaluated numerically. The numerical SNCF value is estimated equal to 7.18, higher than the experimentally evaluated value. According to CIDECT guidelines (2001), the corresponding SCF for the joint under consideration is equal to 9.82, whereas the numerical model results to a SCF value equal to 6.16 using a linear extrapolation and 8.19 using quadratic extrapolation, as shown in Figure 156b. The above differences are attributed to the sensitivity of the strain/stress field near the weld toe in terms of local conditions (notch effect).

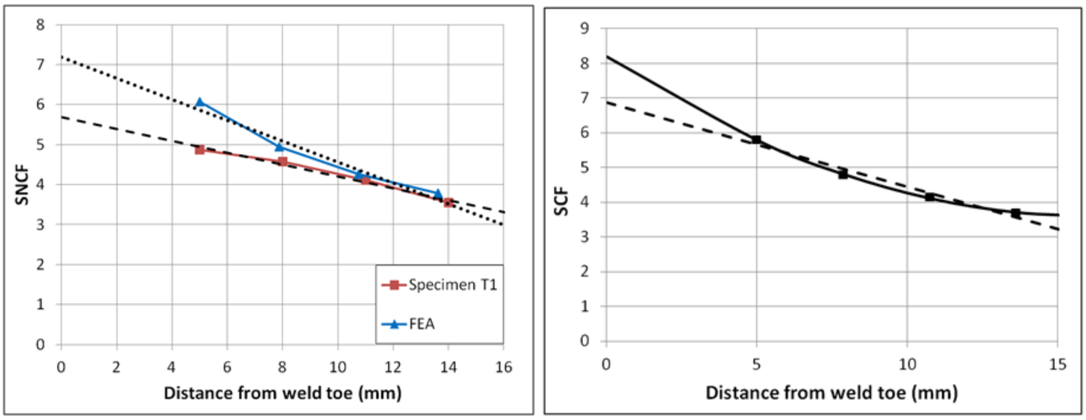

(a) (b)

Figure 156 (a) SNCF and (b) SCF evaluation for out-of-plane bending moments

Towards better understanding of the chord deformation at the weld area, the deformed chord geometry is shown in Figure 159, corresponding to a joint section at the chord middle plane. The concentration of plastic deformation near the weld-toe area is significantly higher than the one located at the weld of the joint, so that the location of cracking initiation at the weld-toe is verified. The deformation mode presented in Figure 159a has been also observed in the experiments and indicates that there is a significant change of chord curvature near the weld toe region, which reaches a critical value at a distance of about 5 times the chord thickness.

1.2 Numerical results for joints under in-plane bending

The same model has been used for the simulation of the IPB tests (monotonic and cyclic). The predictions of the model are in good agreement with the experimental measurements for both types of loading, as presented in Figure 157. The stress concentration factor has been evaluated according to the provisions of CIDECT No. 8 and it is found equal to 3.48. It is observed that the distribution of plastic deformations under this kind of loading is widely spread along the circumference of the weld (Figure 158), which justifies the shear-dominant type of failure observed in the experiments. According the provisions of EN 1993-1-8 and by adopting the actual characteristics of the joint, the joint resistance under IPB is equal to 202 KNm and the failure mode is punching shear, as justified by the numerical results as well. The predicted value is significantly lower than the experimentally measured resistance (32.6% and 24.5% for weld conditions A and B respectively), but lays on the safe side.

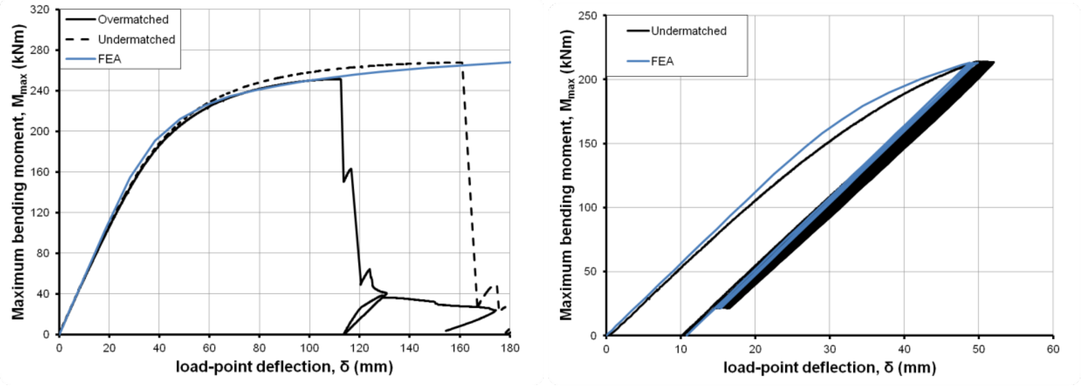

(a) (b)

Figure 157 In-plane bending test and numerical simulation results: (a) Monotonic loading, (b) Cyclic loading

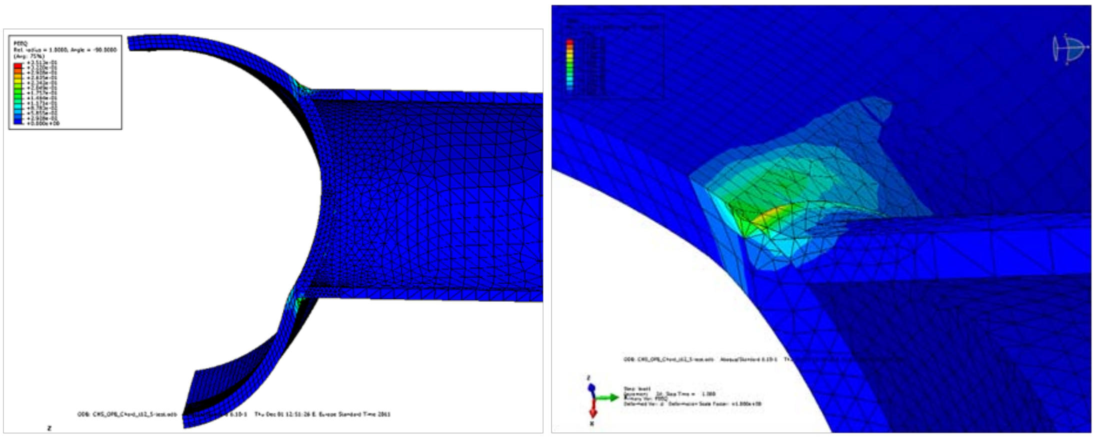

(a) (b)

Figure 158 Out-of-plane bending test simulation. Mid-span section (a) Deformed chord geometry (b) Equivalent plastic strain distribution at the weld-toe area

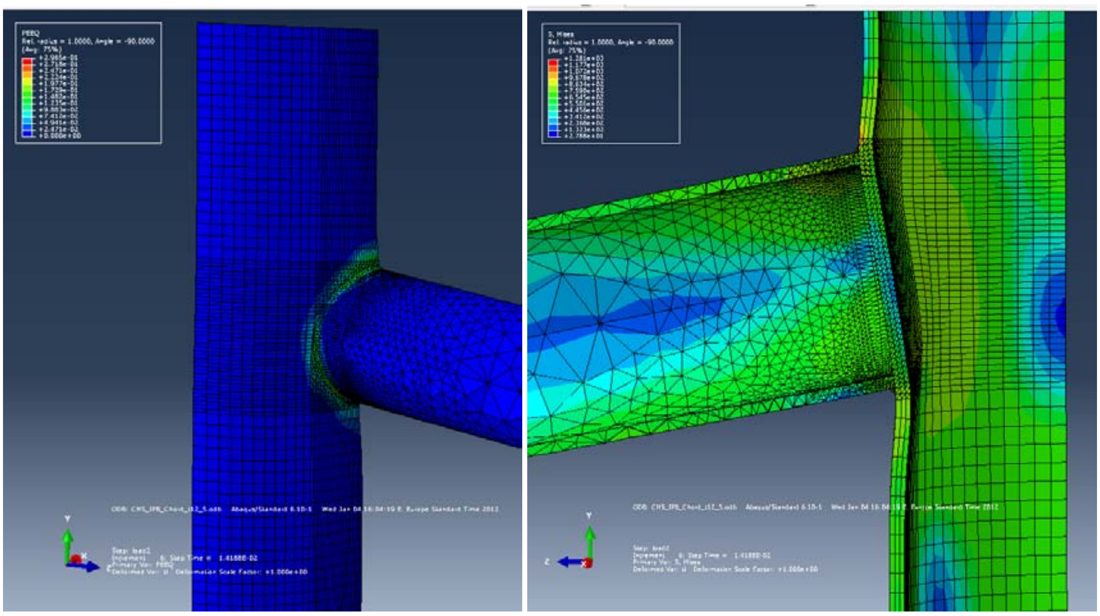

Figure 159 In-plane bending test simulation. (a) Equivalent plastic strain distribution at the weld-toe area, (b) Deformed chord geometry - mid-span section

2. Simulation of bolted connections and joints under strong repeated loading

2.1 Determination of bolt length according to Agreskov's concept

The Agerskov's length (effective length, L_{eff}) for the considered joint configurations can be calculated from the following equation (see Figure 160 for the definition of parameters):

$$L_{eff} = \frac{A_s}{A_b}\left[l_s + 1.43 l_t + 0.71 l_n + 2(0.1 l_n + 0.2 l_w)\right]$$

with the bolt geometrical properties reported in Table 48.

Values of 510 mm and 540 mm are obtained for M27 (joint configuration 1) and M20 (joint configuration 2) respectively. Obviously, only one haft of these length are introduced in the 1/48 part model.

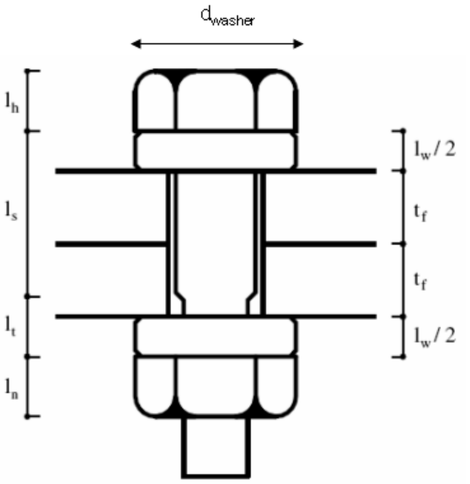

Figure 160 Detailed geometry of the investigated bolts

Table 48 Bolt geometrical properties (see Figure 164)

Bolts	A_b (mm^2)	A_s (mm^2)	t_f (mm)	h_h (mm)	l_n (mm)	l_s (mm)	l_t (mm)	l_w (mm)	d_w (mm)
M27	573	459	15	17	21	30	8	8	50
M20	314	245	20	12,5	15	30	16	6	37

2.2 Natural stress-strain curves for the used materials

By sake of simplicity, multi-linear curves are adopted for the natural σ-ε relations. Two types of σ-ε curves are used for the normal and the high strength steel as shown in Figure 161. The nominal σ-ε curves have been obtained through coupon tests (see WP 4).

The key values to built-up the natural curve are determined as follows: by using the results of the coupon tests, some values are chosen and fixed: ε_B, ε_C, ε_D, E_e, $\sigma_A = \sigma_B$, σ_C, σ_D (Table 49). As described in Deliverable D4.4, the tests on bolts don't give exactly the Young modulus (E_e) and deformation at point D (ε_D); therefore, coupon test results coming from another project [80], for which coupons extracted from the bolt shanks were tested, are used to define these parameters (knowing that the bolts used in both project come from the same production).

Moreover, as the area of section of the coupons after point D was not measured during the tests, the slop of the curve from point D' to point E' (E_{ex}) and the deformation at point E' ($\varepsilon_{E'}$) have been defined referring to [63]. Also, as the tested M27 bolts did not reach failure, the ultimate strength for these bolts is assumed as equal to the one for M20 bolts, as the grade for these two bolts is the same (i.e. 8.8).

Finally, the following values can be calculated:

$\varepsilon_A = \sigma_A / E_e$ $\sigma_{A'} = \sigma_A(1+\varepsilon_A)$; $\varepsilon_{A'} = \ln(1+\varepsilon_A)$; $\sigma_{B'} = \sigma_B(1+\varepsilon_B)$; $\varepsilon_{B'} = \ln(1+\varepsilon_B)$; $\varepsilon_{C'} = \ln(1+\varepsilon_C)$; $\sigma_{C'} = \sigma_C(1+\varepsilon_C)$; $\varepsilon_{D'} = \ln(1+\varepsilon_D)$; $\sigma_{D'} = \sigma_D(1+\varepsilon_D)$; $\sigma_{E'} = \sigma_{D'} + E_{ex}(\varepsilon_{E'} - \varepsilon_{D'})$.

Table 49 and Table 50 present in details the mechanical characteristics of the materials.

For the specimens under monotonic loading, the isotropic hardening material is used, while the kinematical hardening material is adopted for specimens under repeated loading.

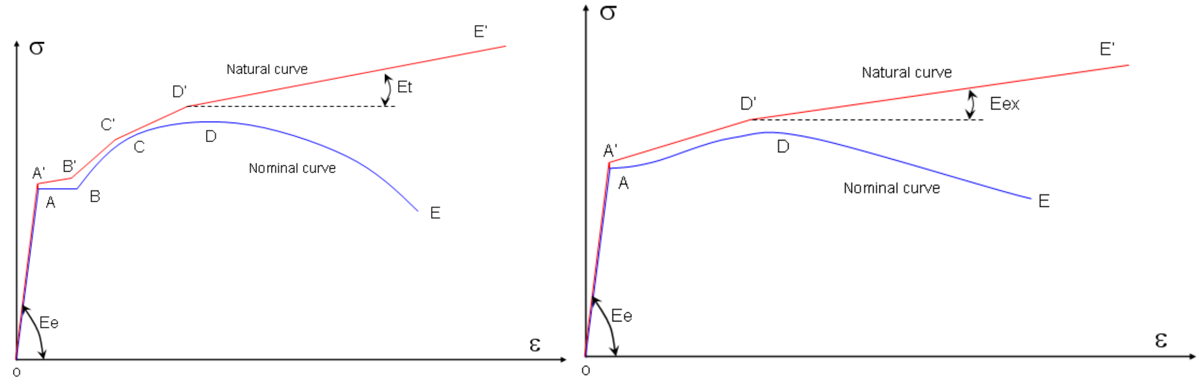

For flanges (mill steel, S355)

For tubes and bolts (high strength steel, TS590)

Figure 161 Material modelling

Table 49 The key values of the nominal curve (mean values)

	Plate 15mm	Plate 20mm	Tube	M27 bolts	M20 bolts
E_e (N/mm2)	210000 (this is a round value with negligible error)				
ε_A (%)	0,18	0,18	0,39	0,41	0,40
ε_B (%)	2	2	-	-	-
ε_C (%)	8	8	-	-	-
ε_D (%)	15	15	8	3	3
σ_A (N/mm2)	387	384	822	857	850
σ_B (N/mm2)	387	384	-	-	-
σ_C (N/mm2)	527	512	-	-	-
σ_D (N/mm2)	544	529	881	930	930

Table 50 The key values of the natural curve

	Plate 15mm	Plate 20mm	Tube	M27 bolts	M20 bolts
E_e (N/mm2)	210000				
E_{ex} (N/mm2)	636			212	
$\varepsilon_{A'}$ (%)	0,18	0,18	0,39	0,4	0,4
$\varepsilon_{B'}$ (%)	1,98	1,98	-	-	-
$\varepsilon_{C'}$ (%)	7,7	7,7	-	-	-
$\varepsilon_{D'}$ (%)	13,98	13,98	7,7	3,0	3,0
$\varepsilon_{E'}$ (%)	100			90	
$\sigma_{A'}$ (N/mm2)	388	385	824	853	853
$\sigma_{B'}$ (N/mm2)	395	391	-	-	-
$\sigma_{C'}$ (N/mm2)	569	553	-	-	-
$\sigma_{D'}$ (N/mm2)	626	608	951	958	958

2.3 Modelling of the initial deformation of the flanges

As a simplification for the meshing procedure, an imperfection is given to the foundation (and not to the flange) to simulate the presence of an initial deformation in the flanges, as illustrated in Figure 162. The bolt axis is defined as perpendicular to the inclined surface of the so-defined rigid foundation.

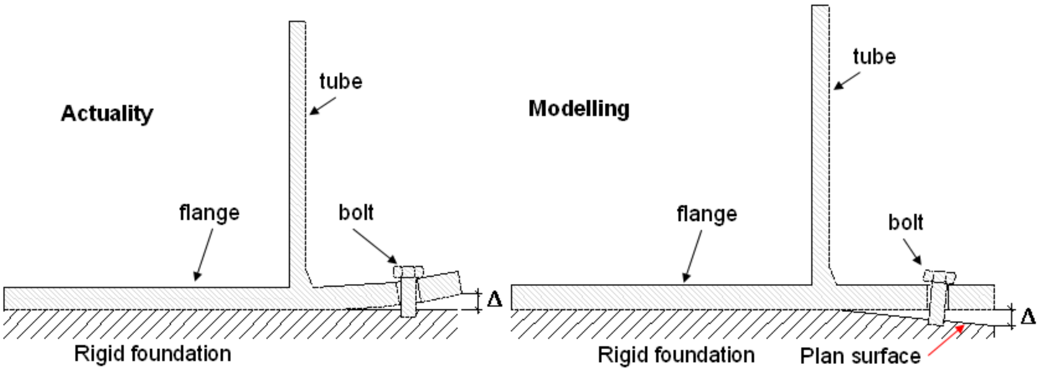

Figure 162 Model of the initial deformation of flanges

2.4 Loading sequence

In order to take into account of the bolt preloading, the loading procedure shown on Figure 163 is used for the monotonic and the repeated loading. Firstly, the load is only applied to the bolt shank, until the mean stress in the bolts reaches the expected value for its preloading. Secondly, the tensile load applied to the tube is increased until failure for the monotonic loading or some load cycles are applied to the simulated specimens for the case of repeated loading. For the case of repeated loading, only the typical hysteretic loop is simulated; the crack development is not considered.

The applied pre-stressing to the bolts is defined in agreement with the recommendations of Eurocode-3, part 1-8 [14] (it corresponds to a stress of 509 N/mm2 for a 8.8 bolt class).

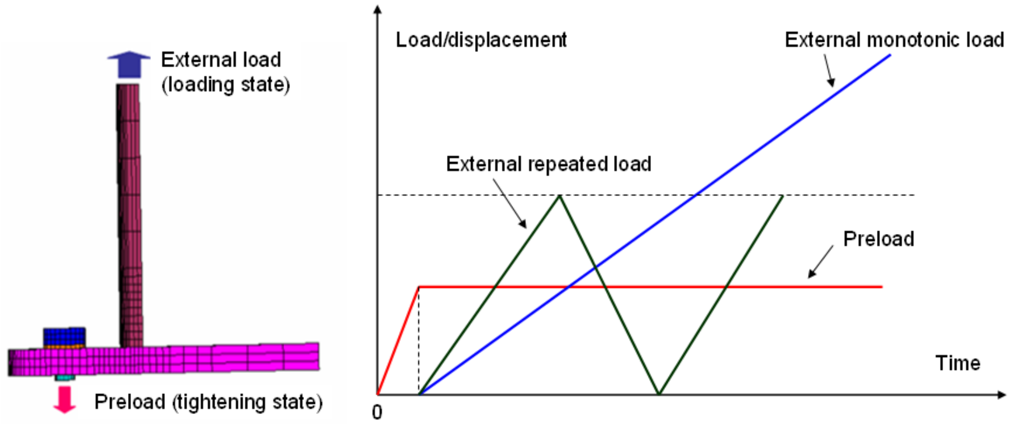

Figure 163 Loading sequence

2.5 Overview of the methods used for the determination of the hot-spot stress

Normally, the stress distribution through plate thickness at the weld toes is nonlinear due to the notch effect. This distribution of stress may be decomposed into three parts: membrane stress, bending stress and the nonlinear peak. The structural hot spot stress is composed of the membrane and the bending stress; the nonlinear peak should not be included (Figure 163) [19].

Three methods are usually used in the literature to determine the hot spot stress in plates at weld toes: (i) Linear surface extrapolation method (LSE) [19], (ii) Through thickness at the weld toe method (TTWT) [20] and (iii) Structural stress from the distance method (Dong method) [21]. Main ideas of the methods are summarized in Figure 165, Figure 166 and Figure 167; more details about these methods may be found in the corresponding references [21] [19] [20] . LSE is a simplified method that can be used for experimental or numerical approaches. On the other hand, the main idea of TTWT and Dong methods is to find a structural stress through plate thickness that is in equilibrium with the notch stress. The comparisons of the methods are also presented in many works [81] [82] [83] .

Remark: only τ_{xz} (Figure 168) is taken into account in Dong proposal [21], but the influence of τ_{yx} and τ_{yz} is also important in some cases [83]. Therefore, τ_{yx} and τ_{yz} are considered in the present work.

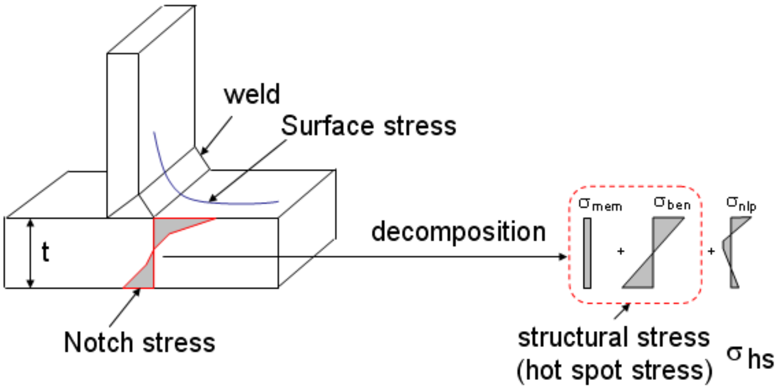

Figure 164 Hot spot stress definition

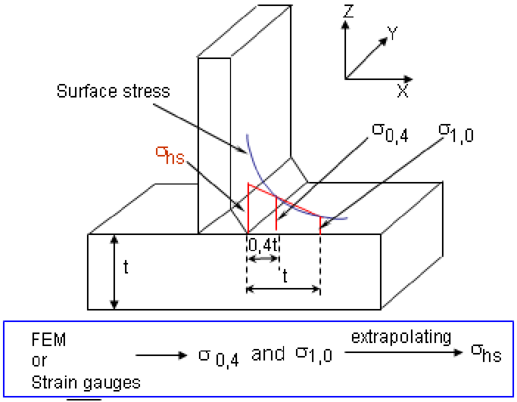

Figure 165 Linear surface extrapolation method

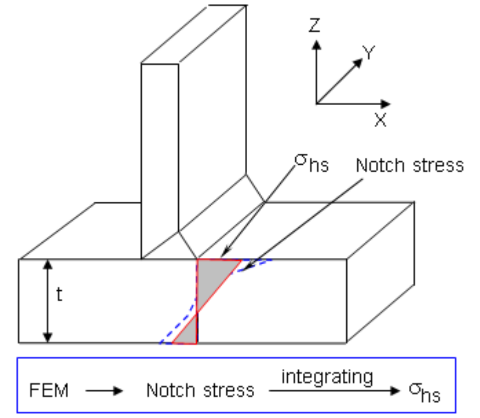

Figure 166 Through thickness at the weld toe method

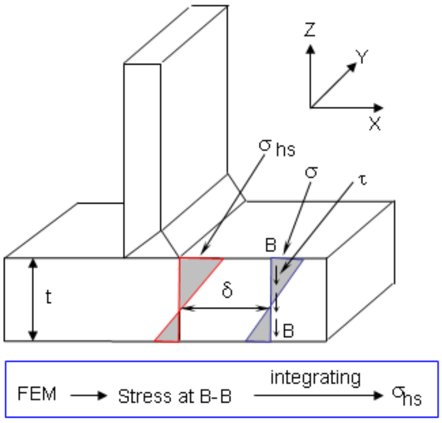

Figure 167 Structural stress from the distance method (Dong method)

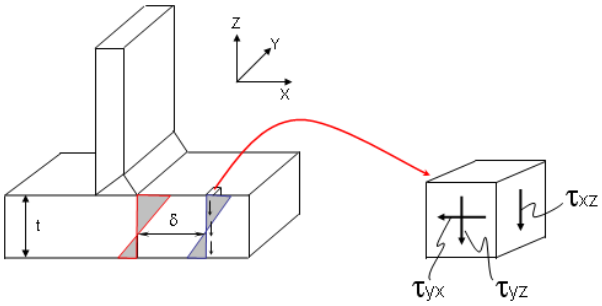

Figure 168 Shear stress components influence to the hot spot stress given by Dong method

The hot spot stress in the flange at the weld toe was calculated using the aforementioned methods. With the Dong's method, the variations of the distance δ and of the shear stress components are considered. The comparison of the hot spot stress given by the methods is carried out. It points out that when the value of δ is small and all components of shear stress are considered, the hot spot stress coming from Dong's method is in agreement with the one of the through thickness at weld toe method. On the other hand, it seems that the linear surface extrapolation method is not recommended in the present case; it may be due to the complicated distribution of stresses in the considered zone. In conclusion, the hot spot stress provided by through thickness method or Dong's method should be used in the calculation of the present modelling.

Appendix F: Numerical simulations of members and Case Studies

1. Simulations of the behaviour of tubular members under strong repeated loading with FE codes

1.1 Simulation of beam-column behavior under monotonic loading

For the simulation of the monotonic experiments conducted by CSM, finite numerical models have been developed using FE program ABAQUS. The 1.5m-long tubular members of section ∅193.7/10 (considered as C specimens) are simulated with four-node reduced-integration shell elements, which have shown to perform very well in nonlinear analysis problems involving large inelastic deformations of relatively thick-walled steel cylinders. Based on thickness measurements, the tubes have been assumed with uniform outer diameter equal to 194.05mm and uniform thickness equal to 10.06mm. The tubular model is assumed perfect and the stiff tube segments which connect the specimen ends to the machine hinges are simulated as rigid members using appropriate beam elements. The numerical analysis allows for the calculation of bending strength under several levels of axial load, in accordance with the experimental procedure; axial load is applied first up to a certain prescribed level and, subsequently, keeping the axial load constant, bending is applied through an arc-length continuation algorithm (Riks) until a maximum bending moment is reached. Upon buckling formation, bending load is continued in the post-buckling range to obtain the buckled shape and compare with the experiments. The finite element results are compared with the experimental ones in terms of interaction diagram and moment-rotation curve a shown in Figure 169 and Figure 170, respectively. The shape of the buckle for the specimen C under combined loading is shown in Figure 171.

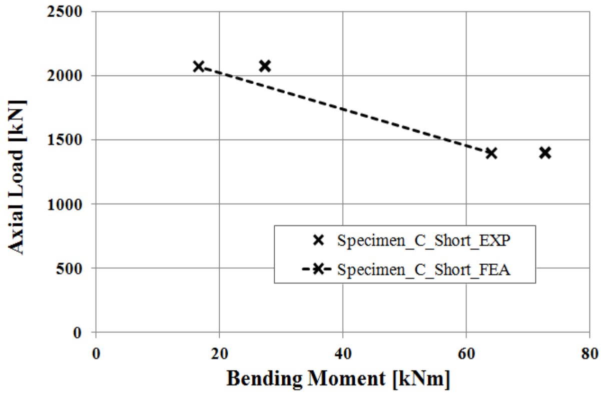

Figure 169 Finite element results in comparison with the experimental for 1.5m-long member of ∅193.7/10 section

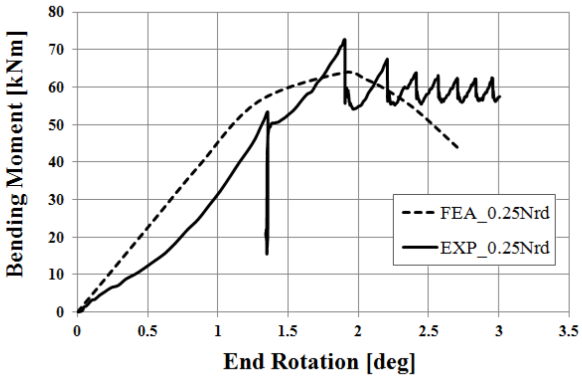

Figure 170 Finite element moment-end rotation curve (M-φ) in comparison with the experimental one for 1.5m-long member of ∅193.7/10 section

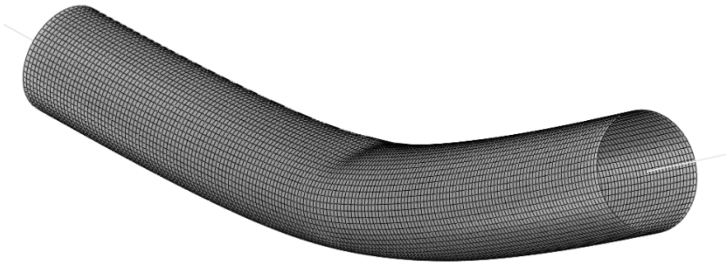

Figure 171 Failure mode of 1.5m-long member of ∅193.7/10 section under combined loading

1.2 Simulation of CHS member behavior under cyclic loading

For the simulation of the cyclic bending tests, detailed numerical models have been developed in ABAQUS FE code. Each specimen was simulated using, 8-node solid (brick) elements with linear-hybrid formulation (C3D8H) adopting the mean measured geometrical characteristics measured before the bending tests started. The stiff beam-type members (referred to as “codolos”) connecting both ends of the specimens with the hinges of the bending device were also modeled using linear beam-type elements (B31) and applying a properly selected profile section in order to take their flexibility into consideration. The connection between the specimen ends and the stiff beams was modeled assuming a kinematic coupling interaction of the end node of the stiff beam and the nodes on the perimeter of the cross-section at the specimen ends. A general view of the developed model for specimen type A is presented in Figure 172. The loading protocol in each test was precisely the one that has been followed in the simulations. Cyclic bending of the specimens was introduced by controlling the end-rotations of the two stiff beams attached to each specimen.

The numerical predictions accuracy is highly depended on the capability of the adopted cyclic plasticity model to capture the cyclic plasticity phenomena (Bauschinger effect, ratcheting) and the change of the cross-sectional geometry (ovalization) that take place during the cyclic bending of the specimens. For the current simulations two plasticity models have been used, namely the von Mises plasticity model with linear kinematic hardening (LKH) and the Tseng – Lee model (TL). The latter is considered as a more advanced model which adopts the “bounding surface” concept and was implemented into ABAQUS through a user-subroutine (UMAT) developed for the purposes of the present project. The material model parameters have been properly calibrated based on the material testing results conducted by CSM.

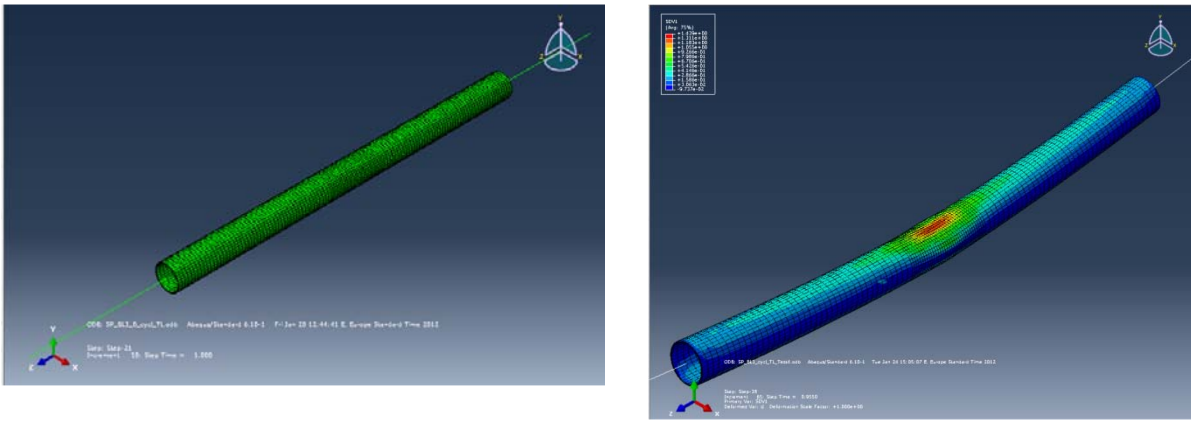

(a) (b)

Figure 172 Finite element numerical model: (a) Undeformed shape, (b) Deformed shape

The comparison between the experimental and numerical results for each test is presented in Figure 173, Figure 174, Figure 175 and Figure 176. In addition, the evolution of flattening in two orthogonal directions of the cross-section and the ovalization are also reported for both models adopted (no test data have been available). The fitting between the experimental and the numerical load-displacement loops is considered satisfactory for the TL model. The LKH model overestimates the range of the elastic behavior of the tube under reverse bending, which is attributed to the fact that this model assumes a constant size of the yield surface throughout the analysis. Moreover, the evolution of flattening and ovalization according to the LKH model is also underestimated for the same reason compared to the predictions of the TL model.

The models also indicate significant accumulation of plastic deformation at the two ends of specimens of type A (Tests No.1 and No.3), which is responsible for cracking, i.e. the failure type observed in tests. On the other hand, for Tests No. 2 and No. 4 that resulted into buckling of the tested specimens, the numerical model with the TL model was able to predict the same failure mode in a slightly increased but very reasonable number of cycles. Generally, the observed differences near the two “corners” of the experimental loops are attributed to measurement acquisition issues and could be neglected. Moreover, the increased number of cycles required to cause buckling according to the numerical model compared with the experimental observations is to be expected since the buckling phenomenon is highly sensitive to the existence of initial imperfections, but such a sensitivity analysis is outside the scope of the present study.

The numerical model developed for the simulation of Test No. 2 has also been used for the examination of the member behavior under symmetric and on-symmetric moment-controlled cyclic bending in a moment level exceeding the elastic limit of the member. The specimen has been subjected to moment-controlled symmetric cyclic bending at ±730 KNm, a moment level which is able to cause plastic deformations on the member but it is lower than the maximum moment the member is able to sustain. The moment-rotation curves, the evolution of flattening and the ovalization evolution are presented in Figure 177. The results indicate that due to the accumulation of plastic deformations and the evolution of the cross-section ovalization, there is a change of the resulting moment-rotation loops and a constant increase of the ovalization as the number of cycles increases. These are strong indications that after a sufficient number of cycles buckling of the specimen is probable to take place.

The case of non-symmetric moment-controlled cyclic bending has been also examined. The specimen under consideration has been subjected to moment-controlled non-symmetric cyclic bending at the level +730/-600 KNm. The resulting moment-rotation loops present a transition towards the higher load direction and the cross-sectional flattening and ovalization is constantly increasing (Figure 178). Again, after a certain number of cycles, local buckling of the specimen is expected. The two observations described above should be taken into consideration in order to introduce design guidelines for the tubular members under consideration.

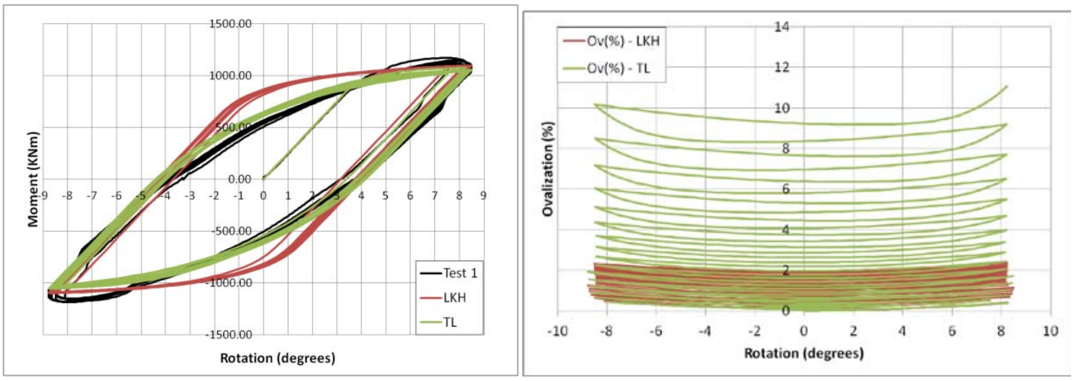

Figure 173 Test No. 1 – Cyclic moment-rotation curve; evolution of ovalization

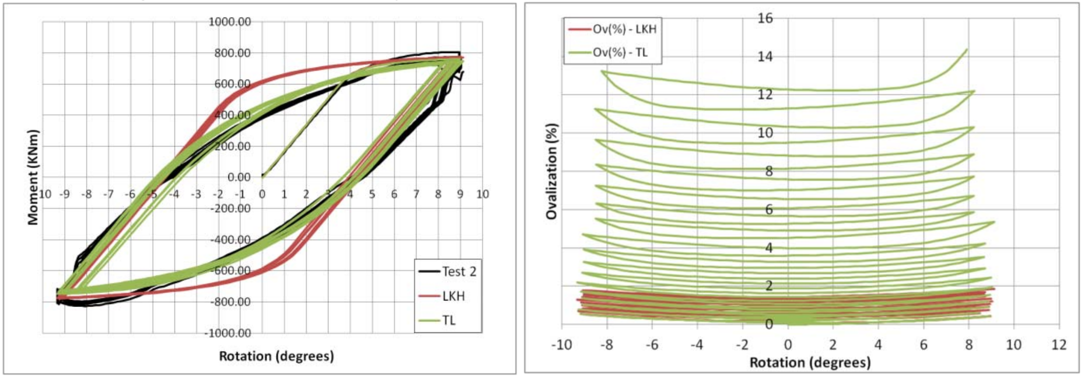

Figure 174 Test No. 2 – Cyclic moment-rotation curve; evolution of ovalization

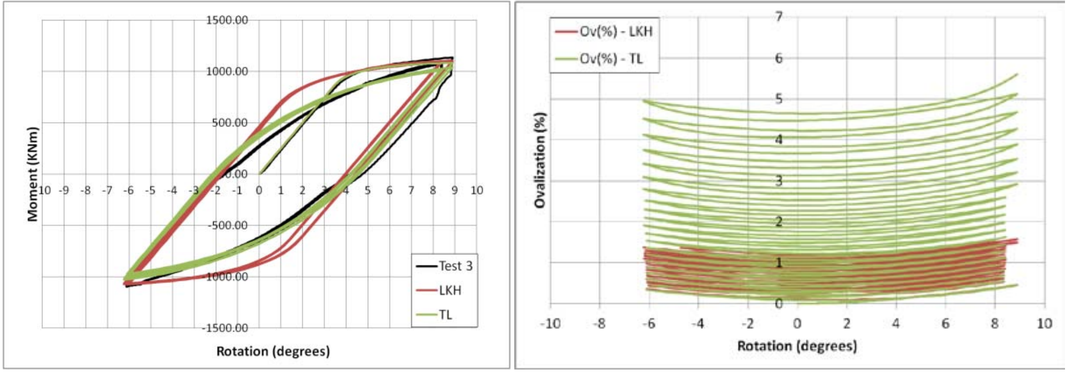

Figure 175 Test No. 3 – Cyclic moment-rotation curve; evolution of ovalization

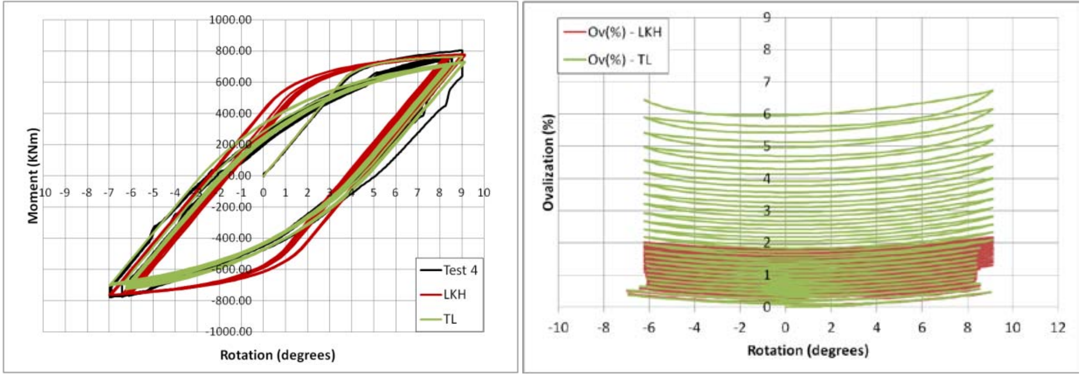

Figure 176 Test No. 4 – Cyclic moment-rotation curve; evolution of ovalization

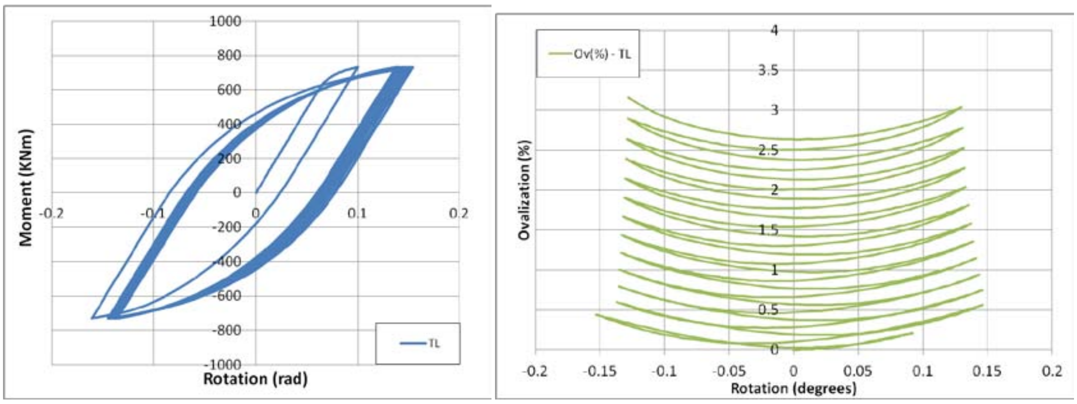

Figure 177 Moment-rotation curve and evolution of ovalization, for symmetric moment-controlled cyclic loading (section type B); numerical results

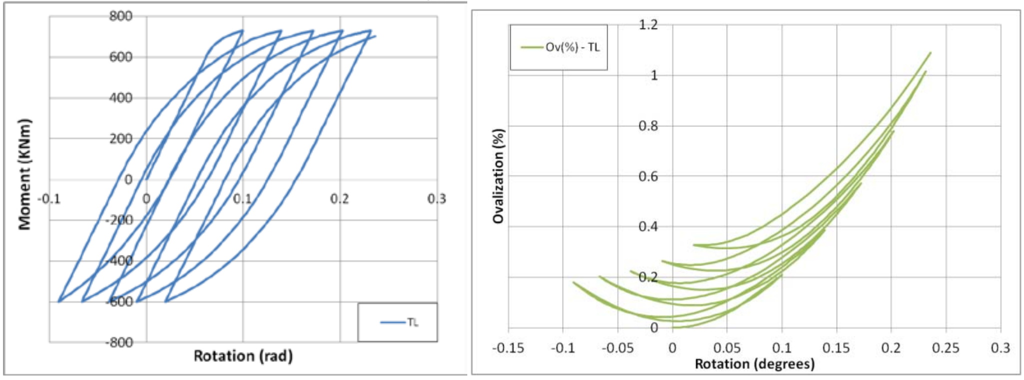

Figure 178 Moment-rotation curve and evolution of ovalization, for non-symmetric moment-controlled cyclic loading (section type B); numerical results

2. Simulation data on case studies and similar structural types

2.1 Model updating and simulations on 'Ponte del Mare' footbridge

The modal properties estimated from the modal testing campaign did not match to that of the numerical model. In order to get a robust FE model capable to simulate the actual behaviour of the footbridge, the initial FE model was updated in the light of the experimental data obtained from the identification of the bridge. The sensitivity based model updating techniques and Powell's Dog-Leg method of optimisation based on the Trust-Region approach were used. The sensitivity matrix was calculated and the 9 most sensitive parameters, shown in Table 51, were selected. The final updated model showed a considerable reduction of errors relevant to frequencies. The MAC values for the 9 updated modes are shown in Figure 179.

Table 51 Updated parameters

No.	Parameter	Initial value	Range 'physical'
1	Elastic Modulus concrete type 1, Ec1	35000000 kN/m^2	±15%
2	Elastic Modulus concrete type 2, Ec2	16000000 kN/m^2	±15%
3	Elastic Modulus structural steel, Es	210000000 kN/m^2	±5%
4	Elastic Modulus cable steel, Es_stay	165000000 kN/m^2	±5%
5	Density concrete type 1, d1	1.5 ton/m3	±30%
6	Density concrete type 2, d2	2.5 ton/m3	±30%
7	Section stiffening coefficient, C_cyc	25.40	±15%
8	Section stiffening coefficient, C_ped_B	5.06	±15%
9	Section stiffening coefficient, C_ped_D	1.15	±15%

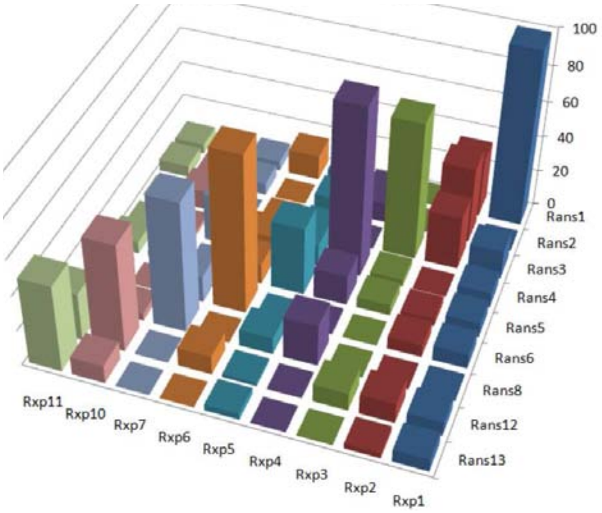

Figure 179 MAC, Rxp- experimental & Rans- ANSYS

The updated FE model was used to reproduce the acceleration response under the actual wind recorded on 25/12/2009 to check the applicability of the model. The mean wind speed near the deck was considered 16.19 m/s, i.e. an average of the measurement obtained from the two anemometers one below the deck and other on the top of the mast. The updated model well reproduced the response of the footbridge under the considered wind loading condition. Moreover and in the case of dampers, it underestimated the acceleration response with respect to the one obtained from measurements. This was due to the fact that, in reality, dampers are characterized by slack up to displacements of 4 mm.

2.2 Simulations of S. Michele and Nomi footbridges

Numerical models of the both footbridges were developed by the ANSYS software. The model frequencies and mode shapes were obtained in order to perform a fatigue check due to pedestrian load on these footbridges as well as on the foot-cycle-bridge of ‘Ponte del Mare’ of Pescara.

Some of the natural frequencies and mode shapes are shown in Table 52 and Figure 180-Figure 181, respectively.

Table 52 Natural frequencies of interest of S. Michele and Nomi footbridges

Mode	1	2	3	4	5	6	7	8
f [Hz] **S. Michele**		0.6704 (L)	0.7178 (L)	0.8823 (L)	1.0676 (L)	1.3377 (V)	1.9322 (V)	2.0038 (V)
f [Hz] **Nomi**	0.73936 (L-arch)	1.2135 (L-V)	1.2159 (V)	1.8762 (L-V arch)	2.1727 (V)			

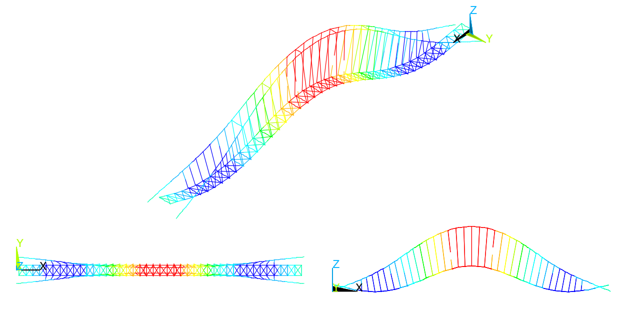

Figure 180 Mode shape 5, S. Michele footbridge

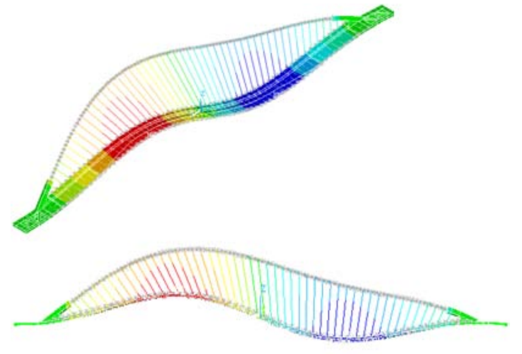

Figure 181 Mode shape 3, Nomi footbridge

2.3 Fatigue checks due to pedestrian loads on footbridges

Footbridges are subjected to vibrations caused by the human walking, which is mainly a dynamic load and may induce relevant oscillations which may compromise the functionality of the structure. This dynamic nature of the load might cause fatigue damage to steel structural members. Safety problems due to overstressing or fatigue may also occur and should also be considered in the design of footbridges, see HIVOSS 2008. Hence, a fatigue check should be performed.

In this respect fatigue check on the three footbridges were performed. For the fatigue analysis the standard EN 1993-1-9 and for pedestrian loading the ‘Technical Guide Setrà’ was used. In the ‘Technical Guide Setrà’ it is possible to find information about the pedestrian load model and a methodology for dynamic analysis for vibrations due to human walking. For fatigue analysis has been adopted this formulation of pedestrian load, because in the EN 1991-2 [46] is explicitly said that the load model given in that section are not applicable for fatigue limit state.

The general steps for the fatigue check were followed in the following order:

Determination of loading events
Stress history at details
Cycle counting
Fatigue life verification

2.3.1 Determination of loading events

The pedestrian load is described as a periodic function that may be resolved into a Fourier series. The three components of the force: a vertical component (v) and two horizontal components i.e., longitudinal (l) and transversal (t), are to be considered. The general formulation of the pedestrian load, according to the Technical Guide Setrà, is reported below:

$$F_j\left(t\right) = F_{st,j} + \sum_i N_{eq}\, G_0 \alpha_i \cos(2\pi\, f_{i,j}\, t)\psi_i \quad , \quad j = v,t,l \tag{1}$$

where: $F_{st,v} = F_{st}$, $F_{st,t} = F_{st,l} = 0$;

$f_{i,v} = f_{i,l} = 2 \cdot f_{i,t}$;

The class chosen for the footbridge is the second, characterised by a dense crowd with a pedestrian density *d* of 0.8 pedestrians/m^2. The following pedestrian actions have been modelled in ANSYS software.

Vertical component:

$$F_v\left(t\right) = F_{st} + \frac{N_{eq}\, G_0}{2 \cdot NNODI} \alpha_v \cos(2\pi\, f_v\, t)\psi_v \tag{2}$$

Transverse horizontal component:

$$F_t\left(t\right) = \frac{N_{eq}\, G_0}{2 \cdot NNODI} \alpha_t \cos(2\pi\ f_t\, t)\psi_t \tag{3}$$

Longitudinal horizontal component:

$$F_l\left(t\right) = \frac{N_{eq}\, G_0}{2 \cdot NNODI} \alpha_l \cos(2\pi\ f_l\, t)\psi_l \tag{4}$$

where: $F_{st} = \frac{G_0 \cdot A_{deck} \cdot d}{2 \cdot NNODI}$, the constant part of the Fourier series for the deck;

G_0=0.7 kN, the mean weight of one pedestrian;

NNODI, number of nodes in each modelled beam for the deck, on which the load is applied;

$N_{eq} = 10.8\sqrt{N\xi}$, number of pedestrians in phase and resonance that will produce the same effect of a crowd of N pedestrians with random phase and frequency;

f_v, f_t, f_l, frequency of the load, taken equal to the natural frequency for each modes;

ψ_v, ψ_t, ψ_l, factor which makes allowance for the fact that the risk of resonance in a footbridge depends, according to the Technical Guide Setrà, from the range of the natural frequency for each modes analysed;

$\alpha_v, \alpha_t, \alpha_l$, reduction factor for the amplitude of the vertical component.

The first harmonic of the Fourier Series will be considered, whereas for the horizontal transverse component only the second harmonic will be considered. This is according to the definition of the coefficients ψ for the three components of the load. Its value depends on the frequency range in which the natural frequency of each mode is.

2.3.2 Stress history at details

Through the implementation of the ANSYS software, a nonlinear dynamic analysis is carried out and the stress history at details is obtained. In each analysis the frequency of the load is in resonance and in phase with the mode analysed and the dynamic load is applied in the direction of the mode shape for each component. The non linear analysis has been articulated in three different phases:
PHASE 1: static non linear analysis for the gravitational loads;

PHASE 2: static non linear analysis for the static part of the pedestrian load;

PHASE 3: application of the dynamic part of the load in the three directions.

By non linear analysis the stresses in the steel structural members of the footbridge have been evaluated. For each typology of structural details, such as welds in arches and decks, the most stressed part has been checked for fatigue. In a successive phase the values of the stress in the elements obtained with ANSYS have been post-processed in order to obtain a graphic representation of the stress history in the detail. A graphic representation of the stress history at the chord-chord welded joint detail of S.Michele footbridge is shown in Figure 182.

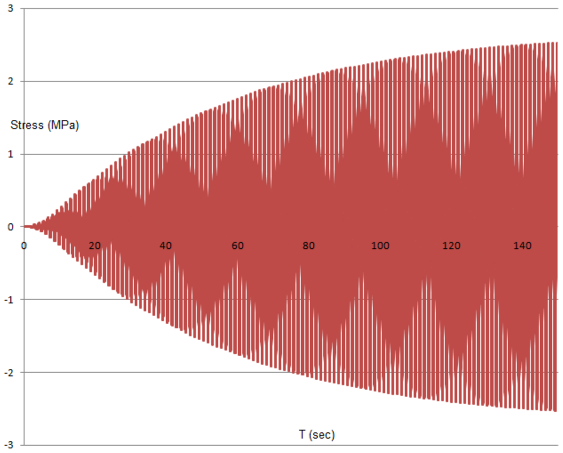

Figure 182 Stress history of the chord-chord welded joint Mode 2 (Element number 346)

2.3.3 Cycle counting

In order to establish the number of pedestrians' passages on the footbridge has been assumed that for 2 hours/day (T_0) the footbridge is loaded with a density of 0.8 pedestrians/m^2, for a period of 50 years (N_{years}). The velocity of human walking is of 1.5 m/s (v_{human}), according to the Technical Guide Setrà .

Number of static laod cycles in 50 years are given as:

$$n_{static} = \frac{N_{years} \cdot 365 \cdot T_0 \cdot 60 \cdot 60}{l_{bridge} / v_{human}} \tag{5}$$

where, l_{bridge} is the mean length of the footbridge. Around each static cycle there are also cycles due to the dynamic part of the load, as shown in Figure 183.

During 50 years there are 131 million seconds in which the footbridge is subjected to the pedestrian load on the different modes. This time has to be divided proportionally to the probability that each mode has to occur. For normal walking, frequency may be described by a Gaussian distribution with 2 Hz average and about 0.175 Hz standard deviation. For each natural frequency is possible to define the probability of resonance and then can be calculated the number of dynamic cycles.

The probability of a mode is represented by the area underneath by the Gaussian distribution between the mean values of two next frequencies, as shown in Figure 184. The dynamic part of the load acts in resonance with each mode and this means that the number of cycles is given by the product of the natural frequency and the number of seconds in which each mode acts.

$$n_{dynamic} = f_i \cdot \left(N_{years} \cdot 365 \cdot T_0 \cdot 60 \cdot 60 \cdot \int_{\frac{f_i - f_{i-1}}{2}}^{\frac{f_{i+1} - f_i}{2}} PDF \cdot df \right) \qquad (6)$$

Where $N_{years}=50$ and i=mode number.

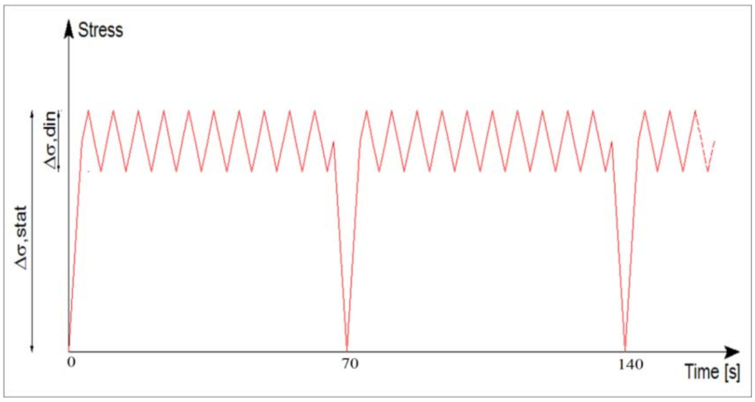

Figure 183 Static and dynamic part of the stress history

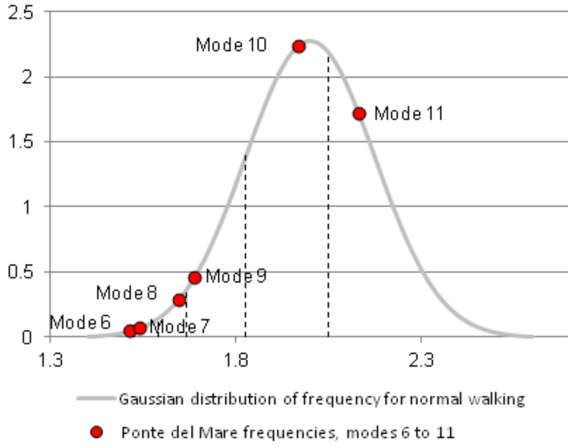

Figure 184 Gaussian distribution of the frequency of human walking

2.3.4 Fatigue life verification

The endurance number of cycles (N_R) can be calculated on the basis of the Wöhler curves as shown in Figure 185, given in the UNI EN 1993-1-9 where:

$\Delta\sigma_C$ is the fatigue strength at 2 million cycles for the detail category considered
$\Delta\sigma_R$ is the stress range in the detail
m is the slope of the Wöhler curve
The detail categories used for full penetration welded joints are characterized by the following curves:

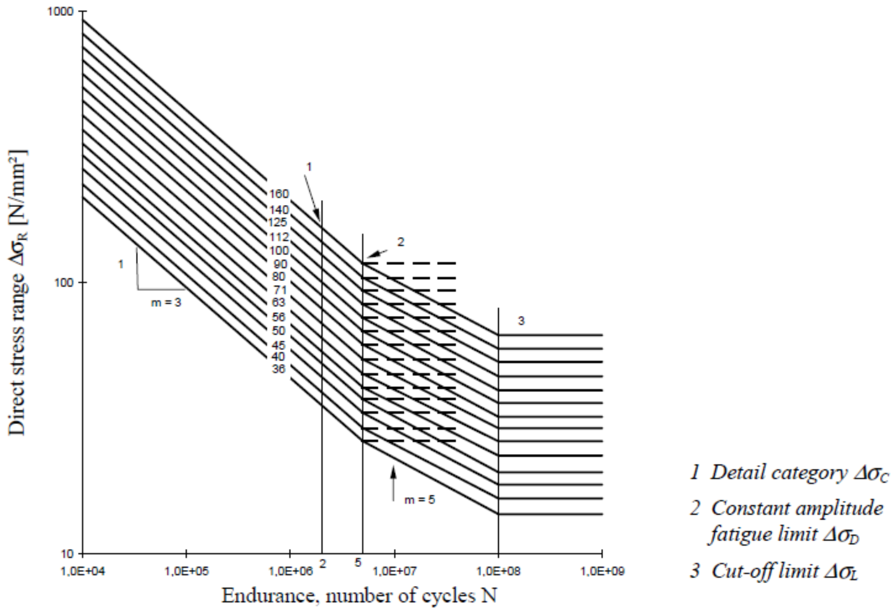

Figure 185 Fatigue strength curves for direct stress ranges

If a structural detail entails stress range values smaller than the cut- off limit, i.e. it is found that $\Delta\sigma_{dyn} < \Delta\sigma_L$ and $\Delta\sigma_{stat} < \Delta\sigma_L$, this is not sensitive to the fatigue..

The fatigue assessment is made through damage verification according to the Palmgren-Miner formula:

$$D = \sum_i \frac{n_i}{N_i} < 1 \tag{7}$$

where n_i, is the number of cycles for each $\Delta\sigma_i$ and N_i is the endurance (in cycles) obtained from the S-N curve for a defined stress range $\Delta\sigma_i$. Moreover, UNI EN 1993-1-9 states that below the cut off limit N_i is equal to 10^{20}. Therefore, if all stress ranges for footbridge details show that $\Delta\sigma_E < \Delta\sigma_L$, so they do not give a relevant contribution to the damage of details.

The simulations and fatigue checks performed on three case studies, i.e. Ponte del Mare of Pescara, S. Michele and Nomi footbridges resulted that none of the footbridge was prone to fatigue problems owing to pedestrians. Therefore, we can conclude that footbridges don’t exhibit fatigue problems due to pedestrians loading.

Appendix G: Design guidelines and recommendations

1. Development of design guidelines for high strength steel for onshore structures under extreme loadings

1.1 Fatigue

In terms of fatigue, there are some variables apart from mechanical mismatching to consider in the analysis such as the welding procedure, post-weld treatments and the weld geometry. The first variable (welding procedure) is one of the most important as HSS is more difficult to weld than conventional steel. The generation of more defects has been observed in macrographs and micrographs taken to these materials. The mechanical post-weld treatments (i.e ultrasonic peening) should be performed in both surfaces (inner and outer) in order to be effective. In the framework of this project, ultrasonic peening treatments were performed on the outer surface of the material resulting in an initiation of the fracture from the inner (not treated) surface. The weld geometry is also critical and actual recommendations of the Eurocode 3- part 9 could be more restrictive as the actual weld overthickness requirements are less than 10% of weld width and smooth transition.

1.2 Toughness

In terms of toughness, there are other variables to consider apart from the mismatch effect as for example the weld width, the crack length and the plate thickness. In the case of the weld width, if the plasticity goes ahead of the weld into the base metal, a similar behavior than that obtained in this project was already noticed by Boothman [84] and Koçak [85]. The explanation is that in undermatched welds, the J-integral should be higher than in overmatched welds due to the strain concentrates in the weld and not in the base metal (see in the Figure 186) and as a result the energy needed for the crack to growth increases. This effect would occur if the size of the plastic zone is higher than the weld thickness. In the case of the HITUBES project, the WPS defines a V butt joint with the weld width between 2 mm (weld root) -15 mm (weld face) (see in the Figure 187). The size of the plastic zone according to the reference [86] and calculated in the case of plane strain conditions is 1.2 mm so we can consider that all the plasticity occurs in the weld metal or at most in the HAZ.

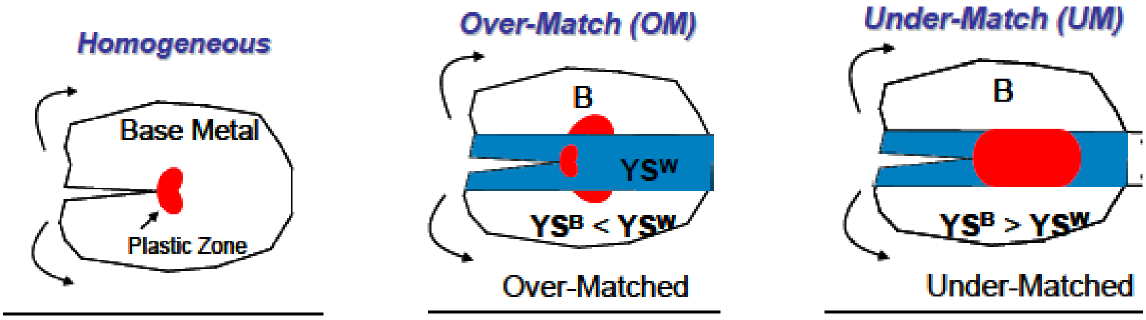

Figure 186 Crack tip plasticity in mismatching welds

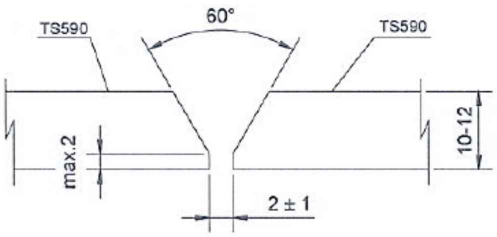

Figure 187 WPS used in HITUBES

1.3 Corrosion

These structures are often exposed to severe corrosive environments with high deposition rates of chlorides and wet conditions. Ordinary high strength steel for offshore structures are usually susceptible to general corrosion and stress corrosion cracking (SCC) including the hydrogen related SCC, also called hydrogen embrittlement. Different corrosion protective measures are commonly employed in order to reduce the extent of corrosion, such as e.g. cathodic protection and coating systems. When cathodic protection is applied it may increase the risk of e.g. hydrogen-induced corrosion cracking [87]. Hydrogen can also be formed during welding processes and enhance the possibility of hydrogen-induced corrosion [88].

Corrosion cracking phenomenon is simultaneously happened in susceptible materials as high-strength steels under the interaction between the specific corrosive environment and an external and/or internal tensile stresses [87] [89] [90]. Failures often take place under tensile stresses lower than the macroscopic yield strength of the material [91]. These stresses could be residual stresses or thermal stresses originated during the steels manufacturing process with increasing stresses the failure time and required time to commence cracking decrease.

The susceptibility to corrosion cracking of high strength steels is closely related to broad range of parameters as e.g. steel compositions, environmental conditions (as e.g. presence of chloride), geometry of the crack, the stress state, the interaction of the dislocations, grain size, orientation of the grains, production history and distribution of the precipitates [92] [93]. Carbon content and its distribution in the material matrix also strongly affect the susceptibility and lower required stress for initiation of the crack. Moreover, both the microstructure of the base metal, welded joints and the strength of the metal have large effects on the materials resistance to hydrogen induced cracking.

2. Development of design guidelines and recommendations for welded connections of onshore structures

2.1 Static strength

For welded tubular X-joints under balanced loading conditions, those equations are

- Axial loading

Chord failure:

$$N_{1,Rd} = \frac{k_p f_{y0} t_0^2}{\sin\theta_1} \frac{5,2}{\left(1 - 0.81\beta\right)} / \gamma_{M5} \tag{1}$$

where k_p is a coefficient that depends on the chord loading.

Punching shear failure $\left(d_1 \le d_0 - 2t_0\right)$:

$$N_{i,Rd} = \frac{f_{y0}}{\sqrt{3}} t_0 \pi d_i \frac{1 + \sin\theta_1}{2\sin^2\theta_1} / \gamma_{M5} \tag{2}$$

- In-plane bending

$$M_{ip,Rd} = 4,85 \frac{f_{y0} t_0^2 d_1}{\sin\theta_1} \sqrt{\gamma}\beta k_p / \gamma_{M5} \tag{3}$$

Punching shear failure $\left(d_1 \le d_0 - 2t_0\right)$:

$$M_{ip,Rd} = \frac{f_{y0} t_0 d_1^2}{\sqrt{3}} \frac{1 + 3\sin\theta_1}{4\sin^2\theta_1} / \gamma_{M5} \tag{4}$$

- Out-of-plane bending

$$M_{op,Rd} = \frac{f_{y0} t_0^2 d_1}{\sin\theta_1} \frac{2,7}{1 - 0.81\beta} k_p / \gamma_{M5} \tag{5}$$

Punching shear failure $\left(d_1 \le d_0 - 2t_0\right)$:

$$M_{op,Rd} = \frac{f_{y0} t_0 d_1^2}{\sqrt{3}} \frac{3 + \sin\theta_1}{4\sin^2\theta_1} / \gamma_{M5} \tag{6}$$

2.2 Fatigue Design

In this perspective, the CIDECT (2001) guidelines can be used as a basis. They adopt the "hot spot" stress method, and they are applicable for a number of cycles greater than 10^3. The methodology consists of two main steps:

1. Stress Concentration Factors (SCF): The parametric SCF equations of CIDECT guidelines can be used for hot spot stress calculations in typical joint geometries. For more complex joint geometries, the corresponding SCF values can be computed through an appropriate finite element analysis, also described in the CIDECT guidelines.

2. Fatigue S-N Curve: The following fatigue S-N design curve proposed by the CIDECT guidelines can be used, which includes the effects of tube thickness. Using the hot spot stress (S) computed through an appropriate SCF value, this curve provides the fatigue design curve (N).

$$\log\left(N_f\right) = \frac{12.476 - 3 \cdot \log\left(S_{rhs}\right)}{1 - 0.18 \cdot \log\left(\frac{16}{t}\right)} \tag{7}$$

The extension of the above methodology into the low-cycle regime can be considered through an "equivalent elastic stress range" through a linear extension of the S-N curves in the log-log scale, connecting (a) the point of fatigue design strength predicted by equation (7), with (b) the point on the vertical axis corresponding to static strength (number of cycles equal to 1). Point (b) for static strength can be predicted by the relevant design equations, properly expressed in terms of the hot-spot stress. Using this approach, the corresponding design methodology results in safe predictions and could be adopted for design purposes in the low-cycle fatigue range. In addition, it can be adopted by EN 1993-1-9 towards a more rational fatigue design methodology for welded tubular connections, based on the hot spot stress.

3. Development of design guidelines and recommendations for bolted connections of onshore structures

Combining the literature review and the experimental and numerical results of the present project the following conclusions can be drawn for the design guidelines to be recommended for bolted joints with circular flanges. With reference to monotonic loading the following methods have been considered: Igarashi method [59], Cao and Belle method [60] [61], Eurocode method [62] and Couchaux method [63]. With regard to the estimation of the plastic failure capacity of the considered joints, all above-mentioned methods are conservative; the observed differences between the method predictions and the experimental results are in a range of 4%-40%. The predictions given by Eurocode method are the most accurate.

With reference to high-cycle fatigue loading, through the preformed investigations it has been demonstrated that the use of “detail number 11” of Table 8.5 in Eurocode 3, part 1-9 (calculating the fatigue strength of the tube at the weld toe) [16] leads to an overestimation of the fatigue strength, which is unconservative. Therefore, it is suggested to use the hot-spot stress concept for this detail. The latter can be estimated through finite element analyses or through analytical methods using stress concentration factors to take into account stress concentration. With this method, it has been demonstrated that a conservative prediction of the fatigue strength can be obtained. The detail number 14 in Table 8.1 of Eurocode 3, part 1-9 [16] may be used to calculate the fatigue strength of the bolts, but the stress range in bolts should be estimated in two steps: (i) using finite element method to computer the stress in the bolts and (ii) applying the “Through thickness at the weld toe” method (see Deliverable 5.3) to calculate the structural stress that may be considered as the “nominal” stress, taking into account the bending and pre-stress effects as requested in Eurocode 3, part 1-9. Detail category 100 as proposed in Eurocode 3, part 1-9 [16] can be applied to estimate the fatigue strength of the flanges at the weld toe. The “Through thickness at the weld toe” method (see Deliverable 5.3) or “Structural stress from the distance” method (i.e. Dong method, see Deliverable D5.3) should be adopted to capture the stress ranges from the stress given by finite element models. The initial deformation of the flanges due to the heat-affect during the weld procedure significantly influences to the stress range on the tubes and on the flange. Therefore, the initial deformation should be taken into account in the finite element modelling if an economic design is needed. As far as low-cycle fatigue loading is concerned, for bolted joints with circular flanges, it is suggested to extend the model of Piluso [64] initially developed for the modelling of T-stubs.

4. Development of design guidelines and recommendations of onshore tubular structures under extreme loadings

The accumulation of deformation can be regarded as the interaction of the effects from two sources:

- At the material level, experiments in steel specimens have indicated that under uniaxial stress-controlled loading conditions in the plastic range about a non-zero mean stress the material exhibits “ratcheting” or “cyclic creep”, where cycle-by-cycle the hysteresis loops translate in the direction of maximum stress, resulting in an increase of the maximum strain. In addition, in the case of strain-controlled loading conditions, while a constant stress is applied on the specimen in a normal direction, a cumulative increase of the strain amplitude in the direction of the applied stress results, a phenomenon referred to as “biaxial ratcheting”. Those phenomena have been well-documented experimentally for several steel materials and several attempts have been made to develop numerical models that describe them in an accurate manner [94] [95].
- At the structural level of the bent tube, it has been widely recognized that the bent tubes exhibit cross-sectional ovalization prior to a maximum moment is reached and well before local buckling occurs. This ovalization reduces the plastic moment and enables the formation of local buckling. Furthermore, it induces hoop stresses and strains in the tube, so that the state of stress and strain in the critical zone of the bent tube is biaxial, referring to the above “cyclic creep” phenomenon.

A typical result from numerical simulation of cyclic bending of a ∅323.9/10 high-strength CHS member, is shown in Figure 188.

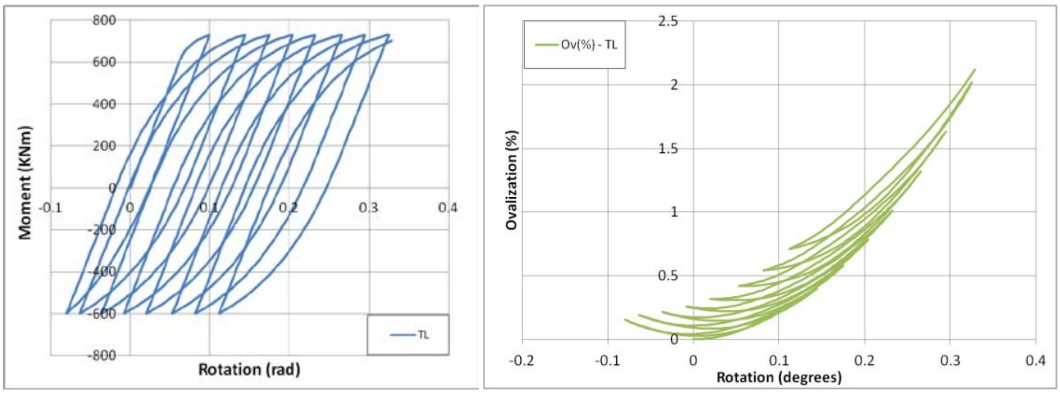

Figure 188 Structural response of a ∅323.9/10 high-strength CHS member, under non-symmetric moment-controlled cyclic loading

Modelling of the above behavior may not be a trivial issue. It is required that the engineer performs a nonlinear analysis, which couples:

- Geometric nonlinearity, in the sense that the numerical model should be able to represent the change of geometry and the flattening of the cross-section [65].
- Material nonlinearity, through the use of advanced numerical models. Cyclic plasticity related phenomena such as the Bauschinger effect and ratcheting [94] [95].

Concerning the material model to be adopted, a simple yet effective model is a J2 flow model with mixed (isotropic and kinematic) hardening. This model is able to predict the abrupt change of the material stress-strain curve when initial yielding occurs, as well as the smooth transition into the plastic range upon load reversal due to Bauschinger effect. Another suitable plasticity model for such applications is the Chaboche model [96]. If this model is adopted, caution should be paid to the increased plastic deformations predicted at the initial loading phase. The two aforementioned models are available in many commercial finite element codes. Finally, other more advanced plasticity models, such as those adopting the "bounding surface" concept (e.g. Dafalias – Popov, Tseng-Lee), that are able to capture the cyclic plasticity phenomena discussed previously are suggested (if available) for this type of simulations. The expected simulation accuracy by this class of models is increased compared to the more simple models.

An important issue towards successful modeling concerns the calibration of the above plasticity models, with respect to appropriately chosen experimental data. Many steel materials exhibit a change (increase or decrease) of the elastic stress range (size of the yield surface) after consecutive loading in the plastic regime. For accurate numerical predictions, it is necessary to define the maximum change of the size of the yield surface and the rate that this takes place with respect to the applied plastic deformations. In addition, the ratcheting rate under stress-controlled plastic cyclic loading should be also predicted accurately. In order to calibrate the adopted plasticity model to predict accurately the aforementioned phenomena, two types of material tests should be conducted:

- Strain-controlled cyclic loading tests at various strain ranges, near the stress-range expected, in order to examine the change of the yield surface size and its rate.
- Stress-controlled cyclic loading tests at various mean stress levels, in order to examine the mean stress effect on the ratcheting rate.

The material parameters of the adopted plasticity model should be calibrated accordingly. For the Chaboche model, a calibration method is described in the reference [97].

5. Time dependent reliability assessment and Bayesian update

5.1 General corrosion model

The resistance of the structure changes due to the reduction of cross-sectional area of tubular steel trusses under corrosion assumed at the outer surface. At any time t, the reduced section area A(t) of a tube truss is given by the following Equation

$$A(t) = \frac{\pi}{4}\cdot\left[\left[D_0 - 2\cdot r_{corr}\cdot W\cdot N\cdot(t - T_{corr})\right]^2 - {D_i}^2\right] \tag{1}$$

where A(t)= area of a truss at time t (mm^2), t= time (years), D_o and D_i = outer and inner diameter of tube under corrosion (mm), T_{corr}= corrosion initiation time (years) – 10 years, r_{corr}=corrosion rate (mm/year) – 0.058 mm/year -, W= a weight coefficient taking into account the global positioning of the trusses w.r.t the sea canal; and N is a random number between 0 and 1 to consider the spreading of corrosion along each member – 0 implies no corrosion; 1 implies complete corrosion along a member -.

5.1.1 Corrosion rate: r_{corr}

The corrosion rate of HSS steel in an environment near the sea (at 1% NaCl from KIMAB tests, see Table 38) is considered as Gaussian distributed with mean value $\mu = 0.058$ mm/year and standard deviation $\sigma = 0.01224$ mm/year. The general formula of a Gaussian probability density function is showed in Eq(2):

$$F(x) = \frac{1}{\sigma\cdot\sqrt{2\pi}}\cdot e^{-\frac{(x-\mu)^2}{2\sigma^2}} \tag{2}$$

The distribution of the resulting corrosion rate r_{corr} of the footbridge is presented in Figure 189a.

5.1.2 Corrosion initiation time: T_{corr}

The distribution of corrosion initiation time is used to determine when corrosion will begin at the trusses surfaces. It has been considered a lognormal (Type1) probability distribution showed in Eq(3) with a mean value $\mu = 10$ years and standard deviation $\sigma = 1.5$ year because an initial painting guarantees for 10 years of corrosion resistence.

$$F(x) = \frac{1}{\sqrt{2\pi}\cdot x\cdot\sigma}\cdot\exp\left(-\frac{1}{2}\cdot\left(\frac{\ln x - \xi}{\delta}\right)^2\right) \tag{3}$$

with $\delta = \sqrt{\ln\left[\left(\frac{\sigma}{\mu}\right)^2 + 1\right]}$ and $\xi = \ln\mu - 0.5\cdot\delta$

The distribution of the resulting corrosion initiation time Tcorr of the footbridge is presented in Figure 189b.

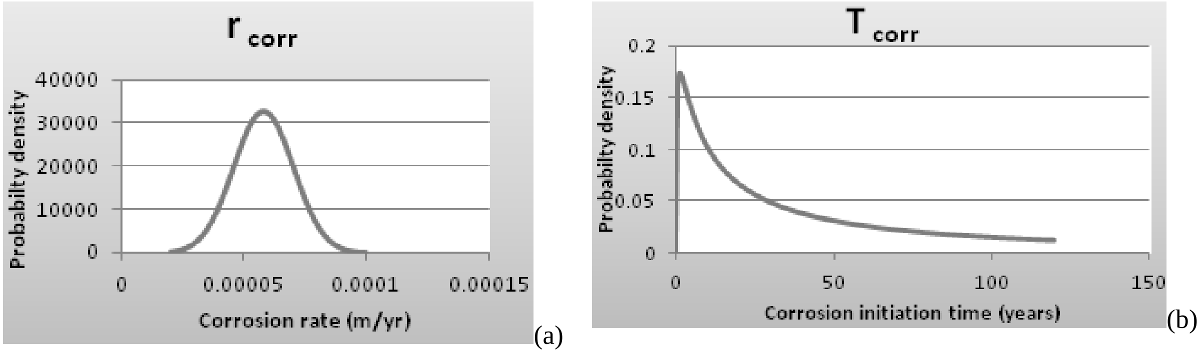

(a) (b)

Figure 189 Probability density function of a) corrosion rate and, b) corrosion initiation time

5.1.3 Local effect of corrosion: N

To take into account the distribution of the corrosion along the truss, it has been defined one parameter N that is a value between 0 (no corrosion) to 1(complete corrosion). It has a uniform distribution according to Eq(4).

$$F(x) = \begin{cases} \frac{1}{b-a} & \text{for } x \in [a,b] \\ 0 & \text{otherwise} \end{cases} \tag{4}$$

5.1.4 Global effect of corrosion: W

W is a weight factor. The trusses located over the sea canal have higher probability of corrosion (W=1) than the one positioned at the ends of the footbridge (W=0.7). This global effect of corrosion is assumed to be linear with the distance from the sea canal (Eq(5)).

Considering the x value as the general point along the deck, the value of W starts from 1 over the sea (10 meters) and ends at the farthest point as 0.7 (at x=65 m and x = - 65 m).

$$W = \begin{cases} 0.004\cdot x + 0.96 & x \in \{-65m; 10m\} \\ -0.005455\cdot x + 1.054545 & x \in \{10m; 65m\} \end{cases} \tag{5}$$

Figure 190 provides the trend of W parameter.

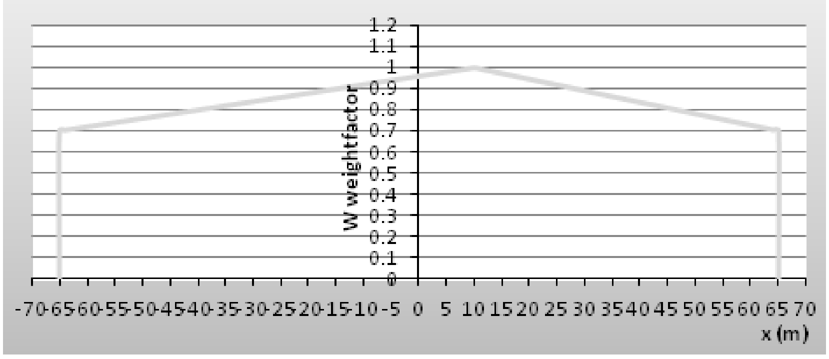

Figure 190 Global effect of corrosion along the footbridge

5.1.5 Yield strength of steel: F_{ys}

A Gaussian distribution is considered for the yield strength of the HSS steel. Its mean value is μ =640 MPa and the standard deviation is σ =16.67 MPa (based on the test data of the project). PDF is shown in Figure 191.

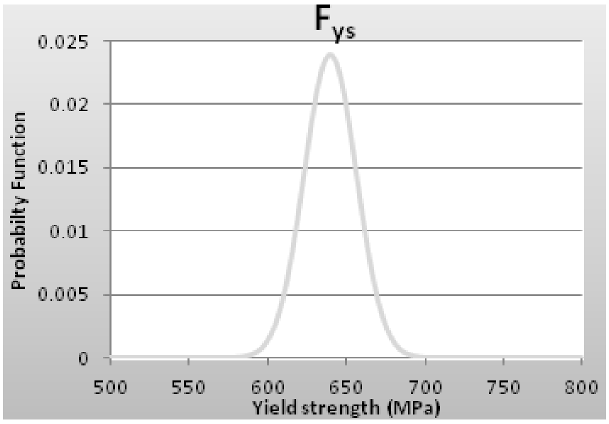

Figure 191 PDF of the yield strength of HSS steel

5.1.6 Wind load

The reliability model incorporates a time-dependent evaluation of the load effects on the deck. The maximum live load is assumed to increase over time since the likelihood of extreme loading conditions increases over time. For the wind load was chosen a Weibull probability density function. This choice distribution is according to [98]. For the ultimate limit state (return period 50 years) the wind speed, from sea to earth is 33.5 m/s and from earth to sea is 27 m/s. These two values come from the CNR DT207-2008 [99].

The corrosion model is implemented with the worst value that is 33.5 m/s. Eq(7) shows the Weibull PDF:

$$F(x) = 1 - e^{-\left(\frac{x}{\lambda}\right)^{k}} \qquad (7)$$

where k is the exponent of the Weibull distribution and λ is the scale factor.

The annual values of the two parameters k and λ were calculated according to [100]. All the formulation is based on the definition of the characteristic value: it’s the value that has the 95% of the probability to occur. So the values of the two parameters of the Weibull distribution are shown in Table 55 and plotted in Figure 192.

Table 53 Values of Weibull distribution parameters for the wind and pedestrian load

	Wind Load		**Pedestrian Load**	
Years	k	λ	k	Λ
5	8.050180849	25.76829918	17.2093990	3.49671724
10	10.37928142	27.59401980	22.19242045	3.614507338
15	11.7952008	28.5362082	25.20095759	3.673781184
20	12.815558	29.1594489	27.36185466	3.712442626
25	13.6136983	29.6202114	29.04883164	3.740751544
30	14.2692432	29.9833163	30.43239207	3.76289963

35	14.8254537	30.281606	31.60505556	3.780989727
40	15.3084739	30.5339203	32.62239641	3.796218943
45	15.7353185	30.7520258	33.52087037	3.809330286
50	16.1176835	30.9437423		

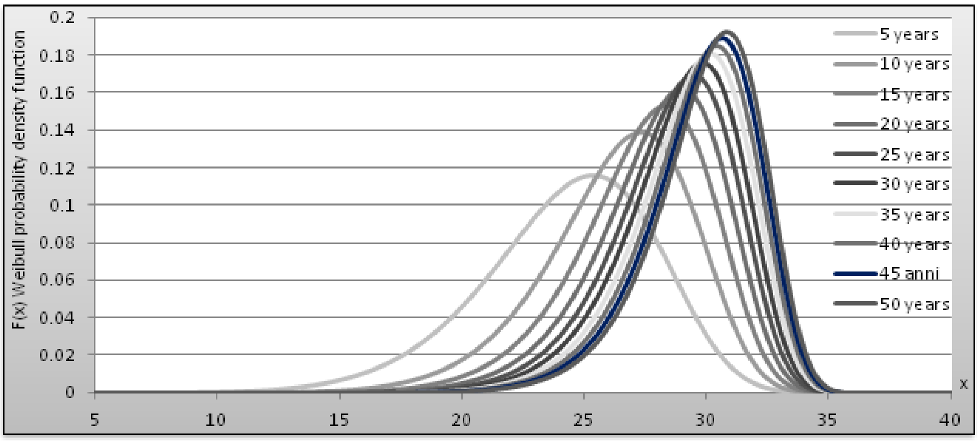

Figure 192 PDF of wind load considering different years

5.1.7 Pedestrian load

It is a load constituted from the compact crowd with intensity of 4 KN/m^2. As said before, the maximum live load is assumed to increase over time since the likelihood of extreme loading conditions increases over time. In other words, as more traffic crosses the bridge over time, the probability that the bridge will have experienced an extreme load increases. For this live load of pedestrian was chosen a Weibull probability density function (Eq(7)).

The annual values of the two Weibull parameters were calculated from the information of the characteristic value of pedestrian load: 4 KN/m^2 in 50 years for 95% confidence level. The results are shown in Table 53 and plotted in Figure 193.

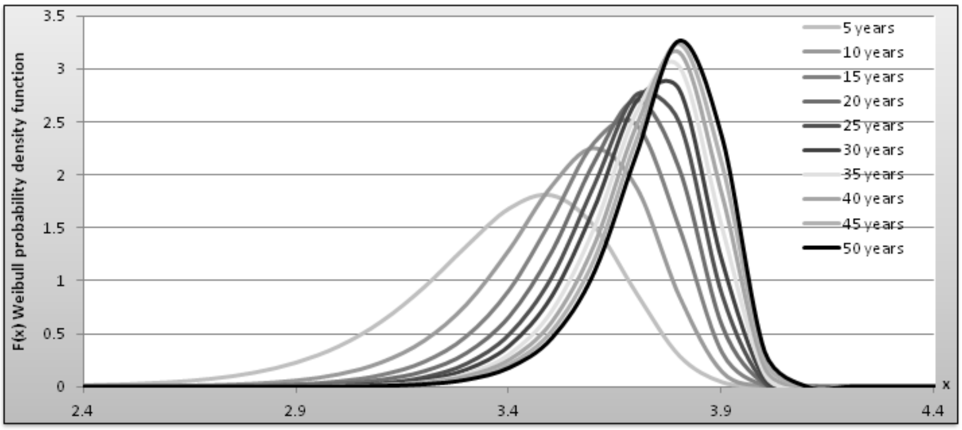

Figure 193 PDF of pedestrian load considering different years

5.2 Simulations in ANSYS and main results

Simulations were performed for 5 to 50 years on the numerical model in ANSYS using Monte Carlo Simulation (MCS) technique and Latin hypercube sampling to accelerate convergence. Two hundred (200) iterations were run for each analysis. Two types of loading conditions were considered, i.e. with the wind and without the wind.

5.2.1 Maximum displacement: Figure 194 illustrates the time variation of the maximum displacement of the footbridge deck.

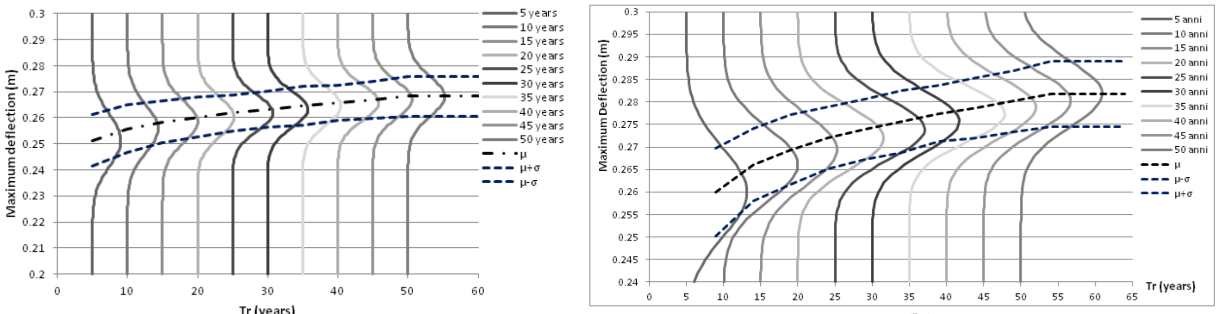

(a) (b)

Figure 194 Maximum deck deflection a) with wind load, b) without wind load

5.2.2 Maximum rotation: The maximum rotation of the deck is shown in Figure 195.

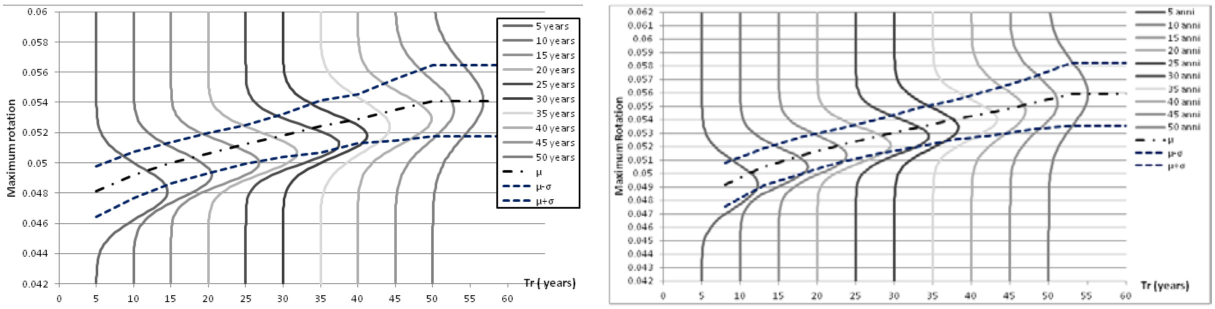

(a) (b)

Figure 195 Maximum rotation of the cycling deck a) with wind load, b) without wind load

5.2.3 Safety Margin: Figure 196 illustrates the change in the predicted safety margin distributions over time for a 50year time horizon.

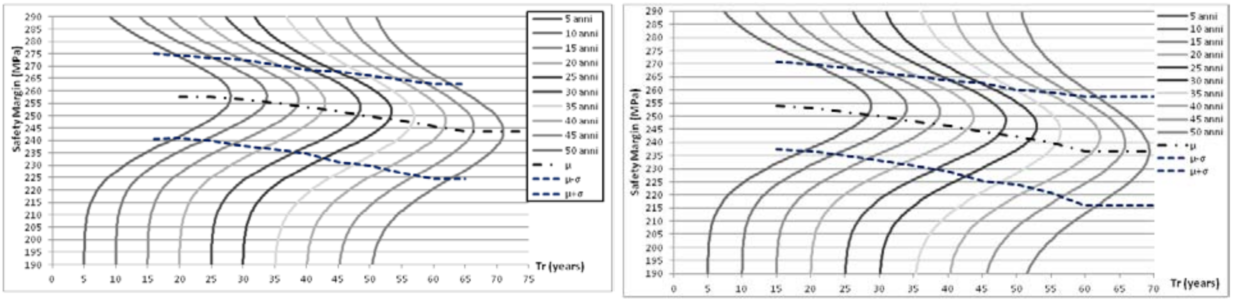

(a) (b)

Figure 196 Safety margin (MPa) of the footbridge deck a) with wind load, b) without wind load

5.2.4 Reliability index and probability of failure

The limit states of the maximum deflection- that should be less than L/500, and the limit state of the safety margin- that should be greater than 0, are satisfied. However, the calculations and the graphics showed that the maximum rotation doesn't respect the value of 5.48%. The reliability index, β is plotted with time for the rotation limit state in Figure 197 for the live load with and without considering the wind. In Figure 197, the limiting value of β is drawn from the Annex C of the Eurocode '0' [66] that means that β should be greater than 1.5 at 50 years.

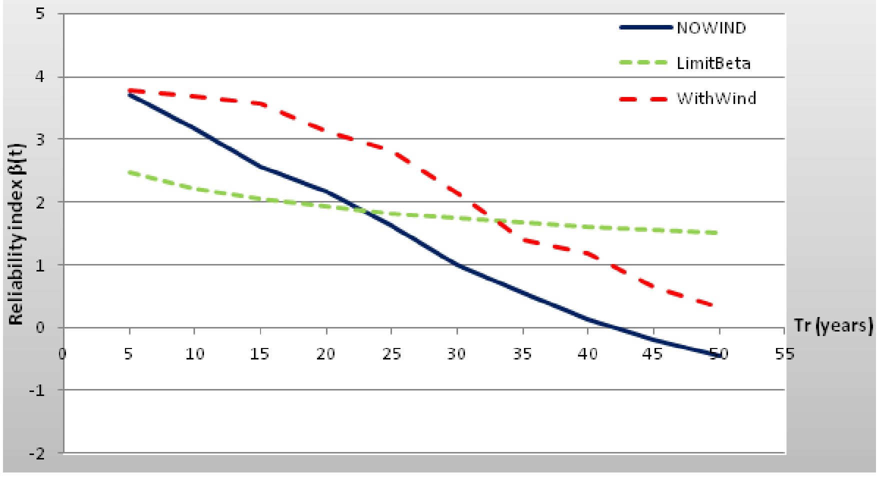

Figure 197 Time variation of reliability index of the footbridge deck

The value of β crosses the limiting value at about 23 years and 33 years for without and with wind consideration. This shows that wind acts to increase the reliability of the footbridge structure. Moreover, the decision should be based on the critical case i.e. without wind. Therefore, the repair and/or retrofit plan should be activated before 23 years of the life of the footbridge to increase its reliability index.

5.2.5 Bayesian estimation

Bayesian updating techniques are very useful when faced with two sets of uncertain information and a planner needs to know which to believe. Bayesian updating uses both the prior information and new inspection information to account for the relative uncertainty associated with each.

Assume that prior to an inspection, a random variable Θ was believed to have a density function $f'(\Theta)$ where Θ is the parameter of that distribution (i.e., the deterioration model). During an inspection, a set of values $x_1, x_2, \ldots, x_n$ representing a random sample from a population X with underlying density function f(x) are observed and are fit to a new density function $f(x_i)$ (i.e., the visual inspection results). The updated or posterior density function $f''(\Theta)$ which uses both sets of information and provides the best use of both can be expressed as [42]

$$f''(\Theta) = kL(\Theta) f'(\Theta) \tag{8}$$

where $L(\Theta)$= likelihood function; and k= normalizing constant. For the case where both $f'(\Theta)$ and $f(x)$ are normally distributed, the posterior function $f''(\Theta)$ is also normally distributed and has the mean value and standard deviation, respectively, as

$$\mu'' = \frac{\mu(\sigma')^2 + \mu'(\sigma)^2}{(\sigma')^2 + (\sigma)^2}, \sigma'' = \sqrt{\frac{(\sigma')^2(\sigma)^2}{(\sigma')^2 + (\sigma)^2}} \tag{9}$$

where μ, μ', and μ'' = mean values of the inspe ction results, the prior distribution, and the posterior distribution, respectively, and σ, σ', and σ'' = standard deviations of those same distributions.

We used the distribution of input parameters r_{corr}, T_{corr}, N, W, U and A_0. Moreover, if the new data are arrived, the posterior distributions of these inputs will change according to Eq (8). Footbridge of 'Ponte del Mare' is newly constructed. Therefore, we don't have the data for Bayesian update. However, by measurement data of wind speed, pedestrian load, distribution of corrosion locally and globally, PDF distributions could be updated. The new distribution values could be used in the model that will give a modified reliability of the footbridge.

Appendix H: Standard test protocols, SWOT analysis & monitoring

1. Definition of the standard test protocols

The test protocols regarding performance of tests have been made and the information in detail about the types of tests, loadings, number of cycles, strain rate and instrumentation has been described. The preliminary numerical simulations have been performed to understand the load-deflection (or stress-strain) behavior of the members and connections in order to prepare the test set-up.
The standards followed are summarized below.

- ASTME 466-06 standard has been followed to extract the test pieces from the specimens in case of tests on the base material and welds.
- For the high cycle fatigue tests on weld materials, the test specimen geometry will be according to the standard ASTM E466-07: “Standard practice for conducting force controlled constant amplitude axial fatigue tests of metallic materials”. The number of cycles to failure is $2x10^6$.
- The strain controlled tests (low cycle), for the base material will be carried out on R=-1, for three different levels of strains between 0.2% and 1%. The specimen geometry will be in agreement with the test standard ASTM E606-04:”Standard practice for strain-controlled fatigue testing”.
- The strain controlled tests (low cycle), for the weld material will be carried out on R>0, for strains between 0.2% and 1%. The specimen geometry will be in agreement with the test standard ASTM E606-04:”Standard practice for strain-controlled fatigue testing”.
- The stress-controlled tests (low cycle) will be done with a negative value of R (0>R>-1) to determine cyclic creep. The value of R will remain constant and the mean stress value will be incrementally increased.
- For the fracture toughness tests the in-service temperature has been decided -20^0 C. Test standard will be ASTM E1820-06: “Standard test method for measurement of fracture toughness” and specimen geometry will be SENB. A specific test standard to measure the fracture toughness properties of welds will be used, BS 7448-2:97:” Fracture mechanics toughness tests: Part 2: Method for determination of KIC, critical CTOD and critical J values of welds in metallic materials”.
- For the moment curvature tests on members ECCS procedure for cyclic testing reported in the ECCS publication no. 45 (1986) will be followed.
- The fatigue tests on the welded X-joints will be carried out with R=0.1 at 1 Hz.
- Bolted joints have been designed following the Eurocode 3. The high cycle fatigue tests will be carried out with number of cycles to failure $2x10^6$ at 1 Hz. The axial load will be derived from the footbridge model analysis.
- As for the high cycle fatigue tests are concern information is available in EN1993: 1-9. For the quantitative relationship between the stress range and number of stress cycles to fatigue failure, used for the fatigue assessment of a particular category of structural detail, can refer EN1990.
- For the low cycle fatigue (LCF) tests on the welded and bolted joints, the simulations on the footbridge will be performed in ANSYS and the real load path (stress vs cycles) will be derived.

2. Strength-Weakness-Opportunity-Threat (SWOT) evaluation of the HITUBES project

The initial SWOT analysis of the HITUBES project is as follows:

2.1 Strengths

1. University-Industry partnership: The working partners of HITUBES project belong to both from the University (UNITN, UNILG and UNITH) and the Industry (CSM, ISQ, ITMA, KIMAB, and STAHLBAU-PICHLER). This enables the better exchange of theoretical and practical knowledge and experience. We are working with a leader in Tubes TENARIS DALMINE.
2. Earlier experience on similar (European) project: Most of the partners of the HITUBES project have already been involved in European projects, so it is very easy for them to understand and to adopt the EC guidelines, rules and regulations.
3. All partners located in Europe: All the partners of HITUBES project are located in Europe, so it is easy for them to communicate and to meet efficiently. They have almost similar work schedule and work culture. This smoothens the overall work process.
4. Partners specialized in there work area: The different partners of HITUBES are specialized in their fields, for e.g. ISQ is specialized in welding, KIMAB is specialized in corrosion and ITMA is specialized in material technology and so on. This gives better reliability of the results of the project.
5. Manufactures (S. Pichler) and Co-ordinator (UNITN) situated nearby: For the success of the tests it is necessary to produce the appropriate specimens for each partner. The producer of the test specimens, S. Pichler is situated near to Trento (Italy). This gives opportunity for better coordination between S. Pichler and UNITN on behalf of the rest of the partners.
6. Innovation: HITUBES project is aimed to work on the latest HSS material and circular hollow sections applied in the field of civil structures such as footbridge and Railway Bridge. This field has

not been explored enough, and the HITUBES project aims to explore it. The partners are motivated to work in the new area.

7. Selection of Case-studies: Two case studies have been chosen: 1. footbridge (Pescara) 2. Railway Bridge (Landegem). The case studies are the footbridge under construction and real existing railway bridge. This gives an opportunity for direct comparison of the results and to assess the usefulness of high strength steel tubular sections in the field of civil engineering structures.

2.2 Weaknesses

1. Many-Partners: HITUBES project involves many partners. It puts a big challenge on efficient coordination among the partners.
2. Limitation of Eurocodes- need of AWS: The working groups in Europe usually follow Eurocodes. But during the design of welds and weld profiles for test specimens, it has been realized that Eurocodes are not complete and we have followed the guidelines of American Welding Society (AWS) codes for this task.
3. HSS un-explored: The high strength steel is not explored sufficiently. So, there is unavailability of enough literatures in this field. We have to utilize very carefully and critically the available literatures and to proceed with our own experience and judgment.
4. Limited HSS-CHS manufacturers: There are limited numbers of steel producers who produce the high strength steel tubes. We do not have many options to compare the price and the quality. In fact, we have compromised with our designed tubular dimensions and HSS grades.
5. Small amount of HSS - CHS need: In HITUBES, for our limited number of experiments on HSS tubes, we need small amounts of steel. Many of the steel mass producers cannot take this order for usual main line production, but can be only produced as an extra to the main production line. This endangers the availability of the steel in time.

2.3 Opportunities

1. Finding HSS tube producer (T. Dalmine) in Italy: Tenaris Dalmine is a well known steel tube manufacturers. The manufactured tubes will be transported to Stahlbau Pichler for the production of specimens. The location of S.Pichler & T. Dalmine, both in the same country and nearby will not only reduce the transportation cost but also reduce some of the bureaucratic processes. In case of defectives production a corrective action can be taken efficiently.
2. Gain in experience: The HITUBES project offers several kinds of experience to the working partners. To work on the high strength steels and tubular members will build their confidence to explore the new materials in a more efficient manner in the future. Apart from technical experience, it offers the experience to work in a team for the single objective.
3. Contact with new Organizations: The progress of HITUBES project has given the opportunity to contact and collaborate with new organizations. We entered in contact with foundations that promote steel tubes: for instance Promozione Acciaio in Italy. We have come in to collaboration with tube producer Tenaris Dalmine and Let's Global for peening treatment of specimens.
4. Monetary Gain: The HITUBES project offers the partner organizations and their employees a direct monetary gain, an upliftment in the standard of living and thus the overall development of the society.

2.4 Threats

1. Pescara Bridge (under construction) case-study – Delay of project objectives One of the chosen case studies, i.e. footbridge in Pescara (Italy) is still under construction. The construction is in the hand of third parties and has already been delayed. The activities of identification and monitoring in work Task 2.3 of the proposal can be fully realized only after completion of the footbridge. This puts an uncertain delay for project activities.
2. Dependency on Tenaris Dalmine (a mass producer) for small amount of TS590 tubes demand – Uncertain delay: Tenaris Dalmine is a mass producer of steel and steel tubes. We had to choose the sections and HSS steel grades from Tenaris Dalmine's production schedule. In doing this, we compromised with our designed steel grades and dimensions. Any error in production will further delay our tube procurement and hence the experimental activities.
3. Mixing of Euro codes & AWS: The weld joints have been designed using Euro codes, while the welds and weld profiles have been detailed using the American Welding Society (AWS) codes. Thus the two different design codes have been used to design and detail weld joints and weld profiles.

3. Monitoring of the project activities

In the beginning of the project the realization of the structural identification and the monitoring experimental activities on the footbridge of the 'Ponte del Mare' was, originally, postponed due to the incomplete construction of the footbridge. Nonetheless, the identification experiments: identification without dampers with dampers, cables and pedestrian were performed in October- December 2009. In addition, the monitoring activities were also completed in December 2010. Moreover, due to the request of the TGS8 committee we analysed two additional case studies, i.e. the footbridge of 'S.Michele' and the footbridge of 'Nomi'.
Due to the difficulty in finding the supplier of the small amount of high strength steel tubes required for the project, there was delay in realization of the specimens and therefore the tests on the base material, welds, connections and members were postpones. However, the specimens were delivered and the experimental activities were completed followed by numerical simulations.

Showing interest in the work on the footbridge, the reviewers of the TGS8 committee requested a fatigue model for pedestrian bridges. A fatigue model for pedestrian bridge is not available in Eurocodes. We proved for three different types of footbridges that fatigue induced by pedestrian is not a limit state that has to be checked. This conclusion applies also to wind loadings. The reviewers of the TGS8 committee have requested to compare the results of this project to that of the HiVoSS project. However, due to the aforementioned conclusion, this comparison is not needed.

In view of the railway bridge analysis, we analysed in depth the IABSE report on high strength steel. It advocates that some post weld treatment techniques such as peening can be beneficial in case of the application of HSS in details and substructures. So, some peening treatment was carried out. Finally with regard to publications/conference presentations resulting from the project, 10 papers and 1 book – in Italian for the time being - were issued; in greater detail, 2 papers published on international journals; 3 papers under preparation; 5 papers presented on international conferences.

A copy of the signed "Technical Annex" (Annex I to the Grant Agreement) or its latest signed amended version if applicable